2019

Computational Modeling and Simulations of Condition Deterioration to Enhance Asphalt Highway Pavement Design and Asset Management

Zul Fahmi Bin Mohamed Jaafar
University of Mississippi

COMPUTATIONAL MODELING AND SIMULATIONS OF CONDITION DETERIORATION TO ENHANCE ASPHALT HIGHWAY PAVEMENT DESIGN AND ASSET MANAGEMENT

A Dissertation
Presented in partial fulfillment of requirements
for the degree of Doctor of Philosophy
in the Department of Civil Engineering
The University of Mississippi

ZUL FAHMI BIN MOHAMED JAAFAR

May 2019

ABSTRACT

A nation's economy and prosperity depend on an efficient and safe transportation network for public mobility and freight transportation. A country's road network is recognized as one of the largest public infrastructure assets. About 93 percent of 2.6 million miles of paved roads and highways in the United States (U.S.) are surfaced with asphalt. Longitudinal roughness, pavement cracking, potholes, and rutting are the major reasons for rehabilitation of asphalt roads. Billions of dollars are required annually for the maintenance and rehabilitation of road networks. If timely maintenance and rehabilitation are not performed, the pavement damages inflicted by heavy traffic repetitions and environmental impacts may lead to life threatening condition for road users. This research is focused on asphalt pavement condition deterioration progression modeling and computational simulations of uncracked and cracked asphalt pavement-subgrade models. The research objectives are to (1) evaluate and enhance asphalt pavement condition deterioration prediction models, (2) evaluate modulus backcalculation approaches for characterizing asphalt pavement layers of selected test sections, (3) develop three dimensional-finite element (3D-FE) asphalt pavement models and study impacts of cracking on pavement structural responses, and (4) implement pavement condition deterioration models for improved structural design and asset management of asphalt highway pavements.

The historical asphalt pavement database records of the Long-Term Pavement Performance (LTPP) research program were used to develop asphalt pavement condition deterioration progression models, considering LTPP regions and maintenance and rehabilitation history. The enhanced condition deterioration prediction equations of the International Roughness Index (IRI), rutting, and cracking distresses were developed and evaluated in this research for LTPP datasets of 2,588 for IRI, 214 for rutting, and 2,240 for cracking. The LTPP regions and major maintenance intervention criteria were common factors considered in all multiple regression equations. The IRI prediction equation also considered the IRI measurement location factor. Additionally, the rutting prediction equation includes additional factors of in situ modulus of pavement layers and base layer type. In comparison, the U.S. national mechanistic empirical pavement design guide (MEPDG) performance prediction models do not include maintenance and rehabilitation and climatic factors which present major limitations of the MEPDG method of pavement thickness design.

Both regression analysis and Artificial Neural Network (ANN) analysis methods were used and the results were compared. The IRI multiple regression equation shows R of 0.633, which is slightly lower compared to the ANN IRI model's R of 0.717. The IRI predictions using the enhanced multiple regression equation are comparable with the ANN results for verification data sets. The prediction equations from multiple regression modeling and ANN modeling of rutting distress show high R values above 0.93 and 0.94,

respectively, and reasonably accurate result of model database and verification section. These model equations have got higher R value compared to the MEPDG's R value.

A new cracking model namely Unified Cracking Index (UCI) was developed in this research by combining all crack types which is not available in the MEPDG. The overall UCI combines the densities (% crack area per total area) of the alligator, block, longitudinal, and transverse cracking types. This approach is practical and easy to implement with intervention criteria of maintenance and rehabilitation for life-cycle asset management of asphalt highway pavements. The UCI equations using multiple regression for log transformation and using sigmoidal transformation for the model database shows the correlation, R, of 0.551 and 0.511 respectively, with 19.5 and 4.1 percent errors in predictions compared to the measured LTPP data. In comparison, the ANN model for UCI showed significant improvements in R value (0.707) with 14.6% error. It also showed high R value (0.861) and low error for the verification data sets.

The MEPDG method includes separate models of alligator crack, longitudinal crack (defined as fatigue induced crack in the MEPDG), and transverse crack. In comparison, this research developed prediction equations not only for alligator, longitudinal, and transverse cracks but for block crack too. Individual ANN model of cracking (alligator, block, longitudinal, transverse) also showed reasonably accurate results.

In situ modulus values of existing pavements are other important material inputs for pavement structural response analysis of overlay thickness design. Several modulus backcalculation software, based on the layer elastic static analysis theory, were evaluated in this research for selected LTPP highway sections. The comparisons indicated that the backcalculated modulus values in the LTPP database were generally unreasonable using the EVERCALC 5.0 software. Overall, the backcalculated modulus values using BAKFAA 2.0 and PEDD/UMPED were generally reasonable for all pavement layers. It was also shown that the thickness design of longer lasting pavement performance depends on seasonal layer modulus values considering extreme weather and climate attribute.

In order to create a structural response database for pavement-subgrade subjected to design truck axle load, the 3D-FE models of uncracked and cracked asphalt pavement layer were developed using the LS-DYNA finite element software. The structural responses such as surface deflections, stresses and strains at different depths in the pavement-subgrade model were analyzed for critical locations. A full factorial experiment for six independent variables at two levels was designed, and the simulations for 64 treatment combinations were executed for the uncracked model. The results of the 3D-FE models showed comparable results with previous studies using the LS-DYNA software and the outputs of the GAMES linear elastic program. An extended analysis was conducted on the cracked model to study the effect of full depth cracked on effective

asphalt modulus values. Based on the full-depth cracked 3D-FE model results, low-level modulus of weak pavements showed a higher reduction of 81.0 % in the asphalt modulus compared to the compared to the asphalt modulus of the uncracked 3D-FE model, while the high-level modulus and thick pavement showed a low reduction of 13.5 % in the asphalt modulus of the uncracked pavement model.

The development of the enhanced pavement condition prediction equations provide significant improvements over the MEPDG method, such as consideration of maintenance and rehabilitation history and climatic regions, using larger number of LTPP datasets, compared to model data sets used in the MEPDG. Therefore, the developed equations are more appropriate for the pavement structural design and asset management of asphalt highways. This implementation will contribute towards longer-lasting asphalt highway pavement assets to serve the public, improve safety, support efficient supply chain and economic growth.

DEDICATION

This dissertation is dedicated to my parents Late Mohamed Jaafar Bin Kadir and Late Che Minah Binti Abdullah, wife Nur Sarhana Binti Ahmad Jamil and children, father and mother in law Ahmad Jamil Bin Abu Bakar and Hamidah Binti Puniman.

LIST OF ACRONYMS

AARG	Average Annual Rate of Growth
AASHTO	American Association of State Highway and Transportation Officials
ANN	Artificial Neural Network
ANOVA	Analysis of Variance
AW	Area from Measured Deflection-Time History
CBO	Congressional Budget Office
CESAL	Cumulative ESAL
CAIT	Center for Advanced Infrastructure Technology
CBR	California Bearing Ratio
CI	Cracking Indicator
CIA	Central Intelligence Agency
CN	Construction Number
CND	Major M&R Intervention Factor
CO_2	Carbon Dioxcide
COV	Coefficient of variance
CS&O	Crack, Seat, and Overlay
CTB	Cement Treated Base
DBSID	Dynamic Backcalculation Procedure with Systems Identification Method

DCP	Dynamic Cone Penetrometer
DEF_{W1}	Peak Deflection under Sensor One
ERDC	Engineering Research and Development Center
ESAL	Equivalent Single Axle Load
FAA	Federal Aviation Administration
FD	Dynamic Friction
FHWA	Federal Highway Administration
FI	Freezing Index
FWD	Falling Weight Deflectometer
FS	Static Friction
GMPro	GeoMedia Professional
GPR	Ground Penetration Radar
GPS	General Pavement Study
HDD	Heating Degree-Days
HDM-III	Highway Design and Maintenance Standards Model
HMA	Hot Mix Asphalt
HWD	Heavy Weight Deflectometer
IRI_0	Initial International Roughness Index
IRI	International Roughness Index
LEAF	FAA Layered Elastic Analysis

LED	Layered Elastic Design
LFA	Lime-Filled Asphalt
LTPP	Long-Term Pavement Performance
LTS	Lime-Treated Subbase
M&R	Maintenance and Rehabilitation
MARE	Mean Absolute Relative Error
MDOT	Mississippi Department of Transportation
MEPDG	Mechanistic Empirical Pavement Design Guide
NALS	Normalized Axle Load Spectra
NHS	National Highway System
NCHRP	National Cooperative Highway Research Program
NDT	Nondestructive Testing
NHTSA	National Highway Traffic Safety Administration
PADAP	Pavement Design System for New and Existing Asphalt Pavements
PCASE	Pavement- Transportation Computer Assisted Structural Engineering
PCR	Pavement Condition Rating
PI	Plasticity Index
PM	Particulate Matter
PMS	Pavement Management System
PRECIP	Precipitation

PSI	Present Serviceability Index
QI	Quarter-Car Index
RAP	Recycled Asphalt Pavement
RD	Rut Depth
RFL	Rainfall Intensity
RMSE	Root Mean Square Error
SD	Standard Deviation
SHRP	Strategic Highway Research Program
SN	Structural Number
TDC	Top-Down Cracking
$TEMP_{AIR}$	Air Temperature
$TEMP_{PAVE}$	Pavement Temperature
TRL	Transportation Research Laboratory
UCI	Unified Cracking Index
UK	United Kingdom
UNDP	United Nations Development Program
U.S.	United States
USDOT	U.S. Department of Transportation
3D-FE	Three Dimensional-Finite Element
WF	Wet-Freeze

WNF	Wet-Non-Freeze
Y_{AC}	UCI for Alligator Crack Density (%)
Y_{AC0}	Initial UCI for Alligator Crack Density (%)
Y_{BC}	UCI for Block Crack Density (%)
Y_{BC0}	Initial UCI for Block Crack Density (%)
Y_{C}	UCI for Combined All Cracks Density (%)
Y_{C0}	Initial UCI for Combined All Crack Density (%)
Y_{I}	IRI per Measurement Year
Y_{I0}	Initial IRI per Measurement Year
Y_{LC}	UCI for Longitudinal Crack Density (%)
Y_{LC0}	Initial UCI for Longitudinal Crack Density (%)
Y_{R}	Average Rut Depth per Measurement Year
Y_{R0}	Initial Average Rut Depth per Measurement Year
Y_{TC}	UCI for Transverse Crack Density (%)
Y_{TC0}	Initial UCI for Transverse Crack Density (%)

ACKNOWLEDGEMENTS

First and foremost I am expressing my profound gratitude and sincere appreciation to my Ph.D. advisor Professor Dr. Waheed Uddin, the Founder Director of Center for Advanced Infrastructure Technology (CAIT), for valuable guidance, constant encouragement and support, and untiring help, which inspired me through all stages of the work. Dr. Uddin's compliments and encouragement were always important to me. Additionally, his advice and critics were equally important to bring the best out of me. Thank you very much, Dr. Uddin.

I acknowledge my profound thanks to my former Master of Science supervisor Professor Dr. Meor Othman Hamzah for suggesting and convincing me to pursue my Ph.D. study at the University of Mississippi with one of the best scholars in the field of asphalt pavement design and asset management. Also, I would like to express my deepest gratitude and appreciation specifically to the School of Civil Engineering of Universiti Sains Malaysia (USM) for choosing me as one of the Bumiputra Academic Training Scheme candidates. Thank you to USM and Ministry of Higher Education Malaysia (MOHE) for continuous financial support throughout my study at The University of Mississippi, Oxford, Mississippi, USA.

I express my heartfelt thanks to my Ph.D. dissertation committee members, Dr. Waheed Uddin as the committee chair, Dr. Yacoub Najjar (Professor and Department Chair of the Civil Engineering Department), Dr. Ahmed Al-Ostaz (Professor of Civil

Engineering), and Dr. Tyrus Mc Carty (Associate Professor of Mechanical Engineering). Thank you very much for the valuable inputs and suggestions that contributed to my dissertation.

I am grateful to all my fellow colleagues at CAIT, Dr. Alper Durmus, Dr. Quang Nguyen, Muhammad Ahlan, Seth Cobb, Tucker Stafford, Robert Richardson, Salma Sultana, and Rulian Barros, for helping me when I needed it, regardless of the subject matter.

I am beyond happy to express my appreciation to my wife for her help in taking care of our children when I was far from home in the United States completing my Ph.D. study. I am eternally grateful for everything you have helped me with and I am wholeheartedly appreciating everything you have done for our family. I am thankful to members of Dermawan Kacak (DK) support group, and other family members for their continuous support and love throughout my doctoral study.

TABLE OF CONTENTS

LIST OF TABLES

LIST OF FIGURES

I. INTRODUCTION

1.1 Background

A nation's economy and prosperity depend on an efficient and safe transportation network for public mobility and freight transportation. Road networks are essential for a nation's military mobilization to ensure public safety and are recognized as one of the largest public infrastructure assets in many countries worldwide. According to the Central Intelligence Agency (CIA) (https://www.cia.gov/index.html), a total of 38,800,476 kilometers of road networks for 223 countries worldwide were reported to the agency, which includes both unpaved and paved roads. The spatial map that shows the total length of the unpaved and paved road networks in the countries worldwide is shown in Figure 1.

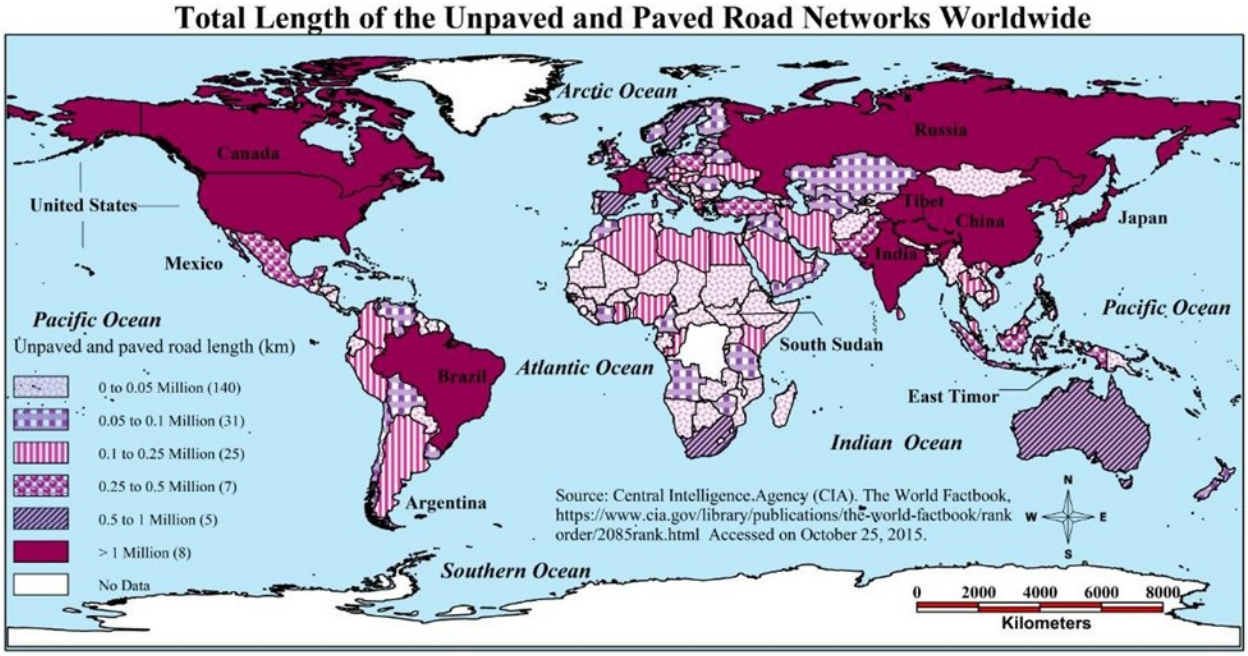

Figure 1. Spatial map of the road length (km) from 216 countries worldwide

The spatial map, developed using the GeoMedia Professional (GMPro) software, shows the distribution of the total unpaved and paved road length for 216 countries. Seven countries are not recognized in the software database. The road length data sets are divided into six different intervals, ranging from less than 50,000 to more than one million kilometers. The majority of 140 countries have less than 50,000 kilometers of road length. About one-quarter of 216 countries worldwide are within the 50,000 to 250,000 kilometers road length group. About 12 countries are observed to have road networks between 250,000 to one million kilometers. There are eight countries reported with road lengths of more than one million kilometers. The top eight countries are the U.S. (6,586,610 km), India (4,689,842 km), China (4,106,387 km), Brazil (1,580,964 km), Russia (1,283,387 km), Japan (1,210,251 km), Canada (1,042,300 km), and France (1,028,446 km).

About 93 percent (%) of 4.2 million kilometers (2.6 million miles) of paved roads and highways in the U.S. are surfaced with asphalt [1]. This is the reason why this research focuses only on the asphalt highway pavement. According to the U.S. Department of Transportation (USDOT), about 2,988.3 billion cumulative vehicle-miles travelled (VMT) were observed in 2013 [2]. These statistics show that road infrastructure is imperative to sustain a road user's movement and ensure a nation's economic competitiveness.

The Congressional Budget Office (CBO) [3] reported that 146 billion USD were spent to build, operate, and maintain highway networks in the U.S. in 2007. This is the actual amount of money spent on maintaining a million miles of nation's ageing highway networks. The real challenge that researchers face today is how to prevent road deterioration, which includes surface cracks. It is hard to find a single mile of asphalt roads that show no cracks. Regardless of how well a road material is mixed, the asphalt layer will eventually crack and degrade over time due

to various factors including environmental conditions. Crack development is quick at the beginning, slows down after a certain time. If no timely maintenance and rehabilitation (M&R) treatments are applied, there are possibilities for the initial longitudinal and transverse cracks to interact and create block cracking. Under repetitive traffic loads, the block cracking deteriorates further to cause alligator cracking and end up with potholes spotted on the road surfaces.

A hairline crack starts it all. A small gap or discontinuity on the asphalt surface will allow water to seep through and accumulate beneath the pavement, which leads to the weaker underlying soil. Over time, rainwater flow through cracks surfaces and the moving traffic caused pumping, which eventually leading to form potholes and damaging the road surfaces. In colder region, water from snow and ice seeps through an opening on the pavement surface. During cold weather, it freezes and expands which eventually leads to pavement and subbase break up. Once the ambient temperature increases, the melting ice leaves a gap inside the pavement. Over repetitive traffic loading, the asphalt eventually fails to support the weight of moving vehicles. Eventually, the asphalt layer disintegrates into smaller pieces, washed away and creating potholes. Potholes are not only among the top 20 causes of car accidents but also contribute to fatal motorcycle accidents in the U.S. [4].

According to the National Highway Traffic Safety Administration (NHTSA), the U.S. road and highway networks posed significant challenges over the last decade. In the U.S, the historical fatalities data revealed that a total of 1,658,458 fatalities occurred from 1975 to 2013 [5]. These statistics refer to a passenger vehicle occupant, motorcyclist, and pedestrian deaths for a 1975 to 2013 analysis period. These fatalities are only 0.53 percent of the total population of 315,091,938 (2013) [6]. But, that small percentage really means something important for those who experienced the loss of family members due to road fatalities. A recent study [7] using data

sets from 2004 to 2013 shows that, out of 340,879 deaths, about 76 percent are passenger vehicle occupants, 12 percent are a motorcyclist, and another 12 percent are road pedestrian. In 2013, a total of 32,719 deaths were reported, or ten deaths per 100,000 population, in the U.S. This is not the statistic to be proud of compared to only four deaths per 100,000 populations in Germany [8].

Another major concern is the number of hours spent on the road due to traffic delays. The data sets from the USDOT Bureau of Transportation [9] showed in 2011, the annual person-hours of highway traffic delay per auto commuter were 52 hours for very large urban areas (> 3 million population), 37 hours for large urban areas (1 to 3 million population), 29 hours for medium urban areas (0.5 to one million population) and 23 hours for small urban areas (> 0.5 million population), respectively. These highway traffic delays caused annual congestion costs per auto commuter of $16,243 for very large urban areas, $23,305 for large urban areas, $21,854 for medium urban areas, and $10,173 for small urban areas [10]. Additionally, highway traffic delays also contribute to higher carbon dioxide (CO_2) and harmful Particulate Matter (PM) and other emissions due to the trucks and cars burning more fossil fuel during highway traffic congestion. Eventually, the emission will cause health problems to an individual who lives in the areas with poor air quality index.

1.1.1 Motivation and Goals

The primary motivation of the research is to (1) address asphalt pavement structural response using the three dimensional-finite element (3D-FE) modeling and nondestructive testing evaluations, (2) enhance the mechanistic empirical design method, and (3) improve the pavement asset management system. Numerous factors affect road condition, including heavy traffic flow, environmental impacts, material degradation over time, and also interactions

between all these factors. If timely maintenance and rehabilitation (M&R) is not performed, road surface condition will deteriorate, in most cases indicated by the severity of surface cracks and rutting. The numerical simulations were conducted using the LS- DYNA software to study cracking distress. Apart from that, this research is also focused on the development of the enhanced roughness, rutting, and cracking prediction models, considering the lifetime M&R histories, the Long-Term Pavement Performance (LTPP) climatic regions, in situ modulus of asphalt layers (rutting and cracking models), and base layer type (rutting model). This research also looks into the material characterization of asphalt highway pavement using nondestructive deflection data. The 3D-FE pavement-subgrade models of uncracked and cracked asphalt layer were developed using the LS-DYNA software. The results from the analysis were used to develop the prediction equations to determine stress and strain parameters at critical depth levels inside the pavement system.

1.2 Needs for Research Issues in Asphalt Pavement Design and Asset Management

Previous discussions on the U.S. road fatalities indicate that there is a need to maintain acceptable road condition over time. This goal is possible if the enhanced predictions models are used in the pavement structural design. The literature review to date indicates that the lifetime M&R history was not considered in asphalt pavement condition deterioration progression modeling. In the historical asphalt pavement database records of the LTPP research program of the National Academy of Sciences, the M&R sequence is denoted by the construction number (CN). Therefore, there is a need to consider the CN in the pavement condition deterioration modeling. Additionally, the method to interpolate the missing Equivalent Single Axle Load (ESAL) data in the LTPP database was proposed.

In the U.S., the LTPP program was started in 1987 under the Strategic Highway Research Program (SHRP) to monitor the performance of more than 2,500 assigned test sections under the actual effect of continuous traffic applications in different climatic regions [11]. In 1992, the LTPP program was transferred to the Federal Highway Administration (FHWA) to continue asphalt pavement performance monitoring for in service state road and interstate highway networks. The LTPP database was established to store all essential information, including Falling Weight Deflectometer (FWD) data [11]. Unfortunately, it was noted that before June 2015, Young's modulus values that describe the stiffness of the materials in different pavement layers were not included in the database. The modulus values are important for pavement layered elastic design of highway pavements.

There is also a need to backcalculate pavement layer modulus values for response analysis and numerical modeling purposes. Although the modulus values are provided in the LTPP database after June 2015, initial evaluation to verify the modulus values from the LTPP database indicates unacceptable modulus values for test sections evaluated in this research. Therefore, the modulus values were backcalculated using several backcalculation software, and the results were compared.

The data sets from the LTPP database [11] were used to develop the asphalt pavement roughness, rutting, and cracking models. However, the research by Mohamed Jaafar et al. [12] on the development of the roughness deterioration prediction models for the LTPP Southern region in the U.S. showed large amounts of missing data from the database. Additionally, the literature review revealed that most of the research related to the development of condition deterioration prediction models show that the models did not consider lifetime M&R history. This includes the IRI roughness and rutting prediction models developed in the National

Cooperative Highway Research Program (NCHRP) 1-37A study. The NCHRP 1-37A was conducted to establish a MEPDG [13] to improve pavement structural design. This national project was completed in February 2004 with an approximately $6.6 million research fund [14]. However, the actual total cost of $15 million spent on MEPDG was reported, and additional money was needed for calibration efforts [15]. The MEPDG was claimed to significantly improve pavement design as compared to 1993 American Association of State Highway and Transportation Officials (AASHTO) guide [16]. Nonetheless, the design aspect alone is not enough to sustain long-lasting pavement but also requires timely M&R treatments [15].

The AASHTOWare software was developed under the NCHRP1 1-37A project. This software did not provide any structural thickness values since it was designed to provide fail or pass criteria only. This software provides a pass or fails criteria for terminal IRI, rut depth, fatigue cracking, combined reflective and alligator cracking, thermal cracking and also the longitudinal cracking (including top-down cracking (TDC)). The numerical models developed under the NCHRP1-37A study were calibrated with pavement performance data from the LTPP program [16]. However, the accuracy of the TDC numerical model is questionable since there is no TDC data available in the LTPP database. The recent AASHTO MEPDG [13] assumed that TDC was caused by repeatedly applied loads. It appears very doubtful that the appropriate regression models were used to predict the TDC. The previous study in Manitoba, Canada, showed that the longitudinal cracking or TDC prediction model in the MEPDG was found to be unreliable [17]. In addition, through a class problem [18] that simulates the U.S. Highway 45 Alternate, the predicted TDC contradicts the findings of visual observations that indicate no TDC distress occurred. Uddin [19] reported an extensive literature review on TDC problems worldwide and field identification methods.

Further analysis is needed to enhance the understanding of the uncracked and cracked asphalt pavement responses using 3D-FE simulations. The latest AASHTO MEPDG assumed that TDC distress happened due to asphalt fatigue failure, which is unlikely. There are no proper models used to predict this distress type, most probably due to the limited amount of data sets related to TDC. As a consequence, TDC was not properly taken into account for the pavement asset management system. This implies that the right M&R related to TDC can be applied, which will improve mechanistic empirical design procedures. Additionally, the universal cracking prediction model is needed to consider different surface cracking types in M&R treatment intervention. This research topic needs urgent attention since surface cracking has become a common surface distress mode of failure in Hot Mix Asphalt (HMA).

In future, further research is needed to highlight the TDC phenomena caused by the surface tensile stresses of wide truck tires, asphalt mix problems, and poor road construction processes [19]. The advancement in nondestructive testing (NDT) technology may contribute to faster road surface condition monitoring. An extensive literature review was conducted to synthesize the potential of the ground penetration radar (GPR) remote sensing technology to map the TDC depth from the surface through asphalt layer thickness [19, 20]. However, based on the review of Uddin's GPR report [19], a nondestructive and noncontact technology operating at highway speed to evaluate TDC was not found in the literature [18, 20].

The use of the 3D-FE is important to study pavement responses for cracked pavement layers, considering that deflection tests are performed on existing pavements which may have cracked. The theory used to analyze deflection data in the commercial modulus backcalculation and pavement analysis software assume pavement layer without cracks or any other discontinuity, which is unlikely in the real world. Uddin et al. [21] successfully evaluated the

performance of jointed concrete pavement by analyzing 3D-FE pavement models created using the ABAQUS software and field condition data. The discontinuity in the concrete pavement was modeled using the unidirectional gap elements. In addition, a cracking model was also developed and applied beneath the concrete layer [21].

Additionally, this research also looks into the development of a universal cracking progression model using the LTPP database [11]. The concept of the universal cracking indicator (CI) was introduced by Paterson in 1994 [22]. The CI considers the extent, intensity, and crack width for transverse, longitudinal, and alligator cracking, respectively. The CI is the summation of the CI for each crack type. The concept of the proposed indicator of cracking was not well explored and reported in the literature review. The development of the enhanced condition deterioration progression model and the universal cracking progression model for a whole life analysis approach improves pavement design and asset management. The preservation of the road network over time demands condition monitoring and intensive financial considerations. The pavement surface condition monitoring and structural integrity assessment on a periodic basis are needed for timely M&R treatments. Application of the improved predictive models contributes toward a better pavement management decision support system for maintenance interventions.

1.3 Research Objectives and Scope

The primary objectives are to:

1) Evaluate and enhance asphalt pavement condition deterioration prediction models.

2) Evaluate modulus backcalculation approaches for characterizing asphalt pavement layers of selected test sections.

3) Develop the 3D-FE asphalt pavement models and study impacts of cracking on pavement structural responses.

4) Implement pavement condition deterioration models for improved structural design and asset management of asphalt highway pavements.

The research scope is limited to:

- Data for LTPP test sections in the U.S. excluding Rhode Island, Guam, and Puerto Rico.
- Only asphalt pavement and no concrete pavement.
- A design truck wheel load single axle dual tires for the 3D-FE structural response analysis.

1.4 Research Methodology

Research methodologies to achieve the objectives consist of the following key steps;

- Evaluation and enhancement of condition deterioration progression models: Multiple linear regressions and Artificial Neural Network (ANN) modeling methods were used to develop asphalt pavement roughness, rutting, and cracking condition deterioration models. The regional factor (Reg_D) and CN are included as the dichotomous (dummy) variables to consider different LTPP climatic regions and lifetime M&R treatments, respectively.
- Material characterization of asphalt pavement using nondestructive deflection data: This research topic characterizes modulus of asphalt pavement, base, subbase, and subgrade layers. The Poisson's ratios are assumed accordingly. Several backcalculation software were used to backcalculate modulus values from the FWD deflection data. The reasonableness of the modulus values was evaluated accordingly. Additionally, response analysis software is used to conduct pavement response analysis.

- 3D-FE numerical modeling of asphalt pavements: Pavement system with uncracked asphalt layers is modeled using LS-DYNA software. The truck wheel load is applied and the pavement responses are observed. The 3D-FE simulation results are compared with the results from the linear elastic program. Next, the cracked asphalt pavement layer were simulated in LS-DYNA. The asphalt pavement responses for uncracked and cracked pavement were compared.
- 3D-FE asphalt pavement modeling of longitudinal cracks: The 3D-FE simulates cracks at different depths in the asphalt pavement layer. The pavement responses under the wheel loads were evaluated and compared with the uncracked pavements.
- Implementation of enhanced condition deterioration models for pavement design and asset management: The enhanced pavement condition deterioration models were implemented in this research to improve asphalt pavement design process. Further discussion highlights the contribution of the enhanced condition deterioration models toward improving asset management.

The research methodology flow chart in Figure 2 shows the milestones of the research topics and their interactions.

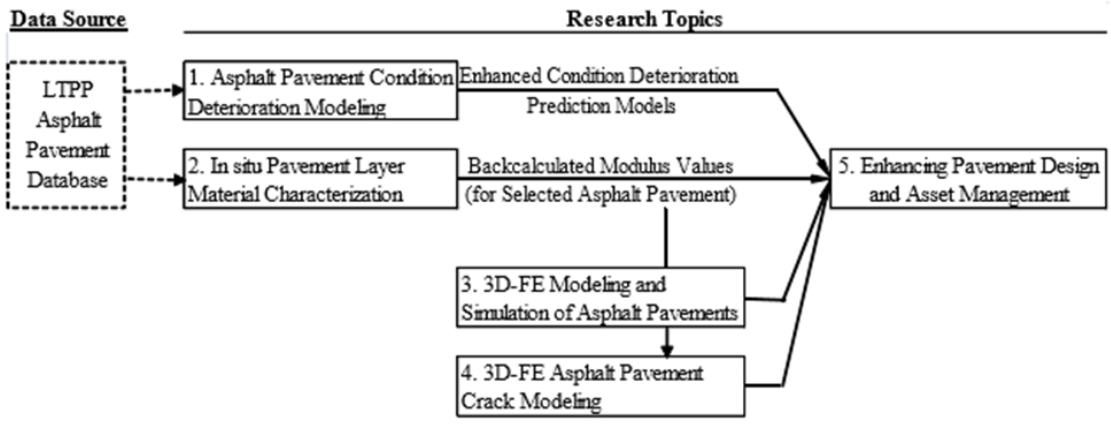

Figure 2. Research methodology flow chart

1.5 Synthesis of Literature Review on TDC

1.5.1 Historical Overview of TDC

Over the last decade, TDC was recognized as one of the common asphalt pavement surface distresses, and either occurred in the wheel path [23] or commonly just outside the wheel path [19]. Most researchers assumed that TDC initiates from the top of the asphalt surface layer and propagates downwards, which is the opposite of the propagation of bottom-up fatigue cracking [19]. Fatigue cracking induced by repetitive traffic load applications propagates from the bottom of the asphalt layer to asphalt surface. However, there is also the possibility that the TDC initiates from the middle of the asphalt mix and moves upwards [23, 24]. The TDC phenomena was noted not only in the U.S. but also a few other countries worldwide. Many studies have been conducted to study TDC which include field observation, laboratory evaluation, and numerical analysis. The new pavement design guide developed under the NCHRP 1-37A discussed and reported the model for TDC distress [25]. Uddin [19] summarized a chronological history of the TDC research worldwide as described in Table 1.

According to Rolt [27], TDC was discovered in the 1970s in UK's Transportation Research Laboratory (TRL) studies. Initially, the presence of TDC distress did not catch any engineers' interest, since it was claimed that this crack type occurred under tropical climates only. From 1973 to 1977, the TRL engineers conducted the first asphalt performance study on eight different sites with different climatic conditions. The goal of the study was to design specification for asphalt layers with 30 to 170 mm thickness, in order to improve asphalt performance under tropical environments. The severity of asphalt rutting, cracking, and deflection was observed throughout the study. Crack propagation was evaluated from cored asphalt samples and it was discovered that some cracks initiated from the top and propagated

downwards. Further analysis indicated that the aged asphalt binder is the key component in the cracking mechanism.

Table 1. Chronological history of TDC distress knowledge base [19]

Years	Continents	Countries	Source of Reports
1970s	Africa	Kenya (Tropical Climate)	[26] Wambura et al (1999)
1980s	Europe Europe Europe Africa	United Kingdom (UK) France The Netherland South Africa	[27] TRL/Rolt (2000) [28] Dauzats and Linder (1982) [29] Gerritsen et al. (1987) [30] Hugo et al. (1982)
1987-1989	North America	USA-SHRP: LTPP Study Started (No TDC reported or considered in experimental design and condition data plans)	
1990s	Asia North America North America	Japan USA – California USA - Florida	[23] Matsuno and Nishizawa (1992) [31] Craus et al. (1994) [32] Myers et. al (1998)
2000s	Europe North America North America North America North America Asia	Portugal USA – Washington State USA – Michigan USA – Indiana USA – Colorado Japan	[33] Freitas et al (2003) [34] Uhlmeyer et al (2000) [35] Svasdisant et al. (2000) [36] Pellinent et al. (2004) [37] Harmelink et al. (2008) [24] Taniguche et al (2009)
2010s	North America	USA-SHRP: LTPP and SHRP 2 Studies on-going (No TDC reported for over 1,000 in-service pavement sections in the U.S. and Canada, September 2013)	
2012-2013	North America	USA - Mississippi	MDOT SS255 Project

The TDC was also reported on highways in France by Dauzats and Linder [28] through their studies in developing a method to evaluate the structural condition of pavements with thick bituminous road bases. In 1987, another study was reported by a French researcher, which related to the mechanism of surface cracking in wearing courses [38]. Gerritsen et al. [29] reported the TDC distress in the Netherlands through their studies on the prediction and prevention of surface cracking in asphaltic pavements. In South Africa, Hugo and Kennedy investigated the effects of load, mix type, and asphalt binder properties that caused the TDC [39].

In Japan, Matsuno and Nishizawa [23] studied the mechanism of longitudinal surface cracking in asphalt pavement. They reported that longitudinal cracks occurred near the wheel path in pavement laid one to five years after construction. However, none of the surface cracking was observed under shadowed areas (for example under bridges). The researcher also stated that very high tensile strains occur at the edge of truck tires which are on asphalt surface layer. These high strain values were observed at specific depths that were close to asphalt surfaces, caused by lower stiffness due to high surface temperatures [19].

1.5.2 TDC studies in the U.S.

In the U.S., TDC was discovered in the late 1990s [19]. Post-2000 studies were conducted in the following states; California [31], Florida [40], Washington State [34], Michigan [41], Indiana [36], Colorado [37], Illinois [42], and North Carolina [43]. Most of the studies were carried out to improve the AASHTO pavement design guide. Uddin [19] clearly summarized previous studies conducted in Michigan through a synthesis study of noncontact evaluation of TDC in an asphalt pavement project for Mississippi Department of Transportation.

In a study for the Washington State Department of Transportation, Uhlmeyer et al. [34] stated that TDC also occurred in thick asphalt pavement in three phases. The TDC distress initiated after three to eight years for pavement sections with proper structural design, acceptable ESAL design, and asphalt layer thicknesses of more than 6.3 inches. Additionally, Uhlmeyer et al. reported that the observed in-service duration before the TDC occurred varies from one to five years in Japan, three to five years in France, five to ten years in Florida, and up to 10 years for the UK.

Harmelink et al. [37] stated that the longitudinal cracks appeared in the pavement surface of a highway section, a year after it was rehabilitated in July 1997. The TDC distress was identified and happened due to aggregate segregation in asphalt mixes. Then, the statewide evaluations on 28 test sections were conducted to study the extent of the TDC phenomena in Colorado. It was discovered that 18 out of 28 sites had TDC distresses. Based on the analysis, aggregate subsurface segregation in asphalt mixes due to mix design and construction practice, caused the TDC. Therefore, the mix design process was improved, and precautionary steps were implemented during the asphalt paving process. It was reported that TDC has been greatly reduced.

Uddin [19] highlighted the importance of TDC consideration in pavement design and construction processes. According to the researcher, most of the current design methods consider bottom-up fatigue cracking, but not TDC. The TDC, which is environmental and climatic induced distress, must be considered in the pavement design as well. Uddin [19] also stated that uses of recycled asphalt pavement (RAP) accelerated binder aging on a surface layer under heavily trafficked roads and eventually caused the TDC distress. This is a major concern since the Superpave asphalt material specification requires the use of lower effective asphalt binder content compared to the traditional methods. The researcher suggested further evaluation of using RAP in asphalt mixes to minimize TDC.

The NCHRP 1-37A assumed that the TDC in the wheel path occurred due to load repetition, which is unlikely in most cases [25]. Another study (NCHRP 1-42A), which was completed in 2009, developed the viscoelastic continuum damage-based crack initiation and the asphalt layer fracture mechanics-based crack propagation model [43]. The NCHRP Project 1-

52A that specifically looked into the development of a mechanistic empirical model for TDC was completed on March 30, 2018 [44].

1.5.3 Causes of TDC distress

Various different causes of TDC have been reported in the reviewed literature. The following studies indicate that asphalt mixes may be an underlying cause of TDC.

• Severe age hardening of asphalt mixes – Wambura et al. [26].

• Age hardening of asphalt mixes, due to a gap or semi gap graded mix design – Hugo and Kennedy [39].

• Poor fatigue performance as a result of high air voids percentage and aging of asphalt mix – Gerritsen at el. [29].

• High surface tensile strains at the edge of the tire during day time and interaction between traffic load with binder aging, temperature gradient, and segregation – Matsuno and Nishizawa [23].

• Stress under the imprint of a truck tire and thermal stress - Myers et al. [40].

• High tensile strain below the pavement surface caused cracking to initiate within the asphalt layer and propagate to the surface – Taniguche et al. [24].

• Aggregate segregation in asphalt mixes – Schorsch et al [45].

• Tensile stresses and strains and interaction of traffic load, temperature, and hardening asphalt binder – Svasdisant et al. [35].

• High surface tensile stresses induced by traffic loads, enhanced by temperature, aging of the asphalt binder, construction material quality, temperature gradient, and compaction effort – Pellinent et al. [36].

• Construction quality, including segregation and compaction procedures - Svasdisant et al. [35], Uhlmeyer et al. [33], Freitas et al. [46], Hermalink et al [42].

1.6 Research Significance

The following statements describe the significance of the research carried out in this dissertation:

- The historical database of LTPP was one of the most comprehensive information on road conditions for more than 2000 test section throughout the US. Various different prediction equations for pavement distress in the MEPDG were developed based on the LTPP data that has M&R histories. However, the mechanistic-empirical pavement design equations do not consider M&R history. Additionally, the actual number of axle-load application used as a traffic parameter is questionable since there are lots of missing traffic data are missing from the LTPP database for yearly data. Hence, a new approach to predict missing traffic data was introduced in this dissertation. Additionally, the newly developed prediction equations consider the M&R as a dummy variable in the equations.
- This research also extends the proposal of universal CI as an indicator of surface crack severity levels in 1994. Instead of evaluating cracks as an individual distress, this research combines four different asphalt pavement crack types as one unique indicator. The Unified Cracking Index (UCI) is objective, relevant to cracking mechanism, and simple in concept.
- A limited number of studies were conducted to consider four point loads (placing two tires on both ends of a single axle) for the 3D-FE parametric studies. Therefore this research simulates truck wheel load under each tire for the 3D-FE simulations and the responses (surface deflection, stress, and strain) based on the factorial design. This implies that the responses at the

critical locations of pavement layers from the 3D-FE simulations of uncracked and cracked pavements are closely simulating the actual loads under rear truck tires.

- A multi-depth cracking approach to simulate longitudinal cracked asphalt pavement in traffic direction was introduced in this research. The small crack area at various different locations inside the asphalt layer was simulated at a lower modulus value, based on the ratio of surface deflection under wheel loads for uncracked and cracked pavements.
- This research intends to enhance pavement performance model for the structural design and asset management of asphalt pavements. Based on the responses at the critical locations from the 3D-FE analysis, this research developed the equations to predict responses (stress and strains) at different various depth levels of pavement structure to improve pavement structural design and asset management practices.

Therefore public road agencies will benefit from longer lasting pavement assets. In general, the road network will have reduced life-cycle costs and lesser disruptions due to less frequent M&R treatment applications. Moreover, road users will benefit from reduced work zone delays and lower vehicle operating costs. A road network maintained in good condition is imperative to serve the public, improve safety, and support efficient supply chain and economic growth.

II. EVALUATION AND ENHANCEMENT OF CONDITION DETERIORATION PROGRESSION MODELS

2.1 Introduction

The LTPP research program was introduced under the SHRP in 1987. The objective of the LTPP program is to collect pavement performance data from more than 2,000 test sections that were set up throughout the U.S. and Canada. This program was conducted for a 5-year period under 150 million USD budget allocations. In 1992, the FHWA took over and managed the LTPP program. Recently, there are approximately 700 test sections that are still under monitoring for continuous pavement performance data collections [47]. Figure 3 shows the LTPP climatic regions in the U.S.. A total of 51 states in the U.S. including Washington, D.C. and ten Canada provinces were considered in the initial selection of the test sections in the LTPP program. There are four climatic regions defined in the LTPP program. Those four regions and their regional codes are the North Atlantic region (LTPP Code: One), North Central region (LTPP Code: Two), Southern region (LTPP Code: Three), and Western region (LTPP Code: Four).

The North Atlantic region (yellow) has 15 states including Washington, D.C. as shown in the spatial map. The North Central region (red) covers 13 states in the U.S. The regional offices that mainly handle data collection and management processes for both the North Atlantic and North Central regions are located at Buffalo, NY.

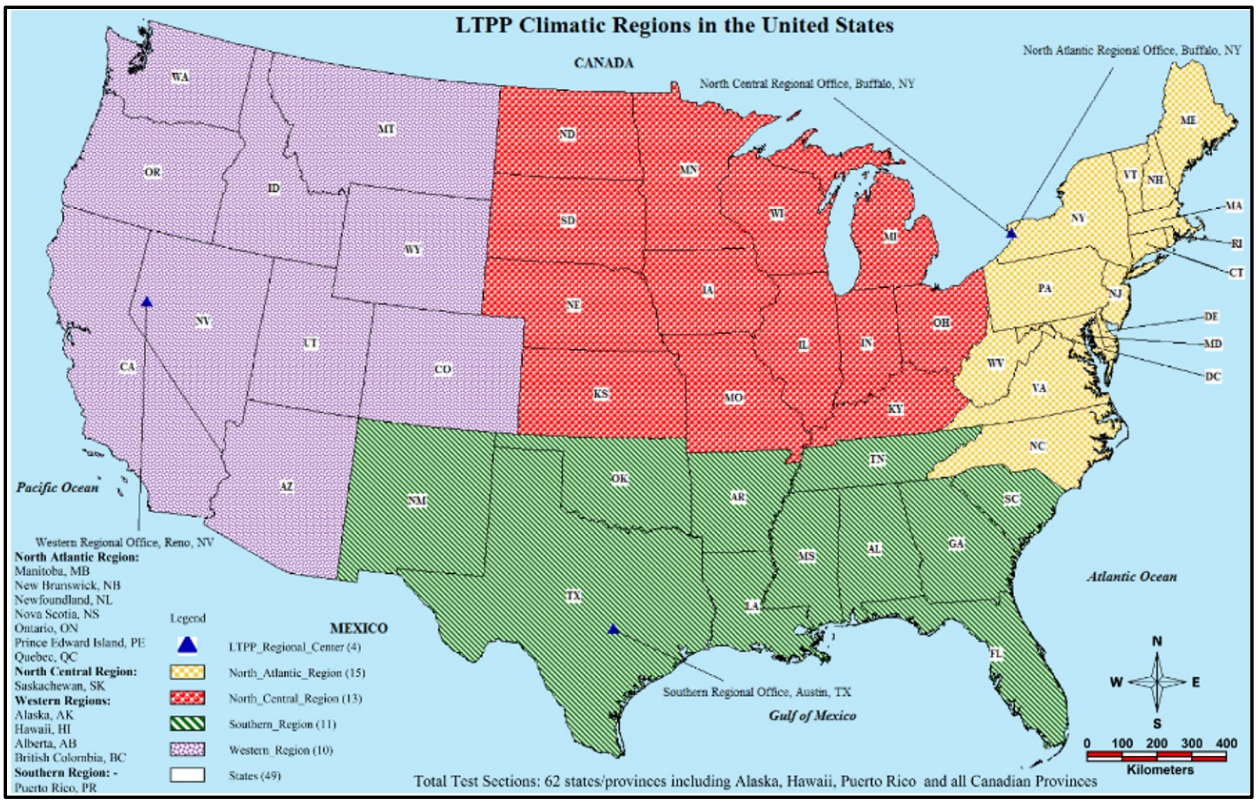

Figure 3. The North Atlantic, North Central, Southern, and Western regions defined in the LTPP program and the LTPP regional office locations [48]

The Southern region (green) includes 11 states in the U.S and the regional office is located in Austin, TX. A total of 12 states are grouped in the Western region (purple) and the office for the central technical support services contractor is located at Beltsville, MD (not shown on the map) [48]. The data were collected at different spatial locations that exhibit values that are different across the LTPP regions. The following LTPP climate zone classification map (Figure 4) was created during the initial recruitment phases of the LTPP test sections [49], which indicates spatial and temporal variability that applied to the collected pavement attributes.

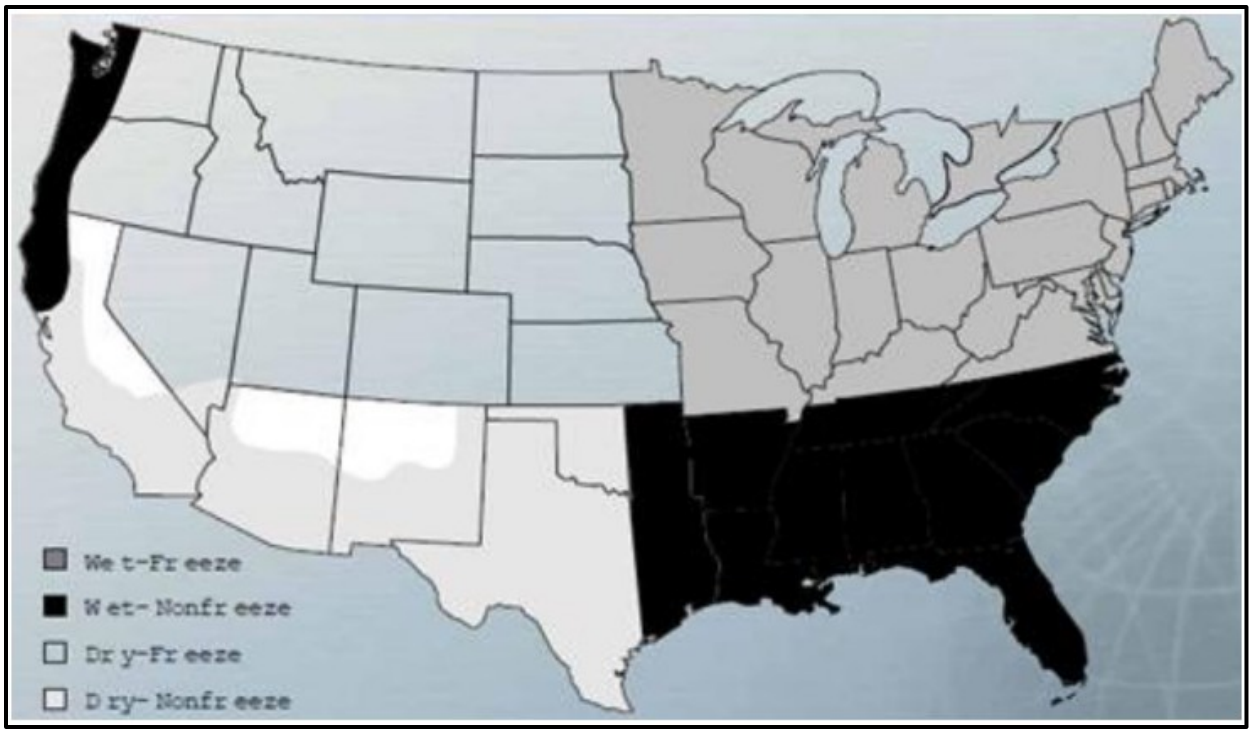

Figure 4. The initial climate zone map created during the LTPP test section recruitments [49]

Four different climates zones were identified namely wet-freeze, wet-nonfreeze, dry-freeze, and dry-nonfreeze zones. In certain areas, this map was altered to state boundaries to ease data collection processes by the regional contractors. However, this climatic zone map was not accurate enough to indicate variability of climatic conditions in the U.S. A more realistic climate zone map was created, which not only considers variations in the temperatures, but also considers the soil conditions (Figure 5). The temperature and soil condition zones follow:

- Low Temperature (A), Freeze-Thaw (B), and High Temperature (C)
- Wet soil all year around (I), Wet soil for only a part of the year (II), Dry soil all year around (III)

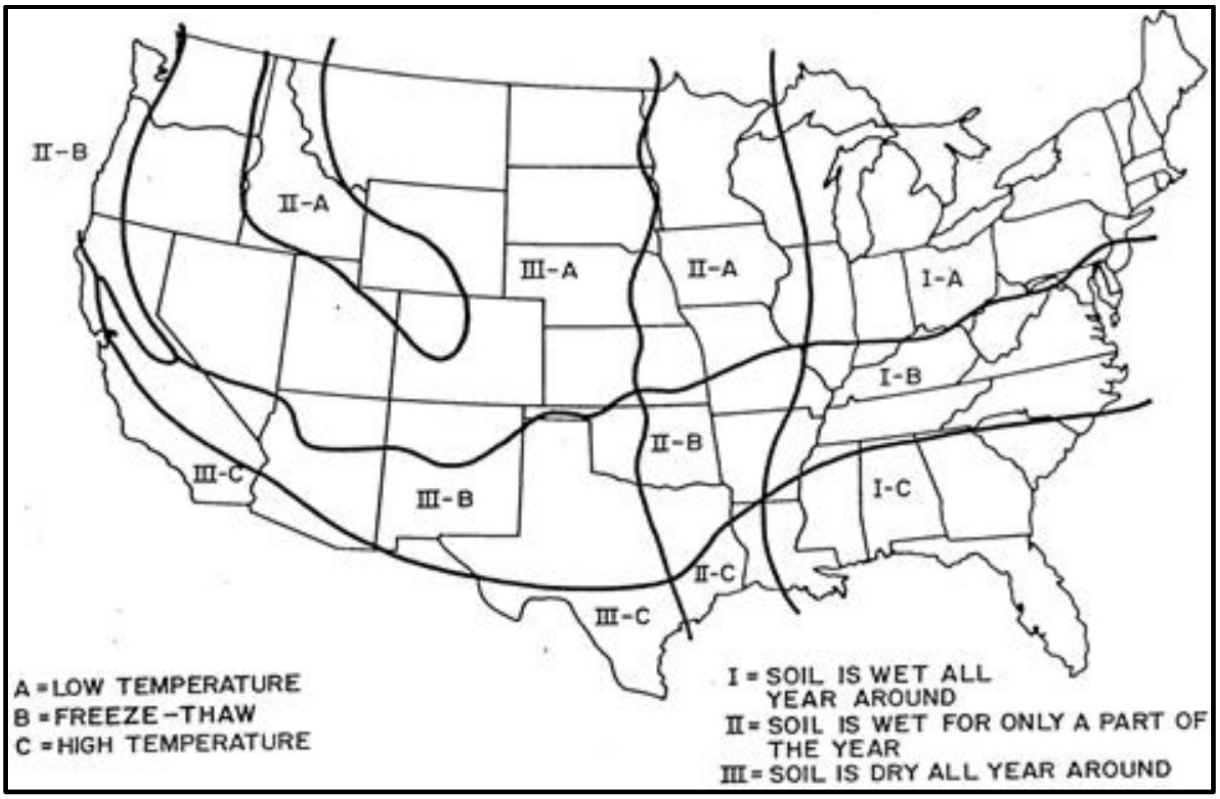

Figure 5. The updated climate zone map considering temperature and soil conditions used in the LTPP program [49]

Based on Figure 5, the northern part of Mississippi is in I-B group climate zone. This implies that in Northern Mississippi, the soil is wet throughout the year especially in winter months, and under extreme high and low temperature variations, which is likely and true as experienced by the author. In contrast, the central and southern parts of Mississippi were grouped as I-C climate zone, which indicates high temperatures and the soil is dry all year around. In 2011, the Mississippi Department of Transportation (MDOT) introduced their own Mississippi microclimate regions for counties group as shown in Figure 6. A total of 82 counties in the Mississippi were divided into nine microclimatic regions. The count for each region is unequal and range from six to 13 counties. The coastal and east climate regions have six counties each,

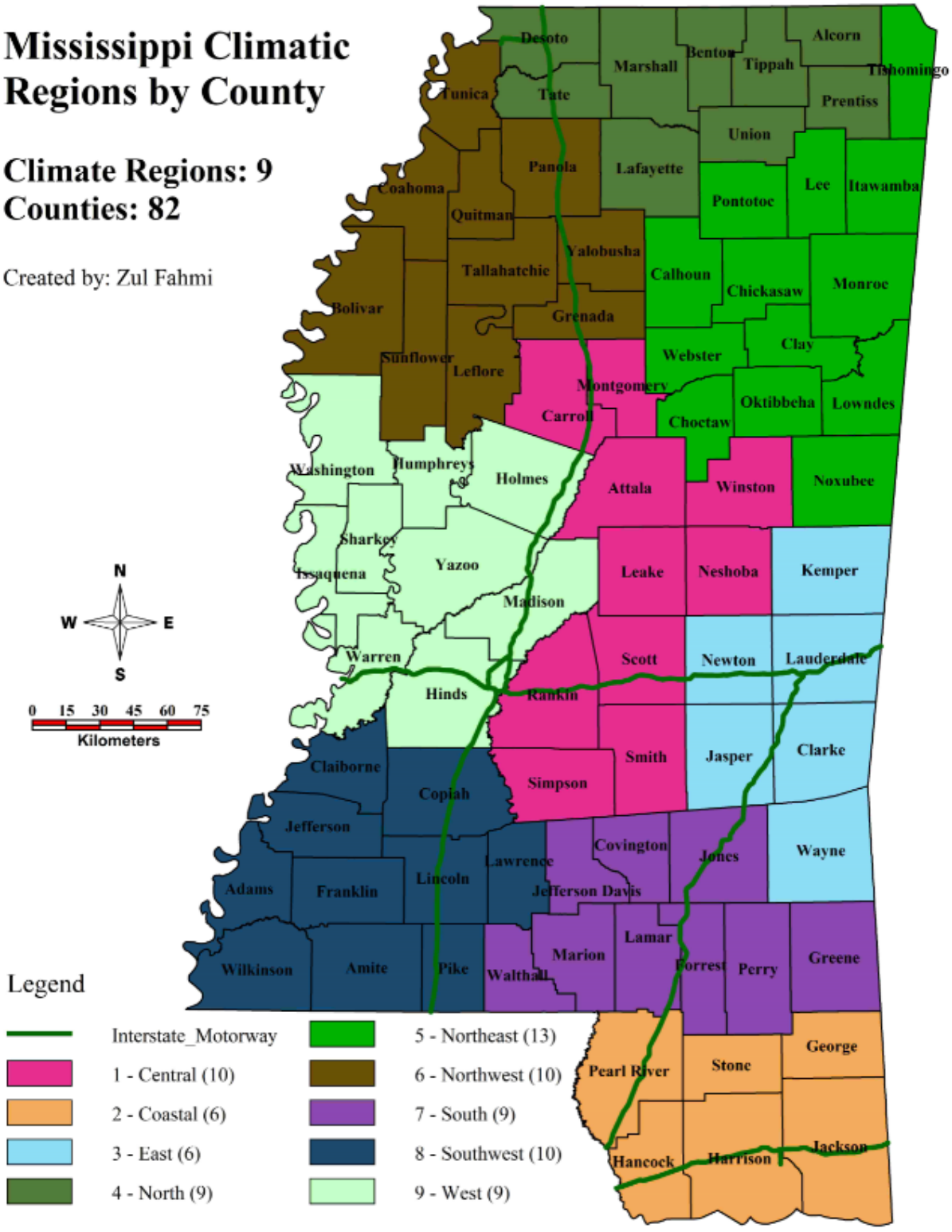

Figure 6. Mississippi county microclimate regions created by Mississippi Department of Transportation [50]

while the Northeast region has the highest number of counties (13 counties). The selection criteria of all the climate regions in Mississippi were not clearly defined in the report [50].

A more comprehensive climatic zone map was created and published by the Office of Energy Efficiency and Renewable Energy [51, 52] as shown in Figure 7. The government agency assigned eight climatic zones based on heating degree-days (HDD), average temperatures, and precipitation. Detail on the climate zones were described by Building America Research Group under similar agency [53].

Figures 3 and 7 indicate that the data in the LTPP database that are related to the pavement layers' attributes that are likely to have high spatial and temporal variations, due to wide spread test section locations, temperature variations, and climate cycle changes.

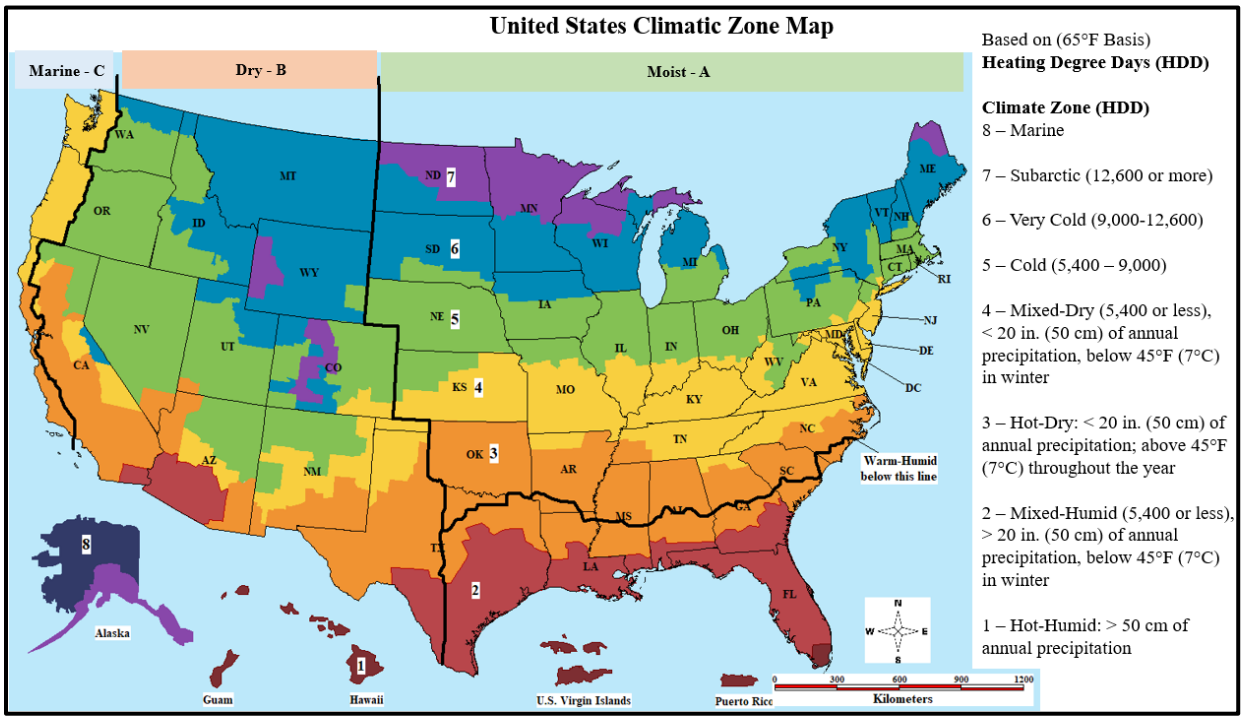

Figure 7. Updated climatic zone map created by the Office of Energy Efficiency and Renewable Energy [51, 52]

Therefore, it is imperative to consider the LTPP regions as one of the independent variables in developing the condition deterioration prediction model equations. The following sections discuss the development of the enhanced asphalt highway condition deterioration prediction equations of the IRI, rutting, and cracking distresses. The LTPP database does not have the TDC data. However, as reviewed in previous section, it's distress manifestation in the MEPDG is shown as the longitudinal crack. The MEPDG database has the alligator, transverse and longitudinal crack performance prediction models, but no block crack model. Therefore, in this research the block crack model is also developed which is nonexistent in the MEPDG.

2.1.1 Review of Literature for Mechanistic Empirical Design of Asphalt Pavement Design

The AASHTO 1993 empirical method of asphalt pavement structural design was developed based on the results of series of experiments and experience of engineers involved in the AASHO Road Test conducted in October 1958 and ended in November 1960 [54]. The AASHO road test was carried out to assess serviceability-performance, load equivalency, create performance database, and distress monitoring under periodical observations [55]. A total of $27 million (1960 dollars) were invested by the U.S. government and industries to study the behavior of both concrete and asphalt highway pavement structures under moving trucks, driven on five out of six closed loops (two-lanes wide) developed for the study. One loop was evaluated under no traffic load repetitions and subjected to climate impacts for two years test period [54].

There were 836 test sections of pavements, representing 200 various different combinations of surface, base, and subbase layers with different thickness levels. This accelerated test was conducted at 18 hours per day and reached 1,114,000 axle load applications per loop during the two-year test. The longitudinal profile, roughness, cracking, patching, rut

depth, and joint faulting were measured and extensively analyzed to develop the relationship between pavement performance, pavement design and load variables [55, 56]. Uddin [57] summarized in detail the key lessons learned from the AASHO (American Association of State Highway Officials) Road Test. There are a few major limitations applied to the empirical equation used in the AASHTO 1993 design guide as follow [57, 58]:

- Low truck traffic volumes (less than 1.8 million ESALs) and do not consider axle load spectra.
- Consider only climate condition and subgrade type at AASHO Road Test location in Ottawa, Illinois.
- Accelerated tests neglect the effects of climate and ageing of construction materials.
- Performance indicator is based only on Present Serviceability Index (PSI).

However, truck induced accelerated damage of highways in 1980's steered to the introduction of the SHRP by Congress in 1987. The LTPP was one of the research programs that was successfully contributed towards compilation and maintenance of the national LTPP pavement performance database at a cost of $190 million from 1987 to 2007 [57]. In post-2000, advancements in computer and software technologies enabled the inclusion of theories of mechanics [58], which contributed to the development of mechanistic-empirical pavement design through NCHRP's Project 1-37 and Project 1-37A [59]. The example of the AASHTOWare Pavement ME Design software inputs is shown in Figure 8. The mechanistic-empirical flexible pavement design approach has provided a huge step towards the betterment of the design by incorporating the following important input parameters through AASHTOWare pavement design software [57, 60]:

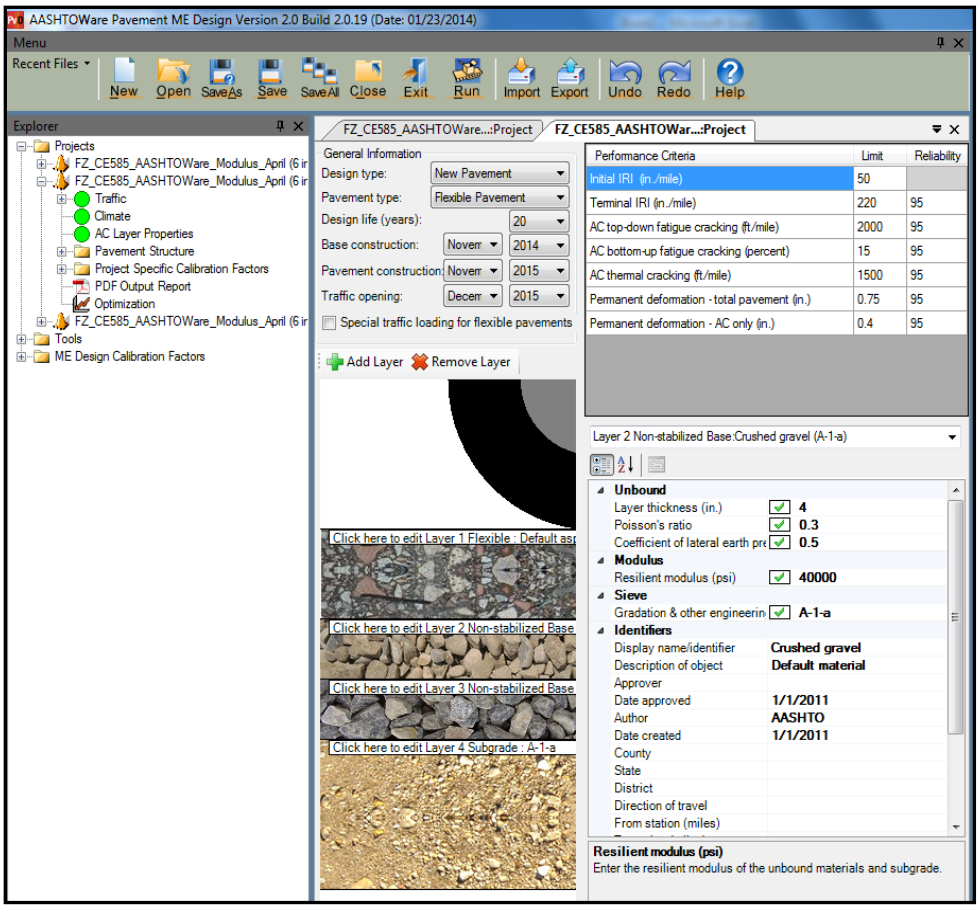

Figure 8. The example AASHTOWare Pavement ME Design software required inputs

- Climate data from climate stations that are spatially distributed throughout the U.S. (more than 10 input data)
- Traffic inputs are normalized axle load spectra (NALS) for each truck class and axle group type, number of axles of each type per vehicle class, percentile truck class volume distribution, truck volume, and truck growth (more than 120 input data).
- Variation of material properties (more than 100 input data) and layer properties (more than 20 input data)
- Six condition deterioration parameters of initial IRI (inches/mile), terminal IRI (inches/mile), rutting in asphalt layer only (inches), total rutting in asphalt and all unbound layers (inches),

fatigue alligator cracking area (% surface area), transverse thermal cracking (feet/mile), and top-down cracking (feet/mile).

These six condition deterioration parameters were separately computed and compared with the threshold values to provide fails or passes criteria over the design period. These criteria are a major improvement of only PSI performance model used in the traditional method. However, there are also some limitations of the MEPDG methodology for asphalt pavements, which include no consideration of major maintenance and rehabilitation intervention as identified by CN in the LTPP database, in the design process. Other limitations are highlighted in detail by Uddin [57] through his appraisal of the MEPDG in the U.S.

2.2 Roughness Modeling using Multiple Linear Regression and Artificial Neural Network (ANN) Method

Historically, pavement longitudinal roughness has been an important component of the serviceability performance concept used in the development of the AASHTO pavement design procedures [61]. Pavement roughness describes the irregularities in the pavement surfaces that affect the ride quality experienced by daily road users. Consequently, rough road surfaces will adversely affect fuel consumption and maintenance cost. In 1986, an International Roughness Index concept was introduced by a group of researchers from the World Bank [62].

The most recent MEPDG includes IRI as one of the criteria for any pavement section evaluations [13]. The IRI roughness (or smoothness called in the post-2000 MEPDG) is measured on an annual basis as part of the highway pavement asset management system [63]. Basic principles of pavement roughness evaluation are described by Plati [64] in a study to establish pavement roughness evaluation criteria. An acceptable prediction of the future IRI

value is closely related to a reasonable formulation of IRI roughness prediction models that consider all major factors such as initial IRI (IRI_O), cumulative traffic ESAL (CESAL) applications, structural number (SN), and pavement age (year). The IRI prediction model is used for life cycle assessment of pavement design alternatives and was selected as one of the important pavement condition attributes in this research.

In the U.S., the IRI for National Highway System (NHS) were measured by each state and the IRI data were compiled in FHWA's Table HM-47A [65]. Figure 9 shows the NHS roughness conditions for all states in the U.S. A total of 157,426 miles of the NHS were surveyed in 2011. The IRI less than 1.5 m/km (95 in./mile) indicates a good ride quality. If the IRI is in between 1.5 m/km (95 in./mile) to 2.7 m/km (171 in./mile), the road surfaces are in medium condition. Additionally, the IRI more than 2.7 m/km (171 in./mile) shows poor road conditions. The state of Texas recorded the highest NHS surveyed length for the IRI in 2011.

Ten out of 51 states reported more than 80% of the surveyed NHS with good ride quality (IRI less than 1.5 m/km) including Florida, Alabama, and Tennessee in the Southern LTPP region. In contrary, Washington D.C. surprisingly showed the worst road conditions with 86.3% of the surveyed NHS are in poor condition. In general, about 65.3% of the NHS in the U.S. are in good condition. About 28.8% of the NHS are in medium condition, and only 5.9% of total NHS surveyed length are in poor condition. However, the statistics indicate that most of the NHS in the East Coast of the U.S. needs major M&R treatments. This implies that most of the surveyed NHS has higher percentages of medium and poor road networks, as compared to the NHS for the states in the Central and West Coast of the U.S.

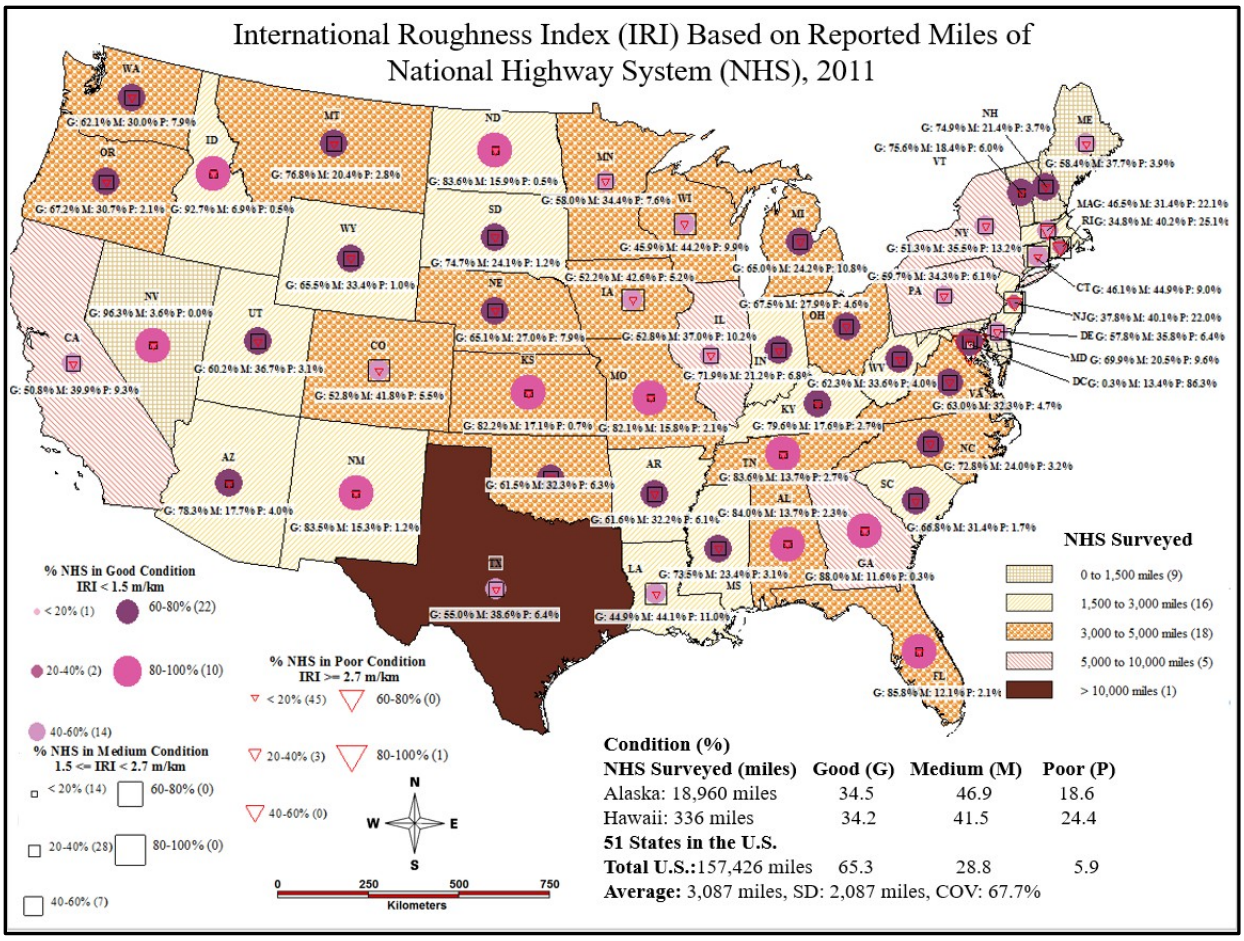

Figure 9. International Roughness Index based on reported miles of National Highway System in 2011 [65]

2.2.1 MEPDG Performance Modeling for Roughness

As mentioned earlier in this chapter, the IRI is one of the important performance criteria used in the design software. Equation 2.1 was developed using 1,926 numbers of datasets from the LTPP database and was embedded in the MEPDG to predict the progression of the IRI over design period for a new and overlay of asphalt pavements [66]. The reported Pearson's R value is 0.75 ($R^2 = 0.56$).

$$IRI = IRI_0 + 0.0150(SF) + 0.400\ (FC_{Total}) + 0.0080\ (TC) + 40.0\ (RD) \quad (2.1)$$

The site factor (SF) was calculated using Equation 2.2.

$$SF = Age[0.02003(PI + 1) + 0.007947(Precip + 1) + 0.000636(FI + 1) \quad (2.2)$$

Table 2 summarizes the independent variables used in the Equations 2.1 and 2.2. The independent variables used in the enhanced IRI multiple regression developed in this research were also shown for comparison purposes. The enhanced IRI multiple regression equation considers independent variables that are easier to use for future IRI value prediction without the needs to use the data from the laboratory tests. Additionally, the enhanced IRI multiple regression equation does not require the measurement of other asphalt surface distresses such as rut depth and area of fatigue cracking prior to the calculation of the future IRI values. Moreover, the enhanced IRI multiple regression equation also considers important factors such as maintenance and rehabilitation intervention factor, LTPP regions factor, and IRI roughness measurement locations.

The independent variables used in the enhanced IRI multiple regression developed in this research were also shown for comparison purposes and will be described in the next sub-chapter. The enhanced IRI multiple regression equation considers independent variables that are easier to use for future IRI value prediction without the needs to use the data from the laboratory tests. Additionally, the enhanced IRI multiple regression equation does not require the measurement of other asphalt surface distresses such as rut depth and area of fatigue cracking prior to the calculation of the future IRI values. Moreover, the enhanced IRI multiple regression equation also considers important factors such as maintenance and rehabilitation intervention factor, LTPP regions factor, and IRI roughness measurement locations.

Table 2. Independent variable used in the enhanced IRI multiple regression equation and MEPDG IRI regression equation

No.	Enhanced IRI multiple regression developed in this research		No.	MEPDG IRI Regression Equation	
1	IRI_0	Initial IRI, m/km	1	IRI_0	Initial IRI after construction, in./mi
2	Age	Pavement age, year	2	Age	Pavement age, year
3	PRECIP	Average monthly precipitation, mm	3	Precip	Average annual precipitation or rainfall, in.
4	SN	Structural number	4	PI	Plasticity Index (%)
5	CESAL	Cumulative ESAL	5	FI	Mean annual freezing index, °F days
6	$TEMP_{AIR}$	Air Temperature, ℃	6	TC_{Total}	Length or transverse crack, ft./mi
7	Reg_D	Dummy variable for LTPP regions, assign 1 for Southern region and 0 for other regions	7	RD	Average rut depth, in.
8	CND	Dummy variable for major M&R, 0 for no major M&R; 1 if M&R has taken place	8	FC_{Total}	FC_{Total} is % area of fatigue cracking (combined alligator, longitudinal, and reflection cracking),
9	IRI_D	Dummy variable for roughness measurement locations, 0 for outside wheel path; 1 for inside wheel path			

2.2.2 Previous Studies on the Development of the Multiple Linear Regression Equations

Many researchers reported different approaches to model and predict IRI in future years. Paterson [67] developed and implemented the performance models in the Highway Design and Maintenance Standards Model (HDM-III). The empirical data used to predict surface roughness were based on initial roughness IRI_0, modified SN, cumulative ESAL traffic, and pavement age since construction, rehabilitation or reconstruction. The reported R value is 0.866. In addition, a correlation between roughness and quarter-car index (QI) was developed, where IRI is equal to QI/13.

In 1989, a new model was developed to predict the progression of roughness over pavement life [68]. It was developed based on field data in the Brazil-United Nations

Development Program (UNDP) road cost study and includes structural, surface distresses and combined environmental-age-condition factors, respectively. The new model predicted the increase of roughness over time and incorporated modified SN, thickness of crack layer, area of cracking in percent, and changes in ESAL per lane. In addition, increase in rut depth, increase in area of surface patching, pavement age, and road surface anomalies such as potholes were also considered as other contributing factors. The model had R value of 0.768. The researcher concluded that the development of road roughness involved a few stages which occurred through multiple mechanisms. The road surfaces degraded over time due to traffic loading, exaggerated by weak pavement strength and exposure to the environment condition over the years [68].

Cardoso and Macron [69] reported several pavement performance models as a function of the pavement age or the number of standard axle load application. Data from the road network of the State of Santa Catarina in Brazil were used and the models were implemented in the Pavement Management System (PMS). Five different models were established including the models to predict QI based on age and cumulative ESAL, respectively. The model predicted QI for three different regions according to subgrade layer types and the R values ranged from 0.332 to 0.831. However, the prediction overestimated the results when compared to previous Brazilian studies by Queiroz [70].

Soncim and Fernandes [71] developed the IRI roughness prediction model, which includes pavement age, ESAL, and rainfall intensity (RFL). An ANOVA was performed from the data collected in 2009 from road roughness surveyed on a 650 km road network in the State of Bahia, Brazil. The model was verified using field data and compared to other IRI roughness prediction models. The results showed a reasonable correlation between the observed and

predicted values with R^2 equal to 0.91. The Soncim and Fernandes's models are shown in Equations 2.3 through 2.6.

$$IRI = 4.55 + 0.57xP(AGE) + 0.86xP(EAL) + 0.38xP(RFL) + 0.25xP(EAL)xP(RFL) \quad (2.3)$$

$$P(AGE) = \frac{AGE-22}{14} \quad (2.4)$$

$$P(EAL) = \frac{EAL-1.1x10^6}{1.6x10^6} \quad (2.5)$$

$$P(AGE) = \frac{RFL-505}{222} \quad (2.6)$$

Where *P(AGE)* is polynomial equation for the age factor; *P(EAL)* is polynomial equation for the accumulated traffic factor; *P(RFL)* is polynomial equation for the rainfall factor.

Meegoda and Gao [72] investigated the time-sequence roughness data of the General Pavement Study (GPS) of the LTPP test sections and developed a model to predict the roughness progression over pavement age. The Meegoda and Gao [72] final model is shown in Equation 2.7.

$$lnIRI_{i+1} - lnIRI_i = (a_{i+1}\, x\, t_{I+1}^{0.9715} - a_{i+1}\, x\, t_i^{0.9715}) \quad (2.7)$$

Where, alpha is described in Equation 2.8 and freezing index (FI) is shown in Equation 2.9.

$$\alpha = \frac{CL^a}{SN^b}c + FI^d e + AP^f g \quad (2.8)$$

$$FI = \sum_{i=1}^{n} 0 - T_i \quad (2.9)$$

Where, the *CL* is cumulative traffic load kilo ESAL per year (KESAL/year); *SN* is structural number; *AP* is annual precipitation; *a, b, c, d, e, f, g* are model parameters; *FI* is freezing index (^{o}C-days); and T_i is average daily air temperature on day *i*.

Madanat et al. [73] developed a performance model to predict the progression of the asphalt pavement roughness. In this study, the MLR equation was developed to predict the incremental roughness progression (ΔIRI) value using the Washington State's PMS database. Eight independent variables were included; (1) IRI in previous year, (2) change in the ESAL in year of observation, (3) cumulative ESAL, (4) base thickness, (5) total asphalt layer thickness, (6) time since last asphalt overlay or bituminous surface treatment (BST) overlay, (7) minimum air temperature, and (8) yearly precipitation. In addition, three dichotomous (dummy) variables for asphalt overlay, BST overlay, and maintenance application were also considered. The multiple linear regression with R^2 of 0.526 was observed in this study.

Rahim et al. [74] evaluated the IRI for asphalt pavement overlays over concrete slab treated with crack, seat, and overlay (CS&O) rehabilitation technique. The IRI prediction models were developed for wet-freeze and wet-no-freeze LTPP regions. An additional model was developed for pavement sections in California. The factors of asphalt overlay thickness and base type (bound or unbound) were evaluated in the study. The independent variables are pavement age, annual ESAL, cumulative ESAL, base type, asphalt and concrete pavement thicknesses. The IRI models for wet-freeze (WF), wet-non-freeze (WNF), and California are shown in Equations 2.10 through 2.12. The observed R^2 are 0.55 (WF), 0.50 (WNF), and 0.62 (California), respectively.

$$IRI_{freeze} = 1.097 + 0.0158(Age^{1.6747})\left(\frac{KESAL^{0.0234}}{H_{ac}}\right) x\ (1 + base)^{-1.103} \quad (2.10)$$

$$IRI_{no-freeze} = 1.652 + 0.0751(Age) - 0.143H_{ac} + 0.57\ (base) \quad (2.11)$$

$$IRI_{CA} = 0.754 + 0.0158(CESAL^{1.07})(\frac{H_{ac}}{H_{pcc}})^{-1.242} \quad (2.12)$$

Where, *age* is pavement age (year); *CESAL* is cumulative ESAL per year (million); *KESAL* is ESAL per year (millions); H_{ac} is depth of asphalt overlay; H_{pcc} is depth of the concrete slab; and *base* is type of base (0 is bound; 1 is unbound).

Choi et al. [75] established the roughness prediction model using the multiple linear regression method. The data sets for the LTPP GPS-1 test sections in the states of Texas, New Mexico and Arizona were used and grouped according to the climatic zones (wet-no-freeze and dry-no-freeze), average daily truck traffic, construction number, and functional class. The multiple linear regression equation with the R^2 of 0.714 is shown in Equation 2.13.

$$IRI = 4.08 - 0.616(SN) - 0.415(AC) + 7.79(P_{200}) + 0.709(CESAL) - 0.48(Thick) \quad (2.13)$$

Where the *SN* refer to the structural number, *AC* is asphalt content, P_{200} is the percent passing no. 200 seize, "*Thick*" represents the thickness of top layer and *CESAL* is the cumulative ESAL in million.

2.2.3 Artificial Neural Network Models for IRI Roughness Prediction

A few studies related to the IRI roughness ANN modeling are reviewed and summarized in this research. Uddin et al. [63] provide good explanations about the ANN modeling method. Attoh- Okine [76] applied the ANN's back-propagation method to evaluate the capabilities of the ANN to predict roughness progression in flexible pavement. An extensive research looked into the structural deformation as the factors of modified SN, incremental traffic loadings, extent of cracking and thickness of cracked layer, and incremental variation of rut depth. In addition, the

surface distresses (changes in cracking, patching, and potholing), environment and other non-traffic-related mechanism were also investigated.

Choi et al. [75] also developed the ANN model ($ANN_{6\text{-}10\text{-}1}$) with the R^2 of 0.723 to predict the IRI roughness value. The models were further evaluated using other data sets that are not included in the model development. The measured vs. predicted IRI plots showed the R^2 of 0.212 and 0.757 for the MLR equation and the $ANN_{6\text{-}10\text{-}1}$ model, respectively. Kargah-Ostadi et al. [77] developed the changes in IRI prediction model for rehabilitation recommendations using the ANN. The statistical analysis for 20 variables was conducted to determine any significant correlation with the IRI. Only eight variables were included in the final model. The R^2 of 0.956 was observed between the predicted and measured IRI values which show that it is feasible to use IRI as the prediction criteria.

In this research the ANN analysis and modeling technique was also adopted for the development of asphalt pavement condition deterioration progression prediction models. The ANN is an advance computing system established from several simple, highly interconnected elements that process information through dynamic responses to the external inputs (independent variables). The basic model for each neuron in a simple ANN is shown in Figure 10. The neural network gains its knowledge through trained feed-forward network. During this process a set of training data consisting of inputs and output (dependent variable) are presented to the network. The resulted output is compared to the target values. Next, back propagation process adjust the connection weight to reduce the error between actual and target values. Once trained, the networks provide an approximate functional mapping of any input pattern onto its corresponding output pattern. Subsequently, the validation process was carried out using data sets that are excluded from model database [63]. The development of the ANN models was carried out using

ANN TRSEQ1 computer program [78]. Sigmoid activation function was embedded in the ANN TRSEQ1 software for data generalization purposes. Figure 11 shows the curve for sigmoid function bounded between zero and one values together with the equation needed for data transformation using sigmoid function (see Figure 11 (i)).

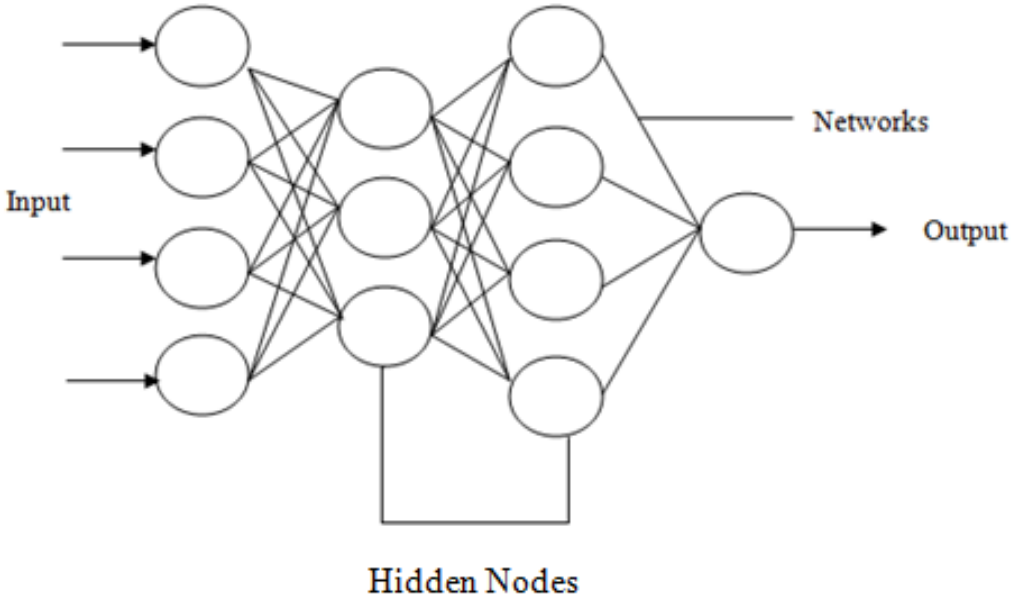

Figure 10. Example of ANN processing elements and interconnection network

This ANN model requires additional pre-processing of the model database prepared for multiple regression analysis, which are:

- Selecting the datasets for training, testing, and validation processes.
- Calculating the normalized minimum and maximum values for dependent and independent variables, respectively.
- Setting up the TRSEQ1 software SPEC and STP input files prior to the analysis.

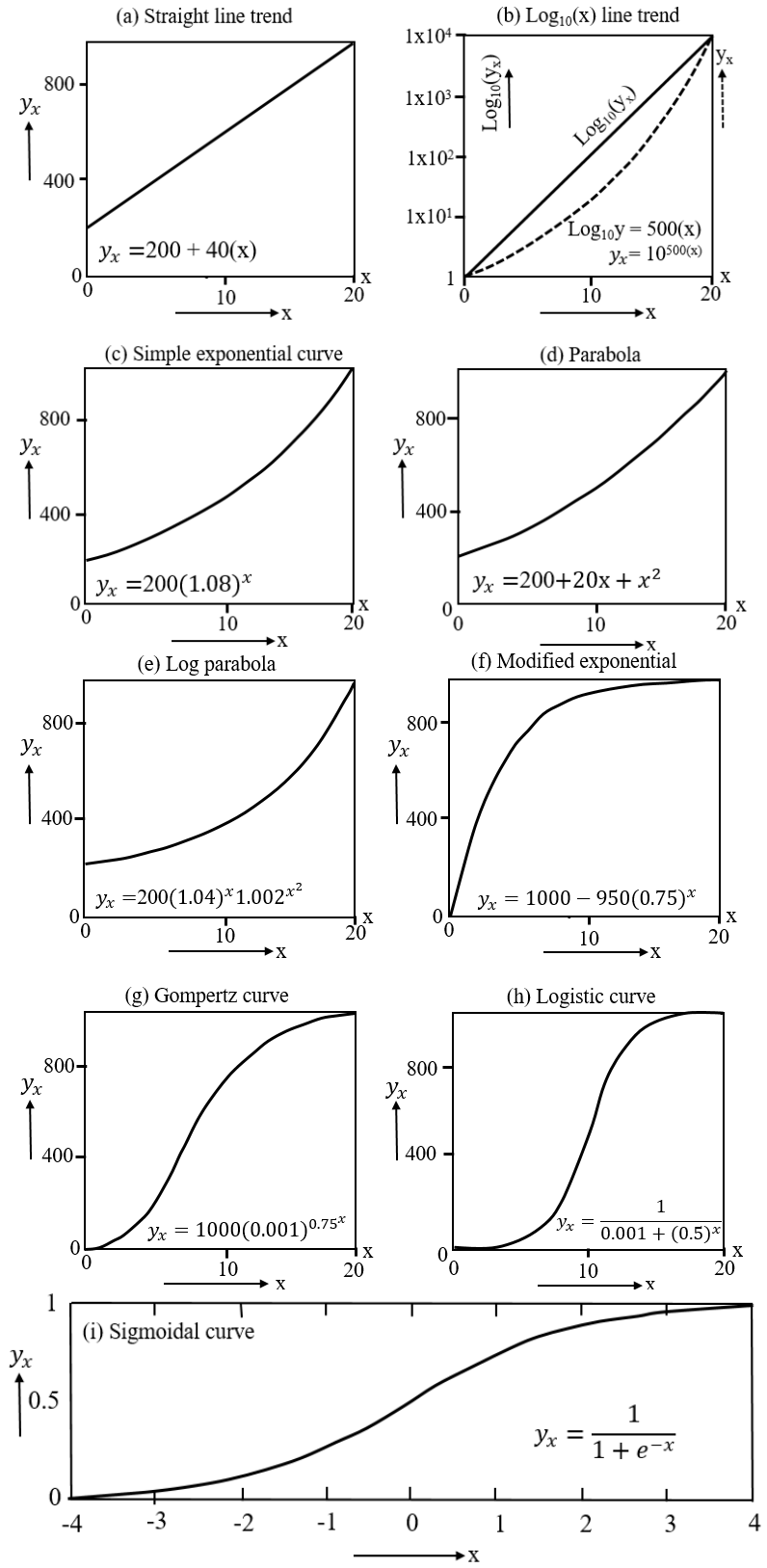

Figure 11. Common data transformation functions used in mathematical modeling as a function of time (x-axis)

2.2.4 LTPP Data Collection

The IRI roughness data for the test sections in 28 states in the U.S. were extracted from the LTPP database under MON_PROFILE_MASTER section [11]. The IRI per measurement year (Y_I) for both inside and outside wheel paths were measured for each 500 feet (152.4 m) test section. The measurements were repeated at least five times, and the average values for each run were also recorded in the LTPP ACCESS database as shown in Table 3.

Table 4 shows the counts and percentages of the Y_I data points for all 28 states in the U.S. that are included in the analysis. The Y_I data used in the model database ranged from 1990 to 2011. A total of 2,588 data points that are comprised of 1,294 Y_I data the inside wheel path, and 1,294 Y_I data outside the wheel path were used in the analysis.

Table 3. Example of IRI data for LTPP test section 1-1011 in Lauderdale County, Alabama

STATE_CODE	SHRP_ID		PROFILE_DA	IRI_LEFT_WH	IRI_RIGHT_W	IRI_AVERAG
1	1011	1	2/11/1992	0.844	0.817	0.831
1	1011	1	2/11/1992	0.86	0.856	0.858
1	1011	1	2/11/1992	0.844	0.854	0.849
1	1011	1	2/11/1992	0.838	0.82	0.829
1	1011	1	2/11/1992	0.841	0.837	0.839
1	1011	1	2/1/1994	0.776	0.827	0.802
1	1011	1	2/1/1994	0.756	0.842	0.799
1	1011	1	2/1/1994	0.74	0.843	0.792
1	1011	1	2/1/1994	0.73	0.813	0.772
1	1011	1	2/1/1994	0.767	0.848	0.807
1	1011	1	8/16/1995	0.814	1.124	0.969
1	1011	1	8/16/1995	0.826	1.093	0.959
1	1011	1	8/16/1995	0.805	1.144	0.974
1	1011	1	8/16/1995	0.851	1.053	0.952
1	1011	1	8/16/1995	0.797	1.1	0.949
1	1011	1	8/12/1998	0.865	1.075	0.97
1	1011	1	8/12/1998	0.849	1.027	0.938
1	1011	1	8/12/1998	0.836	0.983	0.909
1	1011	1	8/12/1998	0.848	1.102	0.975
1	1011	1	8/12/1998	0.867	1.09	0.978
1	1011	2	6/6/2002	1.107	1.391	1.249
1	1011	2	6/6/2002	1.092	1.399	1.245
1	1011	2	6/6/2002	1.172	1.375	1.273
1	1011	2	6/6/2002	1.123	1.386	1.254
1	1011	2	6/6/2002	1.185	1.377	1.281

Total distributions of Y_I data points for each LTPP region follow:

- North Atlantic (716 data points, 27.7%)
- North Central (100 data points, 3.9%)
- Southern (1088 data points, 42%)
- Western (684 data points, 26.4%)

Table 4. State-wise distribution of the Y_I data (number of data points and percentages)

State Code	State Name	LTPP Zone	N	%	State Code	State Name	LTPP Zone	N	%
1	Alabama	SR	62	2.4	32	Nevada	WR	36	1.4
4	Arizona	WR	46	1.8	34	New Jersey	NA	110	4.3
5	Arkansas	SR	64	2.5	35	New Mexico	SR	24	0.9
6	California	WR	328	12.7	36	New York	NA	68	2.6
8	Colorado	WR	34	1.3	37	North Carolina	NA	158	6.1
10	Delaware	NA	32	1.2	38	North Dakota	NC	14	0.5
12	Florida	SR	52	2.0	40	Oklahoma	SR	164	6.3
13	Georgia	SR	88	3.4	41	Oregon	WR	26	1.0
18	Indiana	NC	38	1.5	47	Tennessee	SR	208	8.0
22	Louisiana	SR	12	0.5	48	Texas	SR	162	6.3
24	Maryland	NA	128	4.9	50	Vermont	NA	54	2.1
28	Mississippi	SR	252	9.7	51	Virginia	NA	142	5.5
29	Missouri	NC	48	1.9	54	West Virginia	NA	24	0.9
30	Montana	WR	32	1.2	56	Wyoming	WR	182	7.0
Total number of IRI data points (N) = 2,588									

Dependent Variable

The dependent variable of the multiple regression equation is IRI per measurement Year (Y_I) in meter per kilometer (m/km). Both Y_I measured inside and outside the wheel paths were considered in the analysis for the following reasons;

- The load effects are greater on the outside wheel path. The average Y_I measured outside the wheel path is 1.36 m/km (86.2 in./mile), which is 5.4% more than the Y_I measured inside the wheel path of 1.29 m/km (81.7 in./mile).
- Univariate Analysis of Variance (ANOVA) indicates a statistically significant difference in the means of the measured Y_I inside or outside the wheel paths (see IRI_D) as shown in Table 5. The probability of significance (Sig.), p value is 0.002, which is less than the probability of type 1 error alpha (α) = 0.05.

Table 5. Univariate ANOVA test for the Y_I

Tests of Between-Subjects Effects

Dependent Variable: IRI Per Measurement Year (Y_I)

Source	Type III Sum of Squares	df	Mean Square	F	Sig.
Corrected Model	358.5[a]	105	3.4	12.8	.000
Intercept	1345.1	1	1345.1	5042.4	0.000
State_Code	225.3	24	9.4	35.2	.000
Region	0.0	0			
CND	3.8	1	3.8	14.2	.000
IRI_D	2.5	1	2.5	9.3	.002
State_Code * Region	0.0	0			
State_Code * CND	69.7	21	3.3	12.4	.000
State_Code * IRI_D	8.7	24	0.4	1.4	.114
Region * CND	0.0	0			
Region * IRI_D	0.0	0			
CND * IRI_D	0.3	1	0.3	1.2	.277
State_Code * Region * CND	0.0	0			
State_Code * Region * IRI_D	0.0	0			
State_Code * CND * IRI_D	1.9	21	0.1	0.3	.998
Region * CND * IRI_D	0.0	0			
State_Code * Region * CND * IRI_D	0.0	0			
Error	662.1	2482	0.3		
Total	5537.5	2588			
Corrected Total	1020.6	2587			

a. R Squared = .351 (Adjusted R Squared = .324)

- A dummy or dichotomous variable (IRI_D) with zero and one values were created to represent the IRI measurement locations. Zero value describes the IRI measured outside the wheel path, while one describes the IRI measured inside the wheel path.

Figure 12 plot shows the distribution of the Y_I according to the sequential number or observation number.

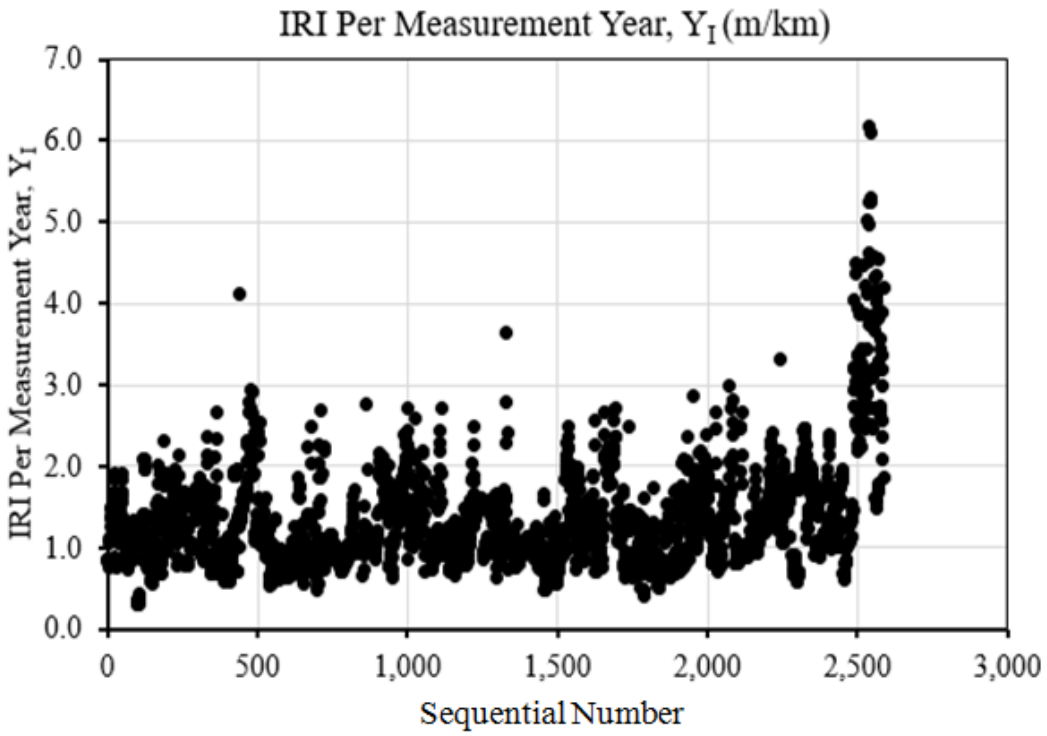

Figure 12. Distributions of the IRI per measurement year data according to sequential number

The following descriptive statistics describes the Y_I for both inside and outside wheel path measurements;

- Most of the data are less than 3 m/km.
- A maximum Y_I of 6.2 m/km was measured on September 6, 1991 for test section 34-1030 located in New Jersey (North Atlantic region)
- A minimum Y_I of 0.31 m/km was measured on February 14, 2002 for test section 4-1065 located in Arizona (Western region)

- The average Y_I is 1.32 m/km
- The Standard Deviation (SD) is 0.63 m/km
- The Coefficient of variance (COV) is 47.5%

Independent Variable

The following independent variables were considered to develop the enhanced IRI condition deterioration prediction equations

- The initial IRI per measurement year (**Y_{I0}**) is the IRI at the first measurement year from the LTPP database. As shown previously in Table 3, test section 1-1011 has the measured Y_I in 1992, 1994, 1995, 1998, and 2002. Therefore, the Y_{I0} for this measurement years is the Y_I that are measured in 1992. It is important to include Y_{I0} in the regression equation since this value describes the road surface condition at the beginning of the analysis period.
- The age (**Age**) attribute is chosen since it reflects the impacts of season and the environment. The pavement age is calculated by subtracting the year when the test section was opened to the traffic from the IRI measurement year. The test section 1-1011 was opened to the traffic in June 1st, 1985. Therefore the corresponding age in 1992 is seven years (1992 to 1985), which explains that the pavement is exposed to traffic loads and the environmental condition for seven years.
- Another important input is the pavement structural number (**SN**) that is used in the 1993 AASHTO and earlier guides [61]. The SN represents the overall structure constructed to sustain the traffic loads. The SN considers structural layer coefficients, layer thicknesses, and base and subbase drainage coefficients. Higher SN exhibits stronger pavement and better load carrying capacity to ensure smooth road surfaces over the service life.

- The next variable selected is cumulative ESAL (**CESAL**) traffic application. The ESAL for certain years are not available in the LTPP database [12]. Mohamed Jaafar et al. [12] show the example of interpolation for missing ESAL data. The missing ESALs are interpolated based on the average annual rate of growth (AARG). The missing values are estimated using the AARG that are determined by averaging growth rate before and after average years. The average year is 8.5, obtained by dividing 17 (number of years from 1990 to 2006) by two. The ESAL values for the missing data are estimated using Equation 2.14.

$$ESALs_y = ESALs_{y-1}\, x\, (1 + AARG) \tag{2.14}$$

Where, y is the year of the measured or interpolated IRI. The latest ESAL depends on the ESAL of the preceding year multiplied with the AARG. Figure 13 shows the example for interpolating the missing ESAL values, as well as the cumulative ESAL at the end of each year. The interpolated total ESAL for each year shows higher ESAL compared to the measured ESAL from preceeding year, corresponding to positive AARG. Some test sections are observed having negative AARG values. Thus, smaller traffic ESAL values are interpolated for those data points. Similar approach is applied to other test sections in order to predict missing traffic ESAL application.

- The air temperature (**$TEMP_{AIR}$**) attributes in degree Celsius (°C) is selected since the asphalt surface temperature data are not available in the LTPP IRI datasets. The changes in daily temperature affect material properties of asphalt pavement. Therefore, the daily temperatures based on the IRI profile date are considered in the analysis.

- Precipitation (**PRECIP**) is another variable considered in the analysis. This attribute describes the amount of rainfall, snow or sleet that each test section experienced, which affects the pavement layers. The engineering properties of bituminous mixtures, granular base course, and underlying subgrade soils are susceptible to both temperature and moisture variations. This research considers monthly average temperature based on the IRI measured date.

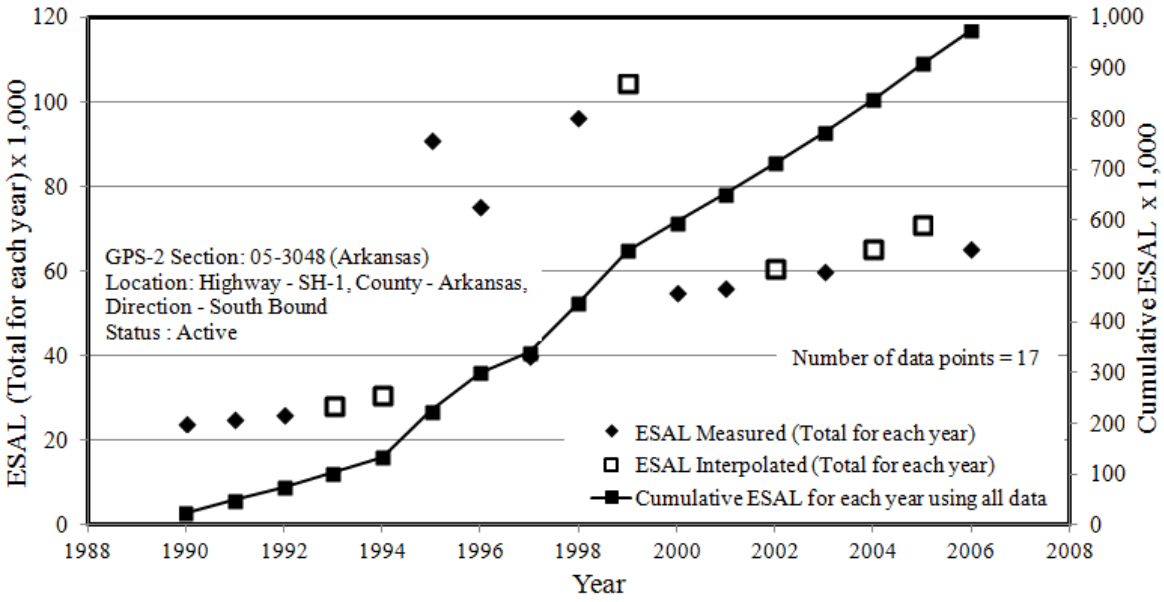

Figure 13. Annual ESAL and cumulative traffic data for GPS 2 test section in Arkansas

- Three dummy variables are also considered in the multiple regression equations. The explanations for each dummy variable follow:

a) Dummy variable for the LTPP regions (**Reg_D**):

Where zero is for the North Atlantic, North Central, and Western regions (defined as other regions in this research), and one is for the Southern region.

Purpose: This dummy variable was used to differentiate IRI roughness data between the Southern region and other LTPP regions.

b) Dummy variable for the major M&R treatment applications intervention factor (**CND**): Where zero is for the test section without any major M&R treatment when Y_I is measured, and one is for the test section that has gone through major M&R treatment when the Y_I is measured.

The CND identifies changes in the pavement structure caused by major M&R treatment events. When the test section first entered the LTPP program, CN1 was assigned. The subsequent M&R changed the section's construction number to CN2, CN3, etc. Mohamed Jaafar et al. [12] described the importance of using the CND in the preliminary multiple regression equation developed for IRI prediction in the Southern region. Another study by Mohamed Jaafar and Uddin [79] highlighted the importance of using the CND in the development of the multiple regression prediction equation for asphalt pavement rutting distress in the Southern region. Both studies [12, 79] discovered that the use of the CND increased the R values of the condition deterioration prediction equations. There is a need to develop condition deterioration models using M&R history which were not considered in the National Pooled Fund Study Tpf-5(013) [80] and NCHRP 1-37 studies [81].

c) Dummy variable for the IRI measurement locations (**IRI_D**):

Where zero represents the Y_I measured outside the wheel path, while one describes the IRI measured inside the wheel path. Detail descriptions related to the IRI_D was already mentioned earlier in this chapter.

Table 6 shows the maximum, minimum, average, SD, and COV for the data sets used in the development of the enhanced IRI condition deterioration prediction equations.

Table 6. Descriptive statistics for the data sets used to develop the enhanced IRI condition

Descriptive Statistics	IRI per measurement year, Y_I (m/km)	Initial IRI per measurement year, Y_{I0} (m/km)	Structural Number (SN)	Age (Years)	Cumulative ESAL	Air Temperature (°C)	Average Monthly Precipitation (mm)
Maximum	6.18	3.55	10.8	48	36,669,857	46	645
Minimum	0.31	0.53	1.4	0	3,000	-8.3	0
Average	1.32	1.22	5.1	17.9	2,323,695	19.5	94
SD	0.63	0.5	1.6	8.5	4,148,364	9.3	76.4
COV (%)	47.5	41.1	31.1	47.7	178.5	47.6	81.3

2.2.5 Methodologies for Enhanced IRI Modeling

1) The initial IRI condition deterioration prediction equation was developed in a previous study [12] as shown in Equation 2.15.

$$IRI_y = 0.99 + 0.3637(IRI_O) - 0.074(SN) + 0.013(Age) - 1.734x10^{-8}(CESAL) + 0.154\ (CND) \quad (2.15)$$

A total of 578 data points from 34 LTPP test sections were used in this study. The IRI_y is the average value of the measured IRI inside and outside the wheel paths. The equation was developed only for the Southern region in the U.S. The Pearson's R for the regression equation is 0.495 or coefficient of determination, R^2 of 0.245. The verification results of the equation predictions have an average difference of -1.6% compared to the mean measured IRI_y value. The predictions using Equation 2.15 gave better prediction as compared to the MEPDG model predictions.

2) An expanded database was prepared for the development of the enhanced multiple regression prediction equations. The expended database considers the Y_I data sets from all four LTPP regions. A total of 2,588 data included in the analysis enables further analysis using the ANN method as well.

3) The data sets used in the analysis must comply with the basic assumptions required for multiple linear regression analysis. Those assumptions are:

- The data are independent: The autocorrelation of the Y_I data sets were assessed using the CORREL function in the Microsoft Excel data sheet. The autocorrelation value that is less than 0.4 shows that the data are independent of each other.
- The data are normally distributed: The Kolmogorov-Smirnov test (K-S test) nonparametric test was conducted and the normality plot from the SPSS [82] was assessed to evaluate that the assumption of normality be met.
- The predicted and measured Y_I should show homogeneity of variance.
- The residual plot must show normal distribution at zero mean value.

4) Many transformations of Y_I were tried including $Log_{10}Y_I$ and Ln Y_I (all IRI data were non-zero data). The regression equations for Y_I, $Log_{10}Y_I$, and Ln Y_I are shown in Equations 2.16 to 2.18, respectively.

$$Y_I = 0.642 + 0.726\ (Y_{I0}) + 0.006\ (Age) - 0.045\ (SN) - 1.542x10\text{-}8\ (CESAL) + 0.002\ (TEMP_{AIR}) \\ -0.000349\ (PRECIP) + 0.08\ (Reg\_D) - 0.105\ (CND) - 0.061\ (IRI\_D) \quad (2.16)$$

$$Log_{10}\ (Y_I) = 0.119 + 0.626\ (Log_{10}Y_{I0}) + 0.002\ (Age) - 0.014\ (SN) - 6.34x10\text{-}8\ (CESAL) + 0.000377 \\ (TEMP_{AIR}) - 0.000112\ (PRECIP) + 0.023\ (Reg\_D) - 0.037\ (CND) - 0.016\ (IRI\_D) \quad (2.17)$$

$$Ln\ (Y_I) = 0.274 + 0.626\ (Ln\ Y_{I0}) + 0.005\ (Age) - 0.032\ (SN) - 1.460x10\text{-}8\ (CESAL) + 0.001 \\ (TEMP_{AIR}) - 0.000258\ (PRECIP) + 0.054\ (Reg\_D) - 0.086\ (CND) - 0.038\ (IRI\_D) \quad (2.18)$$

5) In this research, a high autocorrelation of 0.77 was calculated for the Y_I data. However, there is no physical significance of high auto correlation of 0.77 at lag one because the data were collected on randomly selected and spatially distributed highway pavement test sections across the U.S.

6) The normality test results for Y_I and transformed Y_I data are shown in Table 7.

Table 7. Normality test result for Y_I and transformed Y_I data

Tests of Normality			
Kolgomorov-Smirnov[a]			
	Statistic	df	Sig.
Y_I	.119	2,588	< 0.001
$Log_{10} Y_I$	0.054	2,588	< 0.001
Ln Y_I	.054	2,588	< 0.001
a. Lilliefors Significance Correction			

Kolmogorov-Smirnov is a nonparametric (distribution free) test that is used to test the normality of the data. The test hypotheses for probability of type I error alpha (α) = 0.05 are described, as follow:

Null hypothesis, H_0: The distribution of the Y_I data is normal

Alternative hypothesis, H_A: The distribution of the Y_I data is not normal

The normality test of Y_I data in the LTPP database shows that the probability of significance, p-value is less than the α 0.05 probability of chance error, which is statistically significant. Therefore, the null hypothesis is rejected and the Y_I data is not normally distributed. Figure 14 shows the normality plots for the untransformed and transformed Y_I.

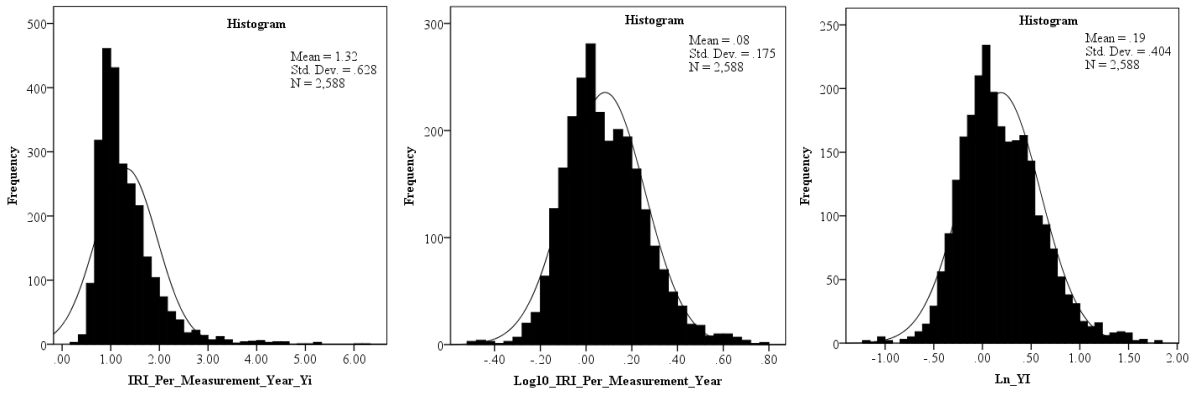

Figure 14. Normality plots for the untransformed and transformed Y_I data

The distributions of the Y_I data do not exactly follow the bell curve of normal distribution. Part of the histogram data are way out of the distribution curve. These histograms indicate that the Y_I data are not normally distributed. The results of the normality test clearly reveal that multiple linear regression modeling may be problematic if residuals are not normally distributed with zero mean value. An alternative method for condition deterioration progression modeling is ANN method.

The reasonableness of the multiple regression equations were evaluated based on the following parameters:

- The R value of the multiple regression equations
- The predicted against measured data plots
- The verifications of the multiple regression equations
- The accuracy measures of the Mean Absolute Relative Error (MARE) and Root Mean Square Error (RMSE)

The MARE was calculated using Equation 2.19.

$$MARE = \frac{\sum_{i=1}^{N}\left|\left(\frac{\hat{y}_i - y_i}{y_i}\right)\right|}{N} x100 \qquad (2.19)$$

Where $\hat{y}_i$ and y are the predicted and observed value of the IRI per measurement year. If the value of the MARE (%) is relatively small, close to zero, it means that the model performance is good. Equation 2.20 was used to calculate the RMSE accuracy measure.

$$RMSE = \sqrt{\frac{\sum_{i=1}^{N}(\hat{y}_i - y_i)^2}{N}} \quad (2.20)$$

Where $\hat{y}_i$ and y are the predicted and observed value of the IRI per measurement year and the N is total number of data sets.

Table 8 summarizes the number of data sets (N), coefficient of correlation (R), coefficient of determination (R^2), average measured Y_I, average predicted Y_I, RMSE, and MARE (%) for the untransformed and transformed Y_I model database. The verification results for Equations 2.16 to 2.18 are shown in Table 9.

Table 8. Accuracy measures for the untransformed and transformed Y_I model database

Regression Equations (SPSS)				Database (Predicted vs Measured)					
Dependent Variable	N	R	R^2	Measured Y_I (m/km)	Predicted Y_I (m/km)	% Difference (Average)	R	RMSE	MARE (%)
Y_I	2,588	0.633	0.401	1.32	1.32	0.0	0.633	0.484	26.8
$Log_{10}(Y_I)$	2,588	0.622	0.387	1.32	1.25	-5.3	0.633	0.494	24.5
$Ln(Y_I)$	2,588	0.622	0.387	1.32	1.25	-5.3	0.633	0.494	24.5

Table 9. Accuracy measures for the untransformed and transformed Y_I model verifications

Verification of IRI Multiple Regression Equations							
(Predicted vs Measured)	Measured Y_I (m/km)	Predicted Y_I (m/km)	% Difference (Average)	N	R	RMSE	MARE (%)
Y_I	2.25	1.74	-22.7	18	0.99	0.21	9.6
$Log_{10}(Y_I)$	2.25	1.61	-28.4	18	0.96	0.38	11.6
$Ln(Y_I)$	2.25	4.23	88.0	18	0.98	3.22	122.2

For model databases, the untransformed Y_I gives the most accurate regression results as shown by the listed accuracy measures. The measured R values are similar for all three equations. However, the average predicted Y_I using equation 2.16 shows no difference as compared to the measured value. Other two equations underpredicted the Y_I (1.25 m/km). The untransformed Y_I has the least RMSE despite a slightly higher MARE of 26.8%. The verification results show that the untransformed Y_I outperformed the other equations based on the average percent difference, RMSE, and MARE. Therefore, Equation 2.16 was selected as the best enhanced IRI prediction equation.

7) The final results are shown in Figures 15 to 17. Figure 17 shows the measured and predicted values using the enhanced multiple regression prediction equation with respect to data sequential number on the x-axis. The ANN model results are shown in Figures 18, 19, and 20, respectively.

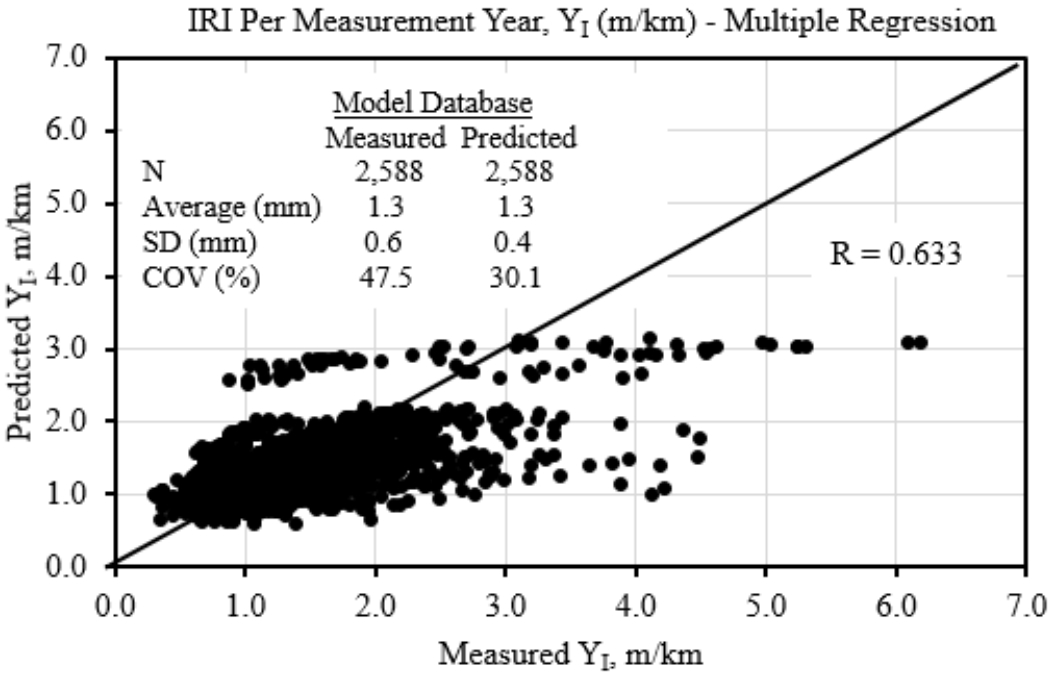

Figure 15. Predicted vs measured plot for IRI multiple regression equation database

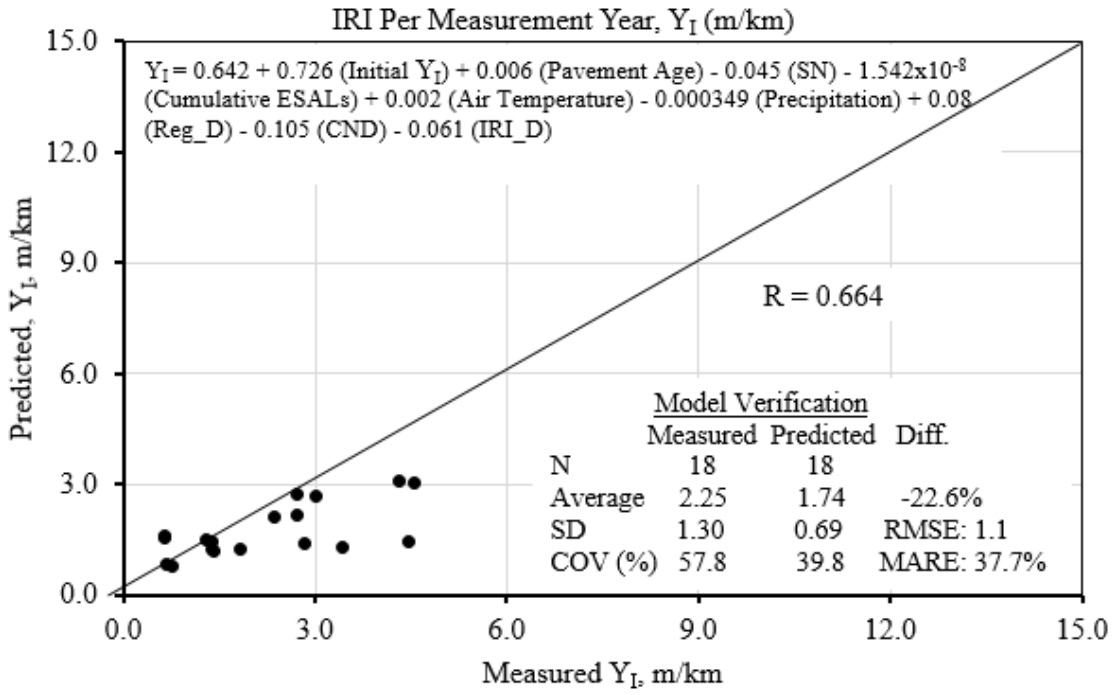

Figure 16. Predicted vs measured plot for IRI multiple regression verification database

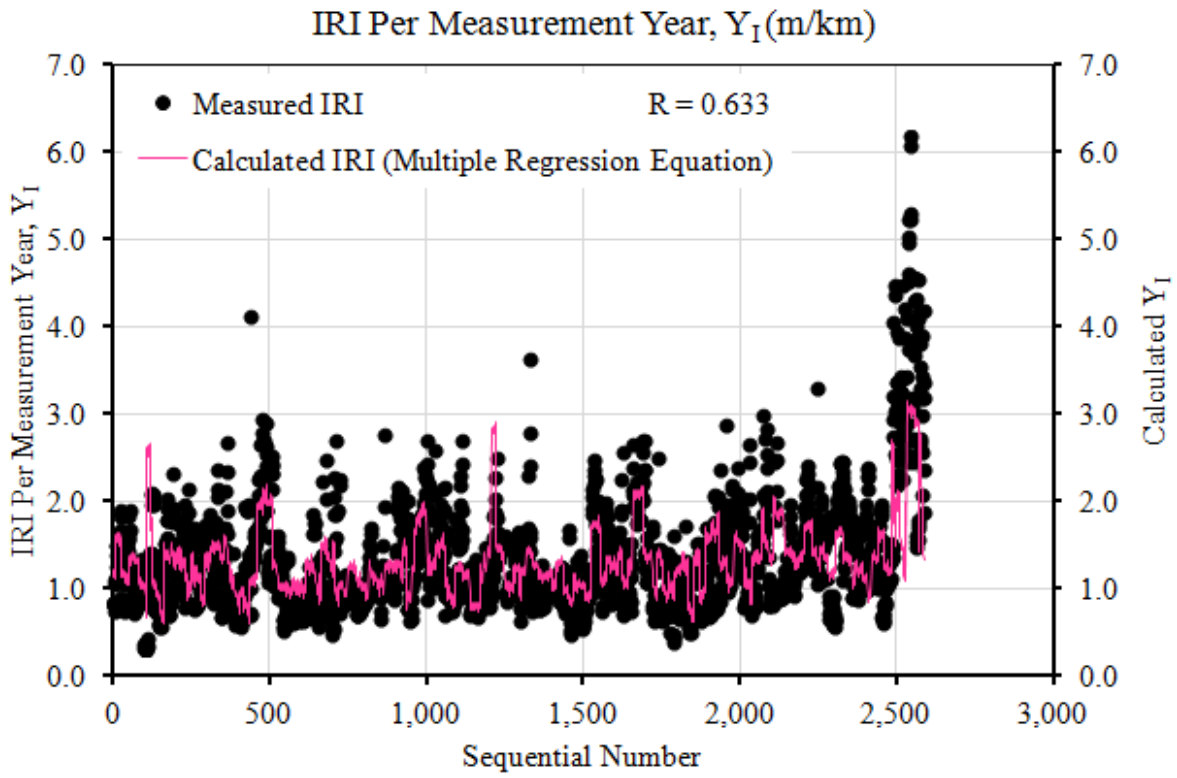

Figure 17. Measured and predicted IRI using multiple regression based on sequential number

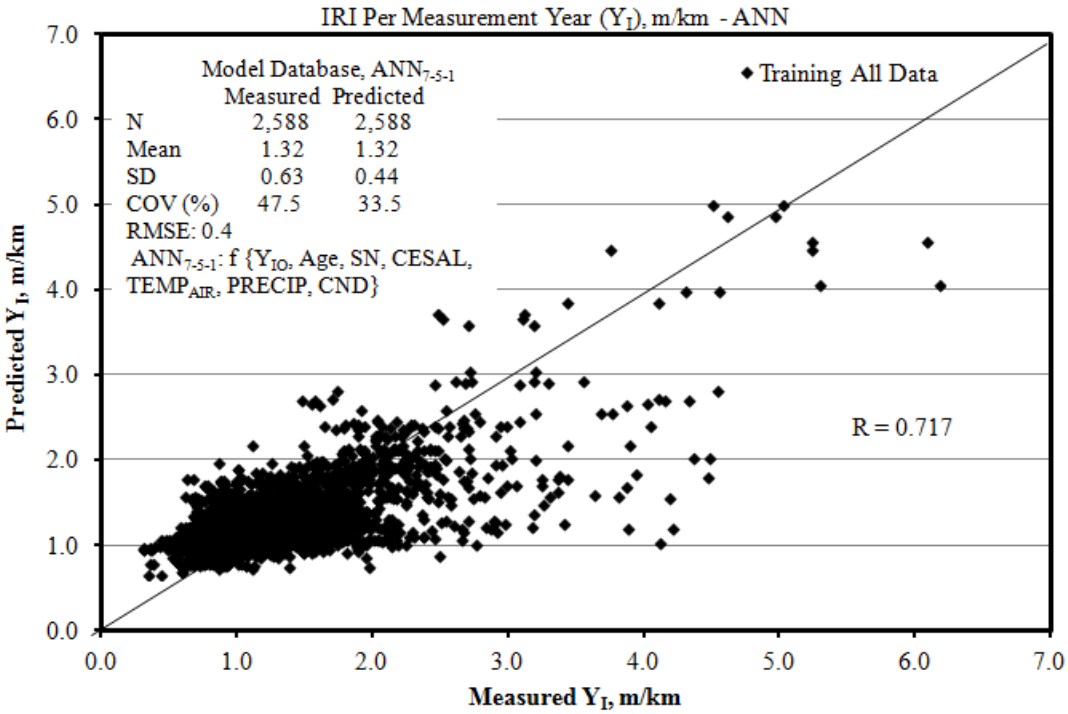

Figure 18. Predicted vs measured plot for IRI ANN model database

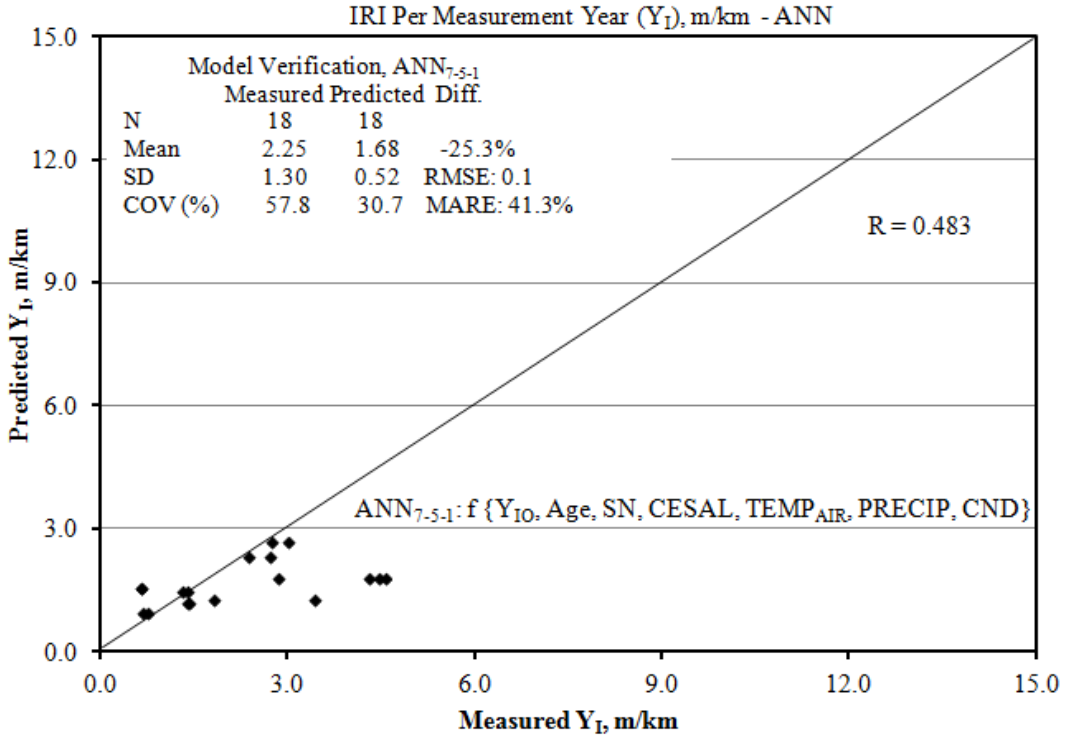

Figure 19. Predicted vs measured plot for IRI ANN verification database

The verification results are better predicted using the enhanced multiple regression model equation for untransformed IRI values. However, both ANN model and the enhanced IRI multiple regression equations are recommended for implementation.

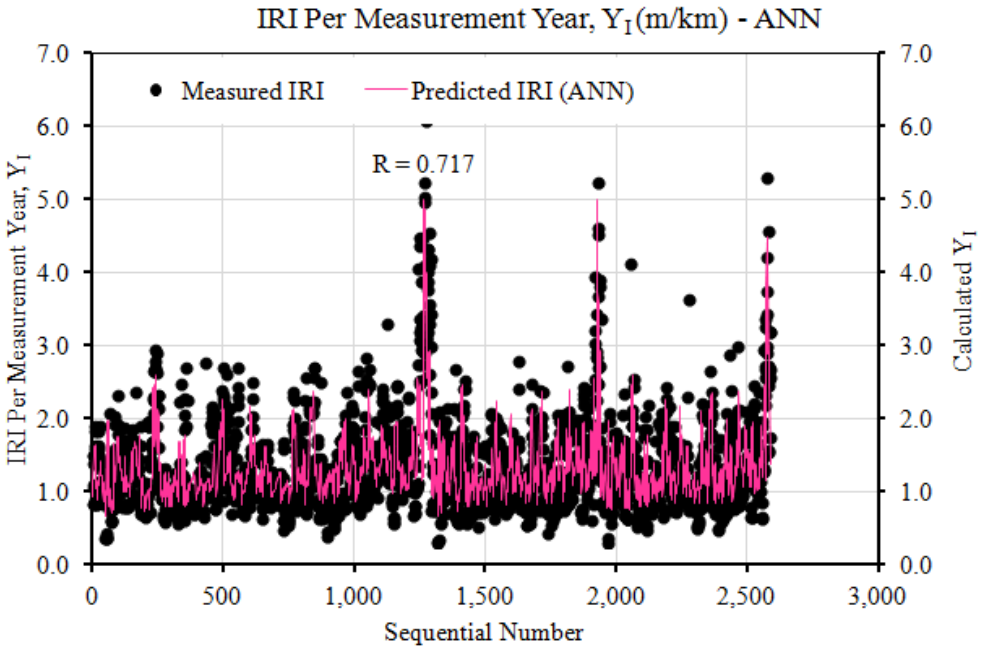

Figure 20. Measured and predicted IRI using ANN model based on sequential number

2.3 Rutting Initiation and Progression Modeling using Multiple Linear Regression and ANN Methods

2.3.1 MEPDG Performance Modeling for Rutting Distress

Asphalt pavement rutting is known as one of the major pavement surface distresses that affect ride quality. The MEPDG defines rutting as a distress that is caused by the permanent vertical deformation in the asphalt surface layer, unbound layers and foundation soils [83]. Equations 2.21 shows the MEPDG's recalibrated model, including new model coefficients used to calculate total rutting in pavement layers [84]. The Pearson's R value for the MEPDG rutting prediction model is 0.76 (R^2 = 0.58), which was developed using 334 data sets.

$$TRUT = 0.51 * ACRUT + 0.32 * BASERUT + 0.33 * SUBGRUT \quad (2.21)$$

Where, TRUT is total rutting, ACRUT is rutting in the asphalt layer, BASERUT is rutting in the base layer, and SUBGRUT is rutting in the subgrade layer.

The field calibrated mathematical equations to estimate incremental distortion or rutting at mid-depth of asphalt layer are shown through Equations 2.22 to 2.24. Table 10 describes the parameters used in Equations 2.22 to 2.25, respectively.

$$\Delta_{p(HMA)} = \varepsilon_{p(HMA)} \, x \, h_{HMA} = \beta_{1r} \, x \, k_z \, x \, \varepsilon_{r(HMA)} \, x \, 10^{k_{1r}} \, x \, n^{k_{2r}\beta_{2r}} \, x \, T^{k_{3r}\beta_{3r}} \quad (2.22)$$

$$k_z = \left(C_1 + C_2 D\right) x \, 0.328196^D \quad (2.23)$$

$$C_1 = -0.1039 \, x \, (H_{HMA})^2 + 2.4868 \, x \, H_{HMA} - 17.342 \quad (2.24)$$

$$C_2 = 0.0172 \, x \, (H_{HMA})^2 - 1.7331 \, x \, H_{HMA} + 27.428 \quad (2.25)$$

Table 10. The parameters used to calculate rutting at the mid-depth of asphalt layer

Parameter	Explanations
$\Delta_{p(HMA)}$	Accumulated permanent or plastic vertical deformation in the HMA layer/sublayer, in
$\varepsilon_{p(HMA)}$	Accumulated permanent or plastic axial strain in the HMA layer/sublayer, in./in
h_{HMA}	Thickness of the HMA layer/sublayer, in./in.
n	Number of axle-load repetitions
T	Mix or pavement temperature, ℉
k_z	Depth confinement factor
$k_{1r,2r,3r}$	Global field calibration parameters (from the NCHRP 1-40D recalibration; k_{1r} = -3.35412, k_{2r} = 0.4791, k_{3r} = 1.5606
$\beta_{ir}, \beta_{2r}, \beta_{3r}$	Local or mixture field calibration constants; for the global calibration, these constants were all set to 1.0
D	Depth below the surface, in
H_{HMA}	Total HMA thickness, in.

The field calibrated mathematical equations to calculate incremental distortion or rutting at mid-depth of all unbound sublayers are shown through Equations 2.26 to 2.29. Table 11 describes the parameters used in Equations 2.26 to 2.29, respectively.

$$\Delta_{p(soil)} = \beta_{s1}\ x\ k_{s1}\ x\ \varepsilon_v\ x\ h_{soil}\ x\ \left(\frac{\varepsilon_o}{\varepsilon_r}\right) x\ \varepsilon^{-(\frac{p}{n})^{\beta}} \quad (2.26)$$

$$Log\beta = -0.61119 - 0.017638\ x(W_c) \quad (2.27)$$

$$\rho = 10^9 x\ \left[\frac{C_o}{(1-(10^9)^{\beta})}\right]^{\frac{1}{\beta}} \quad (2.28)$$

$$C_o = \ln\left[\frac{a_1 M_r^{b_1}}{a_9 M_r^{b_9}}\right] = 0.0075 \quad (2.29)$$

Table 11. The parameters used to calculate rutting at the mid-depth of all unbound sub-layers

Parameters	Explanations
$\Delta_{p(soil)}$	Permanent or plastic deformation for the layer or sublayer, in.,
n	Number of axle-load repetitions
ε_o	Intercept determined from laboratory repeated load permanent deformation tests, in./in
ε_r	Resilient strain imposed in laboratory test to obtain material properties ε_o, ε, and ρ, in./in.,
ε_v	Average vertical resilient or elastic strain in the layer or sublayer and calculated by the structural response model, in./in.
h_{soil}	Thickness of the unbound layer or sublayer, in.
k_{s1}	Global calibration coefficients; k_{s1} = 1.673 for granular materials and 1.35 for fine-grained materials
ε_{s1}	Local calibration constant for the rutting in the unbound layers; the local calibration constant was set to 1.0 for the global calibration effort
W_c	Water content (%),
M_r	Resilient modulus of the unbound layer or sublayer, psi,
$a_{1,9}$	Regression constant; a_1 = 0.15 and a_9 = 20.0
$b_{1,9}$	Regression constants; b_1 = 0.0 and b_9 = 0.0
W_c	Water content (%)

About 20 input parameters are required to predict future rut depth using the MEPDG rutting prediction equation. The only load-related response parameter is $\varepsilon_{v,}$, which is the average vertical resilient or elastic strain in the asphalt layer or sublayers. The vertical strain was computed using the Jacob Uzan Layered Elastic Analysis (JULEA) multilayer elastic analysis computer program [83].

In general, the MEPDG rutting prediction model was developed to be used with the computer program, but not for manual calculation considering the complex input parameter that are based on the laboratory tests. In contrast, the enhanced rutting multiple regression equation developed in this research is easier to use for future rutting prediction considering reasonable input parameters such as initial rut depth value, cumulative traffic ESAL, layer modulus values, and asphalt thickness, total layer thicknesses, pavement age, SN, and air temperature. Moreover, the enhanced rutting multiple regression equation also considers important factors such as maintenance and rehabilitation intervention factor, LTPP regions factor, and base layer types.

2.3.2 LTPP Data Collection

The rutting data available for test sections in 24 states in the U.S. are extracted from the LTPP database under MON_RUT_DEPTH_POINT section [11]. The rut depths are commonly measured at 11 equal intervals for both outside and inside wheel paths throughout 500 feet (152.4 m) test section. Table 12 shows the example of rut depth data sets for test section 1-1011 in Lauderdale County, Alabama. In this research, only the average rut depth per measurement year (Y_R) is considered in the analysis. Total rut depth values from 11 points outside wheel path, and rut depth values from 11 points inside wheel path were divided by eleven to get the average values on both sides, respectively. Next, the average rut depth values on both sides were divided

by two to obtain an average rut depth per measurement year, measured in millimeter (mm). For example, the average rut depth per measurement year for test section 1-1011 is 3.14 mm. A total of 214 data sets were used in the development of the enhanced Y_R multiple regression and ANN model equations. Distribution of rut depth data sets based on LTPP regions (Reg_Actual), base type (Base_D), and major M&R intervention factor (CND) is shown in Table 13. Figure 21 shows the distribution of the rut depth per measurement year data used in this research.

Table 12. Example of rut depth data sets for test section 1-1011 in Lauderdale County, Alabama

SHRP_ID	STATE_COD	CONSTRUC	SURVEY_D	POINT_LO	LEFT_RUT_	RIGHT_RUT_
1011	1	1	3/30/1993	0	4	6
1011	1	1	3/30/1993	15.3	2	5
1011	1	1	3/30/1993	30.5	3	4
1011	1	1	3/30/1993	45.8	2	4
1011	1	1	3/30/1993	61	2	3
1011	1	1	3/30/1993	76.3	2	4
1011	1	1	3/30/1993	91.5	2	4
1011	1	1	3/30/1993	106.8	2	5
1011	1	1	3/30/1993	122	2	4
1011	1	1	3/30/1993	137.3	1	3
1011	1	1	3/30/1993	152.5	2	3

Table 13. Distribution of rut depth data sets based on LTPP regions (Reg_Actual), base type (Base_D), and major M&R intervention factor (CND)

Between-Subjects Factors

Group		Value Label	N	Percentage
Reg_Actual	1	North Atlantic	7	3.3%
	2	North Central	23	10.7%
	3	Southern	175	81.8%
	4	Western	9	4.2%
Base_D	0	Stabilized Base	83	38.8%
	1	Granular Base	131	61.2%
CND	0	No Major M,R&R	159	74.3%
	1	Major M,R&R Applied	55	25.7%

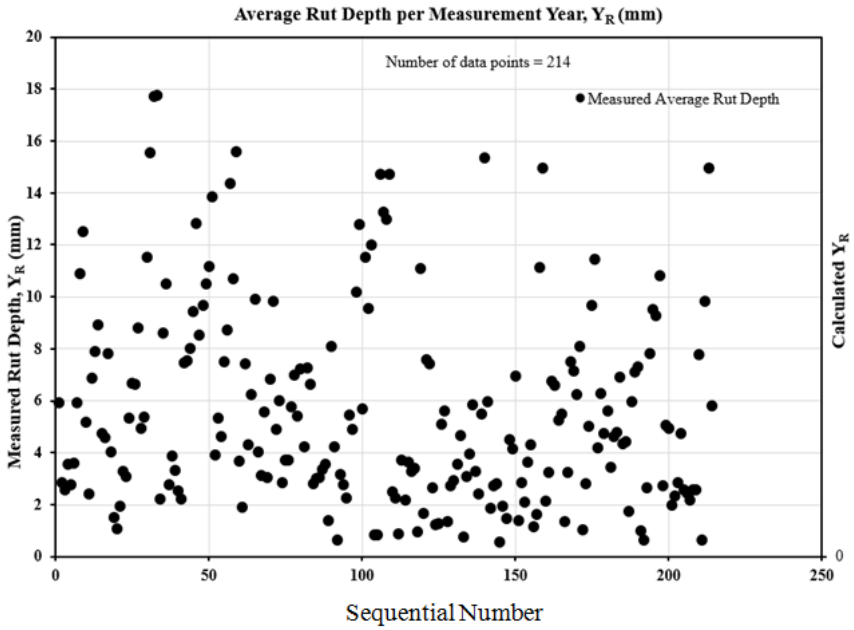

Figure 21. Distribution of the rut depth per measurement year data according to sequential number

2.3.3 Methodologies for Enhanced Rutting Modeling

The following key steps are considered to develop rutting progression prediction model equation:

1. Data screening indicated a few test sections with zero average rut depth values (Table 14) and therefore, the data were removed from the database.

Table 14. Lists of test section in the LTPP database with zero rut depth values

No.	Test Sections	Survey Date for Rut Depth	Reasons
1	28-3083	11/8/1995	Zero average rut depth values
2	28-3085	11/9/1995	
3	28-3091	9/1/1978	
4	36-1644	5/4/1992	
5	48-1048	5/20/1991	
6	48-3835	12/9/1991	
7	47-9024	4/18/1995	

2. Further observation showed the average rut depth data for test section 47-3101 were suspected for error. This test section had rut depth data sets for 1990, 1991, and 1995, and assigned as CN one to CN three as shown in Table 15. The rut depth data surveyed on 4/20/1995 were not supposed to have zero value since the road was opened to traffic on 1/1/1980, and there was no major maintenance and rehabilitation treatment taking place. In 1995 the major maintenance of road milling and overlay with asphalt pavement (LTPP code: 51) only happened about 50 weeks after the measurement of the rut depth on 4/20/1995. Therefore the zero values of rut depth were ambiguous and questionable, which resulted in the termination of the data set from the model database.

Table 15. Test section 47-3101: Rut depth survey date and CN attributes

SHRP ID	CN	CN Assigned Date	CN Change Reason	Rut Depth Survey Date	Rut Depth Data
47-3101	1	1/1/1987		11/16/1990	Available
	2	9/1/1995	51	18/14/1991	Available
	3	5/15/1998	25	4/20/1995	**Zero Values**

3. After several iterations, it was noticed that the average rut depth per measurement year data need transformation using a $\log_{10}$ function to obtain a linear relationship between two variables. Additionally, a dependent variable of $\text{Log}_{10}(Y_R+0.5)$ was used to allow zero rut depth zero rut depth value to be considered in the development of the enhanced model equations. This variance stabilizing transformation was in this research and it appears that the data were more compressed and less scattered as compared to the rut depth data without log base 10 function. A total of 214 normally distributed data sets were considered in the database for the development of the enhanced rutting prediction equation.

4. Prior to the development of multiple regression model equation, the data were evaluated to ensure that the data are (1) random, (2) independent of each other, and (3) normally distributed. Additionally, the variance between the measured and predicted average rut depth per measurement year data must be homogenous. The results follow:

- The data were random because the average rut depth data are measured for different test sections in different states throughout the U.S.
- The data were independent of each other since the average measured rut depth data are for different years. The autocorrelation test shows a low value of 0.42, which suggests that data were independent of each other.
- The normality test has proved that the data are normally distributed with a mean of 0.70 mm and a standard deviation of 0.28 mm. Table 16 shows the result of Kolmogorov-Smirnov normality test.

Table 16. Test of normality for average rut depth per measurement year data sets

	Kolmogorov-Smirnov[a]		
	Statistic	df	Sig.
$Log_{10}(Y_R+0.5)$	.040	214	0.200*
*This is lower bound of the true significance a. Lilliefors Significance Correction			

The test hypotheses for probability of type I error α equal to 0.05 follows:

Null hypothesis, H_0: The distribution of the average rut depth data per measurement year data is normal

Alternative hypothesis, H_A: The distribution of the average rut depth data per measurement year data is not normal

The normality test for average rut depth data per measurement year data in the LTPP database showed that the probability of significance, p-value (Sig.) was more than the α 0.05 probability of chance error, which is not statistically significant for Kolmogorov-Smirnov normality test. Therefore, the test failed to reject null hypothesis and the average rut depth data per measurement year data are normally distributed. Figure 22 shows histogram plot of average rut depth per measurement year with descriptive statistics and normal distribution plot for the data used in this research.

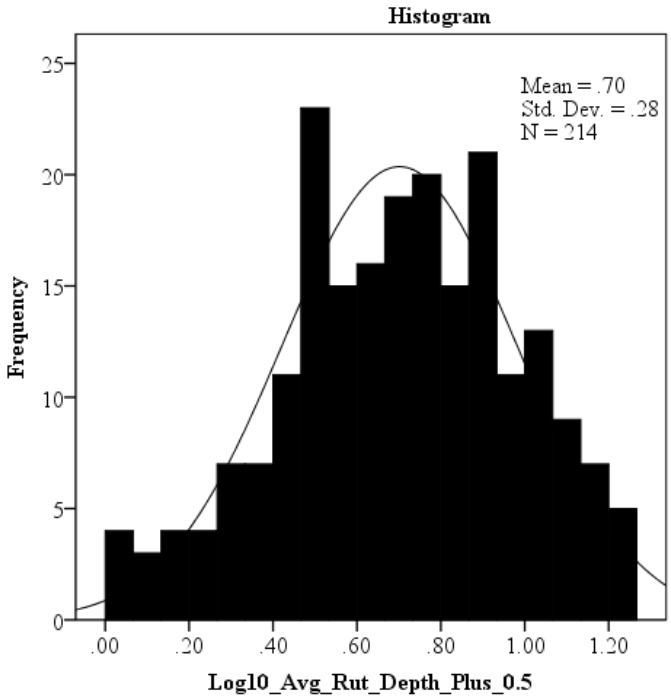

Figure 22. Histogram plot of average rut depth per measurement year with descriptive statistics and normal distribution curve

The distribution of the data follows the bell curve of normal distribution. This histogram supports the results from the normality test, which indicates that the average rut depth data per measurement year are normally distributed.

5. The ANOVA test assesses the effects of M&R history, LTPP climatic regions, and base type (stabilized and granular) on the average rut depth per measurement year data and the results are shown in Table 17. For CND factor, there is statistically significant difference in the average rut depth per measurement year before and after major M&R treatments. The main effects of the base type (Base_D) factor and LTPP climatic region (Reg_D) alone are not showing statistically significant difference in the means of the average rut depth per measurement year. However, the interactions of CND with base type, and CND with LTPP climatic region show statistically significant difference in the means of the average rut depth per measurement year. Therefore, the CND, Base_D, and Reg_D factors are used as the dummy variables in both multiple regression and ANN modeling of rutting prediction equations.

Table 17. ANOVA tests of between-subjects effects for average rut depth per measurement year

Source	Type III Sum of Squares	df	Mean Square	F	Sig.
Corrected Model	389.703[a]	13	29.977	2.250	.009
Intercept	1169.695	1	1169.695	87.792	.000
Reg_Actual	35.386	3	11.795	.885	.450
Base_D	6.625	1	6.625	.497	.482
CND	63.208	1	63.208	4.744	.031
Reg_Actual * Base_D	25.093	2	12.546	.942	.392
Reg_Actual * CND	110.183	3	36.728	2.757	.044
Base_D * CND	58.478	1	58.478	4.389	.037
Reg_Actual * Base_D * CND	41.711	2	20.856	1.565	.212
Error	2664.706	200	13.324		
Total	9771.050	214			
Corrected Total	3054.409	213			

a. R Squared = .128 (Adjusted R Squared = .071)

6. Table 18 shows the independent variables used to develop the enhanced rutting multiple regression equation and ANN model equation. The age, SN, CESAL, $TEMP_{AIR}$, PRECIP, Reg_D, and CND variables are already described in previous sub-chapter (IRI roughness modeling).

Table 18. List of independent variables for the rutting progression prediction model equation

No.	Independent Variable	Notes	Unit
1	$Log_{10}\ Y_{R0}$	Log_{10} Initial average rut depth per measurement year	-
2	Age	Pavement age	Year
3	CESAL	Annual cumulative ESALs	Year
4	$TEMP_{AIR}$	Air temperature during rut depth measurement	°C
5	E_1	Asphalt modulus	psi
6	E_2	Base modulus	psi
7	E_3	Subbase modulus	psi
8	E_4	Subgrade modulus	psi
9	T_1	Asphalt thickness	inch
10	T_T	Total thicknesses (T_T), Asphalt thickness (T_1), base layer thickness (T_2), and subbase layer thickness (T_3): $T_T = T_1 + T_2 + T_3$	inch
11	SN	Structural Number	-
12	CND	Dummy variable for CN (0 if no major M&R treatment history, 1 if major M&R treatment has taken place)	-
13	Reg_D	Dummy variable for LTPP climatic regions (zero for Southern region, one for other regions)	-
14	Base_D	Dummy variable for base layer type (zero for stabilize base, one for granular base)	-

Since rutting is a structural related problem, additional independent variables that are related to structural integrity of pavement layers (layer thicknesses and modulus values) are introduced in the enhanced rutting multiple regression equation and ANN model equation. The modulus values for asphalt (E_1), base (E_2), subbase (E_3), and subgrade (E_4) layers are calculated using the equations developed by Uddin [85]. If the calculated layer modulus values are less than

or more than the minimum and maximum modulus values, respectively, change the modulus values based on the ranges proposed by Uddin [85]. However, best judgments are required to decide whether or not to keep or discard the modulus values that are slightly above or below the proposed ranges.

Initially, the modulus value for subgrade layer is calculated, followed by the asphalt layer modulus value. Then the modulus values for base layer and subbase layers are calculated, respectively. Uddin [85] developed separate multiple regression equations for stabilized and granular base, respectively, in order to calculate modulus values for all layers as described in the following paragraph.

Subgrade Layer (Modulus values typically between 10,000 to 50,000 psi)

Subgrade layer modulus value (E_4) for pavement system with stabilized base layer is calculated using Equation 2.30. Meanwhile, subgrade layer modulus for pavement system with granular base layer is calculated using Equation 2.31.

$$E_4 = 10^y;\ y = 5.42783 + 0.00894\ (X_7) - 0.14851\ (X_9) - 0.86213(X_{13}) \quad (2.30)$$

Where:

$X_7 = \text{Log}_{10}(1+T_3)$; T_3 is thickness of subbase layer (inches)

$X_9 = \text{Log}_{10}(R_2 \times W_2)$; R_2 is radial distance of FWD sensor number two from the center of loading area (12 inches), W_2 is peak deflection under sensor number two (mils) for FWD load normalized to 1,000 lbs.

$X_{13} = Log_{10}(R_6 \times W_6)$; R_6 is radial distance of FWD sensor number six from the center of loading area (60 inches), W_6 is peak deflection under sensor number six (mils) for FWD load normalized to 1,000 lbs.

$$E_4 = 10^y; \; y = 5.43813 - 0.15369\,(X_9) + 0.04114\,(X_{10}) - 0.90072\,(X_{12}) \quad (2.31)$$

Where:

$X_9 = Log_{10}(R_2 \times W_2)$; R_2 is radial distance of FWD sensor number two from the center of loading area (12 inches), W_2 is peak deflection under sensor number two (mils) for FWD load normalized to 1,000 lbs.

$X_{10} = Log_{10}(R_3 \times W_3)$; R_3 is radial distance of FWD sensor number three from the center of loading area (24 inches), W_3 is peak deflection under sensor number three (mils) for FWD load normalized to 1,000 lbs.

$X_{12} = Log_{10}(R_5 \times W_5)$; R_5 is radial distance of FWD sensor number five from the center of loading area (48 inches), W_5 is peak deflection under sensor number five (mils) for FWD load normalized to 1,000 lbs.

Asphalt Layer (Modulus values typically between 100,000 to 1,000,000 psi)

Asphalt layer modulus value (E_1) for pavement system with stabilized base layer is calculated using Equation 2.32. Meanwhile, asphalt layer modulus value for pavement system with granular base layer is calculated using Equation 2.33.

$$E_1 = \frac{10^y}{(T_1)^3} \quad (2.32)$$

Where;

$y = 2.91794 + 3.51615 (X_5) - 3.28093 (X_8) + 5.97415 (X_9) - 4.76039 (X_{10}) + 1.49939 (X_{13})$

$X_5 = Log_{10} (1+T_1)$; T_1 is thickness of asphalt layer (inches)

$X_8 = Log_{10} (R_1 \times W_1)$; R_1 is radial distance of FWD sensor number one from the center of loading area (0 inch), W_1 is peak deflection under sensor number one (mils) for FWD load normalized to 1,000 lbs. Set $R_1 \times W_1$ to zero value due to zero R_1.

$X_9 = Log_{10} (R_2 \times W_2)$; R_2 is radial distance of FWD sensor number two from the center of loading area (12 inches), W_2 is peak deflection under sensor number two (mils) for FWD load normalized to 1,000 lbs.

$X_{10} = Log_{10} (R_3 \times W_3)$; R_3 is radial distance of FWD sensor number three from the center of loading area (24 inches), W_3 is peak deflection under sensor number three (mils) for FWD load normalized to 1,000 lbs.

$X_{13} = Log_{10} (R_6 \times W_6)$; R_6 is radial distance of FWD sensor number six from the center of loading area (60 inches), W_6 is peak deflection under sensor number six (mils) for FWD load normalized to 1,000 lbs.

$$E_1 = \frac{10^y}{(T_1)^3} \tag{2.33}$$

Where; $y = -22.82457 + 2.35850 (X_5) - 4.37037 (X_8) + 6.60322 (X_9) - 3.21414 (X_{10}) + 4.83214 (X_{16})$

$X_5 = Log_{10} (1+T_1)$; T_1 is thickness of asphalt layer (inches)

$X_8 = Log_{10}(R_1 \times W_1)$; R_1 is radial distance of FWD sensor number one from the center of loading area (0 inch), W_1 is peak deflection under sensor number one (mils) for FWD load normalized to 1,000 lbs. Set $R_1 \times W_1$ to zero value due to zero R_1.

$X_9 = Log_{10}(R_2 \times W_2)$; R_2 is radial distance of FWD sensor number two from the center of loading area (12 inches), W_2 is peak deflection under sensor number two (mils) for FWD load normalized to 1,000 lbs.

$X_{10} = Log_{10}(R_3 \times W_3)$; R_3 is radial distance of FWD sensor number three from the center of loading area (24 inches), W_3 is peak deflection under sensor number three (mils) for FWD load normalized to 1,000 lbs.

$X_{16} = Log_{10}(X_{15})$

Where; $X_{15} = (R_6 \times W_6 \times E_4)$; R_6 is radial distance of FWD sensor number six from the center of loading area (60 inches), W_6 is peak deflection under sensor number six (mils) for FWD load normalized to 1,000 lbs, E_4 is modulus value for subgrade layer.

Base Layer (Modulus values typically between 22,500 to 80,000 psi for granular base layer, and 25,000 to 600,000 psi for stabilized base layer)

Base layer modulus value (E_2) for pavement system with stabilized base layer is calculated using Equation 2.34. Meanwhile, base layer modulus value for pavement system with granular base layer is calculated using Equation 2.35.

$$E_2 = \frac{10^y}{(1+T_2)^3} \tag{2.34}$$

Where; $y = 31.99946 - 1.20607 (X_5) + 2.40370 (X_6) - 1.22023 (X_8) - 3.19149 (X_9) + 2.84323(X_{12}) - 4.68852 (X_{16})$

$X_5 = Log_{10}(1+T_1)$; T_1 is thickness of asphalt layer (inches),

$X_6 = Log_{10}(1+T_2)$; T_2 is thickness of base layer (inches),

$X_8 = Log_{10}(R_1 \times W_1)$; R_1 is radial distance of FWD sensor number one from the center of loading area (0 inch), W_1 is peak deflection under sensor number one (mils) for FWD load normalized to 1,000 lbs. Set $R_1 \times W_1$ to zero value due to zero R_1.,

$X_9 = Log_{10}(R_2 \times W_2)$; R_2 is radial distance of FWD sensor number two from the center of loading area (12 inches), W_2 is peak deflection under sensor number two (mils) for FWD load normalized to 1,000 lbs,

$X_{12} = Log_{10}(R_5 \times W_5)$; R_5 is radial distance of FWD sensor number five from the center of loading area (48 inches), W_5 is peak deflection under sensor number five (mils) for FWD load normalized to 1,000 lbs,

$X_{16} = Log_{10}(X_{15})$

Where; $X_{15} = (R_6 \times W_6 \times E_4)$; R_6 is radial distance of FWD sensor number six from the center of loading area (60 inches), W_6 is peak deflection under sensor number six (mils) for FWD load normalized to 1,000 lbs, E_4 is modulus value for subgrade layer.

$$E_2 = \frac{10^y}{(1+T_2)^3} \tag{2.35}$$

Where; $y = 27.17619 - 1.23502 (X_4) - 0.50339 (X_5) + 3.38241(X_6) - 0.59163(X_8) - 1.32598(X_9) - 2.9170 (X_{16})$

$X_4 = Log_{10}(E_4)$; E_4 is modulus value for subgrade layer,

$X_5 = Log_{10}(1+T_1)$; T_1 is thickness of asphalt layer (inches),

$X_6 = Log_{10}(1+T_2)$; T_2 is thickness of base layer (inches),

$X_8 = Log_{10} (R_1 \times W_1)$; R_1 is radial distance of FWD sensor number one from the center of loading area (0 inch), W_1 is peak deflection under sensor number one (mils) for FWD load normalized to 1,000 lbs. Set $R_1 \times W_1$ to zero value due to zero R_1,

$X_9 = Log_{10} (R_2 \times W_2)$; R_2 is radial distance of FWD sensor number two from the center of loading area (12 inches), W_2 is peak deflection under sensor number two (mils) for FWD load normalized to 1,000 lbs,

$X_{16} = Log_{10} (X_{15})$

Where; $X_{15} = (R_6 \times W_6 \times E_4)$; R_6 is radial distance of FWD sensor number six from the center of loading area (60 inches), W_6 is peak deflection under sensor number six (mils) for FWD load normalized to 1,000 lbs, E_4 is modulus value for subgrade layer.

Subbase Layer (Modulus values typically between 10,000 to 50,000 psi)

Subbase layer modulus value (E_3) for pavement system with stabilized base layer is calculated using Equation 2.36. Meanwhile, subbase layer modulus value for pavement system with granular base layer is calculated using Equation 2.37.

$$E_3 = \frac{10^y}{(T_3)^3} \tag{2.36}$$

Where; $y = 4.55483 - 0.17133 (X_5) - 0.27774 (X_6) + 3.44927 (X_7) - 1.81765 (X_{10}) + 1.52304 (X_{13})$

$X_5 = Log_{10} (1+T_1)$; T_1 is thickness of asphalt layer (inches),

$X_6 = Log_{10} (1+T_2)$; T_2 is thickness of base layer (inches),

$X_7 = Log_{10} (1+T_3)$; T_3 is thickness of subbase layer (inches),

$X_{13} = Log_{10}(R_6 \times W_6)$; R_6 is radial distance of FWD sensor number six from the center of loading area (60 inches), W_6 is peak deflection under sensor number six (mils) for FWD load normalized to 1,000 lbs,

$X_{10} = Log_{10}(R_3 \times W_3)$; R_3 is radial distance of FWD sensor number three from the center of loading area (24 inches), W_3 is peak deflection under sensor number three (mils) for FWD load normalized to 1,000 lbs.

$$E_3 = \frac{10^y}{(T_3)^3} \tag{2.37}$$

Where; $y = -9.14746 - 0.37575(X_5) - 0.23825(X_6) + 3.42105(X_7) - 1.05695(X_9) - 0.93991(X_{10}) + 1.36417(X_{13}) + 2.61730(X_{16})$

$X_5 = Log_{10}(1+T_1)$; T_1 is thickness of asphalt layer (inches),

$X_6 = Log_{10}(1+T_2)$; T_2 is thickness of base layer (inches),

$X_7 = Log_{10}(1+T_3)$; T_3 is thickness of subbase layer (inches),

$X_9 = Log_{10}(R_2 \times W_2)$; R_2 is radial distance of FWD sensor number two from the center of loading area (12 inches), W_2 is peak deflection under sensor number two (mils) for FWD load normalized to 1,000 lbs,

$X_{10} = Log_{10}(R_3 \times W_3)$; R_3 is radial distance of FWD sensor number three from the center of loading area (24 inches), W_3 is peak deflection under sensor number three (mils) for FWD load normalized to 1,000 lbs,

$X_{13} = Log_{10}(R_6 \times W_6)$; R_6 is radial distance of FWD sensor number six from the center of loading area (60 inches), W_6 is peak deflection under sensor number six (mils) for FWD load normalized to 1,000 lbs,

$X_{16} = Log_{10}(X_{15})$

Where; $X_{15} = (R_6 \times W_6 \times E_4)$; R_6 is radial distance of FWD sensor number six from the center of loading area (60 inches), W_6 is peak deflection under sensor number six (mils) for FWD load normalized to 1,000 lbs, E_4 is modulus value for subgrade layer.

7. Table 19 shows the maximum, minimum, average, SD, and COV (%) for the data sets used in the development of the enhanced rutting condition deterioration prediction equations.

Table 19. Descriptive statistics for independent variables used to develop rutting model equations

Descriptive Statistics	Rut depth per measurement year, Y_R (mm)	Initial rut depth per measurement year, Y_{R0} (mm)	Age (Year)	Cumulative ESAL, CESAL	Air Temperature, $TEMP_{AIR}$ (°C)	Asphalt Modulus, E_1(psi)
Maximum	17.8	15.4	28.0	7,612,665	31.1	1,183,987
Minimum	0.5	0.5	0.0	3,000	-3.0	100,000
Average	5.6	5.1	13.2	491,616	19.7	553,611
SD	3.8	3.2	6.3	928,150	7.7	398,513
COV (%)	67.7	63.6	47.7	189	39.2	72

Descriptive Statistics	Base Modulus, E_2 (psi)	Subbase Modulus, E_3 (psi)	Subgrade Modulus, E_4 (psi)	Asphalt Thickness, T_1 (inches)	Total Thickness, T_T (inches)	SN
Maximum	862,470	129,359	53,270	14.6	34.7	8.8
Minimum	0	0	9,034	0.9	7.2	1.0
Average	198,122	18,726	19,128	4.9	18.7	4.0
SD	218,557	25,293	9,970	3.2	6.5	1.5
COV (%)	110	135	52	65.3	34.8	38.5

8. The enhanced rutting multiple regression equation and ANN model equation were developed and the reasonableness of the multiple regression and ANN model equations were evaluated based on the following parameters:

- The R value of the multiple regression equations

- The predicted against measured data plots
- The verifications of the multiple regression equations
- The accuracy measures of the MARE and RMSE

9. Initially two enhanced rutting multiple regression equations were developed as shown in Equations 2.38 and 2.39, respectively. Equation 2.38 contains additional variable of peak deflection values under sensor one (DEF_{W1}) normalized to 1,000 lbs FWD load and measured in mils. Due to difficulty to predict future value for $DEF_{W1,}$ this independent variable was not selected in the final multiple regression equation. Therefore Equation 2.39 without DEF_{W1} variable was proposed as the final enhanced rutting multiple regression equation.

$$Log_{10}(Y_R+0.5) = 0.032 + 0.952\,(Log_{10}(Y_{R0}+0.5)) - 0.000447\,(Age) + 2.607\times10^{-9}\,(CESAL) + 0.023\,(SN) + 1.843\times10^{-8}\,(E_1) - 1.158\times10^{-7}\,(E_2) - 3.465\times10^{-8}\,(E_3) + 4.855\times10^{-7}\,(E_4) - 0.000173\,(TEMP_{AIR}) + 0.013\,(DEF_{W1}) + 0.003\,(Reg\_D) + 0.006\,(CND) - 0.037\,(Base\_D) + 8.145\times10^{-6}\,(T_T) - 0.01\,(T_1) \quad (2.38)$$

$$Log_{10}(Y_R+0.5) = 0.058 + 0.952\,(Log_{10}(Y_{RO}+0.5)) - 0.000481\,(Age) + 2.962\times10^{-9}\,(CESAL) + 0.021\,(SN) + 2.562\times10^{-8}\,(E_1) - 1.356\times10^{-7}\,(E_2) - 1.171\times10^{-7}\,(E_3) + 2.348\times10^{-7}\,(E_4) - 0.000141\,(TEMP_{AIR}) + 0.010\,(Reg\_D) + 0.006\,(CND) - 0.041(Base\_D) + 0.000259\,(T_T) - 0.011\,(T_1) \quad (2.39)$$

10. Subsequently, the $ANN_{15\text{-}3\text{-}1}$ was observed to give the optimum network for the prediction of future rutting value using the ANN model equation. The $ANN_{15\text{-}3\text{-}1}$ refers to a total of 15

inputs ($Log_{10}(Y_{R0}+0.5)$, Age, CESAL, SN, E_1, E_2, E_3, E_4, $TEMP_{AIR}$, Reg_D, CND, Base_D, T_T, T_1, DEF_{W1}), three hidden nodes, and one output ($Log_{10}(Y_R+0.5)$.

11. The final results are shown in Figure 23 and Figure 24. Figure 25 shows the measured and predicted values using the enhanced multiple regression prediction equation with respect to data sequential number on the x-axis.

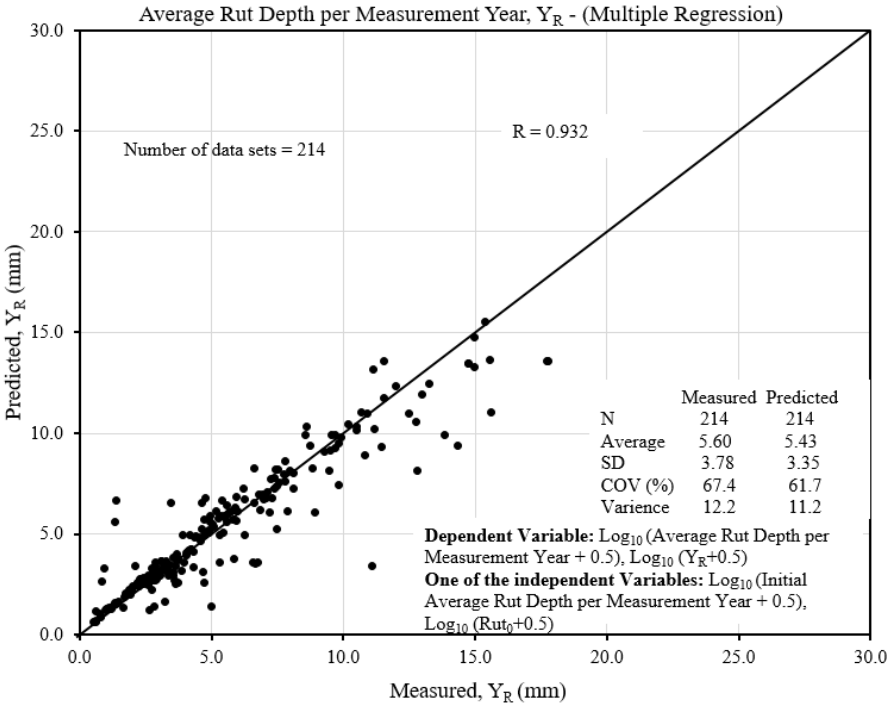

Figure 23. Predicted vs measured plot for rut depth multiple regression equation database

The average rut depth per measurement year data that were transformed using log_{10} form, showed lesser variances in the measured and predicted values as shown in Figure 23. This is the best transformation model to reduce the variance of the average rut depth per measurement year data. The data are less scattered and aligned closely to the equity line with a higher R of 0.932. This implies that the variances are more uniform between the measured and predicted values,

with only -8% difference compared to the measured average rut depth per measurement year. Therefore the assumption of the homogeneity of the variance is met.

The ANN model results are shown in Figures 26 to 28. The model database and verification results are outstanding for both enhanced multiple regression model equation and ANN model equation. Therefore, both enhanced rutting IRI multiple regression equations and ANN model equation are recommended for implementation.

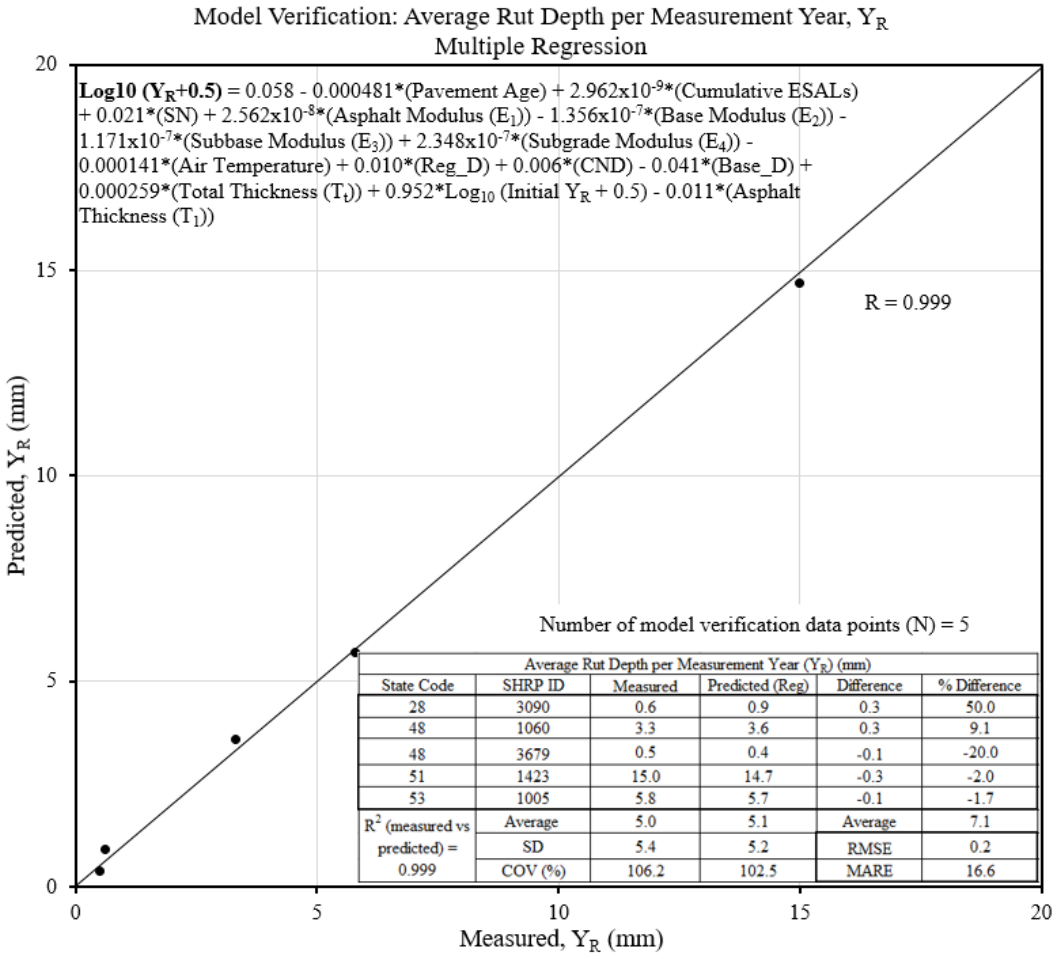

Average Rut Depth per Measurement Year (Y_R) (mm)

State Code	SHRP ID	Measured	Predicted (Reg)	Difference	% Difference
28	3090	0.6	0.9	0.3	50.0
48	1060	3.3	3.6	0.3	9.1
48	3679	0.5	0.4	-0.1	-20.0
51	1423	15.0	14.7	-0.3	-2.0
53	1005	5.8	5.7	-0.1	-1.7
R^2 (measured vs predicted) = 0.999	Average	5.0	5.1	Average	7.1
	SD	5.4	5.2	RMSE	0.2
	COV (%)	106.2	102.5	MARE	16.6

Figure 24. Predicted vs measured plot for rut depth multiple regression verification database

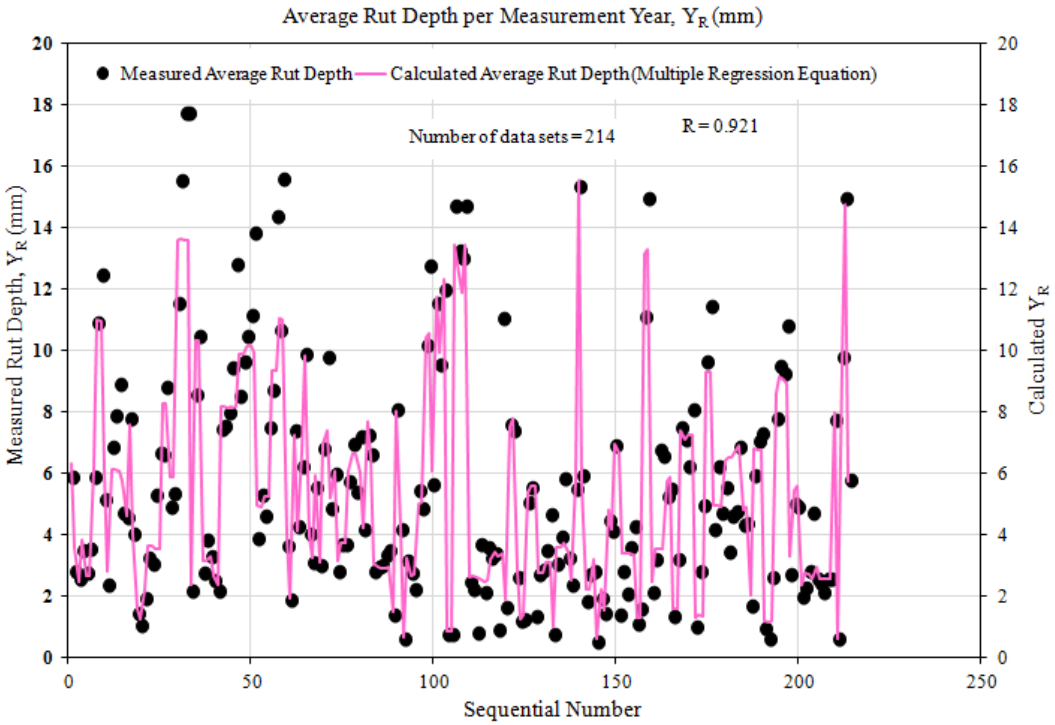

Figure 25. Measured and predicted rut depth using multiple regression based on sequential number

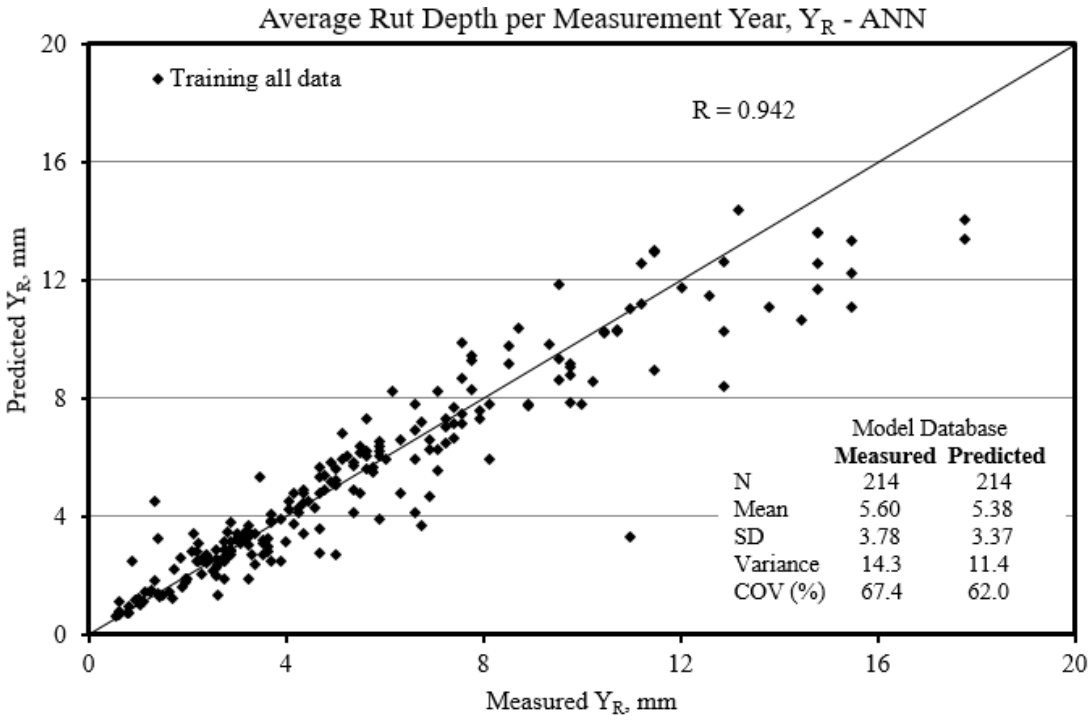

Figure 26. Predicted vs measured plot for rut depth ANN model database

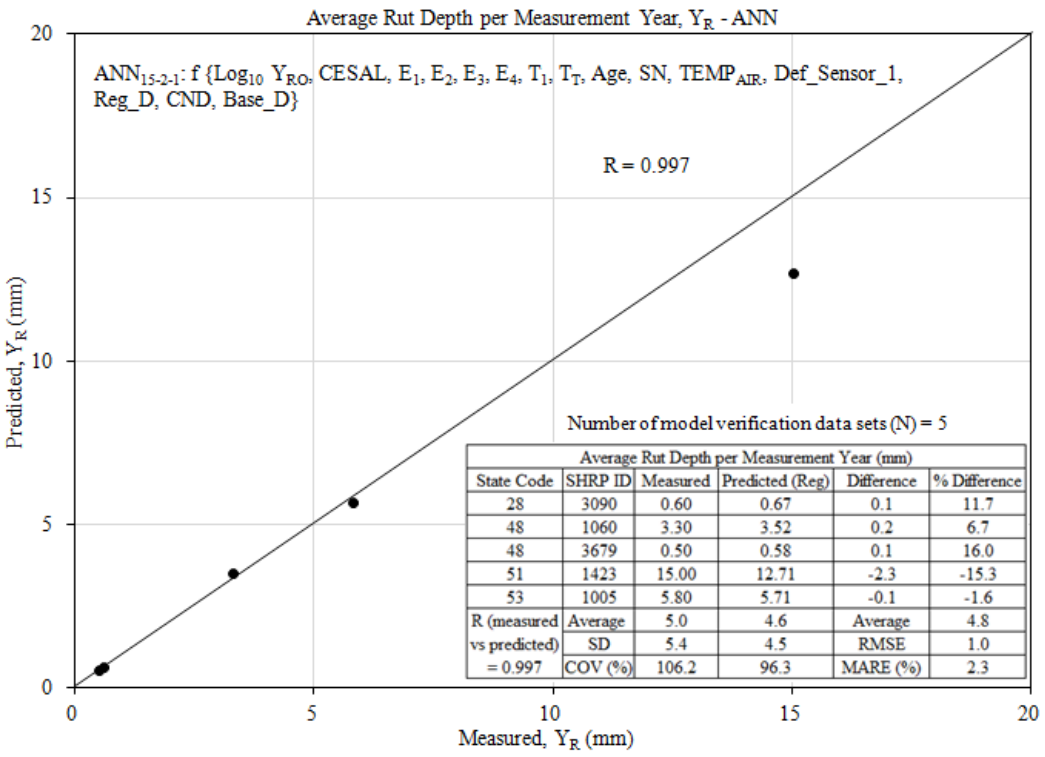

Average Rut Depth per Measurement Year (mm)					
State Code	SHRP ID	Measured	Predicted (Reg)	Difference	% Difference
28	3090	0.60	0.67	0.1	11.7
48	1060	3.30	3.52	0.2	6.7
48	3679	0.50	0.58	0.1	16.0
51	1423	15.00	12.71	-2.3	-15.3
53	1005	5.80	5.71	-0.1	-1.6
R (measured	Average	5.0	4.6	Average	4.8
vs predicted)	SD	5.4	4.5	RMSE	1.0
= 0.997	COV (%)	106.2	96.3	MARE (%)	2.3

Figure 27. Predicted vs measured plot for rut depth ANN verification database

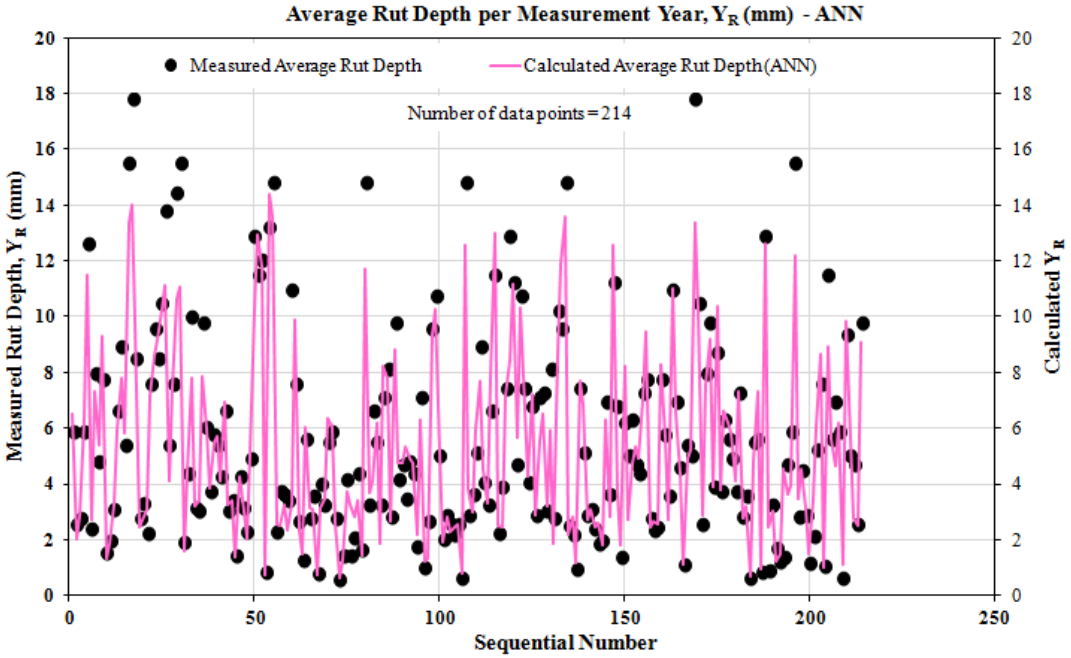

Figure 28. Measured and predicted rut depth using ANN model equation based on sequential number

The enhanced rutting multiple regression equation developed in this research is easier to use for future rutting prediction considering reasonable input parameters such as initial rut depth value, cumulative traffic ESAL, layer modulus values, and asphalt thickness, total layer thicknesses, pavement age, SN, and air temperature. Moreover, the enhanced rutting multiple regression equation also considers important factors such as maintenance and rehabilitation intervention factor, LTPP climatic region factor, and base layer types.

2.4 Unified Cracking Index (UCI) Development and Predictive Model Equations

In the MEPDG, asphalt surface cracking distresses are classified as load-related cracking (alligator cracking and longitudinal cracking), non-load related cracking (transverse crack), and reflective cracking type. However, the latter is not one of the cracking distress types that are in favor of this research. The following subchapters show the performance models for cracking distress predictions.

2.4.1 Load-Related Cracking (Alligator and Longitudinal Cracks)

The MEPDG describes alligator crack as a load related distress that initiate from initiate from the bottom of asphalt layer and propagate upwards due to traffic load repetitions. In contrast, the longitudinal cracks are assumed to initiate from the asphalt surface [84]. The incremental damage index approach was used to predict both alligator and longitudinal crack distresses. Equations 2.40 to 2.49 were used in the mechanistic-empirical design method of asphalt pavements.

$$N_{f-HMA} = k_{f1}\ x\ (C)\ x\ (C_H)\ x\ \beta_{f1}\ x\ (\varepsilon_t)^{k_{f2}\beta_{f2}}(E_{HMA})^{k_{f2}\beta_{f3}} \quad (2.40)$$

$$C = 10^{M} \quad (2.41)$$

$$M = 4.84\,x\,\left[\frac{V_{be}}{V_a+V_{be}} - 0.69\right] \quad (2.42)$$

The MEPDG determine the thickness correction term, C_H for alligator crack and longitudinal crack based on Equation 2.43 and Equation 2.44, respectively.

$$C_H = \frac{1}{0.000398+\frac{0.003602}{1+e^{(11.02-3.49H_{HMA})}}} \quad (2.43)$$

$$C_H = \frac{1}{0.01+\frac{12.0}{1+e^{(15.676-2.8186H_{HMA})}}} \quad (2.44)$$

The incremental damage index (ΔDI) is calculated by dividing the actual number of axle loads by the allowable number of axle as described in Equation 2.45.

$$DI = \sum(\Delta DI)_{j,m,l,p,T} = \sum\left(\frac{n}{N_{f-HMA}}\right)_{j,m,l,p,T} \quad (2.45)$$

Finally, the area of alligator cracking (FC_{BOTTOM}) is predicted using Equation 2.46. Equation 2.49 is used to calculate the longitudinal fatigue cracks (FC_{TOP}) [84].

$$FC_{Bottom} = \left(\frac{1}{60}\right)\left(\frac{C_4}{1+e^{(C_1C_1^*+C_2C_2^*\log(DI_{Bottom}*100))}}\right) \quad (2.46)$$

$$C_1^* = -2C_2^* \quad (2.47)$$

$$C_2^* = -240874 - 39.748(1 + H_{HMA})^{-2.856} \quad (2.48)$$

$$FC_{TOP} = 10.56\left(\frac{C_4}{1+e^{(C_1-C_2\log(DI_{TOP}))}}\right) \quad (2.49)$$

Table 2.4A summarizes the explanations for each parameter used in the MEPDG equations to calculate the alligator and longitudinal cracks.

Table 20. List of parameters used in the MEPDG equations to calculated alligator and longitudinal cracks

Parameters	Explainations
N_{f-HMA}	Allowable number of axle-load applications for a flexible pavement and HMA overlays
ε_t	Tensile strain at critical locations and calculated by the structural response model, in./in
E_{HMA}	Dynamic modulus of the HMA measured in compression (psi),
k_{f1}, k_{f2}, k_{f3}	Global field calibration parameters (from the NCHRP 1-40D re-calibration; k_{f1}= 0.007566, k_{f2}= -3.9492, k_{f3}= -1.281
$\beta_{f1}, \beta_{f2}, \beta_{f3}$	Local or mixture specific field calibration constants; for the global calibration effort, these constants were set to 1.0
V_{be}	Effective asphalt content by volume, %,
V_a	Percent air voids in the HMA mixture
C_H	Thickness correction term, dependent on type of cracking
H_{HMA}	Total HMA thickness, in.,
n	Actual number of axle-load applications within specific time period
j	Axle-load interval
m	Axle-load type (single, tandem, tridem, quad, or special axle configuration
l	Truck type using the truck classification groups included in the MEPDG
ρ	Month
T	Median temperature for the five temperature intervals or quintiles used to subdivide each month, ˚F
FC_{Bottom}	Area of alligator cracking that initiates at the bottom of the HMA layers, % of total lane area
DI_{Bottom}	Cumulative damage index at the bottom of the HMA layers
$C_{1,2,4}$	Transfer function regression constants; C_4 = 6,000; C_1 = 1.00; and C_4 = 1.00
H_{HMA}	Total HMA thickness, in
FC_{Top}	Length of longitudinal cracks that initiate at the top of the HMA layer, ft/mi
DI_{Top}	Cumulative damage index near the top of the HMA surface
$C_{1,2,4}$	Transfer function regression constants; C_1= 7.00; C_2= 3.5; C_4= 1,000

The MEPDG also provides specific equation to calculate fatigue crack in the Cement Treated Base (CTB) layer as shown in Equation 2.50 and Equation 2.51. Equation 2.50 is used to determine the number of load application N_{f-CTB} for fatigue cracks in the CTB layers.

$$N_{f-CTB} = 10^{\left[\frac{k_{C1}\beta_{C1}\left(\frac{\sigma_t}{M_R}\right)}{k_{c2}\beta_{c2}}\right]} \quad (2.50)$$

$$FC_{CTB} = C_1 + \frac{C_2}{1+e^{(C_3 - C_4 \log(DI_{CTB}))}} \quad (2.51)$$

Equation 2.52 is used to calculate the damaged elastic modulus within each time period for calculating critical pavement responses in the CTB and other pavement layers. Table 21 summarizes the explanations for each parameter used in the MEPDG equations to calculated fatigue crack in the CTB layer.

$$E_{CTB}^{D(T)} = E_{CTB}^{Min} + \left(\frac{E_{CTB}^{Max} - E_{CTB}^{Min}}{1+e^{(-4+14(DI_{CTB}))}}\right) \quad (2.52)$$

Table 21. List of parameters used in the MEPDG equations to calculated alligator and longitudinal cracks

N_{f-CTB}	Allowable number of axle-load applications for a semi-rigid pavement
σ_t	Tensile stress at the bottom of the CTB layer (psi),
M_R	28-days modulus of rupture for the CTB layer, psi. Value used in the calculations is 650 psi
σ_t	Tensile stress at the bottom of the CTB layer (psi)
DI_{CTB}	Cumulative damage index of the CTB or cementitious layer determined in accordance with Equation 3e
k_{c1}, k_{c2}	MEPDG used 1.0 for these values
β_{c1}, β_{c2}	Local calibration constants; these values are set to 1.0 in the software
FC_{CTB}	Area of fatigue cracking, sq ft
$C_{1,2,3,4}$	Transfer function regression constants; C_1= C_2= 1.0, C_3= 0, and C_4= 1,000 (this value are not calibrated and may change once the transfer function has been calibrated
$E_{CTB}^{D(T)}$	Equivalent damaged elastic modulus at time t for the CTB layer (psi),
E_{CTB}^{Min}	Equivalent elastic modulus for total destruction of the CTB (psi),
E_{CTB}^{Max}	28-days elastic modulus of the intact CTB layer, no damage (psi)

2.4.2 Non-Load Related Cracking – Thermal Cracking (Transverse Cracking)

The MEPDG describes transverse cracking as a distress that is non-load related and predominantly perpendicular to the traffic direction. The low temperatures thermal cracking is

the main reason for this type of cracking distress. The following Equations 2.53 to 2.57 are used to predict the thermal cracking.

$$\Delta C = A(\Delta K)^n \tag{2.53}$$

$$A = 10^{k_t \beta_t (4.389 - 2.52 \log(E_{HMA} \sigma_m n))} \tag{2.54}$$

$$n = 0.8\left[1 + \frac{1}{m}\right] \tag{2.55}$$

$$K = \sigma_{tip}\left[0.45 + 1.99{C_o}^{0.56}\right] \tag{2.56}$$

$$TC = \beta_{t1} N\left[\frac{1}{\sigma_d} \log\left(\frac{C_d}{H_{HMA}}\right)\right] \tag{2.57}$$

Table 22 summarizes the explanations for each parameter used in the MEPDG equations to calculated fatigue crack in the CTB layer. Figure 29 shows typical crack distress types observed on asphalt surfaced road network.

Table 22. List of parameters used in the MEPDG equations to calculated alligator and longitudinal cracks

ΔC	Change in the crack depth due to a cooling cycle
ΔK	Change in the stress intensity factor due to a cooling cycle
A, n	Fracture parameters for the HMA mixture
k_t	Coefficient determined through global calibration for each input level (Level 1 = 50; Level 2 = 1.5; and Level 3 = 3.0)
E_{HMA}	HMA indirect tensile modulus(psi),
σ_m	Mixture tensile strength (psi),
m	The m-value derived from the indirect tensile creep compliance curve measured in the laboratory
β_t	Local or mixture calibration factor
σ_{tip}	Far-fields stress from pavement response model at depth of crack tip (psi
C_o	Current crack length, ft
TC	Observed amount of thermal cracking, ft/mi
β_{t1}	Regression coefficient determined through global calibration (400),
$N[z]$	Standard normal distribution evaluated [z],
σ_d	Standard deviation of the log of the depth of cracks in the pavement (0.769), in
C_d	Crack depth, in.,
H_{HMA}	Thickness of HMA layers, in

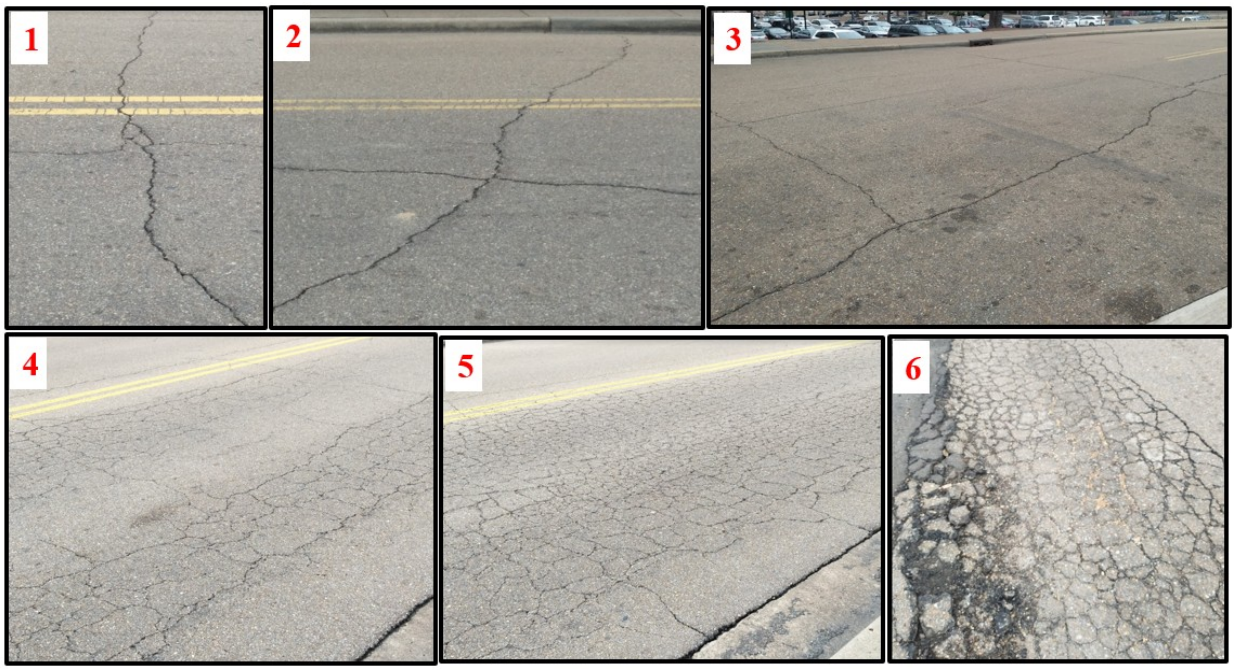

Figure 29. Typical crack distress types observed on asphalt surfaced road network

- Transverse crack: Initiation of block cracking, reflection cracking due to deterioration of cement or lime stabilized base or subbase (1)
- Longitudinal crack: Initiation of fatigue cracking, top-down cracking, poor longitudinal joint. (Fatigue is manifested as alligator cracking) (2)
- Block crack: Primarily due to low temperature thermal cracking (3)
- Alligator crack: Primarily due to traffic load repetitions (4, 5, and 6)

2.4.3 UCI for Cracking Distress Indicator

In a road section, the severity levels of asphalt pavement surface distress of cracking and rutting are important factors for the M&R intervention. The most recent MEPDG method of pavement design for any road section requires passing six design distress criteria of: TDC, fatigue cracking, low-temperature thermal cracking, rutting in total pavement system, and rutting only in asphalt layer [59]. These criteria indicate the importance of considering cracking distress

not only for pavement design, but also for maintenance management and road infrastructure asset management. Therefore, it is imperative to consider reasonably accurate and reliable asphalt cracking deterioration initiation and progression prediction models for future prediction of distressed areas.

The mechanisms involved in developing different types of cracking distresses include: layer thickness, base material type, subgrade, traffic applications, and climate data. Eventually all cracked distress areas are treated similarly for the M&R actions. Therefore, in this research, a new approach is proposed to rationally combine all cracking distresses into one parameter.

The Patterson concept of universal Cracking Indicator (CI) [86] highlights the need for a distress indicator that combined different cracking distress types as a unique indicator. The proposed cracking indicator is the simple product of three primary physical dimensions of the amount of cracking (Equation 2.58). Figure 30 is used to describe the CI concept as proposed by the researcher.

$$CI = \text{extend} \times \text{intensity} \times \text{crack width} \tag{2.58}$$

Where,

Extend = area of cracked pavement defined within a sample area, expressed as a percentage of total pavement area,

Intensity = total length of cracks within the area defining the extend, and

Crack width = mean width of crack opening at the surface of a set of cracks

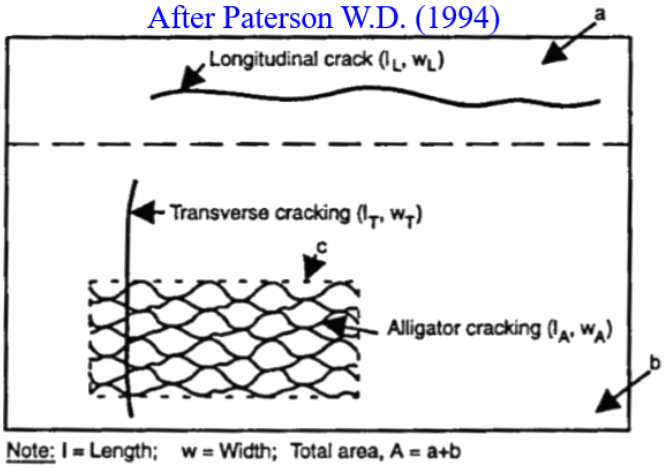

Figure 30. Example of computational of CI [86]

Equations 2.59 and 2.60 are used to calculate CI for longitudinal cracks. Equation 2.61 and 2.62 are used to calculate CIs for alligator crack and transverse crack, respectively. The combined CI for all crack types is calculated using Equation 2.63.

Longitudinal Cracking

$$CI_L = 100\left[\frac{a}{A}.\frac{l_L}{a}.W_b + \frac{b}{A}.\frac{0}{b}.0\right] = \frac{100 l_L W_L}{A} \quad (2.59)$$

Or calculating in the basis of the whole section

$$CI_L = 100\left[\frac{(a+b)}{A}.\frac{l_L}{(a+b)}.W_L\right] = \frac{100 l_A W_A}{A} \quad (2.60)$$

Alligator Cracking

$$CI_A = 100\left[\frac{C}{A}.\frac{l_A}{C}.W_A\right] = \frac{100 l_A W_A}{A} \quad (2.61)$$

Transverse Cracking

$$CI_T = 100\left[\frac{A}{A}.\frac{l_T}{A}.W_T\right] = \frac{100 l_T W_T}{A} \quad (2.62)$$

Combined CI

$$CI = \frac{100[l_L W_L + l_A W_A + l_T W_T]}{A} \quad (2.63)$$

Important information on CI follows:

- CI is cracking indicator (dimensionless)
- Extent is area of cracked pavement (% of total pavement area)
- Intensity is total length of crack within the area defining the extent (m/m^2), and
- Crack width is crack opening (mm)
- Scaling factors: a) 100 (percentage area), b) 1,000 (mm/m)
- Range 0 – 10,000.
- Example CI of 3,200 may comprise of 2,000 alligator, 700 longitudinal, 500 irregular cracking.

However, adapting this concept in this research requires some alteration due to the following reason;

- The intensity term requires the length of alligator cracking distress for low, medium, and high severity levels. Unfortunately, the length parameter of alligator cracking distress type was not available in the LTPP database.
- No block cracking model, which is an important distress of low-temperature cracking.

Therefore, the development of the UCI that simplifies and considers the combination of various different cracking distress types including block cracking was proposed in this research. In the MEPDG database, the alligator and block cracking distresses are calculated as an area (square meter) for low, medium, and high severity levels, respectively. Longitudinal and transverse cracking distresses are reported based on the observed lengths (meter) for low, medium, and high severity levels, respectively. However, the crack width range for each severity

level is small and not practical for new UCI approach. The crack width for low severity level was assumed as 0.05 meter, while the crack width of 0.1 meter was assumed for both medium and high severity levels of cracking distresses. Equations 2.64 to 2.66 show the calculation of the combined UCI (Y_C), which is the combination of the UCI for alligator crack (Y_{AC}), block crack (Y_{BC}), longitudinal crack (Y_{LC}), and transverse crack (Y_{TC}). There is no TDC data in the LTPP database. Therefore, the UCI equation is not account for the TDC distress. The UCI values are express in percentage of total LTPP test section area.

$$Y_C(\%) = \sum\left[\left(\frac{a_{AL}+a_{AM}+a_{AH}}{A_T}.100\right)+\left(\frac{a_{BL}+a_{BM}+a_{BH}}{A_T}.100\right)+\left(\frac{l_{LL}W_{LL}+l_{LM}W_{LM}+l_{LH}W_{LH}}{A_T}.100\right)+\left(\frac{l_{TL}W_{TL}+l_{TM}W_{TM}+l_{TH}W_{TH}}{A_T}.100\right)\right] \quad (2.64)$$

$$Y_C(\%) = \sum\left[\left(\frac{a_{AL}+a_{AM}+a_{AH}}{A_T}.100\right)+\left(\frac{a_{BL}+a_{BM}+a_{BH}}{A_T}.100\right)+\left(\frac{a_{LL}+a_{LM}+a_{LH}}{A_T}.100\right)+\left(\frac{a_{TL}+a_{TM}+a_{TH}}{A_T}.100\right)\right] \quad (2.65)$$

$$Y_C(\%) = (Y_{AC} + Y_{BC} + Y_{LC} + Y_{TC}) \quad (2.66)$$

Where;

a_{AL} = area of alligator crack for low severity level,

a_{AM} = area of alligator crack for medium severity level,

a_{AH} = area of alligator crack for high severity level,

a_{BL} = area of block crack for low severity level,

a_{BM} = area of block crack for medium severity level,

a_{BH} = area of block crack for high severity level,

a_{LL} = area of longitudinal crack for low severity level,

a_{LM} = area of longitudinal crack for medium severity level,

a_{LH} = area of longitudinal crack for high severity level,

a_{TL} = area of transverse crack for low severity level,

a_{TM} = area of transverse crack for medium severity level,

a_{TH} = area of transverse crack for high severity level,

l_{LL} = length of longitudinal crack for low severity level,

l_{LM} = length of longitudinal crack for medium severity level,

l_{LH} = length of longitudinal crack for high severity level,

l_{TL} = length of transverse crack for low severity level,

l_{TM} = length of transverse crack for medium severity level,

l_{TH} = length of transverse crack for high severity level,

A_T = total test section area in square meter (sq. m).

Note: All areas are in square meter and lengths are measured in meter.

The cracking data available for test sections in 47 states in the U.S. are extracted from the LTPP database under MON_DIS_AC_REV section. The cracking distresses were observed for the whole 500 feet test section and were observed on the same day when the FWD test was carried for structural assessment of pavement layers. A total of 2,240 data sets were used in the development of the enhanced UCI multiple regression and ANN model equation. Distribution of combined UCI data sets based on LTPP climatic regions (Reg_Actual) and major M&R

intervention factor, CND are shown in Table 23. Figure 31 shows the distribution of the UCI data sets per measurement year used in this research.

Table 23. Distribution of UCI data sets based on LTPP climatic regions (Reg_Actual) and major M&R intervention factor (CND)

Between-Subjects Factors				
Group		Value Label	N	Percentage
Reg_Actual	1	North Atlantic	386	17.2%
	2	North Central	230	10.3%
	3	Southern	976	43.6%
	4	Western	648	28.9%
CND	0	No Major M,R&R	1,316	58.8%
	1	Major M,R&R Applied	924	41.2%

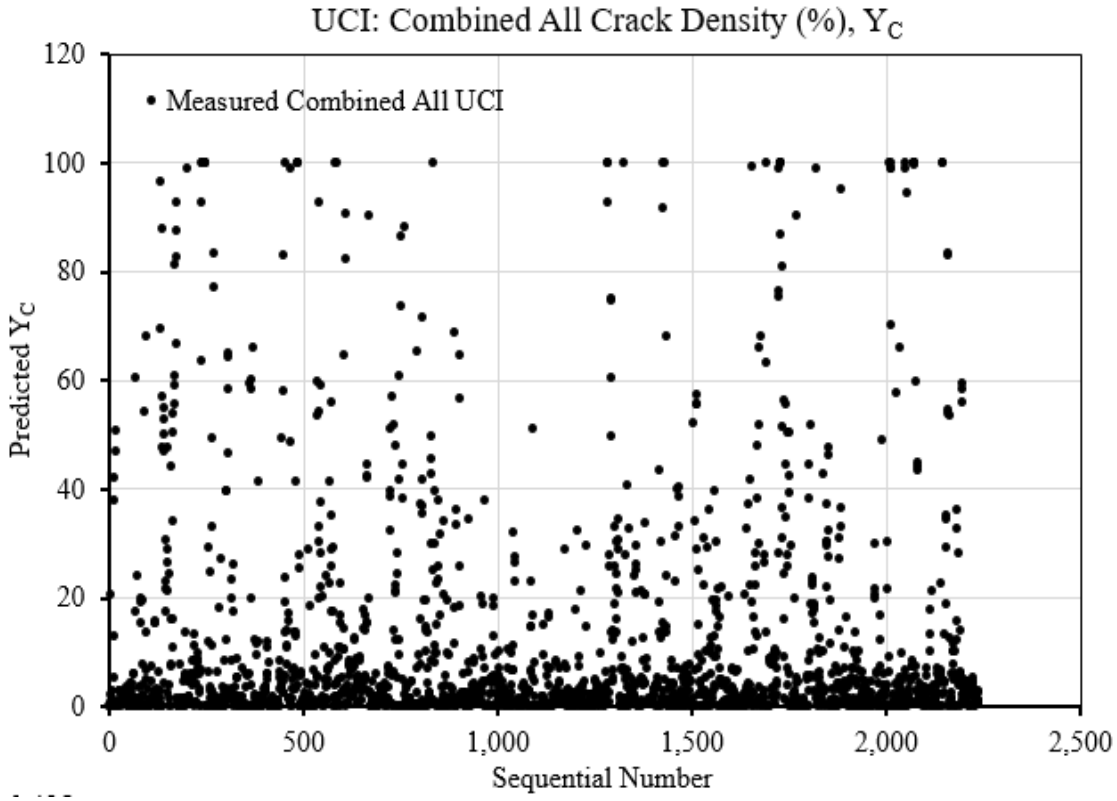

Figure 31. Distribution of the UCI per measurement year data according to sequential number

2.4.4 Methodologies for Enhanced Cracking Modeling

1. Cracking distress data were extracted from the LTPP database and converted to the UCI for each cracking distress type (alligator, block, longitudinal, transverse). The individual UCI, which is the density of crack area in % for each crack was added to form a combined UCI. The combined UCI data were transformed using a few transformation functions including $Log_{10}(Y_C+0.5)$, which works really well for rutting data as explained in previous sub-chapter. Table 24 shows the result for combined UCI data transformed using $Log_{10}(Y_R+0.5)$ function.

Table 24. Test of normality for combined UCI data sets

	Kolmogorov-Smirnov[a]		
	Statistic	df	Sig.
$Log_{10}(Y_R+0.5)$	.113	2,240	< 0.001*
*This is lower bound of the true significance a. Lilliefors Significance Correction			

The test hypothesis for probability of type I error α equal to 0.05 follows:

Null hypothesis, H_0: The distribution of the combined UCI data is normal

Alternative hypothesis, H_A: The distribution of the combined UCI data is not normal

The normality test for the combined UCI showed that the probability of significance, p-value (Sig.) was less than the α 0.05 probability of chance error, which is statistically significant. Therefore, the null hypothesis is rejected and the combined UCI data is not normally distributed. Figure 32 shows histogram plot for combined UCI with descriptive statistics and normal distribution curve.

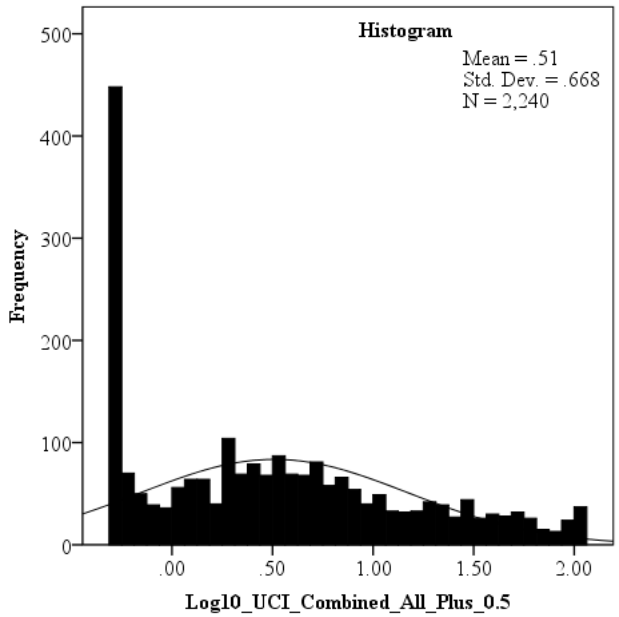

Figure 32. Normality plots for the combined UCI data transformed using $Log_{10}(Y_C+0.5)$ function

2. The effect of major M&R was further analyzed by selecting 25 test sections and tested for CND factor on the UCI means. The hypothesis testing using T-Test for UCI data before and after major M&R for all 25 test sections follow:

Step by Step Procedure

Step 1: Setup null hypothesis and alternative hypothesis.

Null Hypothesis: H_0: $\mu 1 = \mu 2$

The UCI means before and after major M&R treatments are equal.

Alternative Hypothesis: H_A: $\mu 1 \neq \mu 2$

The UCI means before and after major M&R treatments are not equal.

Step 2: Select α probability of Type 1 chance error for α level of statistical significance.

$\alpha = 0.05$

$\alpha/2 = 0.025$ (for two-tailed test)

Figure 2.4.4B shows two-tailed t-test probability distribution.

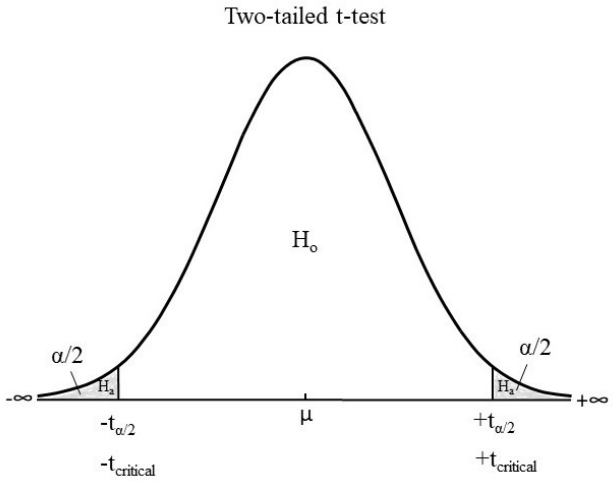

Figure 33. Two-tailed t-test probability distribution graph

Step 3: Define test criteria and decision rule for rejecting H_0.

Test criteria: $t_{critical} = 1.96$ for degree of freedom (dof) = 185 and $\alpha/2 = 0.025$

Decision Rule: Reject H_0 if t-test statistics t_{test} exceeds the absolute value of $t_{critical}$ ($t_{test} > t_{critical}$) and probability of significance value, $p \leq$ Probability of Type-1 chance error, $\alpha/2$.

Step 4: Calculate t test statistics, t_{test}, and p-significance value.

$t_{test} = 4.93$

Probability of significance, p-value < 0.001

Step 5: Interpret the results.

$t_{test}(4.93) > t_{critical}(1.96)$ and $p (< 0.001) < \alpha/2 (0.025)$

Therefore, the test rejected the null hypothesis. The results show that the difference in the means of the UCI values before and after major M&R treatments for all 25 test sections are

statistically significant at α/2, 0.025 level probability of chance error. The t-test was conducted to give good estimate of population's UCI data.

3. The T-Test was also conducted for each test section to observe the effect of major M&R on the UCI values. As can be seen, Figure 34 shows eight out of 25 sections t test showed that there are statistically significance different in the means of the UCI values before and after the most recent major M&R treatments.

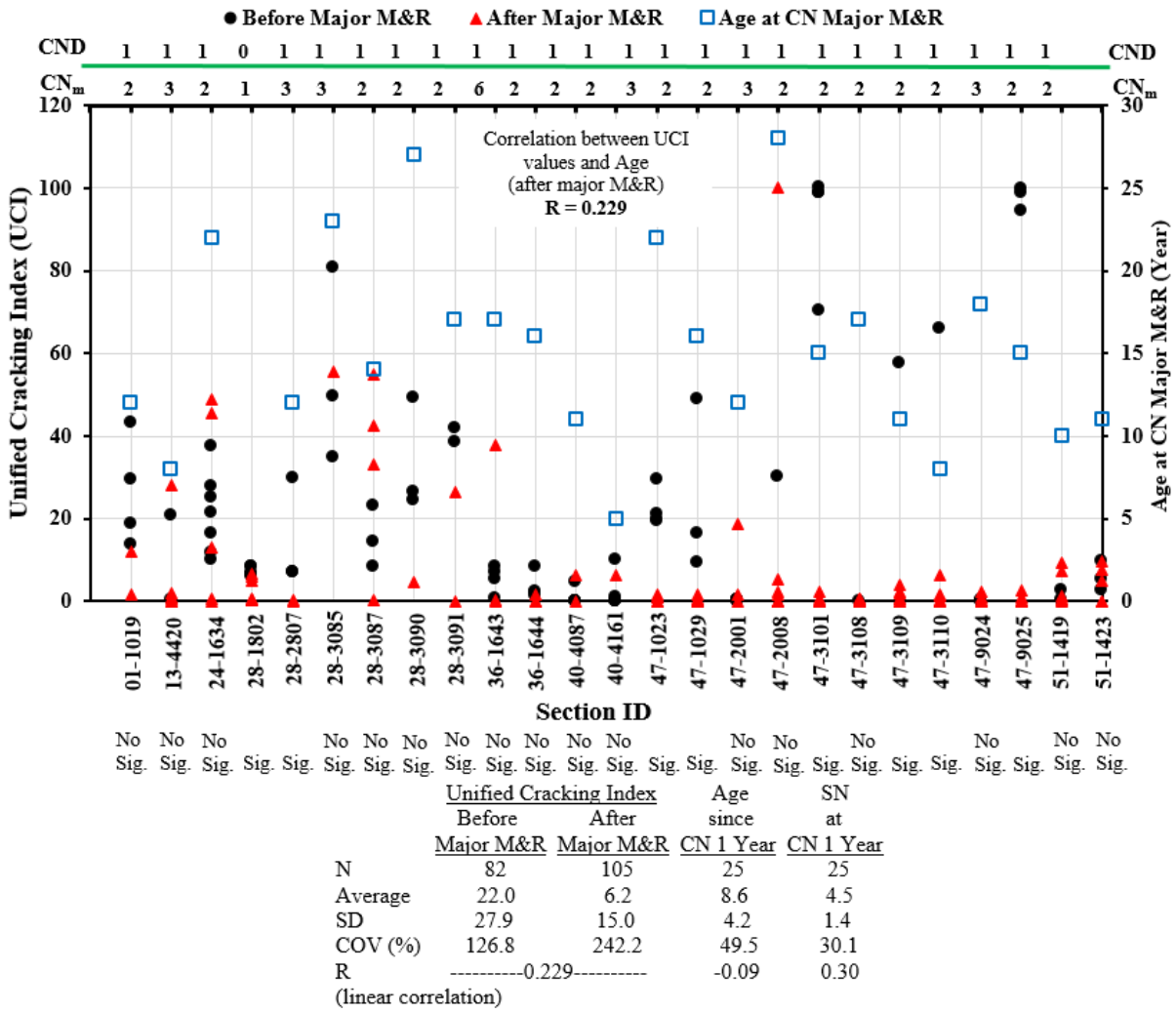

Figure 34. Asphalt pavement age (years) at the most recent CN major M&R (CN_m) with crack data before and after major M&R treatment

Therefore, based on these results of 25 samples, the most recent CN for major M&R on a whole entire asphalt surface is considered as a candidate dichotomous or dummy variable for multiple regression modeling together with other independent variables. It is important to use dummy variable to consider the effect of M&R in the equation.

4. Figure 35 shows the UCI plot for LTPP test section 47-3101 in Tennessee. There is a significant decrease in the UCI values after major M&R of milling of existing asphalt layer and overlay with new hot mix asphalt layer. Therefore the CN 1 was assigned as CND 0, while CN 2 and CN 3 were assigned as CND 1 in the model database.

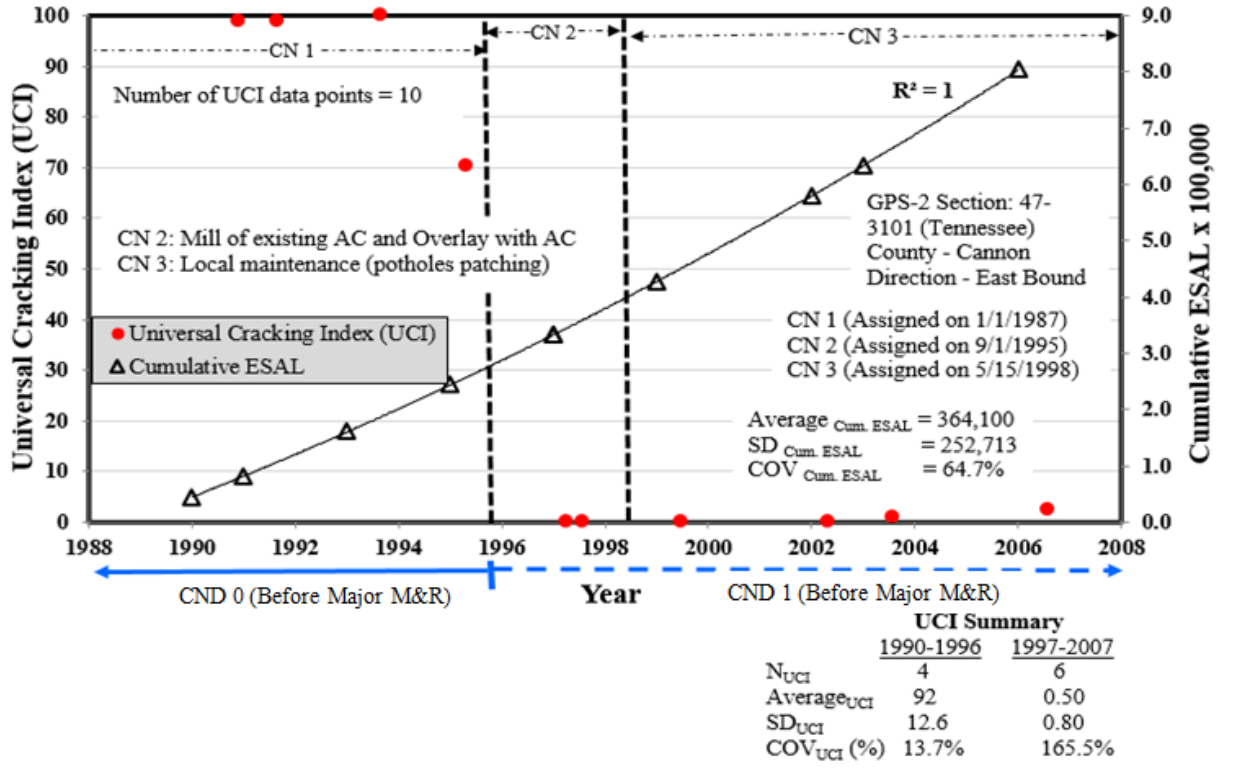

Figure 35. UCI data plot for test section 47-3101 in Tennessee

Step by Step procedure

Step 1: Setup null hypothesis and alternative hypothesis.

Null Hypothesis: H_0: $\mu 1 = \mu 2$

The UCI means before and after major M&R treatments are equal.

Alternative Hypothesis: H_A: $\mu 1 \neq \mu 2$

The UCI means before and after major M&R treatments are not equal.

Step 2: Select α probability of Type 1 chance error for α level of statistical significance.

$\alpha = 0.05$

$\alpha/2 = 0.025$ (for two-tailed test)

Step 3: Define test criteria and decision rule for rejecting H_0.

Test criteria: $t_{critical} = 2.306$ for degree of freedom (dof) = 8 and $\alpha/2 = 0.025$

Decision Rule: Reject H_0 if t-test statistics t_{test} exceeds the absolute value of $t_{critical}$ ($t_{test} > t_{critical}$) and probability of significance value, p ≤ Probability of Type-1 chance error, α/2.

Step 4: Calculate t test statistics, t_{test}, and p-significance value.

$t_{test} = 15.8$

Probability of significance, p-value < 0.001

Step 5: Interpret the results.

t_{test} (15.8) > $t_{critical}$ (2.306) and p (< 0.001) < α/2 (0.025)

Therefore, the test does not reject the null hypothesis. The results show that the difference in the means of the UCI values before and after major M&R treatments for test section 47-3101

are statistically significant at α/2 0.025 level probability of chance error. This implies that there is a need to consider dummy construction number CND 0 (before major M&R treatments) and CND 1 (after major M&R treatments) in the multiple linear regression prediction equations.

5. Further transformation using Y_{Beta} and Sigmoid functions were also tested in this research. Equation 2.67 and 2.68 were used to transform combined UCI data (dependent variable) into Y_{Beta}, and sigmodal function (Y_{CS}), respectively. However, the normality tests for these data sets (Y_{Beta} and Y_{CS}) also showed that data were not normally distributed. Therefore, alternative method for condition deterioration progression modeling is ANN method.

$$Y_{Beta} = \frac{1}{3.1429x\sqrt{Y}\,x\sqrt{1-Y}} \tag{2.67}$$

$$Y_{CS} = \frac{1}{\left[1+e^{-Y_{CP}}\right]};\ Y_{CP} = \frac{Y_C}{100} \tag{2.68}$$

6. The ANOVA test was conducted to evaluate the effects of M&R history and LTPP climatic region factors on the combined UCI data sets and the results are shown in Table 25. For CND factor, there are statistically significant differences in the means of combined UCI values before and after major M&R treatments. Additionally, the LTPP climatic region factor also showed statistically significant difference in the means of the combined UCI values. Therefore, both CND and Reg_D factors are used as the dummy variables in both multiple regression and ANN modeling of cracking distress prediction equations.

Table 25. ANOVA tests of between-subjects effects for combined UCI data sets

Source	Type III Sum of Squares	df	Mean Square	F	Sig.
Corrected Model	30080.818[a]	7	4297.260	10.768	.000
Intercept	187354.202	1	187354.202	465.539	.000
LTPP_Region	10603.508	3	3534.503	8.783	.000
CND	13333.051	1	13333.051	33.130	.000
LTPP_Region * CND	4089.964	3	1363.321	3.388	.017
Error	898258.999	2232	402.446		
Total	1173237.740	2240			
Corrected Total	928339.817	2239			

a. R Squared = .032 (Adjusted R Squared = .029)

7. Table 26 shows the independent variable used to develop the enhanced cracking multiple regression equation and ANN model equation. The modulus values for pavement layers were calculated using the same procedures applied for rutting distress modeling. The interaction terms between two variables that showed significant correlation were also considered as one of the independent variables. For example, T_1 x E_1 explains the interaction between the thickness of asphalt layer with the modulus value of asphalt layer, which has significant interaction and considered in the model database.

8. Table 27 shows the maximum, minimum, average, SD, and COV (%) for the data sets used in the development of the enhanced cracking condition deterioration prediction equations.

9. The enhanced cracking multiple regression equation and ANN model equation were developed and the reasonableness of the multiple regression and ANN model equations were evaluated based on the following parameters:

- The R value of the multiple regression equations

- The predicted against measured data plots
- The verifications of the multiple regression equations
- The accuracy measures of the MARE and RMSE

Table 26. List of independent variables for the enhanced cracking progression prediction model equation

No.	Independent Variable	Notes	Unit
1	$Log_{10}\ Y_{C0}$	Log_{10} Initial UCI value per measurement year	-
2	Age	Pavement age	Year
3	CESAL	Annual cumulative ESALs	Year
4	$TEMP_{PAVE}$	Pavement temperature measured during the assessment of cracking distress	°C
5	E_1	Asphalt modulus	psi
6	E_2	Base modulus	psi
7	E_3	Subbase modulus	psi
8	E_4	Subgrade modulus	psi
9	T_1	Asphalt thickness	inch
10	T_T	Total thicknesses (T_T), Asphalt thickness (T_1), base layer thickness (T_2), and subbase layer thickness (T_3): $T_T = T_1 + T_2 + T_3$	inch
11	SN	Structural Number	-
12	PRECIP	Average monthly precipitation	mm
13	CND	Dummy variable for CN (0 if no major M&R treatment history, 1 if major M&R treatment has taken place)	-
14	Reg_D	Dummy variable for LTPP climatic regions (zero for Southern region, one for other regions)	-
15	$T_{1\ x}\ E_1$	Interaction between asphalt thickness and asphalt modulus	-
16	$TEMP_{PAVE}$ x E_1	Interaction between pavement temperature and asphalt modulus	-
17	SN x CESAL	Interaction between SN and cumulative ESAL	-
18	T_T x CND	Interaction between total thickness and CND	-
19	$TEMP_{PAVE}$ x PRECIP	Interaction between pavement temperature and precipitation	-
20	Age x $Log_{10}(Y_{C0}+0.5)$	Interaction between age and $Log_{10}(Y_{C0}+0.5)$	-
21	CESAL x $Log_{10}(Y_{C0}+0.5)$	Interaction between CESAL and $Log_{10}(Y_{C0}+0.5)$	-

Table 27. Descriptive statistics for independent variables used to develop enhanced cracking condition deterioration prediction equation

Descriptive Statistics	Combined UCI, Y_C (%)	Initial Combined UCI, Y_{C0}	Asphalt Modulus, E_1 (psi)	Base Modulus, E_2 (psi)	Subbase Modulus, E_3 (psi)	Subgrade Modulus, E_4 (psi)	Asphalt_Thickness, T_1 (inch)
Minimum	0	0	93,859	0	0	9,003	0
Maximum	104	100	1,238,563	1,351,856	604,293	53,655	25
Mean	10	9	445,043	210,162	16,545	17,697	7
SD	20	19	373,055	245,297	24,032	8,535	4
COV (%)	194.7	222.9	83.8	116.7	145.3	48.2	54.2

Descriptive Statistics	Total Thickness, T_T (inch)	Age (Year)	SN	Cumulative ESAL, CESAL	Pavement Temperature, $TEMP_{PAVE}$ (°C)	Precipitation, PRECIP (mm)
Minimum	6	0	1	2,000	(12)	0
Maximum	58	48	10	56,568,503	68	381
Mean	21	19	5	2,364,607	24	76
SD	8	8	2	4,605,857	12	63
COV (%)	40.7	42.8	34.1	194.8	49.3	81.9

10. The development of new cracking model using UCI combines all crack types (alligator, block, longitudinal, and transverse) and beneficial for pavement asset management purposes. The UCI is practical and applicable for decision support system for the maintenance and rehabilitation programs. However, this research also developed the enhanced multiple regression equations and ANN models for alligator crack, block crack, longitudinal crack, and transverse crack, respectively. These individual enhanced multiple regression and ANN model equations are practical and applicable for pavement structural design purposes. The independent variables used in the development of multiple regression equations and ANN model equations for each crack type are similar to the independent variables used in the equations for combined all crack types.

11. Initial approaches to develop ANN model equations using only 50% training data sets showed less promising outputs for both combined and individual crack model equations. Therefore, additional analysis using 100% training data sets were conducted and the results showed significant improvement for both model database and verification data sets. The results are shown in the following sub-chapter.

2.4.5 Final Enhanced UCI Multiple Regression and ANN Model Equations

This sub-chapter discusses the results from the analysis using enhanced multiple regression equations and ANN model equations. For model database, the following criteria were evaluated to decide the best performing model equation.

- Average predicted values (%),
- Average % difference,
- R and R square values, and
- RMSE

Additional accuracy measure of MARE was used to decide the best performing model for model verifications. The MARE was not calculated for model database due to zero values of certain cracking distress data sets. The analysis was conducted using SPSS software and the outputs that showed the coefficients for all multiple regression equations developed in this research were described in Appendix A.

2.5 Recommendations for Implementation of Condition Deterioration Progression Model Equations

The recommendations for implementation of the enhanced condition deterioration progression model equations follow:

- IRI Roughness: Both enhanced multiple regression and ANN model equations are recommended for asphalt pavement IRI roughness modeling and prediction for future IRI value.
- Rutting: Both enhanced multiple regression and ANN model equations are recommended for asphalt pavement rutting modeling and prediction for future rut depth value.
- Cracking: ANN model equations are better predictors for future UCI values and recommended for implementation in both asphalt pavement structural design and asphalt pavement asset management. However, it is also recommended to calibrate the enhanced regression prediction equations using condition and traffic data for selected pavement sections, if desired to implement in other geographic and different climatic regions.

III. MATERIAL CHARACTERIZATION OF ASPHALT PAVEMENT USING NONDESTRUCTIVE DEFLECTION DATA

3.1 Literature Review of Pavement Modulus Backcalculation Methods Based on Layered Elastic Static Analysis

3.1.1 Layered Elastic Theory

The basic pavement structural design is genuinely based on these two famous theories which are one layer linear elastic theory by Boussinesq reported in 1885, followed by Burmeister's two and three layers theory back in 1943 and 1945 [87, 88]. These theories were explored as a result of great interest among scholars to understand the behavior of materials used to form a complete pavement system. Asphalt pavement system composed of horizontal layers with different material types, contributed to further research to study mechanistic responses (stress, strain, and deflection) at critical locations to understand the mechanism of pavement deteriorations such as rutting and other distress types.

Boussinesq's one layer linear elastic theory was traditionally used for soil foundation design. The researcher assumed that the material is elastic, isotropic, and homogenous semi-infinite half space. Half space is defined as an infinite large horizontal plane area with semi-infinite depth. Another general assumptions include the load is point load, the stress imposed is bell-shaped whose amplitude decreases with depth, and maximum stress is near surface and theoretically reduced to zero at an infinite depth. Equations 3.1 and 3.2 show a Boussinesq

approach to calculate vertical stress (σ_z) due to a point load at the surface (Figure 36). In general, σ_z is a function of P, z, and r, assuming no material properties, weightless, and no temperature effect.

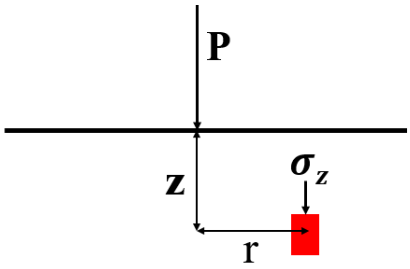

Figure 36. Illustration of a point of interest to calculate vertical stress based on Boussinesq's approach

$$\sigma_z = k\left(\frac{P}{z^2}\right) \tag{3.1}$$

$$k = \left(\frac{3}{2\pi}\right)\left(\frac{1}{[1+(r/z)^2]^{5/2}}\right) \tag{3.2}$$

Where σ_z is vertical stress, P is point load, Z is depth, and r is radial distance.

Furthermore, under an assumed circular loaded area, the modulus of elasticity (E) of the underlying soil can be determined if the applied pressure, the radius of loaded area, and the surface deflection are known (Figure 37). Equations 3.3 to 3.5 show the mathematical equations derived to determine equation to determine modulus value and surface deflection for flexible plate (Equation 3.6) [89]. Equations 3.7 and 3.8 were derived to determine modulus value and surface deflection for rigid plates (Equation 3.9) [89].

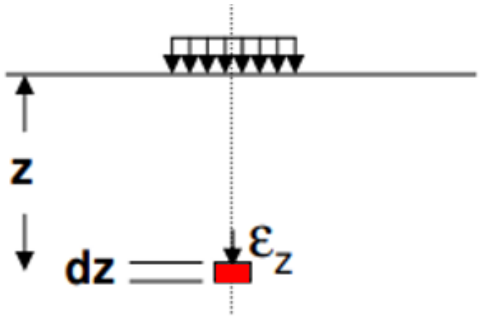

Figure 37. Illustration of the point of interest to calculate deflection value on Boussinesq's approach (After [89])

$$\Delta_z = \int_{\infty}^{z} \varepsilon_z \, dz: \; \Delta_z = \frac{(1+\mu)p*a}{E}\left[\frac{a}{(a^2+z^2)^{0.5}} + \frac{1-2\mu}{a}\left[(a^2+z^2)^{0.5} - z\right]\right] \tag{3.3}$$

For μ = 0.5, $\Delta_z = \frac{3pa^2}{2E(a^2+z^2)^{0.5}}$ (3.4)

At z = 0, $\Delta_z = \frac{2(1-\mu^2)}{E} p * a$ (3.5)

At z = 0 and μ = 0.5, $\Delta_z = \frac{1.5pa}{E}$ or $E = \frac{1.5pa}{\Delta_z}$ (Flexible plate) (3.6)

Based on the research [89], the distribution of pressure under a rigid plate follows;

$$p(r) = \frac{pa}{2(a^2-r^2)^{0.5}} \tag{3.7}$$

By integrating a point load over the contact area of the plate, it can be derived that

$$\Delta_o = \frac{\pi(1-\mu^2)}{2E} p * a \quad (3.8)$$

If μ = 0.5, then, $\Delta_o = \frac{1.18pa}{E}$ or E $= \frac{1.18pa}{\Delta_o}$ (Rigid plate) (3.9)

Where,

Δ = Deflection at the center of the loaded area associated with the surface pressure

E = Young's modulus of elasticity of the material

p = Unit pressure applied to the surface of the loaded area

a = radius of the loaded area

μ = Poisson's ration of the material

However, the one layer linear elastic theory has a few limitations as follow:

- The assumptions are suitable only for pavement with a thin surface
- It is unreasonable to neglect the effects of stiffer and thicker pavements since it greatly affects the stress, strain and deflection values
- Tensile stress and strain analysis were neglected. Unfortunately, stress and strain analyses were very important for fatigue failure analysis of concrete and asphalt pavements, respectively.

Therefore, in the early 1940s, Burmeister introduced more appropriate approaches to consider material stiffness and thicknesses through two layers and three layer systems [87, 88, 89, 90]. The approach is more reasonable for a pavement system that has different layers with various different material properties. Burmester's theory maintains the basic assumptions for one layer theory. Additional assumptions follow:

- The intermediate layer thickness is finite, while the bottom layer is assumed to be semi-infinite.
- Full friction between the layers.
- There is no shear stress at the surface.
- The material is assumed as linear elastic and the constitutive behavior of the material is defined by Young's elastic modulus and Poisson's ratio.
- The load is assumed to be static and uniformly distributed over a circular area.

Advancement through computer engineering contributed to the development of various different computer programs based on multi-layer linear elastic theory to predict stress, strain, and deflection values for pavement structural design. Researchers [87, 88, 90] describe the examples of that computer programs in detail.

3.1.2 Review of Literature for Backcalculation Methods Based on Layered Elastic Analysis

One of the most useful data available in the LTPP database is the deflection data sets obtained from the FWD nondestructive test to assess the structural integrity of the pavement system [85, 91, 92, 93]. The FWD test was conducted to measure asphalt pavement deflection using seismic sensors placed at different distances from the center point of the test load drop location [94]. The deflection data sets extracted from the LTPP database are based on the computation of seven FWD geophone sensors located at 0, 8, 12, 18, 24, 36, and 60 inches from the center of the 5.91 inches loading plate. Typically four different load weight levels are tested, four drops for each level which resulted in a total of 16 deflection basins. According to the FHWA [94], the FWD simulated the pavement surface deflection caused by a fast-moving truck.

The load pulse generated by dropping a specific weight was transmitted through the loading plate and caused the elastic deflections of pavement layers. The deflection basin corresponding to each drop load was determined from the sensor data. Uddin and Garza [93] provide detailed information related to the FWD test through their study on numerical simulation and dynamic response analysis of FWD impact test on asphalt pavement.

For years, Young's modulus values which describe the stiffness of the pavement layers were not reported for most of the test sections in the LTPP database. The modulus values are required for pavement evaluation and rehabilitation design [95], response analysis, and numerical studies of the the pavement system for the specific test section. Therefore, the backcalculation using deflection data from the FWD test is essential to obtain modulus values for asphalt, base, subbase and subgrade layers, respectively. The backcalculated modulus values are important to evaluate the structural integrity of the pavement system after a series of M&R treatments [96].

The FHWA through SHRP carried out the extensive literature review and summarized important information for 17 different backcalculation programs [92]. The review looked into program developers and forward calculation methods which used either multi-layer elastic theory, a method of equivalent thickness, finite element, or other closed-form solutions. In addition, the review also reported forward calculation subroutine approaches including BISAR, MET, FEACONS III, ELSYM5, CHEVRON, and WESLEA. Moreover, nonlinear or linear methods, requirements of seed modulus values, and ranges of acceptable modulus values are among other criteria evaluated in the study. Six backcalculation programs were selected for detail evaluations which are ELCON and ELI-BACK for rigid pavement, and ISSEM4, MODCOMP3, MODULUS, and WDEF for flexible pavements. The results were evaluated

based on reasonableness, robustness and stability, the goodness of fit and suitability of SHRP purposes. The top three programs selected are MODCOMP3, MODULUS, and WESDEF. Further evaluations were conducted on these three programs. The user repeatability, reasonableness of results, deflection matching errors, ability to match the calculated modulus value from simulated deflection basins, and versatility are among the criteria assessed. Final evaluations revealed that the MODULUS backcalculation program was superior compared to the other two programs. The guideline for review and evaluation of backcalculation results are available in a report published in 2006 [95]. However, the final LTPP deflection data analysis was conducted not using the reasonable backcalculation program, as discussed later.

According to Ameri et al. [96], there are three modes of backcalculation available which include (1) radius of curvature, (2) deflection basin fit, and (3) Finite Element Method (FEM) or Linear Elastic Theory (LET) or Method of Equivalent Thickness (MET). All these modes are described in a comparative study for static and dynamic backcalculation approaches for asphalt, base and subgrade layers. In this study, for static analysis, the MODULUS 6.0, ELMOD 5.0 and EVERCALC 5.0 were analyzed, while the Dynamic Backcalculation Procedure with Systems Identification Method (DBSID) program was employed for the dynamic backcalculation process. Ameri et al. [96] concluded that MODULUS 6.0 was the most appropriate software to backcalculate modulus values. The comparison between the MODULUS 6.0 and DBSID indicated that the dynamic analysis approach showed higher modulus for asphalt and subgrade layers compared to the static approach. In contrast, the backcalculated modulus value using a static approach showed a higher value for the base layer.

One of the widely used backcalculation software for military airports and roads is the Pavement- Transportation Computer Assisted Structural Engineering (PCASE) developed at

Transportation Systems Center and Engineering Research and Development Center (ERDC) of the U.S. Army Corps of Engineers [97]. This software was used as a tool for pavement design and repair alternatives for both airfield and road networks (flexible and rigid pavements). Users are prompted to choose an either empirical or layered elastic design (LED) approaches. The empirical design requires California Bearing Ratio (CBR) or modulus of subgrade reaction (k) values. The LED requires Young's modulus values and Poisson's ratio for each layer. This software used the WESDEF layered linear elastic backcalculation routine to backcalculate modulus values. There is a limited number of research papers related to modulus backcalculation available for review using the PCASE 2.09 backcalculation software.

Priddy [98] used the PCASE 2.09 software to determine the required thickness of the PCC slab for a 100-ft-length by 60-ft-wide test section construction. The study assumed the PCC airfield flexural strength of 650 psi, k equal to 15 pci, six inches aggregate base thickness, no drainage layer required, and a design life of 50,000 C-17 aircraft passes. The PCASE software proposed a 14 inches thick PCC slab with specific locations for one-inch diameter of rebar. The test section was constructed with 15 20-ft by 20-ft PCC slabs placed at three by five configurations. Three types of repair methods were evaluated. Repair one, two, and three explain the replacement of quarter, half and full slab, respectively. Prior to the repair, the PCC slabs were sawed at quarter, half, and full slab area at certain locations. A single 10-ft by a 10-ft concrete panel with dowel bars was used to replace quarter slab. Additionally, the removed half slab was replaced with two concrete panels and four concrete panels replaced the removed full slab, respectively. A multi-wheel load cart simulating a C-17 aircraft landing gear was used to simulate aircraft passes, until 10,000 passes or until the PCC slab failed.

The heavy weight deflectometer (HWD) tests were conducted using the Dynatest model 8081 equipment. The HWD tests were conducted on a newly constructed test section (pre-repair) and post-traffic for both slabs and panels at different locations. Before the construction of the test section, the dynamic cone penetrometer (DCP) tests were carried out to determine the subgrade modulus value. Subsequently, the DCP estimated moduli in psi were determined by multiplying CBR values with 1500. The results showed no changes in pre-repair and post traffic PCC slabs modulus values. Less than three percent reductions for the backcalculated base and subbase modulus values were observed compared to pre-repair slabs conditions. This implies that no major loss in foundation support beneath the test section that could lead to early deterioration of the repairs. For PCC panel cases, the post-traffic panels showed approximately 60 percent reductions in PCC modulus value. Additionally, about 40 percent reductions in the backcalculated modulus values were observed for the base layer and 53 percent reductions for subgrade layer, compared to pre-repair panels. The significant reductions of the modulus values are not due to a reduction in foundation support but attributed to the deterioration of the panels during traffic simulation processes [98].

Priddy et al. [99] evaluated procedures for backcalculation of airfield pavement modulus values and compared the backcalculated modulus values using the WESDEF, BAKFAA and ELMOD6 backcalculation software. Both FWD and HWD deflection data sets from five army airports in the U.S and one in South Korea were used for backcalculation purposes. The backcalculated modulus values were evaluated to determine the number of allowable aircraft passes and allowable loads before the failure. The findings indicated that the analysis procedures for backcalculation and structural analysis vary between each software. Reasonable modulus can be obtained either using the WESDEF or BAKFAA although the users are inexperienced or have

limited knowledge performing backcalculation using the software. The modulus values calculated from the BAKFAA and WESDEF software are more reasonable as compared to ELMOD6 software. The modulus values calculated using ELMOD6 over predicted subgrade modulus for most of the sections analyzed.

Recently, the FHWA has updated the LTPP database with layers' modulus values backcalculated using the EVERCALC 5.0 [100] backcalculation software. It is noted that this software ranked high in previous comparative studies [92, 95, 96]. The backcalculated modulus values are different for each CN for all test sections in the LTPP database InfoPave (https://infopave.fhwa.dot.gov/) which includes test section 28-2807 located at Highway 6 East, Lafayette County, Mississippi.

3.1.3 Previous Studies for Test Section 28-2807 in Mississippi

The preliminary research for backcalculation of the modulus values was conducted for the LTPP test section 28-2807 on Highway 6 East, Lafayette County, MS. The pavement structure and backcalculation of Young's modulus for similar test section were initially analyzed in previous studies between 1998 to 2003 by Uddin [101], Uddin et al. [102], and Boriboonsomsin and Momm [103]. Uddin [101] backcalculated modulus values for pavement structure using the PEDD1 computer program. The nondestructive deflection data based on the FWD test and other data sets were used to determine the in situ backcalculated modulus values without making any correction for temperature. The modulus values were compared with the WESDEF and MODULUS5 backcalculation programs. The PEDD1 backcalculated modulus values of 473,000 psi for asphalt layer, 600,000 psi for asphalt base, 57,000 psi for CTB, and 43,600 psi for subgrade layer were more reasonable compared to other programs. These modulus

values represented the pavement layer in a good condition without any crack and rutting in the test area. Further analysis using The 3D-FE analysis was conducted using the modulus values from the PEDD1 software to study surface deflection and pavement structural response subjected the FWD dynamic load pulse.

Uddin et al. [102] backcalculated modulus values for similar test sections using the UMPED static backcalculation program [104] which is a simplified version of the PEDD program. The PEDD is the Windows version of PEDD1, adjusted to adapt to the current changes in the computer technologies. The PEDD and UMPED embedded a self-iterative equivalent linear elastic procedure to correct the backcalculated modulus values for unbound subbase and subgrade layers. The modulus values were corrected based on the normalized shear modulus versus shear strain curves implemented in earthquake engineering [101].

Uddin et al. [102] used the FWD deflection data in 1993 and 1998 from the LTPP database for pavement structure with four layers and assigned different CN. The FWD test in 1998 was conducted for one inch thicker asphalt pavement layers and tested in 25.5°F higher air temperature compared to the 1993 FWD test condition. The deflection recorded by the first sensor placed closest to the drop location showed higher values for 1998 data sets due to a warmer temperature. Additionally, deflection data detected by this sensor showed the highest variability since the first sensor indicated traffic and environmental effects on the asphalt layer. On the other hand, sensor seven, placed at the longest distance from the load center point, recorded the lowest variability. In general, the backcalculated modulus values for asphalt pavement and asphalt base varies with temperatures and traffic applications. However, the backcalculated modulus values for subgrade soil showed no obvious changes. From 1993 FWD data sets, the in situ backcalculated modulus values were 623,300 psi for asphalt pavement,

623,600 psi for asphalt base, 90,500 psi for CTB, and 19,240 psi for subgrade layer. The calculated modulus values from 1998 FWD data sets were 264,600 psi for asphalt pavement, 236,400 psi for asphalt base, 91,400 psi for CTB, and 24,810 psi for subgrade layer.

Boriboonsomsin and Momm [103] backcalculated the modulus values using the UMPED program using FWD deflection data sets collected in 1990, 1991, 1992, 1993, 1995, and 1998. This study highlighted the importance of the CN, which is the intervention factor for maintenance and M&R on the backcalculated modulus values. The only major M&R for this test section was conducted on January 31, 1994, which involved milling of 1.1-inch uppermost asphalt pavement layer and overlaid with 2.1 inches of new HMA. The asphalt layer is one inch thicker, while other layers remain the same. The FWD test data before (August 3, 1993) and after (December 1, 1995) the milling and resurface rehabilitation intervention were analyzed and the backcalculated modulus values were compared. The results showed approximately 42 percent higher modulus values for the asphalt layer and 33 percent higher for asphalt base layer, exaggerated by 26.8°F lower air temperature in 1995. Additionally, 29 percent and 39 percent higher modulus values were observed for the subbase and subgrade layers, respectively. The UMPED modulus values in 1998 were selected as the most reasonable modulus and used for preliminary finite element analysis [102].

3.2 Evaluation of Candidate Backcalculation Methods using Selected Asphalt LTPP Deflection Data

The LTPP test section 28-2807 located at Highway 6 East in Lafayette County, MS was opened to traffic on January 1, 1982. This test section was assigned the CN value of one when the LTPP program started in 1987. The test section comprises of four layers of asphalt, asphalt

base, CTB, and subgrade layers. The subgrade soil type is sandy lean (low plasticity) clay with a CBR value of eight. For analysis purposes, the Poisson's ratio for asphalt pavement and asphalt base is set to 0.35. Ali et al. [105] studied the influence of Poisson's ratio on the surface deflection of layered systems. The deflection factors obtained from laboratory evaluation were compared with the theoretical values. A Poisson's ratio of 0.35 is the ideal value for asphalt material. The use of a higher value of 0.5 for asphalt material resulted in an increased deviation between the calculated modulus using theoretical and experimental approaches. The Poisson's ratio of 0.25 and 0.45 was set for the CTB and subgrade layers, respectively. Since 1987, the test section was subjected to six series of FWD tests from 1990 to 1998 as shown in Table 28.

Table 28. Basic information for LTPP test section 28-2807 in Lafayette County, MS

State Code	SHRP ID	Construction Number, CN	CN Assigned Date	CN Change Reason Code	FWD Test Date
(MS)	2807	1	1st Jan. 1987		11th Oct 1990
					19th July 1991
		2	15th May 1992	25	24th June 1992
					3rd August 1993
		3	31st Jan. 1994	51	1st Dec. 1995
		4	15th May 1997	24	9th July 1998

CN Change Reason
25: Patch potholes-hand spread, compacted with the truck
51: Mill of asphalt concrete and overlay with asphalt concrete
24: Full depth patch of AC pavement (removing damaged material, repairing supporting layer)

Four different CNs were assigned to this test section. The CN is an intervention factor which describes any M&R event that has been applied to the pavement section. The local maintenance to patch potholes has changed the CN to CN two. The FWD tests were conducted annually from October 11, 1990, until August 3, 1993. The thickness of asphalt, base, and subbase layers under CN one and two are 5.5, 5.1, and 6.6 inches, respectively and the subgrade

layer is semi-infinite in depth. The major M&R treatment was conducted on January 31, 1994, and the test section was assigned the CN three. About 1.1 inches of asphalt top layer was milled and resurfaced with 2.1 inches of HMA. Therefore, asphalt layer thickness increased to 6.5 inches and the thicknesses for the base and subbase layers remain unchanged. The FWD tests were continued in 1995 and 1998 to assess the structural integrity of the pavement structure under continuous traffic ESAL applications and environmental factors.

Table 29 shows annual and cumulative ESAL from 1982 until 2001. The annual ESALs show a steady increase in vehicles from 1982 until 1989.

Table 29. ESAL data for test section 28-2807 in Lafayette County, MS

State Code	SHRP ID	Age (Year)	Traffic Year	Annual ESAL	Cumulative ESAL
28	2807	1	1982	53,000	53,000
		2	1983	55,000	108,000
		3	1984	57,000	165000
		4	1985	51,000	216,000
		5	1986	61,000	277,000
		6	1987	65,000	342,000
		7	1988	69,000	411,000
		8	1989	85,000	496,000
		9	1990	72,000	568,000
		10	1991	74,000	642,000
		11	1992	91,000	733,000
		12	1993	94,000	827,000
		13	1994	97,000	924,000
		14	1995	100,000	1,024,000
		15	1996	103,000	1,127,000
		16	1997	106,000	1,233,000
		17	1998	109,000	1,342,000
		18	1999	135,000	1,477,000
		19	2000	140866	1,617,866
		20	2001	146986	1,764,852

In 1990 the recorded annual ESAL reduced by 15.3% compared to the previous year data (1989). Then the traffic count gradually increases until 1998, but a rapid increase of ESAL was observed in 1999. In the LTPP database, traffic data for 2000 and 2001 are missing, so the number is estimated based on the formula proposed in this study. Therefore, the calculated average annual rate of growth is 4.3%. In this case, the estimated annual ESAL for the year 2000 and 2001 are 140,866 and 146,986, respectively. The cumulative ESAL for 20 years are calculated and shown in Table 29.

Table 30 shows the applied loads and corresponding deflections in mils for test section 28-2807. The FWD test was conducted on October 11, 1990.

Table 30. The FWD drop loads and peak deflections (Test section 28-2807, October 11, 1990)

28-2807 Drop No.	Drop Load (lbs)	Area sq. in., Radius = 5.9 in.	Peak Deflections (mils) Test date: October 11, 1990						
			Sensor 1	Sensor 2	Sensor 3	Sensor 4	Sensor 5	Sensor 6	Sensor 7
1	6,207	109.4 sq. in.	3.56	3.00	2.71	2.36	2.10	1.65	1.05
2	6,203		3.54	3.00	2.71	2.35	2.11	1.65	1.05
3	6,218		3.55	3.00	2.71	2.35	2.11	1.66	1.06
4	6,216		3.53	2.99	2.70	2.34	2.10	1.65	1.05
5	9,109		5.17	4.50	4.07	3.53	3.17	2.50	1.60
6	9,163		5.19	4.52	4.10	3.55	3.18	2.52	1.61
7	9,157		5.20	4.52	4.10	3.55	3.18	2.50	1.61
8	9,155		5.19	4.51	4.09	3.54	3.18	2.51	1.60
9	12,534		7.20	6.17	5.59	4.86	4.35	3.43	2.18
10	12,566		7.24	6.20	5.61	4.88	4.37	3.45	2.19
11	12,563		7.24	6.20	5.62	4.88	4.37	3.45	2.19
12	12,560		7.25	6.21	5.62	4.89	4.38	3.45	2.20
13	17,682		9.91	8.54	7.75	6.72	6.03	4.75	3.01
14	17,689		9.96	8.58	7.78	6.75	6.05	4.77	3.00
15	17,690		9.96	8.60	7.79	6.77	6.06	4.78	3.01
16	17,671		9.95	8.59	7.78	6.75	6.05	4.77	3.02
Mean	11,399		6.5	5.6	5.0	4.4	3.9	3.1	2.0
SD	4,407		2.5	2.1	1.9	1.7	1.5	1.2	0.7
COV	38.7%		38.1%	38.4%	38.5%	38.5%	38.5%	38.6%	38.1

For comparison purposes, each software was analyzed using deflections measured at load levels closest to standard 9,000 lbs level of load. Typically, the pavement structural design is based on a loaded axle of 18,000 lbs (9,000 lbs per one-half of the axle). In this research, only the deflection data for drop number eight is used to backcalculate modulus values.

3.2.1 Backcalculation Software Evaluated for Preliminary Study in This Research

The FWD data for test section 28-2807 was extracted from the LTPP database and used as an input in the PCASE 2.09, BAKFAA 2.0, and EVERCALC 5.0 backcalculation software. The PCASE 2.09 software was developed under collaboration between the Transportation System Center and ERDC of the U.S. Army Corps of Engineers [97]. The PCASE 2.09 software allows the the user to backcalculate pavement layers modulus values and evaluates response analysis for both asphalt and concrete pavements. Users are required to provide traffic data, pavement layers with specific thicknesses, seed modulus values, Poisson's ratio, interface parameter for each layer, monthly air temperatures, and FWD data. A maximum of ten iterations for each drop is allowed for evaluation of the backcalculated modulus.

The BAKFAA 2.0 software was developed by the Federal Aviation Administration (FAA) and more straight forward as compared to the PCASE 2.09 software. This software used FAA Layered Elastic Analysis (LEAF) backcalculation subroutine [106]. The required inputs for analysis are pavement layers (up to 10 layers), seed modulus values, Poisson's ratio, interface parameter for each layer, FWD sensor location, and deflection data. The maximum number of 5,000 iterations was reported [99].

The EVERCALC 5.0 software was developed by Mahoney et al. [107] and included as one of the EVERSERIES software packs developed by the Washington Department of

Transportation [100]. The software adopted CHEVRON forwarded subroutine and an iterative subroutine for backcalculation process. The required inputs for analysis are pavement layers which are limited to limited to four layers including stiff layer, seed modulus values, Poisson's ratio, interface parameter for each layer, pavement temperature, and FWD data. The maximum of 10 iterations are set for analysis and the deflection tolerance is based on percent RMS error. The LTPP database InfoPave (https://infopave.fhwa.dot.gov/) is now populated with the backcalculated modulus values using this software [100].

3.2.2 Methodology for Modulus Values Backcalculation Process

The following key steps were implemented for the backcalculation of pavement layer modulus values:

1) Assign pavement layer configurations including layer thicknesses and Poisson's ratio are referred to the previous study on test section 28-2807 by Uddin et al [102].

2) Extract FWD data conducted in 1990, 1991, 1992, 1993, 1995 and 1998 from the LTPP database.

3) Provide seed modulus values which are required by each backcalculation software used in this research.

The default seed modulus values for BAKFAA 2.0 and PCASE 2.09 [99], and EVERCALC 5.0 [100] are shown in Table 31. On the other hand, no seed modulus values are used by the UMPED software.

4) Run backcalculation process using the PCASE 2.09, BAKFAA 2.0, EVERCALC 5.0, and UMPED software. Calculate the RMSE as shown in Equation 3.10.

5) Compare the modulus value with the backcalculated modulus values from the previous study by Boriboonsonsin and Momm [103] as shown in Table 32. The most acceptable modulus values were selected for further analysis using the finite element software.

Table 31. Default seed modulus values used in this research

Default seed modulus values used in this research (psi) *Default, **Automatically generated from UMPED			
Layer	*BAKFAA (2.0)	*EVERCALC (5.0)	*PCASE (2.09)
Asphalt	500,000	150,000	350,000
Asphalt Treated Base (ATB)	500,000	50,000	300,000
Cement Treated Base (CTB)	750,000	400,000	300,000
Subgrade	7,000	10,000	15,000

$$RMS\ error\ (\%) = \sqrt{\frac{1}{n_d} x\ \sum_{i=1}(d_{ci} - d_{mi})^2}\ \text{x } 100 \quad (3.10)$$

Where,

d_{ci} = Calculated surface deflection at sensor i,

d_{mi} = Measured surface deflection at sensor i, and

n_d = Number of deflection sensors used in the FWD test

For the asphalt layer, the seed modulus value for BAKFAA 2.0 is the highest compared to other software. The modulus of 150,000 psi which is in the proposed ranges of 100,000 to

200,000 psi was used for EVERCALC 5.0 software. The asphalt modulus value for the PCASE 2.09 is 350,000 psi. For the base layer, BAKFAA 2.0 specified 500,000 psi for a stabilized base layer. The PCASE 2.09 software used 300,000 psi for asphalt base layers. In EVERCALC 5.0 manual, only lime stabilized and cement stabilized modulus values are specified [100]. Therefore, similar modulus value of 50,000 psi was used for asphalt base layer. For the CTB layer, the modulus values vary from 300,000 to 750,000 psi. The proposed values are significantly higher compared to the modulus value backcalculated by Uddin et al. [102]. The subgrade modulus values are 7,000 psi for BAKFAA 2.0, 10,000 psi for the EVERCALC 5.0 and 15,000 psi for the PCASE 2.09 software, respectively.

Table 32. Modulus values from previous study by Boroboonsonsin and Momm [103]

FWD Date Test	Air Temp. (°F)	CN	Backcalculated Young's Modulus Summary Results (psi)				
			Statistics	Layer 1 Asphalt	Layer 2 Asphalt Base	Layer 3 CTB	Layer 4 Nonlinear (Subgrade)
Oct. 11, 1990	43.3	1	Mean COV (%)	989,900 50	1,093,300 57	119,100 41	24,160 15
July 19, 1991	77.7	1	Mean COV (%)	536,200 32	655,600 40	102,800 35	20,160 19
June 24, 1992	85.5	2	Mean COV (%)	403,500 32	367,800 29	74,600 25	17,720 18
Aug. 3, 1993	77.6	2	Mean COV (%)	623,300 32	623,600 40	90,500 41	19,240 16
Dec 1, 1995	50.8	3	Mean COV (%)	884,00 49	826,800 63	116,800 45	26,700 16
July 9, 1998	96.3	4	Mean COV (%)	264,600 44	236,400 54	91,400 45	18,010 18
Average				616,917	633,917	99,200	20,998
Standard Deviation (SD)				253,863	282,150	15,601	3,316
Coefficient of Variation (%)				41.2	44.5	15.7	15.8

The modulus values in Table 33 are referred for comparison with the backcalculated values from other software. The backcalculated modulus values for subgrade layer are corrected

for the nonlinear behavior corresponding to the effect of the design wheel load [103]. On the other hand, no correction to the modulus values of the asphalt base and the CTB layers are applied due to the fact that these are the stabilized layers. The important findings from the study [103] follow:

- The modulus values for asphalt pavement and asphalt base layers increase caused by the lower air temperature during the FWD tests due to visco-elastic properties of the asphalt layer. This implies that the backcalculated temperature-dependent modulus values for asphalt pavement and asphalt base layers for higher temperature (1991, 1992, 1993, and 1998) are smaller compared to the modulus values at lower temperatures for 1990 and 1995.
- The modulus values for the CTB layer show a decreasing trend over time. Under constant temperature, the modulus value for the CTB in 1991 is about 12 percent lower compared to the modulus in 1993. This implies that under continuous traffic loads application, the CTB is prone to crack-related degradation and age-related degradation [102].

The modulus values for subgrade layer show no obvious changes with only less than 20% in COV. The relatively small variation indicates almost homogenous soil layer, and most importantly, the subgrade layer is not affected by the seasonal changes. According to Uddin et al [102], the modulus value for the subgrade layer usually four to six times less than the CTB layer. Additionally, the increase in subgrade modulus values is closely related to the variations in moisture content in the subgrade layer. It can be seen that lower subgrade modulus values are observed during summer months due to frequent rainfall compared to the modulus values in winter months.

3.3 In Situ Material Characterization of Selected Asphalt Pavement Structures

This sub-chapter compares the stiffness of asphalt pavement, asphalt treated base, cement treated base, and subgrade layers based on the modulus values calculated using different computer programs. In general, material characterization focuses on two main parameters, which are Young's modulus, and the Poisson's ratio.

The reasonableness of the backcalculated modulus values is evaluated by comparing modulus values from different software as shown in Table 33. The FWD test date, CN, air and surface temperatures, layer thicknesses, and RMS error in percent for test section 28-2807 are included in the table. The reasonableness of the backcalcalculated modulus is assessed based on sensitivity to temperature changes for the first two layers, changes of the CTB layer modulus values over time, acceptable changes of the modulus values for the subgrade layer for different years, and must be within the specified modulus ranges.

In general, although the same deflection data sets are used, the backcalculated modulus values from each software are greatly differ. This implies that the analysis subroutine for each software is different. The BAKFAA 2.0 used LEAF [99] subroutine, a layered elastic computational program. The EVERCALC iteration is based on CHEVRON subroutine [99]. The PCASE 2.09 adopted WES5 subroutine [99], and the UMPED used the BASIN backcalculation analysis subprogram incorporated in the PEDD software [108, 109]. Comparison with the previous study [103] shows the inconsistency of the backcalculated modulus values using BAKFAA 2.0 and PCASE 2.09 which are noted through the huge unexpected increase in the modulus values for the CTB layer. The BAKFAA 2.0 software also shows an unreasonable asphalt base modulus value that in most cases was excessively higher than asphalt layer modulus value.

For data sets in 1990, the EVERCALC 5.0 software over-predicted asphalt base modulus value, almost double the modulus value for asphalt pavement. Additionally, for all other cases, the EVERCALC 5.0 software shows excessively low modulus values for the asphalt base and the CTB layers. For test section 28-2807 in MS, the backcalculated modulus values from the LTPP database are unreasonable due to very low values compared to the Boriboonsonsin and Momm study [103]. Only the UMPED software shows reasonable modulus values for all cases. In general, the modulus values relatively decrease as the distances of the underlying layers are farther from the asphalt surface. The comparison between the measured and calculated surface deflection values for each backcalculation software is shown in Figure 38.

The RMS error in percent depends on the deviation between the calculated and measured deflections. The BAKFAA 2.0, EVERCALC 5.0 from the LTPP database, and the PCASE 2.09 software show the least error compared to the measured deflection values. This implies that the differences between the measured and final calculated deflections are relatively small. However, it is noted that the backcalculation subroutine used in that software tries to minimize the RMS error by repeating the iteration processes, but compromise the reasonableness of the backcalculated modulus values. The deflection values calculated using the EVERCALC 5.0 software are very poor compared to other software. Both PCASE 2.09 and EVERCALC have been set to a maximum of 10 iterations. Maximum number of iterations is 455 for the BAKFAA2.0 software in this research.

For the UMPED software, after a single iteration for each layer, the calculated deflections at sensors one, six and seven show very small differences compared to the measured deflection values. Generally, the deviation between the measured and calculated deflections at sensor one reflects the asphalt layer modulus values. On the other hand, the differences between the

measured and calculated deflection for sensor six and seven affect the modulus value for the subgrade layer.

Table 33. Backcalculated modulus values for test section 28-2807 in Mississippi

			Backcalculated Moduli (psi)					
SHRP_ID 28 (MS)-2807	Layer (Thickness)	Backcalculation Method	Asphalt Surface	Asphalt Base	Cement Treated Base	Subgrade	No. of Iterations	RMS Error (%)
FWD Test Date: 10/11/1990	Asphalt (5.5 in.)	BAKFAA 2.0	943,693	899,389	126,802	28,096	408	1.3%
Construction Number: 1	Asphalt Treated Base (5.1	EVERCALC 5.0 (From	170,569	27,011	3,599	4,241	-	1.3%
Temperature:	Cement Treated Base (6.6	EVERCALC 5.0 (Calculated)	446,740	847,440	35,000	43,600	10	21.1%
Air: 43.3°F, Surface: 32.7°F	Subgrade	PCASE 2.09	2,195,236	115,301	1,029,395	17,105	3	0.8%
		UMPED	1,200,000	90,000	70,000	36,650	1	78.6%
			Backcalculated Moduli (psi)					
SHRP_ID 28 (MS)-2807	Layer (Thickness)	Backcalculation Method	Asphalt Surface	Asphalt Base	Cement Treated Base	Subgrade	No. of Iterations	Avg. RMS Error
FWD Test Date: 07/19/1991	Asphalt (5.5 in.)	BAKFAA 2.0	1,083,350	66,789	862,736	22,155	192	4.4%
Construction Number: 1	Asphalt Treated Base (5.1	EVERCALC 5.0 (From	170,569	27,011	3,599	4,241	-	1.3%
Temperature:	Cement Treated Base (6.6	EVERCALC 5.0 (Calculated)	1,687,500	35,000	35,000	43,600	10	26.0%
Air: 77.7°F, Surface: 103.1°F	Subgrade	PCASE 2.09	598,751	180,249	463,786	16,626	2	0.8%
		UMPED	1,029,300	89,300	70,000	29,760	1	42.1%
			Backcalculated Moduli (psi)					
SHRP_ID 28 (MS)-2807	Layer (Thickness)	Backcalculation Method	Asphalt Surface	Asphalt Base	Cement Treated Base	Subgrade	No. of Iterations	Avg. RMS Error
FWD Test Date: 06/24/1992	Asphalt (5.5 in.)	BAKFAA 2.0	501,588	107,923	191,511	21,894	365	3.2%
Construction Number: 2	Asphalt Treated Base (5.1	EVERCALC 5.0 (From	75,547	22,063	3,320	3,696	-	1.3%
Temperature:	Cement Treated Base (6.6	EVERCALC 5.0 (Calculated)	828,100	35,000	35,000	43,600	10	31.1%
Air: 85.5°F, Surface: 122.0°F	Subgrade	PCASE 2.09	377,683	128,154	281,308	15,290	4	2.6%
		UMPED	789,800	90,000	60,000	20,060	1	14.9%
			Backcalculated Moduli (psi)					
SHRP_ID 28 (MS)-2807	Layer (Thickness)	Backcalculation Method	Asphalt Surface	Asphalt Base	Cement Treated Base	Subgrade	No. of Iterations	Avg. RMS Error
FWD Test Date: 08/03/1993	Asphalt (5.5 in.)	BAKFAA 2.0	1,125,212	206,918	127,573	23,359	288	1.3%
Construction Number: 2	Asphalt Treated Base (5.1	EVERCALC 5.0 (From	75,547	22,063	3,320	3,696	-	1.3%
Temperature:	Cement Treated Base (6.6	EVERCALC 5.0 (Calculated)	1,538,460	35,000	35,000	43,600	10	27.8%
Air: 77.6°F, Surface: 95.5°F	Subgrade	PCASE 2.09	1,033,789	142,985	340,384	15,880	2	0.8%
		UMPED	1,091,100	85,600	70,000	28,530	1	40.5%
			Backcalculated Moduli (psi)					
SHRP_ID 28 (MS)-2807	Layer (Thickness)	Backcalculation Method	Asphalt Surface	Asphalt Base	Cement Treated Base	Subgrade	No. of Iterations	Avg. RMS Error
FWD Test Date: 12/01/1995	Asphalt (6.5 in.)	BAKFAA 2.0	1,761,351	96,012	307,207	27,436	455	1.2%
Construction Number: 3	Asphalt Treated Base (5.1	EVERCALC 5.0 (From	167,557	29,613	3,961	4,371	-	1.4%
Temperature:	Cement Treated Base (6.6	EVERCALC 5.0 (Calculated)	2,295,000	35,000	35,000	43,600	10	18.2%
Air: 50.8°F, Surface: 44.7°F	Subgrade	PCASE 2.09	1,652,768	54,809	1,195,041	18,157	10	5.5%
		UMPED	1,200,000	90,000	70,000	36,900	1	68.5%
			Backcalculated Moduli (psi)					
SHRP_ID 28 (MS)-2807	Layer (Thickness)	Backcalculation Method	Asphalt Surface	Asphalt Base	Cement Treated Base	Subgrade	No. of Iterations	Avg. RMS Error
FWD Test Date: 07/09/1998	Asphalt (6.5 in.)	BAKFAA 2.0	146,430	738,211	66,901	24,480	295	1.6%
Construction Number: 4	Asphalt Treated Base (5.1	EVERCALC 5.0 (From	35,517	32,432	2,841	3,991	-	1.3%
Temperature:	Cement Treated Base (6.6	EVERCALC 5.0 (Calculated)	433,100	35,000	35,000	43,600	10	29.6%
Air: 96.3°F, Surface: 117.5°F	Subgrade	PCASE 2.09	215,763	76,104	800,768	16,096	3	0.6%
		UMPED	559,900	90,000	63,300	21,110	1	11.2%

The UMPED backcalculation subroutine calculates seed modulus values as a function of the peak test load, measured deflections, and pavement layer thicknesses. Then it starts the iteration initially for the subgrade layer. Once the modulus value for the subgrade layer is determined, the iteration process continues for the asphalt layer and other intermediate layers [109]. Although the RMS error is higher compared to other software, the UMPED is more

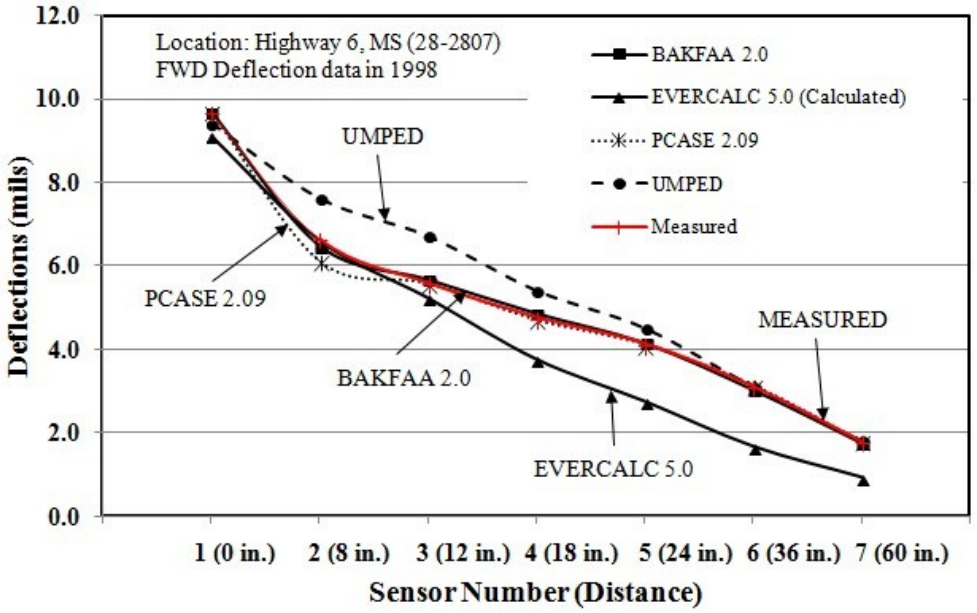

Figure 38. Comparison between the measured and calculated deflections in 1998

efficient in predicting reasonable modulus values since those values are computed only after one iteration. The modulus values from Table 33 were plotted as shown in Figures 39 through 42 for asphalt, asphalt base, CTB, and subgrade layers, respectively. For asphalt layer (Figure 39), only the modulus values determined using the PCASE 2.09 and UMPED software show higher modulus values as the temperatures decrease. The calculated modulus using the EVERCALC 5.0 gave unacceptable modulus of more than 2.2 million psi at 50.8ºF air temperature, which is too high for asphalt pavement.

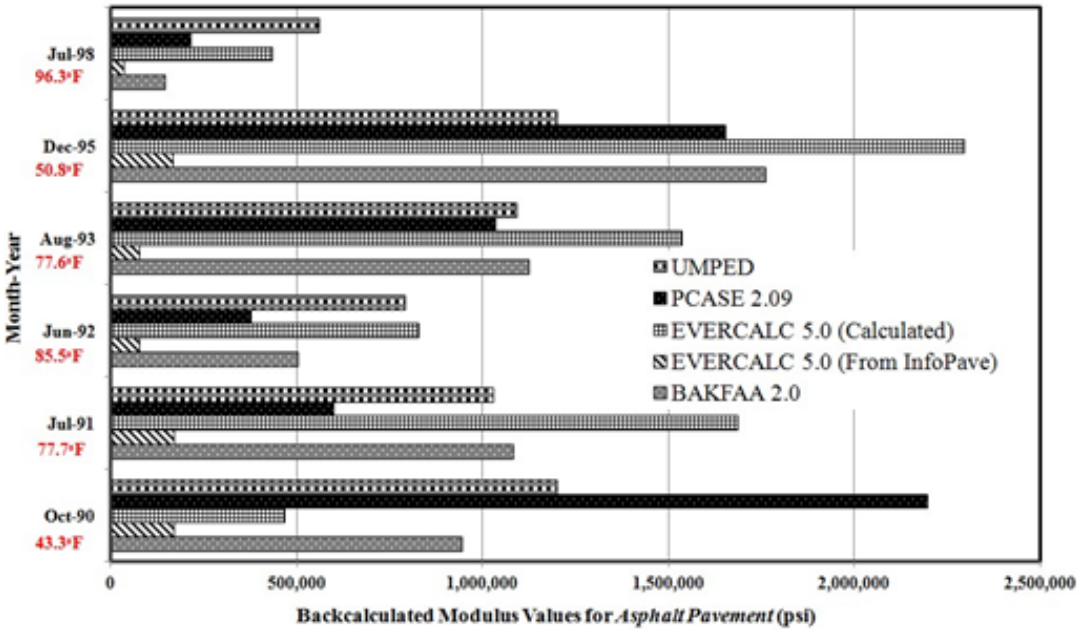

Figure 39. Backcalculated modulus values for asphalt surface layer

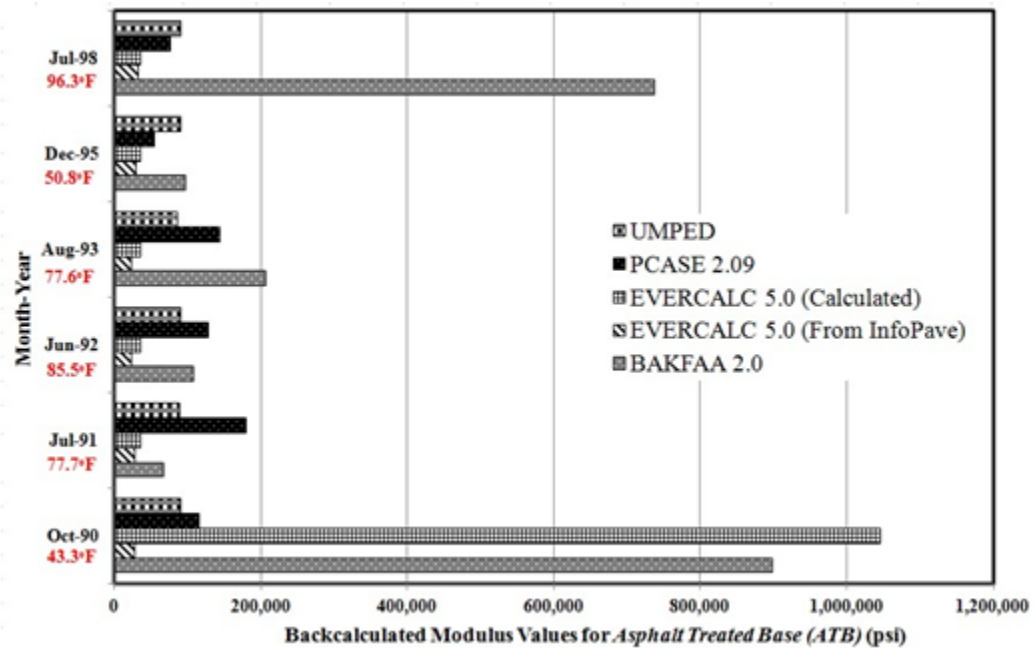

Figure 40. Backcalculated modulus values for asphalt treated base layer

The modulus values from the LTPP InfoPave database are very low for all years. In general, the modulus values are higher than the backcalculated values from the previous study

[103]. However, according to Priddy et al. [99], the acceptable ranges are in between 70,000 to 3,625,000 psi for the asphalt layer.

For the asphalt treated base layer (Figure 40), the modulus values are relatively low for all cases compared to Boriboonsonsin and Momm [103] predictions. The modulus value of 899,389 psi (1990) determined using the BAKFAA 2.0 software is reasonable for the FWD deflection data measured during a near freezing condition. Additionally, this value is slightly lower than asphalt pavement modulus and higher than modulus values for the CTB (Figure 41) and subgrade layers, respectively. The proposed range for asphalt base is 100,000 to 3,625,000 psi [99].

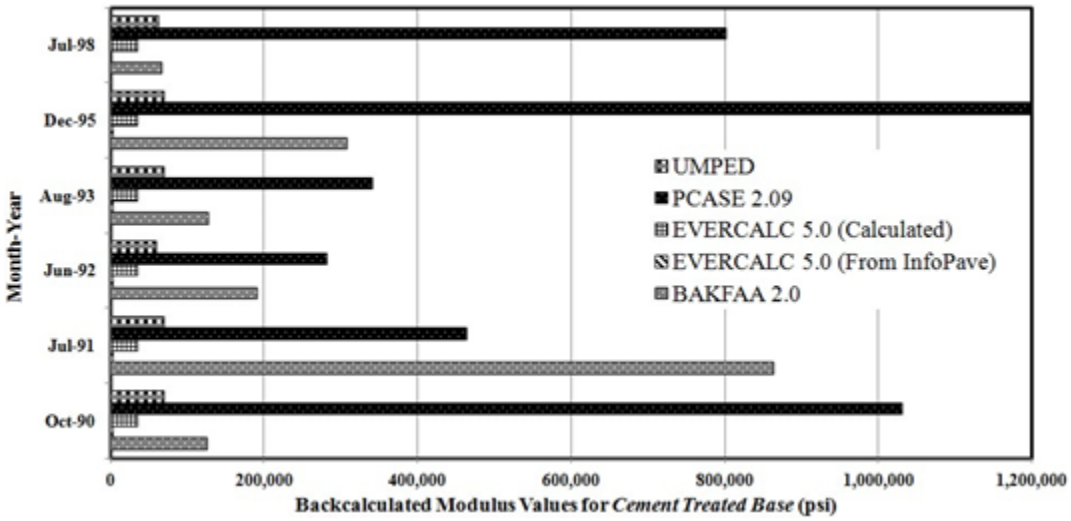

Figure 41. Backcalculated modulus values for CTB layer

For the CTB, only the UMPED and PCASE 2.09 software indicate decreasing values over time from 1990 to 1992 due to possible crack in the CTB layer under continuous traffic application. The reasonable modulus values are in between 10,000 to 1,000,000 psi for the stabilized base [99]. The backcalculated modulus values using the EVERCALC 5.0 from the LTPP InfoPave database are very low and unreasonable.

The backcalculated modulus values for the subgrade layer are compared and shown in Figure 42. A reasonable range for subgrade modulus is from 1,000 to 30,000 psi [99]. Only the PCASE 2.09 software shows the least variation in subgrade modulus values from 1990 to 1998. In contrast, the UMPED and BAKFAA 2.0 have more than 25% difference between the lowest and the highest modulus values. The variation is expected as moisture content changes throughout the year and over the life of the pavement. The subgrade modulus values calculated using the EVERCALC 5.0 software are very low for all cases. Overall, the 1998 FWD test data analyzed by the BAKFAA 2.0 software and the UMPED backcalculation software provide reasonable in situ modulus values for all pavement layers.

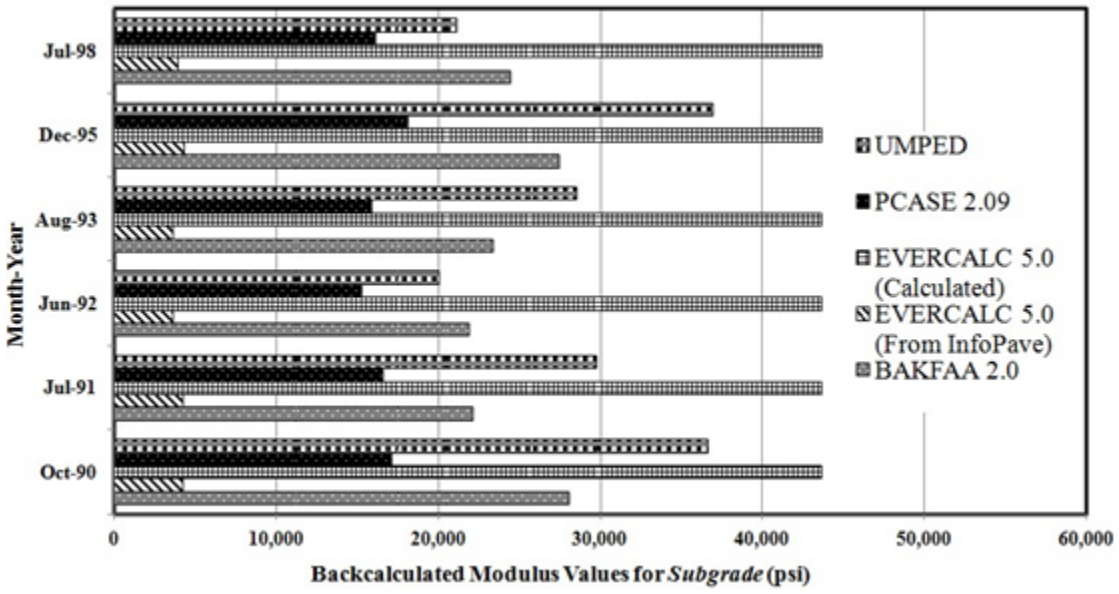

Figure 42. Backcalculated modulus values for the subgrade layer

Based on the research, it can be concluded that the UMPED software shows a consistent reasonable set of backcalculated modulus values for FWD data collected over the years for all layers. The next-reasonable modulus values were backcalculated using the BAKFAA 2.0 software using the FWD deflection data collected in 1998 (Table 33). It is observed that the

modulus values of both asphalt layers are higher than expected. The output for 1998 data shows 295 iterations and RMS of 1.6 percent, respectively. On the other hand, the most reasonable modulus values backcalculated using the UMPED software for 1998 data are 559,900 psi (asphalt surface layer), 90,000 psi (asphalt treated base), 63,300 psi (CTB), and 21,110 psi (subgrade layer), respectively for 1998 data. These values were calculated after one iteration only with RMS of 11.3 percent. Therefore, this research suggests that the backcalculated modulus values for the year 1998 using the BAKFAA 2.0 software and the UMPED software for deflection data in 1998 are reasonable and recommended to be used for the 3D-FE numerical analysis, if desired.

3.4 Review of FWD Dynamic Analysis for Backcalculation of Asphalt Pavement Layer Modulus Values and Comparison with Layered Elastic Static Analysis Results

The FWD is a testing device used to evaluate the physical properties of the pavement. It provides the structural capacity evaluation of the pavement system, which is important for load-carrying capacity analysis. Figures 43 shows an illustration of the FWD test set up and the locations of geophone sensors. Once a specific magnitude of FWD load is dropped on top of a circular steel plate, a load pulse is transmitted on the pavement surface. This action creates a deflection that simulates wheel load caused by a moving vehicle, for example, a heavy truck. The geophone sensor automatically determines the vibration amplitude, depending on the magnitude of the FWD loads. Subsequently, complex formulation of the computer program will calculate the deflections under each sensor. The line indicates the deflection basin usually obtained from

the FWD test. The deflection values under each sensor are used for the backcalculation process to determine the modulus of asphalt, base, subbase, and subgrade layers.

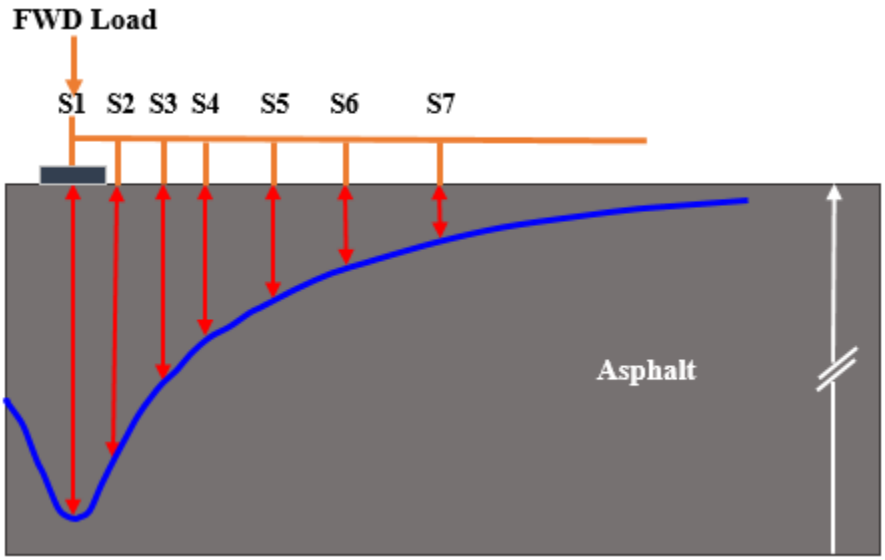

Figure 43. Approximate illustration of FWD load point and the locations of geophone sensors (not to scale)

The previous sub-chapter highlighted the estimation of modulus values using a static backcalculation approach based on the layered elastic analysis. Unfortunately, the computer programs developed for backcalculation of modulus value did not consider the dynamic load of the FWD test. It is noted that the structural response of an asphalt pavement is time-dependent and affected by load-time history [90, 104, 110]. For that reason, a more advanced approach to study the effects of the FWD load on pavement structural responses using the 3D-FE modeling was introduced by a few researchers [104, 110]. Garza [111] has developed a 3D-FE model using LS-DYNA software to further evaluate the effect of dynamic loading based on the load-time history curve. The sizes of the elements are set in a way that the location of the nodes in the 3D-FE matched with actual distances from the loading point of the geophone sensors used in the

FWD testing device. Figure 44 shows the 3D-FE model of uncracked asphalt that consists of asphalt, base, subbase, and subgrade layers used in the previous study [111].

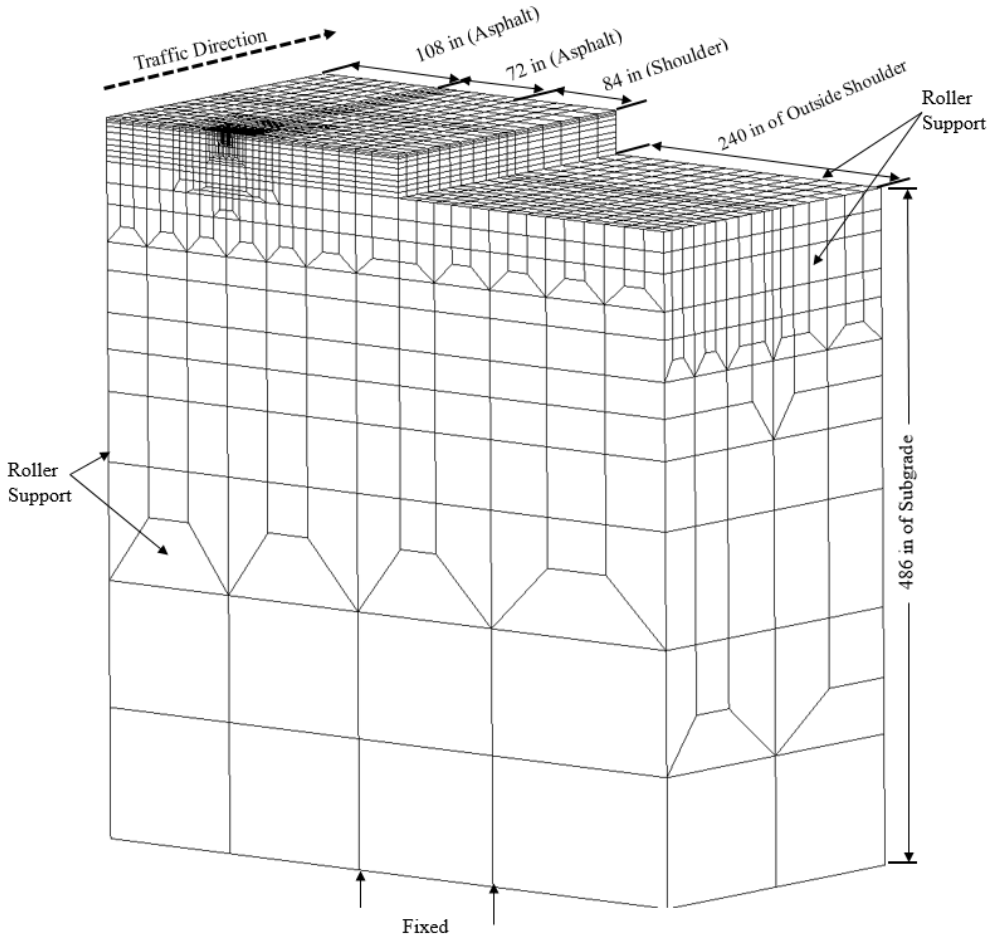

Figure 44. Garza's 3D-FE model used to evaluate responses under the FWD load [111]

Garza's runs multiple 3D-FE simulations under the FWD load and observed the responses at specific nodes of the elements. Subsequently, the responses from the 3D-FE analysis based on factorial design were used to develop the multiple regression equations to predict modulus value for asphalt, base, subbase, and subgrade layers, respectively.

From previous discussion, it was observed that the UMPED [104] static modulus backcalculation program developed at the University of Mississippi showed among the most reasonable predictions of modulus for the section 28-2807 in Mississippi. Based on this

statement, this research intends to further evaluate the reasonableness of the predicted modulus values using UMPED static analysis, with Garza's multiple regression equations to predict modulus values for all four layers. Table 34 summarized the backcalculated modulus values for asphalt layer, Lime-Filled Asphalt (LFA) base layer, Lime-Treated Subbase (LTS) layer, and subgrade layer [111].

Table 34 shows the backcalculated modulus values for all layers using UMPED for drop number two. The outputs for seven sensors are selected for comparison with the modulus values calculated using multiple regression based on the 3D-FE analysis.

Table 34. Summary of modulus values from UMPED for US45N North Project, Section 1, Station 461+05 (After Garza [111])

Cycle	Method		Modulus Values: MPa (psi)				
			Asphalt	LFA	LTS	Subgrade	
3	Backcalculation UMPED Drop 2	Thickness mm (inch)	152.4 (6)	152.4 (6)	152.4 (6)	Semi-infinite	Nonlinear Modulus
		Sensor 1-7	4,624 (670,600)	1,040 (150,800)	110 (15,900)	160 (23,240)	118 (17,180)
		Sensor 1-6	4,619 (670,000)	612 (88,700)	176 (25,500)	163 (23,680)	116 (16,870)

3.4.1 Evaluation of Asphalt Pavement Modulus using Predictive Equations Developed from the 3D-FE Numerical Analysis

The multiple regression equations were developed based on the area under deflection-time history method which was described in detailed by Garza [111]. The following parameters are required to calculate the modulus values based on the regression constant and coefficient values:

- The area from measured deflection-time history (AW) for US 45N as shown in Table 35 [After 111]
- The area under FWD load/peak load-time history curve (LA = 24.4 msec)
- Radial distances of each sensor (R_1 = 0 in., R_2 = 12 in., R_3 = 24 in., R_4 = 36 in., R_5 = 48 in., R_6 = 60 in., R_7 = 72 in.) [91]
- The plate is a 4-segmented plate with a radius of 5.91 inches
- Layer thicknesses for asphalt, base, and subgrade layers as shown in Table 35 too [After 111]

Table 35. Areas from measured deflection-time history for US45N, Cycle 3, Drop 2 [After 111]

AW_1	246.79 mils-msec	LA	24.40 msec
AW_2	183.73 mils-msec	T_1	6 inches
AW_3	122.38 mils-msec		
AW_4	83.94 mils-msec	T_2	6 inches
AW_5	61.13 mils-msec		
AW_6	47.32 mils-msec	T_3	6 inches
AW_7	36.79 mils-msec		

In order to obtain the modulus values for all layers, the subgrade modulus must be calculated first, since the subgrade modulus value is required to predict the modulus values for other layers. Equations 3.11 to 3.14 are used to predict modulus values for subgrade layer (E_4), subbase layer (E_3), base layer (E_2), and asphalt layer (E_1), respectively.

$$\text{Log}_{10}(E_4) = 10.005 - 0.0289*\text{Log}_{10}(1+T_2) - 0.05*\text{Log}_{10}(1+T_3) + 0.2940*\text{Log}_{10}(AW_1) + 1.418*\text{Log}_{10}(AW_3 \times R_3) - 3.0270*\text{Log}_{10}(AW_4 \times R_4) + 5.6790*\text{Log}_{10}(AW_5 \times R_5) - 4.3820*\text{Log}_{10}(AW_6 \times R_6) - 1.1090*\text{Log}_{10}(LA \times AW_2 \times R_2) - 0.025*\text{Log}_{10}[(1+T_1) \times (1+T_2) \times (1+T_3)] \quad (3.11)$$

$$\text{Log}_{10}[E_3 \text{ x } (1+T_3^3)] = 13.760 - 0.3730*\text{Log}_{10}(1+T_1) - 0.4850*\text{Log}_{10}(1+T_2) + 3.1030*\text{Log}_{10}(1+T_3) + 0.0616*\text{Log}_{10}(AW_1) - 5.26*\text{Log}_{10}(AW_3 \text{ x } R_3) + 1.5030*\text{Log}_{10}(AW_4 \text{ x } R_4) - 3.3620*\text{Log}_{10}(AW_5 \text{ x } R_5) + 3.2190*\text{Log}_{10}(AW_6 \text{ x } R_6) + 3.09*\text{Log}_{10}(LA \text{ x } AW_2 \text{ x } R_2) - 1.3210*\text{Log}_{10}(AW_6 \text{ x } R_6 \text{ x } E_4) \quad (3.12)$$

$$\text{Log}_{10}[E_2 \text{ x } (1+(T_2^3)] = 21.84 - 0.753*\text{Log}_{10}(1+T_1) - 0.2230*\text{Log}_{10}(1+T_3) + 1.01*\text{Log}_{10}(AW_1) + 8.1160*\text{Log}_{10}(AW_3 \text{ x } R_3) - 6.0220*\text{Log}_{10}(AW_4 \text{ x } R_4) + 7.8720*\text{Log}_{10}(AW_5 \text{ x } R_5) - 8.6540*\text{Log}_{10}(LA \text{ x } AW_2 \text{ x } R_2) + 3.3790*\text{Log}_{10}(E_4) - 4.2450*\text{Log}_{10}(AW_6 \text{ x } R_6 \text{ x } E_4) + 2.9030*\text{Log}_{10}[LA \text{ x Radius x } (1+T_2)] \quad (3.13)$$

$$\text{Log}_{10}[E_1 \text{ x } (1+T_1^3)] = -21.182 - 0.0169*\text{Log}_{10}(1+T_2) + 0.0232*\text{Log}_{10}(1+T_3) - 4.1970*\text{Log}_{10}(AW_1) - 9.7050*\text{Log}_{10}(AW_3 \text{ x } R_3) + 3.7740*\text{Log}_{10}(AW_4 \text{ x } R_4) - 3.9660*\text{Log}_{10}(AW_5 \text{ x } R_5) + 11.478*\text{Log}_{10}(LA \text{ x } AW_2 \text{ x } R_2) - 2.17*\text{Log}_{10}(E_4) + 2.4160*\text{Log}_{10}(AW_6 \text{ x } R_6 \text{ x } E_4) + 3.3010*\text{Log}_{10}[LA \text{ x Radius x } (1+T_1)] \quad (3.14)$$

The use of logarithms to base 10 was noted in the equations. This implies that data transformation using logarithms to base 10 give a better correlation coefficient, R values of 0.978, 0.851. 0.889. 0.959 for equations 3.11 to 3.14, respectively [111]. Based on the previous study by Uddin [85], it was discovered that the radial distance of the sensors helped to improve the R-value. Therefore, Garza [111] has incorporated the interaction between the area under the deflection-time history curve, radial distance, and modulus value as part of the independent variables in the developed equations. Table 36 summarizes the comparison between the UMPED

outputs as compared to the predictions from multiple regression models developed based on the 3D-FE responses.

Table 36. Comparison between UMPED and regression model using areas under deflection-time history data

Highway US45N, North Project, Section 1, Cycle 3, Drop 2			
Layers \ Methods	Regression Model using Areas under Deflection-Time History Curves, psi [98]	Backcalculated Modulus, psi (UMPED)	% Difference UMPED vs Regression Model
Asphalt, E_1	613,584.4	670,700.0	9.3%
LFA Base, E_2	95,894.7	150,800.0	57.3%
LTS Subbase, E_3	12,351.0	15,900.0	28.7%
Subgrade, E_4	19,692.1	17,180.0	-12.8%

As shown in Table 36, reasonable good results were backcalculated for the asphalt and subgrade layers within ± 15%. The UMPED predicted 9.3% higher asphalt modulus compared to multiple regression prediction models. Additionally, the UMPED calculated 12.8% less subgrade modulus value compared to another method, which is also acceptable for a high variability soil condition. Percent difference in the subgrade modulus could be higher, however, the UMPED has incorporated certain algorithm to correct for nonlinear behavior of subgrade soil. On the other hand, the base and subbase layers showed much higher discrepancies in backcalculated modulus values using the two approaches. As demonstrated by Uddin [85], the surface deflection values are relatively insensitive to modulus values of two intermediate layers.

3.5 Climate Impacts on Pavement Layer Modulus Values and Structural Capacity

An in-depth study was conducted to assess climate impacts using the Pavement Design System for New and Existing Asphalt Pavements (PADAP) asphalt pavement design and

analysis software. This software was developed for the Mississippi Department Of Transportation and was used for climate impact assessment [112, 113]. Additionally the PADAP software provides a mechanistic methodology to pavement designers for modeling the effects of in-service environmental and load conditions for enhanced and realistic structural designs of pavement-subgrade system. Uddin et al. [114] provide detail sensitivity analysis of mechanistic-empirical pavement structural design methods considering climate impacts on layer modulus values. Climate data for Water Valley, Mississippi was used to select maximum air temperature days during the period of 1991 to 2016. The analysis indicates that the thickness design of longer lasting pavement performance depends on correct layer modulus values considering extreme weather and climate attributes [114].

IV. THREE DIMENSION-FINITE ELEMENT (3D-FE) MODELING OF UNCRACKED ASPHALT PAVEMENTS

4.1 Literature Review

The 3D-FE modeling allows the user to view the pavement system from multiple perspectives. Through observation, the 3D-FE helps to improve the visualization of the stress-strain and deflection behavior in pavement layer subjected to dynamic loads. Furthermore, the 3D-FE allows the user to improve impact and sensitivity analysis, and identify potential consequences of changing material properties and layer thicknesses on pavement response analysis. Once the final 3D-FE model is developed, it can be used to estimate modifications to implement any changes to the real pavement systems. According to Uddin et al. [21], the FE numerical analysis helps users to realistically model pavement structure, evaluate, and visually check the integrity of the model. Most importantly, the 3D-FE analysis helps to reuse or reapply part of the existing information and knowledge from previous studies.

Uddin and Garza [93] evaluated the dynamic effects such as damping, load pulse duration, and dynamic response analysis of FWD impact load tests on asphalt pavements. The study was conducted to quantify the needs of pavement response analysis considering load-time history and related dynamic effects, which have been neglected in most of the modulus backcalculation programs. The traditional programs used only peak deflections, peak FWD load, and static linear response analysis to backcalculate the Young's modulus value. A 3D-FE half model asphalt pavement section was modeled using LS-DYNA software to verify the in situ

backcalculated modulus values for the U.S. Highway 45 North project, and compared with the UMPED backcalculated modulus values. Uddin and Garza [93] concluded that the effect of damping on the calculated dynamic FWD deflections and backcalculated modulus is very small and negligible. On the other hand, the load pulse duration of the FWD affected the backcalculated modulus values using dynamic analysis. A range of 40 to 100 millisecond (msec) for the load pulse was found to generate good dynamic response and provide a better simulation of moving highway traffic. Uddin and Garza [93] provide a thorough explanation of implicit and explicit analysis using ABAQUS, and only explicit analysis using LS-DYNA. The authors concluded that the explicit analysis is more accurate for pavements subjected to FWD dynamic loads [93].

Wang et al. [115] studied the 3D-FE model of an asphalt pavement structure using the ABAQUS software. Instead of assuming an average tire pressure applied at only one position, Wang et al. simulated possible effects of changing load position due to wander in wheel path. Additionally, the stop, braking, and turning actions of a moving vehicle caused variations in applied direction and force due to wheel loads. In order to simulate different load pressures on pavement surface, a reasonable wheel-load model was developed and used for the 3D-FE analysis. The wheel-load model consisted of a pair of the simulated longitudinal tire thread contours with simulated pressure values ranging from 460 to 870 kPa (66.7 to 126.2 psi). For details of the 3D-FE model, see Wang et al. [115].

Wang et al. [115] modeled asphalt, cement stabilized macadam, and lime stabilized layers with the thicknesses of 15 in, 30 in, and 40 in, respectively. The modulus values ranged from 174,045 psi, 217,557 psi, 116,030 psi, and 5,802 psi, respectively from top to the bottom layers. The Poisson's ratios were 0.25 (asphalt), 0.25 (base), 0.30 (subbase) and 0.35(subgrade),

respectively. Asphalt pavement layer with different thicknesses was modeled and the maximum tensile stress and maximum shear stress at specific locations were computed. Wang et al. believed that the maximum shear stress on asphalt pavement surface has initiated the TDC. Maximum tensile stress at the bottom of subbase was also believed to cause reflective cracking initiation. The research also showed pavement thicknesses have no obvious effects on the maximum shear stress. However, thicker asphalt pavement contributed to lower tensile stress and surface deflections [115].

The dimensions (length, width, thickness) of the 3D-FE model developed by Garza [111] for the U.S Highway 45 North project subjected to FWD load was used as the reference for the new 3D-FE asphalt pavement models developed using the LS-DYNA software.

4.2 LS-DYNA 3D-FE Modeling and Simulations of Uncracked Asphalt Pavements Subjected to Truck Axle Load – Time History

The step by step approaches to develop the 3D-FE model subjected to truck axle loading follow:

1) Make a sketch of the proposed asphalt pavement cross section manually before creating the 3D-FE model using the LS-DYNA software. Take note of the important coordinates of nodes, sizes of the elements, pavement layer thicknesses, overall dimension of the 3D-FE model, and the proposed loading area subjected to truck wheel loads.

2) Create the cross section of pavement system in the LS-DYNA software from asphalt pavement surface layer at the top to the underlying subgrade layer at the bottom. Figure 45 shows the completed 3D-FE model of pavement-subgrade system developed in this research.

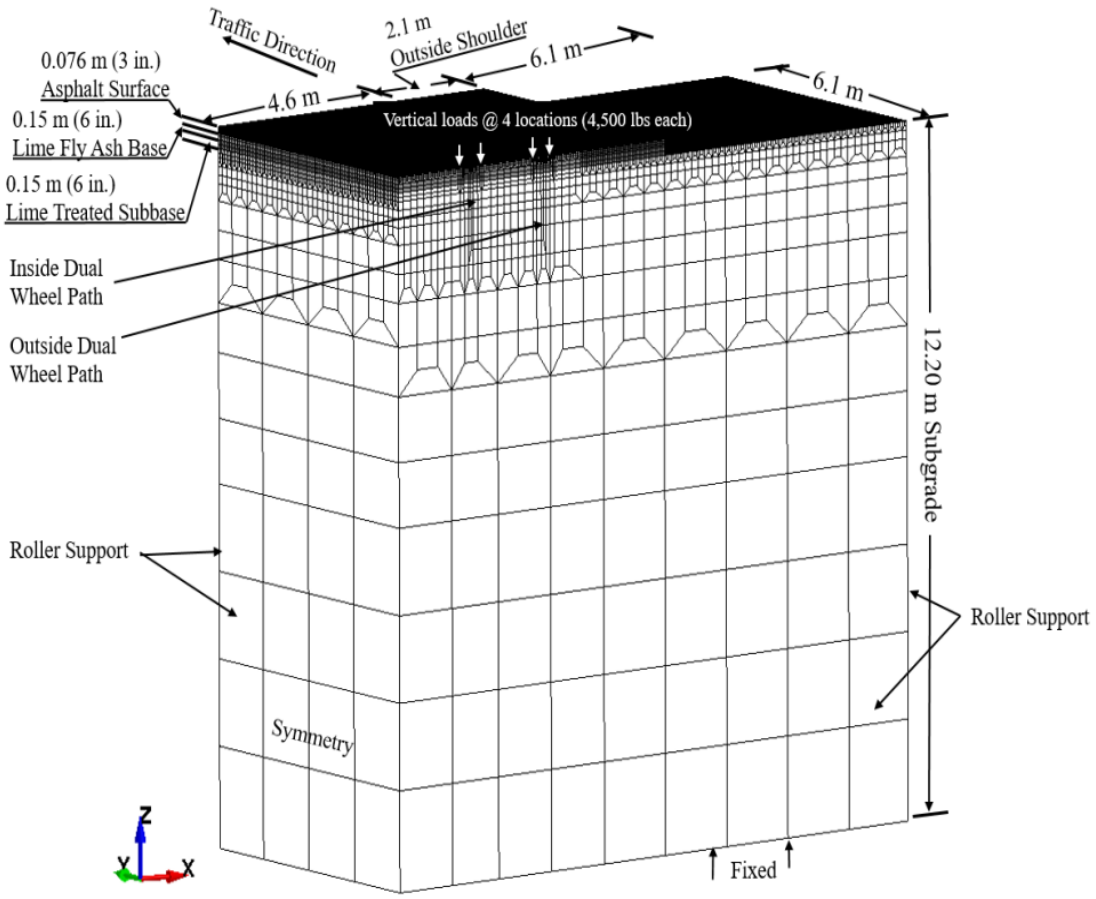

Figure 45. Example of the 3D-FE model of pavement-subgrade system subjected to truck axle loading

3) Create each layer as a unique part. In this model a total of 26 parts are created to simulate the 3D-FE half model of uncracked asphalt pavement system (Figure 46).

- 6 parts of asphalt pavement layer (left side), 6 parts of asphalt pavement layer (right side)
- 4 parts of LFA base layer (left side), 4 parts of LFA base layer (right side)
- 2 parts of lime treated subbase (left side), 2 parts of lime treated subbase (right side)
- 1 part of subgrade, 1 part of outside shoulder

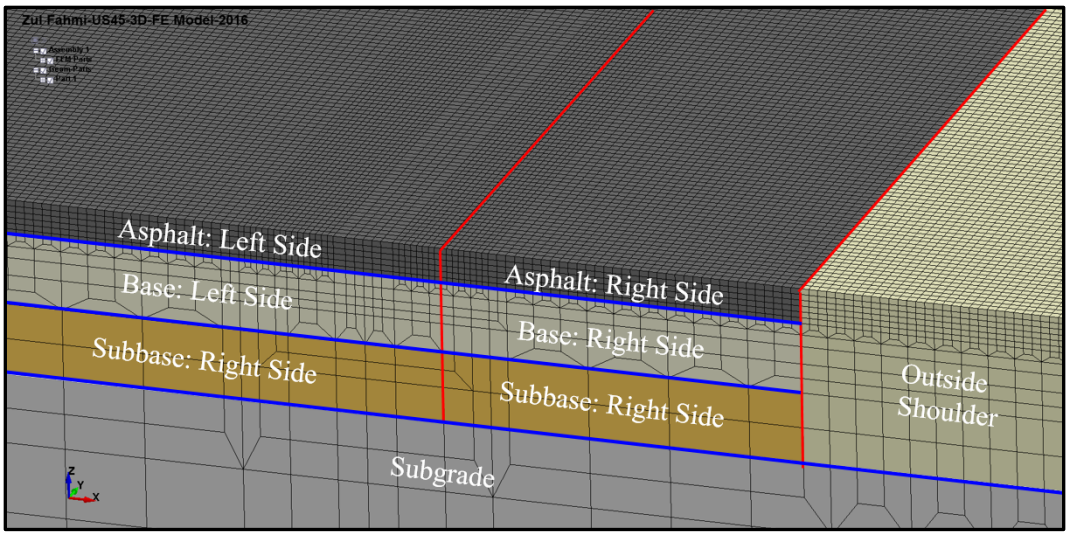

Figure 46. Example of pavement-subgrade 3D-FE model of uncracked pavement developed using LS-DYNA software

Figure 46 shows the close-up view of asphalt, base, subbase, subgrade layers and outside shoulder parts from the final 3D-FE half model. The following description of the 3D-FE model under in situ condition applies:

- Asphalt, base, and subbase layers were developed not as a single layer, but as a combination of a few thinner layers. The thinner layer was developed as a unique part with specific part identification number.
- The asphalt layer was developed with six thinner layers of asphalt pavement (six parts). The thickness for each asphalt layer is 12.7 mm (0.5 in.), therefore the total thickness is 76.2 mm (3 inches).
- The base layer consists of four different parts. The total base layer thickness of 152.4 mm (6 inches) is the combination of four thinner layers of 25.4 mm (1 in.), 25.4 mm (1 in.), 38.1 mm (1.5 inches), and 63.5 mm (2.5 inches), respectively, from the first to the fourth layers.
- The subbase layer consists of two different parts. This layer was divided into two different parts with 76.2 mm (3 inches) thick, respectively.

- The subgrade layer consists of only one part, with a total thickness of 12,192 mm (480 inches).
- A total of 26 parts were used to develop the model including one part of outside shoulder section. The undeformed 3D-FE model of uncracked asphalt pavement is shown in Figure 47.

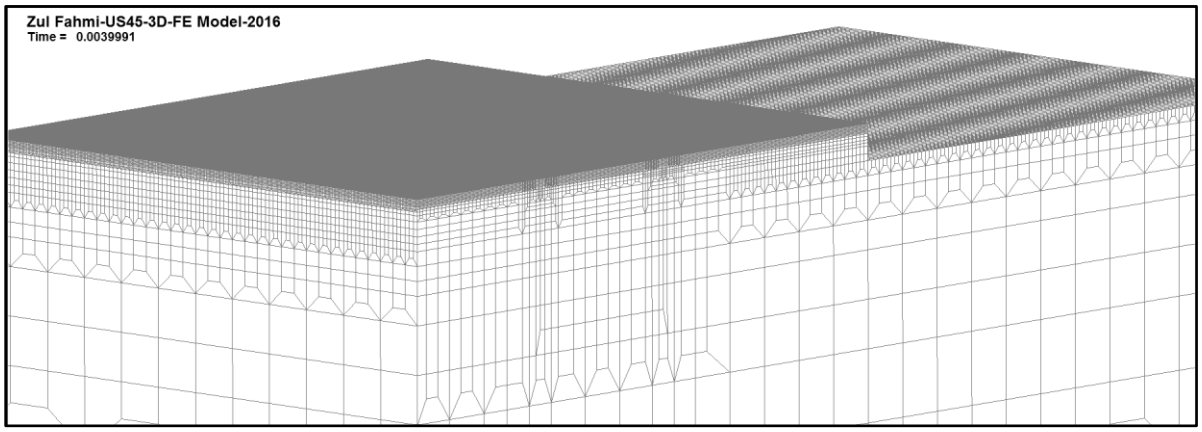

Figure 47. Undeformed 3D-FE model of uncracked asphalt pavement

4) Each layer was assigned with a proper color codes as shown in Figure 48.

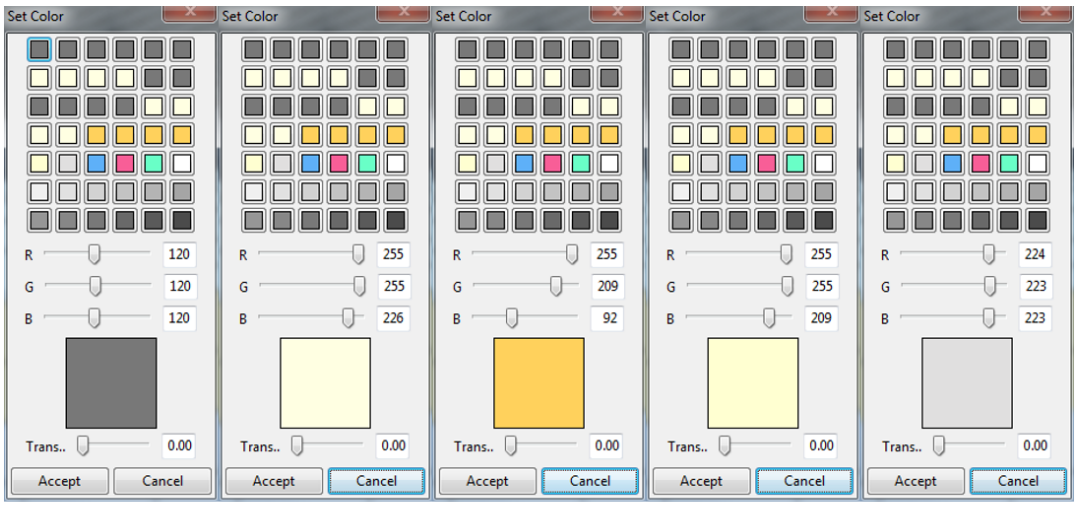

Figure 48. Color codes assigned to pavement-subgrade 3D-FE model

5) Truck rear axle load-time history curve was created based on previous study by Hajj et al. [116]. The researchers studied the influence of tire-pavement stress distribution, shape, and braking performance predictions for asphalt pavement. The comprehensive stress curve for rear axle was traced on a piece of transparent paper. More than 150 points of time (x-axis) and compressive stress (y-axis) coordinates were noted, as shown in Figure 49. Next, the peak stress ratios were calculated by dividing each compressive stress value with the maximum compressive stress of 42.5 kPa. Figure 50 plot shows the stress ratios bounded between zero to one ratios. The stress ratios were then converted to simulate maximum tire pressure of 100 psi with 200 miliseconds time-history curve as shown in Figure 51.

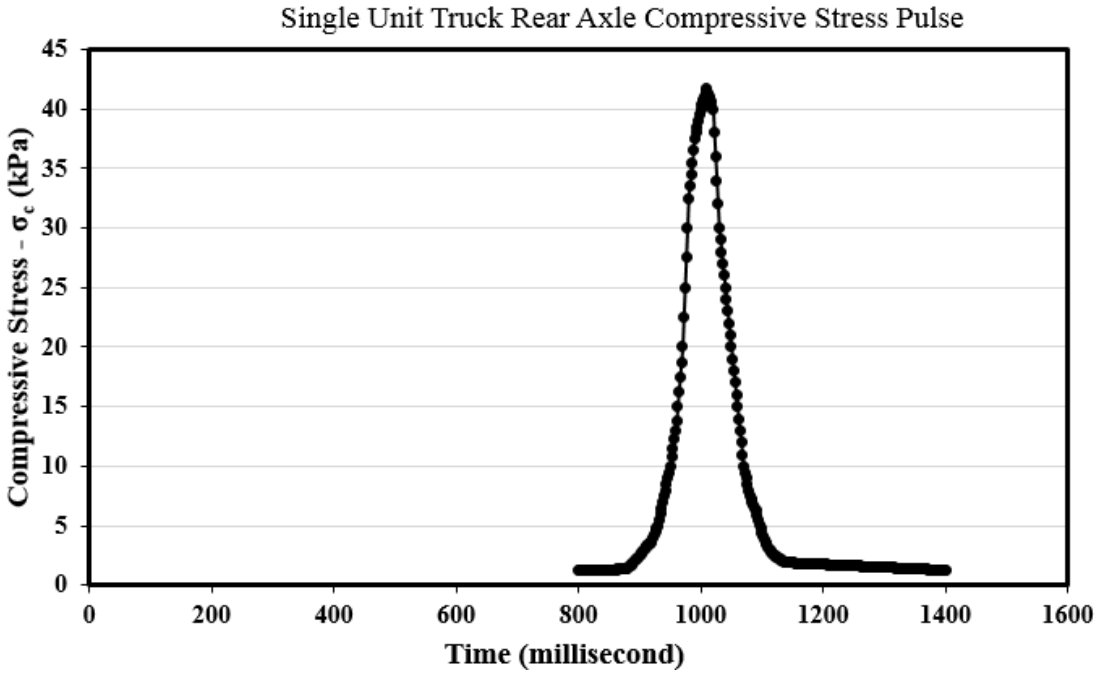

Figure 49. Single unit truck rear axle compressive stress pulse

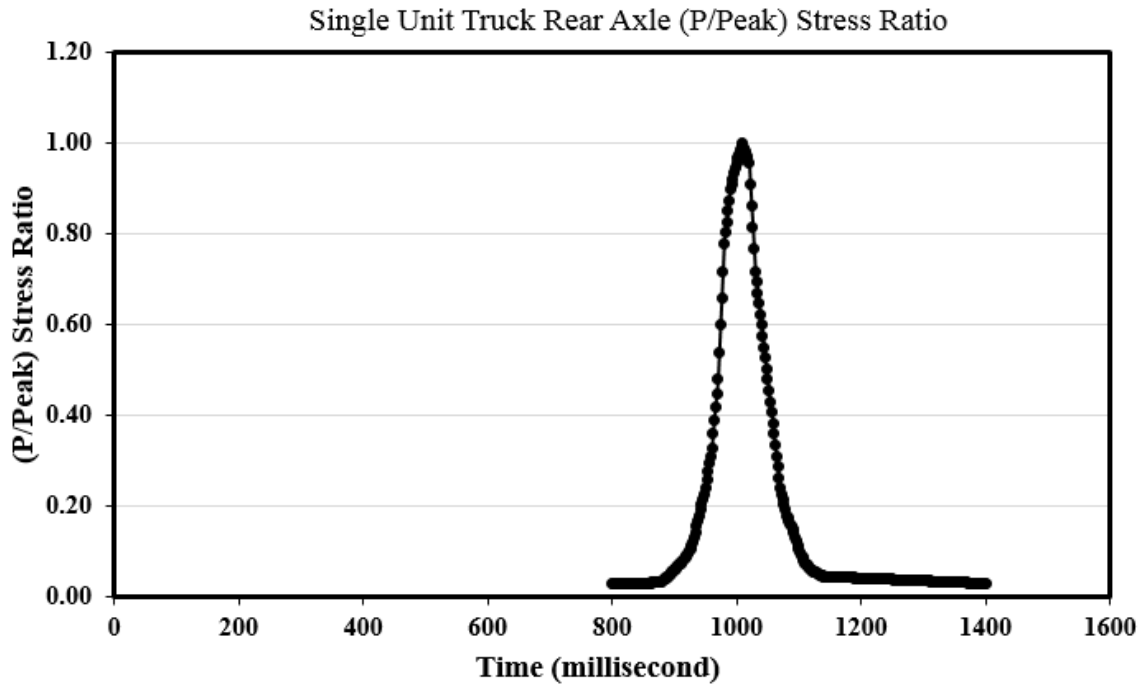

Figure 50. Single unit truck rear axle (P/Peak) stress ratio

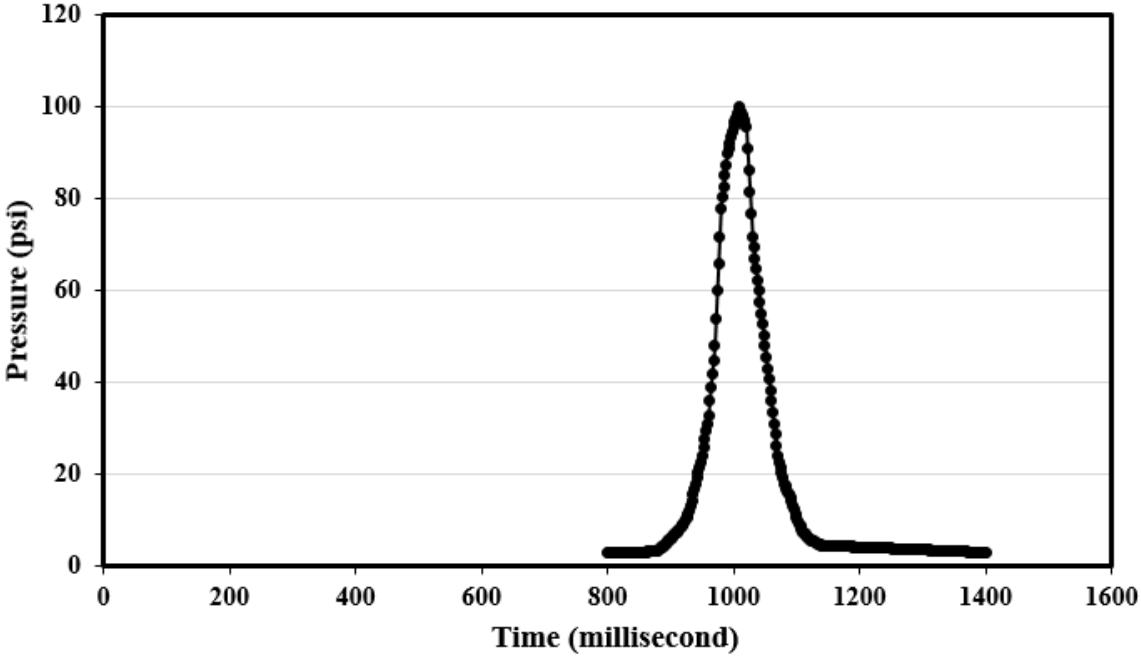

Figure 51. Surface pressure (psi) used in the LS-DYNA analysis

6) In the 3D-FE dynamic analysis, the nodal force association with mass, damping and stiffness attributes is explained through Equation 4.1 [111].

$$M\ddot{U} + C\dot{U} + KU = F(t) \quad (4.1)$$

Where, M is the mass matrix, C is the damping matrix, K is stiffness matrix, $\ddot{U}$ is the vector of acceleration, $\dot{U}$ is the vector of velocity, and U is the vector of displacement. F(t) is the vector of nodal forces. In this research, the effect of damping is ignored because the duration of the truck axle load pulse is short (less than one second) and does not affect the results of the analysis.

7) Next, truck wheel contact area was assigned on top of asphalt pavement surface. The initial set up was discarded due to elongated oval shape as shown in Figure 52. The final truck wheel contact area set up (Figure 53) shows a more reasonable footprint of the truck wheel contact area. The calculated contact area in the 3D-FE half model is 22.5 in^2.

8) The 3D-FE model was subjected to an 18,000 lbs (18-kips) single axle truck wheel loads with four tires. This research simulates 4,500 lbs of truck wheel load on each tire as shown previously in Figure 45. For the 3D-FE half model, the required load is 2,250 lbs (4,500 lbs divide by two) and the tire pressure is 100 psi. By dividing the required load with the tire pressure (2,250 lbs / 100 psi), the calculated truck wheel contact area under one tire is 22.5 in^2. Therefore the applied peak load was 4,500 lbs. The LS-DYNA calculated peak deflections are normalized to 4,500 lbs by multiplying the calculated peak deflections with 1.0 (4,500 lbs / 4,500 lbs).

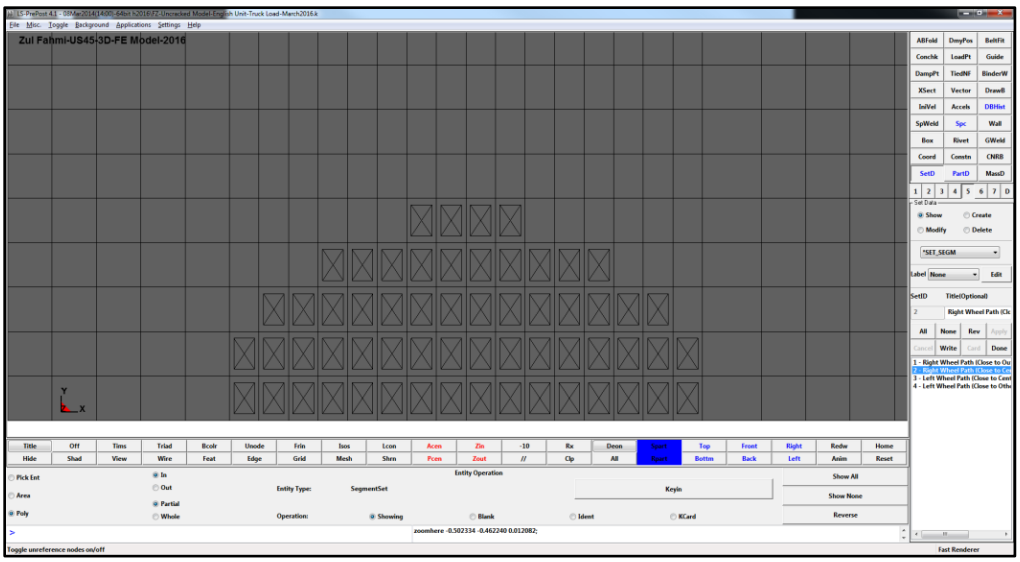

Figure 52. Initial set up for truck wheel contact area for 3D-FE Half model

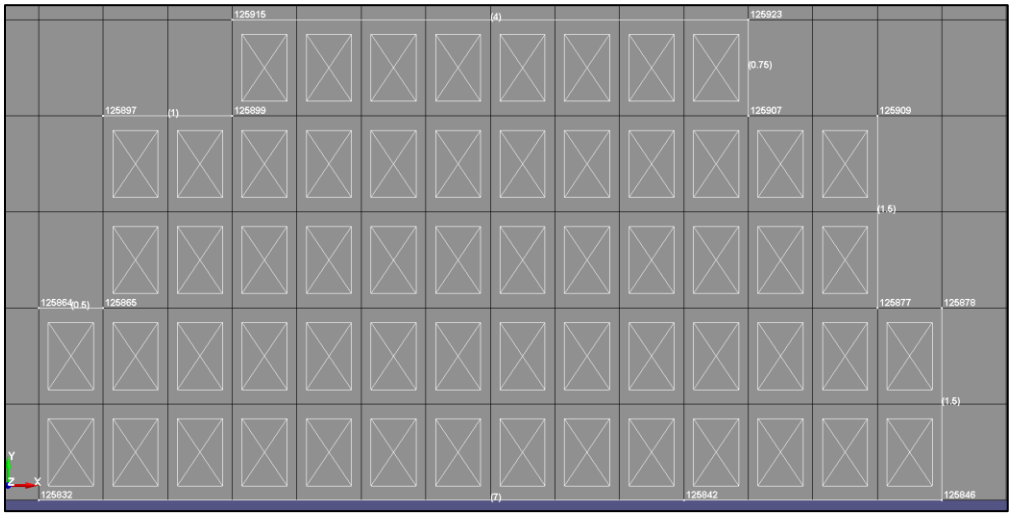

Figure 53. Final truck wheel contact area set up for 3D-FE Half model

9) The boundary conditions were modeled by using BOUNDARY_SPC_NODE function in the LS-DYNA software. Figure 54 shows the required set up to simulate roller support at the front and back sides of the 3D-FE model. Figures 55 to 57 show the nodes used to simulate roller support, observed from the front and back views of the 3D-FE model.

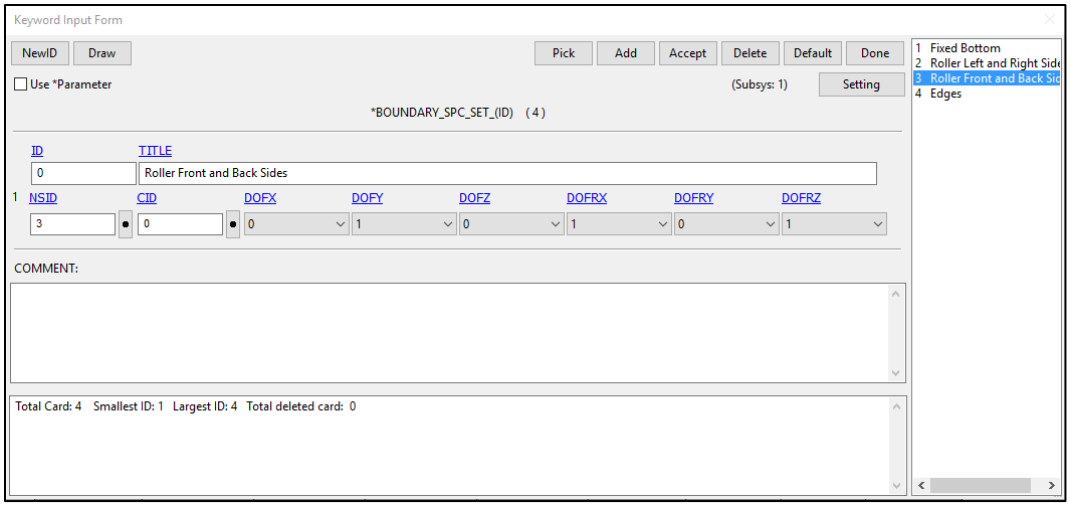

Figure 54. Boundary condition set up for front and back sides of 3D-FE Half Model

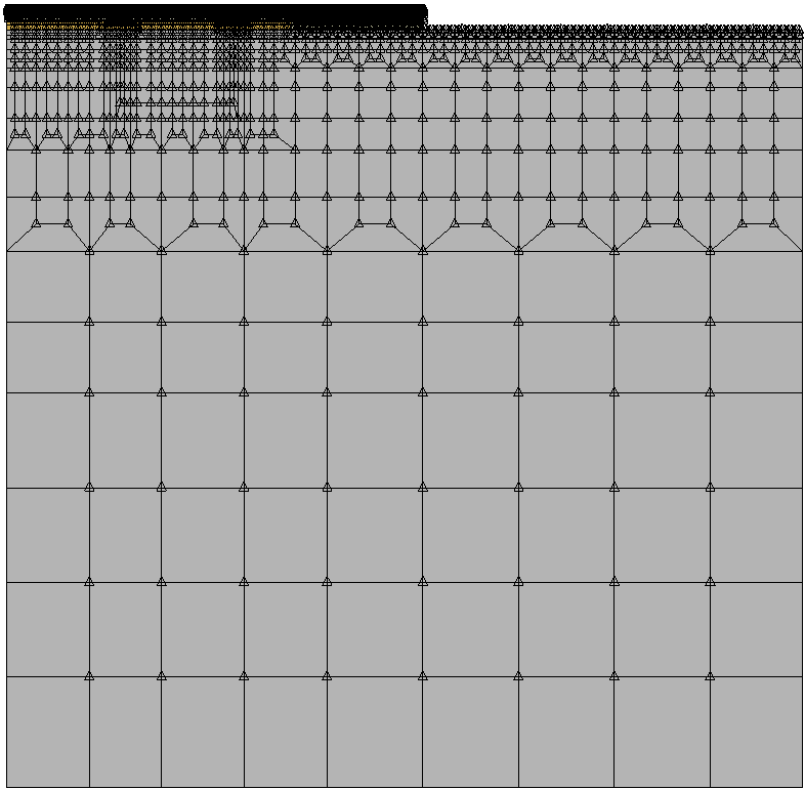

Figure 55. Nodes used to set boundary condition (front view of 3D-FE Half Model)

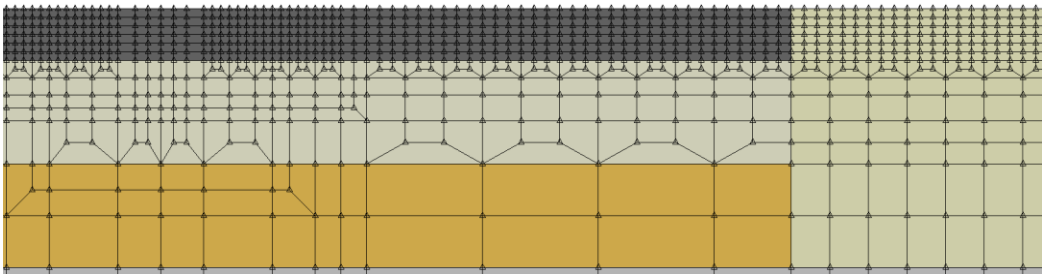

Figure 56. Close-up view of asphalt layers (front view of 3D-FE Half Model)

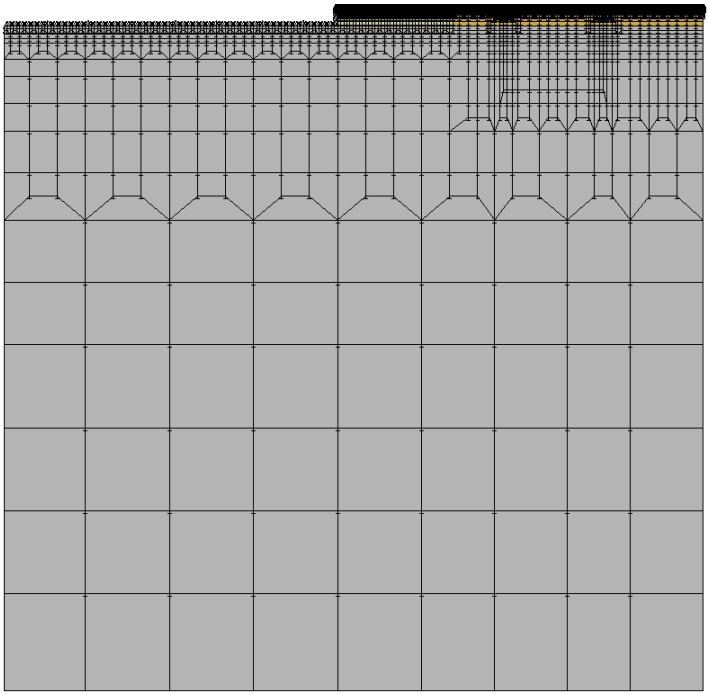

Figure 57. Nodes used to set boundary condition (back view of 3D-FE Half Model)

10) Once the 3D-FE model is ready, make a few trial runs to ensure the model is functional and reliable for further analysis. Run the simulations based on the proposed full factorial experiment design. Connor and Zelen [117] provide the guideline for partial factorial design that consideres a subset of a full factorial design to reduce number of simulations, if necessary.

4.3 Comparison of 3D-FE Half Pavement Simulation Results with Layered Elastic Static Analysis Results

In order to assess the reliability of the developed 3D-FE model of uncracked pavement, the deflection values at the center of loading area were extracted and compared with the following data sets:

- Measured asphalt surface deflection value subjected to FWD load (Figure 58), and
- Calculated asphalt surface defection values using GAMES linear elastic static analysis software [118] subjected to truck axle loading.

Table 37 shows in situ linear elastic material properties for Highway US45N, North Project, where the FWD data was measured and used for comparison purposes. Table 38 describes the thickness values, degree of freedom, number of nodes and elements for asphalt, base, subbase, subgrade layers and include outside shoulder as well. Other important information for the 3D-FE analysis subjected to the FWD load is shown in Table 39.

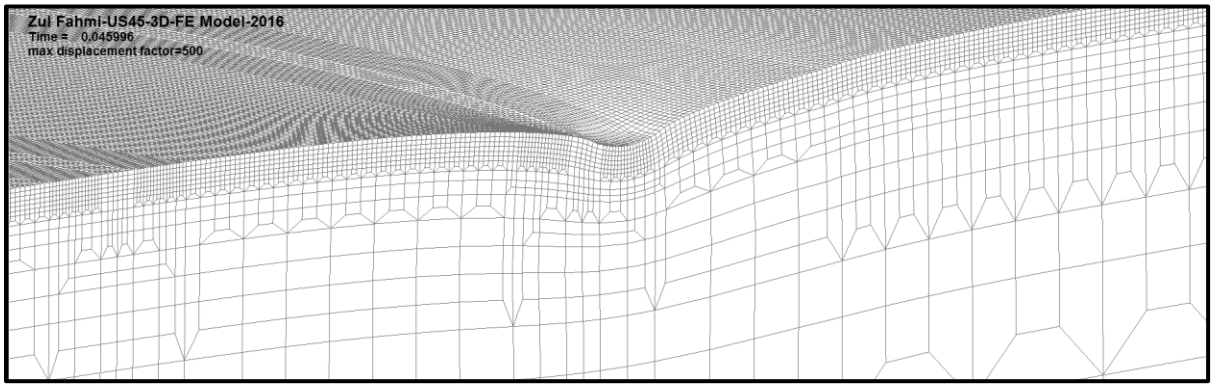

Figure 58. Deformed 3D-FE model subjected to FWD load

The LS-DYNA peak deflections for this analysis were calculated using a pressure value of 579.2 kPa (84 psi) over an area of 344.8 cm^2 (53.45 in^2), therefore the applied peak load was 39.94 kN (8,979.6 lbf). The LS-DYNA calculated peak deflections were normalized to 40kN (9,000 lbf), multiplying the calculated peak deflections by the factor 1.002 (9,000 / 8,979.6) [119].

Table 37. Linear elastic material properties for Highway US45N, North Project, Section 1, Station 461+05, Cycle 2, Drop 2

Layer	Material	Thickness mm (inches)	Young's Modulus MPa (psi)	Poisson's Ratio	Mass Density (lb-sec^2/in^4)
1	Asphalt	76.2 (3)	2,290 (332,200)	0.35	0.000230
2	LFA	152.4 (6)	914 (132,500)	0.30	0.000210
3	LTS	152.4 (6)	281 (40,800)	0.30	0.000187
4	Subgrade	1,219.2 (480)	122 (17,740)	0.45	0.000173
Outside Shoulder	Compacted Layer	381 (15)	69 (10,000)	0.45	0.000165

Table 38. Degree of freedom, number of nodes and elements for the US45N 3D-FE model

Layer	Material	Thickness mm (inches)	Degree of Freedom	No. of Nodes	No. of Elements
1	Asphalt	76.2 (3)	3,036,894	1,016,232	502,686
2	LFA	152.4 (6)	845,192	283,646	180,821
3	LTS	152.4 (6)	59,394	20,196	10,272
4	Subgrade	1,219.2 (480)	174,273	60,049	48,700
Outside Shoulder	Compacted Layer	381 (15)	877,597	296,295	321,268

The GAMES linear elastic static analysis software allows simulation of point loads at four different locations (Figure 59) similar to the loading configurations embedded to the 3D-FE models of uncracked asphalt pavement (Figure 60). The GAMES linear elastic static analysis

software assumes no discontinuity on asphalt pavement surfaces. Table 40 shows the parameters related to the dynamic analysis using 3D-FE half model subjected to 4,500 lbs truck wheel loads.

Table 39. Parameters for 3D-FE half model with FWD load

No.	Model Parameters	Total
1	Type of Element: Eight-node solid element (C3D8R)	
2	Number of Elements	1,039,413
3	Number of Nodes	1,113,195
4	Degree of Freedom	3,313,429
5	CPU Time, sec – Window 7 Computer (Xi®MTower™-S/N: 039617; 16 GB RAM, 64-bit Operating System	2,280
6	Peak Deflection (Load Center)	13.8 mils
7	Initial model preparation time, days	14
8	Load set up time, minutes	5

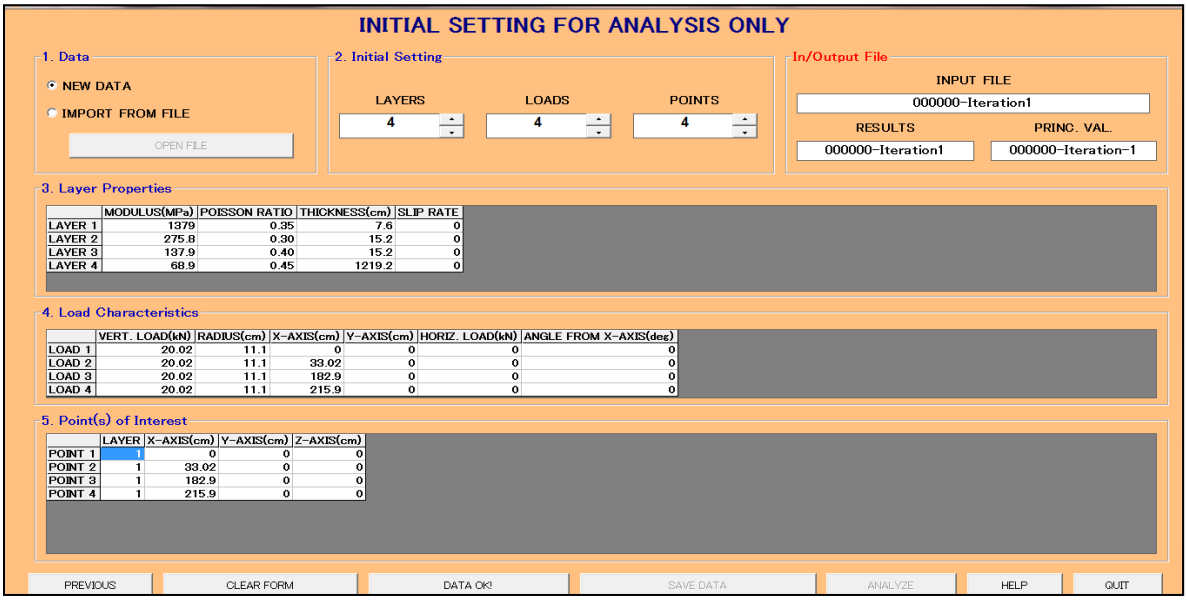

Figure 59. Example of GAMES software interface for initial set up prior to the structural analysis

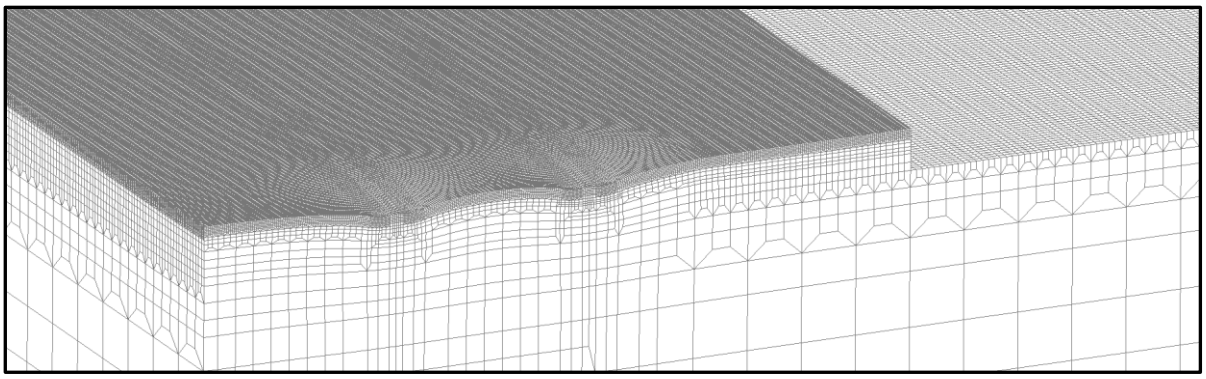

Figure 60. Deformed 3D-FE model subjected to a single axle dual tire loads

Table 40. Parameters for 3D-FE half model with 4,500 lbs truck wheel loads

No.	Model Parameters	Total
1	Type of Element: Eight-node solid element (C3D8R)	
2	Number of Elements	1,039,413
3	Number of Nodes	1,113,195
4	Degree of Freedom	3,313,429
5	CPU Time, sec - Window 7 Computer (Xi®MTower^{TM}-S/N: 039617; 16 GB RAM, 64-bit Operating System	8,880
6	Peak Deflection (Load Center)	13.5 mils
7	Initial model preparation time, days	14
8	Load set up time, minutes	8

Table 41 shows the measured FWD peak deflection value, peak surface deflection value (13.9 mils) extracted from the 3D-FE half model developed in previous study by Garza [111], and surface deflection value (13.8 mils) extracted from the 3D-FE model developed in this research. The calculated deflection value (14.3 mils) using the GAMES software was also shown in Table 41. A low error of -1.7% was calculated based the 3D-FE model developed in this research.

Table 41. Measured and calculated peak surface deflections subjected to FWD load (normalized to 9,000 lbf)

	FWD Measured	Garza 2003 (3D-FE half model using LS-DYNA)		GAMES (Layered elastic analysis)		Fahmi's 3D-FE half model using LS-DYNA	
Sensor Distance mm (in)	Peak Deflection* µm (mils)	Peak Deflection* µm (mils)	% Error †	Peak Deflection* µm (mils)	% Error †	Peak Deflection* µm (mils)	% Error †
0 (0)	357 (14.04)	354 (13.93)	-0.8	362.6 (14.27)	1.64	350.5 (13.8)	-1.71

** Deflections normalized to 40kN (9,000 lbf)*

† Percentage error compared to the measured peak deflections

Further analysis was conducted to compare peak surface deflection values calculated using 3D-FE model and GAMES software subjected to truck wheel loads (4,500 lbf) and the results are shown in Table 42. A low error of -4.4% was calculated for the 3D-FE model prepared with in situ modulus values. For the 3D-FE model of uncracked asphalt with various different combinations of factorial design (Table 43), a maximum error of -6.5% was recorded. These low error values indicate that the 3D-FE model of uncraked asphalt pavement developed in this research is reliable, practical for asphalt pavement structural response analysis, and recommended for future studies.

Table 42. Comparison of the peak surface deflections calculated using 3D-FE and GAMES software subjected to truck wheel loads (4,500 lbf)

Center of Outside Truck Wheel Contact Area	3D-FE half model developed in this research		GAMES (Layered elastic analysis)	
Distance mm (in)	Peak Deflection* µm (mils)	% Error **	Peak Deflection* µm (mils)	% Error
0 (0)	342.9 (13.50)	-4.40%	358.6 (14.12)	-
** Deflections normalized to 20kN (4,500 lbf)*				
*** Percentage error compared to the layered elastic analysis(GAMES)*				

Table 43. Comparison of measured and calculated peak deflections from LS-DYNA finite element software and GAMES layered elastic static analysis software (FWD load)

	Factorial Design	Thickness, in (cm)		Young's Modulus, psi (MPa)				Deflection at the center of loading area, (cm)		
		Asphalt Layer (T_1)	Subbase Layer (T_2)	Subgrade (E_4)	Base (E_2)	Subbase (E_3)	Asphalt (E_1)	Uncracked Pavements (3D-FE)	GAMES	% Diff.
1	000000	3 (7.6)	6 (15.2)	10,000 (68.9)	40,000 (275.8)	20,000 (137.9)	200,000 (1,379)	0.070	0.071	-1.5
2	000011	3 (7.6)	6 (15.2)	10,000 (68.9)	40,000 (275.8)	100,000 (689.5)	1,000,000 (6,894.8)	0.049	0.050	-2.9
3	000111	3 (7.6)	6 (15.2)	10,000 (68.9)	200,000 (1,379)	100,000 (689.5)	1,000,000 (6,894.8)	0.039	0.041	-4.3
4	001000	3 (7.6)	6 (15.2)	50,000 (334.7)	40,000 (275.8)	20,000 (137.9)	200,000 (1,379)	0.035	0.034	3.7
5	001011	3 (7.6)	6 (15.2)	50,000 (334.7)	40,000 (275.8)	100,000 (689.5)	1,000,000 (6,894.8)	0.021	0.021	0.4
6	001111	3 (7.6)	6 (15.2)	50,000 (334.7)	200,000 (1,379)	100,000 (689.5)	1,000,000 (6,894.8)	0.014	0.014	-3.1
7	111111	9 (22.9)	12 (30.5)	50,000 (334.7)	200,000 (1,379)	100,000 (689.5)	1,000,000 (6,894.8)	0.009	0.010	-6.5

4.4 3D-FE Modeling and Simulations using Factorial Design for Uncracked Asphalt Pavements

The dynamic analysis is conducted for a broad range of asphalt sections representing normal and strong pavement structures. The 3D-FE half model simulated highway pavement sections that consist of four different layers namely asphalt surface, base, subbase, and soil subgrade layer. The developed 3D-FE model also considers an outside shoulder that has the combined thicknesses of asphalt, base, and subbase layers, respectively.

Six factors are considered in this full factorial experiment design for 3D-FE simulations. Each factor has two levels: medium and high, which contributes to full factorial experiment design with a total of 64 possible treatment combinations (2^6). All 64 treatment combinations are used in the analysis to understand the effects of different asphalt and subbase layer thicknesses, and Young's modulus values for all four layers on pavement responses at critical locations. The

thickness of base layer is fixed to six inches throughout the analysis since it is a requirement by Mississippi Department of Transportation for highway construction procedures. The thickness of subgrade layer is fixed to 480 in based the successful applications in previous studies.

The treatment combinations was assigned in the following form: the first two numbers represent asphalt thickness (T_1) and subbase thickness (T_2) layers; the last four numbers represent the levels for Young's modulus for subgrade (E_4), base (E_2), subbase (E_3), and asphalt (E_1) layers as shown in Figure 61. Tables 44 shows the arrangement and treatment combinations used in this research. Treatment combinations one and 64 describe the weakest and the strongest asphalt pavements, respectively. Figures 62 to 65 show the front views of model 000000, model 010000, model 100000, and model 110000, respectively. Layer thicknesses and modulus values for all 64 treatment combinations is shown in Appendix B.

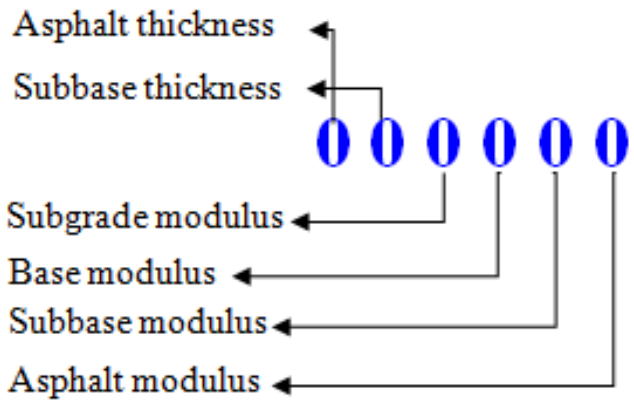

Figure 61. Treatment combination of the factorial design used for 3D-FE simulations

Table 44. Treatment combinations for full factorial experiment design (six factors and two levels) [85, 117]

Levels of the factors				Layer Thickness - mm (in)			
				0 Asphalt - 76.2 (3)		1 Asphalt - 228.6 (9)	
Young's Modulus, E - MPa (ksi)				0	1	0	1
Subgrade (SG)	Base (B)	Subbase (SB)	Asphalt (A)	Subbase -152.4 (6)	Subbase - 304.8 (12)	Subbase -152.4 (6)	Subbase - 304.8 (12)
0 E_{SG1} - 68.9 (10)	0 E_{B1} - 275.8 (40)	0 E_{SB1} - 137.9 (20)	0 E_{A1} - 1,379 (200)	1 000000	2 010000	3 100000	4 110000
			1 E_{A2} - 6,894.8 (1,000)	5 000001	6 010001	7 100001	8 110001
		1 E_{SB2} - 689.5 (100)	0 E_{A1} - 1,379 (200)	9 000010	10 010010	11 100010	12 110010
			1 E_{A2} - 6,894.8 (1,000)	13 000011	14 010011	15 100011	16 110011
	1 E_{B2} - 1,379 (200)	0 E_{SB1} - 137.9 (20)	0 E_{A1} - 1,379 (200)	17 000100	18 010100	19 100100	20 110100
			1 E_{A2} - 6,894.8 (1,000)	21 000101	22 010101	23 100101	24 110101
		1 E_{SB2} - 689.5 (100)	0 E_{A1} - 1,379 (200)	25 000110	26 010110	27 100110	28 110110
			1 E_{A2} - 6,894.8 (1,000)	29 000111	30 010111	31 100111	32 110111
1 E_{SG2} - 344.7 (50)	0 E_{B1} - 275.8 (40)	0 E_{SB1} - 137.9 (20)	0 E_{A1} - 1,379 (200)	33 001000	34 011000	35 101000	36 111000
			1 E_{A2} - 6,894.8 (1,000)	37 001001	38 011001	39 101001	40 111001
		1 E_{SB2} - 689.5 (100)	0 E_{A1} - 1,379 (200)	41 001010	42 011010	43 101010	44 111010
			1 E_{A2} - 6,894.8 (1,000)	45 001011	46 011011	47 101011	48 111011
	1 E_{B2} - 1,379 (200)	0 E_{SB1} - 137.9 (20)	0 E_{A1} - 1,379 (200)	49 001100	50 011100	51 101100	52 111100
			1 E_{A2} - 6,894.8 (1,000)	53 001101	54 011101	55 101101	56 111101
		1 E_{SB2} - 689.5 (100)	0 E_{A1} - 1,379 (200)	57 001110	58 011110	59 101110	60 111110
			1 E_{A2} - 6,894.8 (1,000)	61 001111	62 011111	63 101111	64 111111

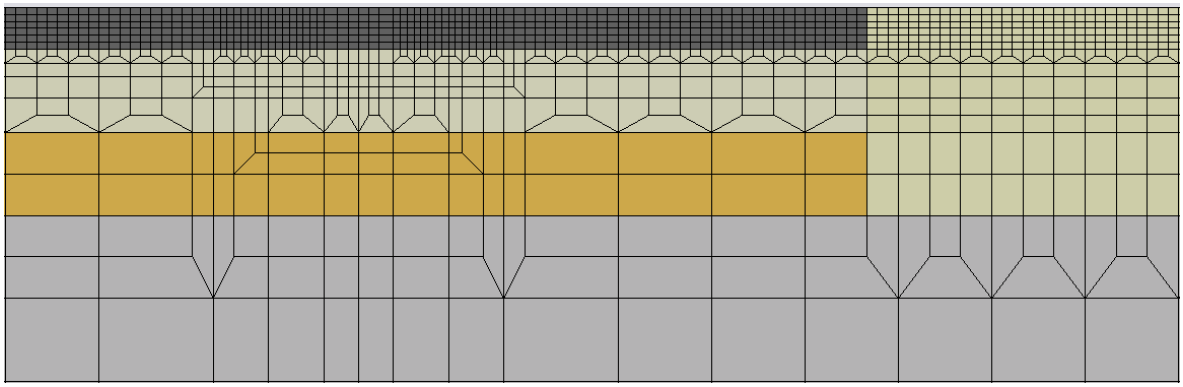

Figure 62. Front view of Model 000000 (Asphalt = 3 in, Base = 6 in, Subbase = 6 in, and Subgrade = 480 in)

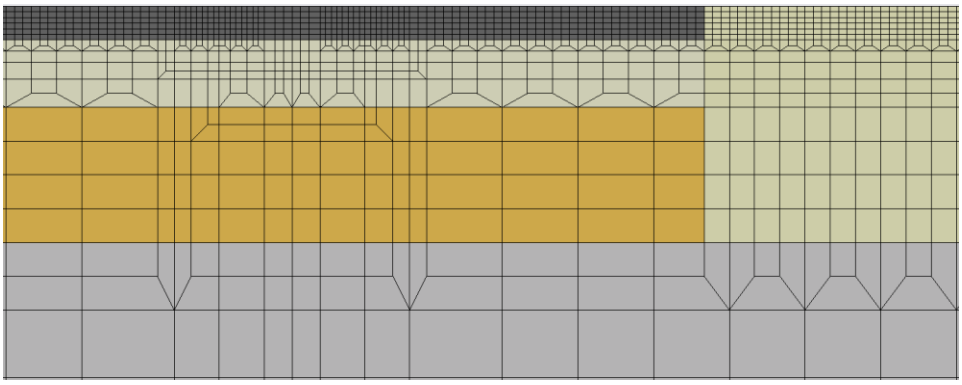

Figure 63. Front view of Model 010000 (Asphalt = 3 in, Base = 6 in, Subbase = 12 in, and Subgrade = 480 in)

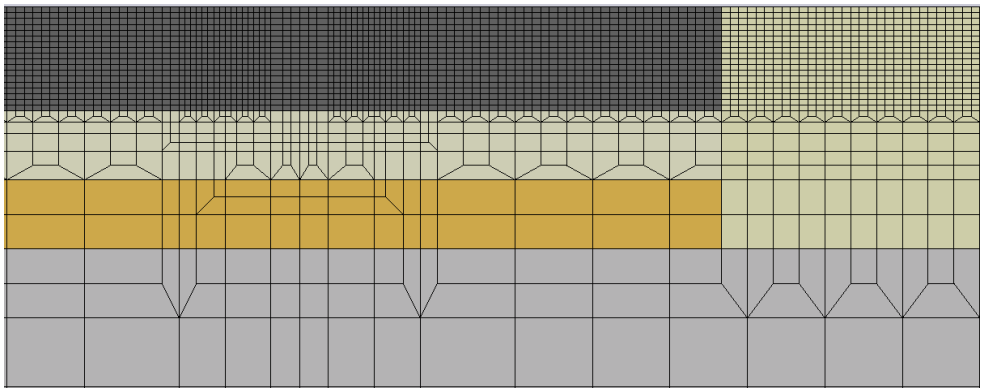

Figure 64. Front view of Model 100000 (Asphalt = 9 in, Base = 6 in, Subbase = 6 in, and Subgrade = 480 in)

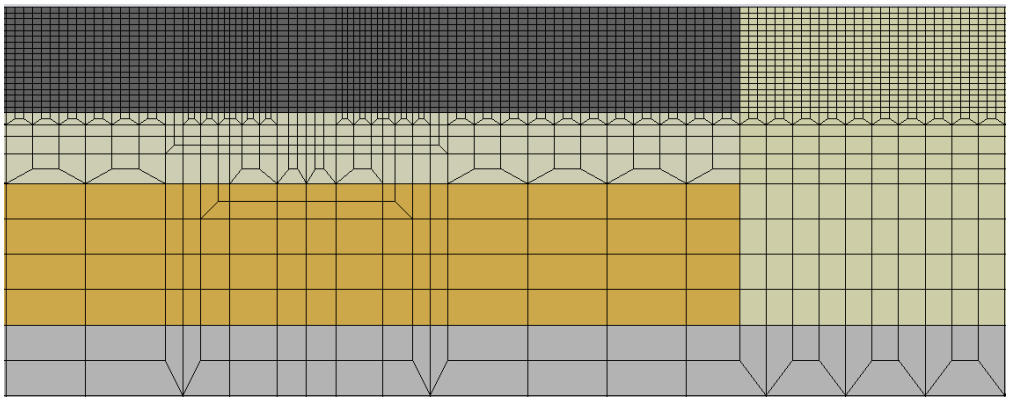

Figure 65. Front view of Model 100000 (Asphalt = 9 in, Base = 6 in, Subbase = 12 in, and Subgrade = 480 in)

4.5 Structural Response Database using 3D-FE Simulations of Uncracked Pavements Subjected to Axle Truck Loading

In this research, the analysis requires large number of 3D-FE dynamic analysis using the LS-DYNA software to generate a comprehensive asphalt pavement structural responses database for asphalt pavement thickness design. Those structural responses are surface deflections, stresses and strains at a few critical pavement response locations as follow and illustrated in Figure 66.

- Asphalt pavement surface deflection under loading area
- Compressive vertical stress in the middle of asphalt layer
- Tensile horizontal strain at the bottom of asphalt layer
- Compressive vertical strain in the middle of base layer
- Tensile horizontal strain at the bottom of base layer
- Compressive vertical stress in the middle of subbase layer
- Compressive vertical strain on top of subgrade

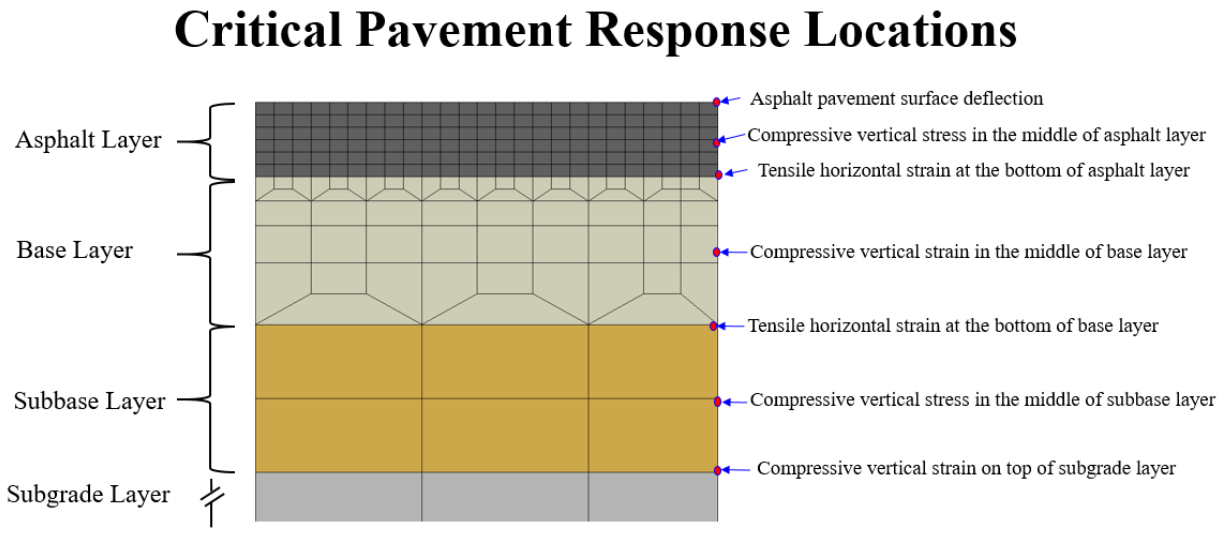

Figure 66. Critical asphalt pavement response locations

These structural responses are required for the following purposes:

- Asphalt pavement surface deflection under loading area is important for backcalculation of asphalt pavement modulus value.
- Compressive vertical stress in the middle of asphalt layer, compressive vertical strain in the middle of base layer, compressive vertical stress in the middle of subbase layer, and compressive vertical strain on top of subgrade are important for rutting distress evaluation in the mechanistic-empirical pavement design method.
- Tensile horizontal strain at the bottom of asphalt layer and tensile horizontal strain at the bottom of base layer are important for assessment of load-related cracking such as alligator crack and longitudinal crack.

The full factorial simulations were conducted for low and high levels and the surface deflections, stresses, and strains for all treatment combinations of uncracked asphalt are summarized in Table 45. Cells highlighted in yellow color indicate maximum values, while cells highlighted in blue color describe the minimum values for all pavement responses extracted from the 3D-FE analysis.

However, for future research, it is recommended to create a full factorial design of uncracked pavements by including medium level of thickness and medium level of modulus values for asphalt, base, subbase, and subgrade layers too. Once more data sets are compiled, the structural response prediction equations using the 3D-FE response database will be developed and these equations will provide an easier approach to predict structural responses in asphalt pavement layers.

Further analysis was conducted to assess the effects of thickness and modulus values on asphalt pavement surface deflection response. The selected treatment combinations, asphalt and

Table 45. Surface deflections, stresses, and strains for all treatment combinations of uncracked asphalt

Uncracked Asphalt Pavement Responses		1		2	3	4	5	6	7
Full Factorial Design (2^6)		Surface Deflection at the center of loading area		Compressive vertical stress in the middle of asphalt layer (psi)	Tensile horizontal strain at the bottom of asphalt layer (÷**1000**)	Compressive vertical stress in the middle of base layer (psi)	Tensile horizontal strain at the bottom of base layer (÷**1000**)	Compressive vertical stress in the middle of subbase layer (psi)	Compressive vertical strain on top of subgrade layer (÷**1000**)
No.	Treatment Combinations	mils	inches						
1	000000	27.6	0.028	80.5	0.26750	23.7	0.19791	8.4	0.53100
2	010000	26.1	0.026	80.5	0.26600	24.3	0.18291	7.2	0.35950
3	100000	18.8	0.019	22.9	0.17200	7.0	0.09522	3.7	0.26450
4	110000	18.2	0.018	49.2	0.09375	7.4	0.08814	3.4	0.20050
5	000001	22.8	0.023	66.0	0.12900	14.6	0.14872	6.5	0.43700
6	010001	21.6	0.022	66.2	0.12550	15.2	0.13593	5.7	0.30950
7	100001	13.5	0.014	44.8	0.21695	3.3	0.04394	2.1	0.15100
8	110001	13.1	0.013	45.1	0.03830	3.5	0.04114	2.0	0.12700
9	000010	23.2	0.023	81.4	0.24900	28.0	0.07378	8.3	0.37150
10	010010	20.2	0.020	81.5	0.25400	29.8	0.06548	7.9	0.22600
11	100010	16.8	0.017	50.0	0.07980	8.8	0.03809	3.7	0.20250
12	110010	15.2	0.015	50.4	0.07445	10.2	0.02845	3.8	0.14300
13	000011	19.1	0.019	67.1	0.11300	17.8	0.05219	6.3	0.31550
14	010011	16.5	0.017	67.4	0.10850	19.6	0.04090	6.3	0.20100
15	100011	12.5	0.013	45.6	0.03450	4.2	0.02120	2.2	0.12750
16	110011	11.5	0.012	45.9	0.03155	5.1	0.01517	2.3	0.10130
17	000100	21.0	0.021	93.3	0.04800	25.5	0.10550	5.9	0.37500
18	010100	20.1	0.020	93.3	0.51000	26.1	0.09797	5.2	0.28100
19	100100	16.3	0.016	53.4	0.03440	8.5	0.05833	2.9	0.19900
20	110100	15.9	0.016	53.5	0.03375	7.9	0.05511	2.7	0.16000
21	000101	17.8	0.018	79.4	0.00035	16.8	0.09415	4.4	0.29550
22	010101	17.1	0.017	79.3	0.05620	17.2	0.08810	4.0	0.22550
23	100101	12.3	0.012	48.0	0.02560	4.0	0.03644	1.9	0.12850
24	110101	12.1	0.012	48.0	0.02500	4.2	0.03497	1.8	0.10950
25	000110	18.0	0.018	93.9	0.05345	31.1	0.05210	6.3	0.28550
26	010110	15.6	0.016	94.0	0.06310	32.9	0.04036	6.2	0.18450
27	100110	14.9	0.015	54.1	0.02815	10.1	0.03337	3.1	0.16750
28	110110	13.6	0.014	54.4	0.02725	11.6	0.02547	3.3	0.12150
29	000111	15.3	0.015	80.1	0.05130	21.5	0.05109	4.8	0.23300
30	010111	13.4	0.013	80.4	0.05125	23.4	0.03925	4.9	0.15600
31	100111	11.5	0.012	48.7	0.02165	5.5	0.02445	2.0	0.11550
32	110111	10.6	0.011	49.0	0.01965	6.6	0.01951	2.1	0.09010
33	001000	13.6	0.014	80.9	0.27800	26.1	0.16683	12.7	0.16250
34	011000	14.8	0.015	80.8	0.27900	25.4	0.17824	9.8	0.11200
35	101000	8.7	0.009	26.6	0.48128	9.1	0.07570	6.2	0.08475
36	111000	9.2	0.009	49.6	0.09085	8.6	0.00380	5.0	0.34180
37	001001	10.0	0.010	66.7	0.12100	17.1	0.11511	10.3	0.07689
38	011001	11.0	0.011	66.5	0.12388	16.4	0.12558	8.1	0.09720
39	101001	4.9	0.005	24.7	0.03456	4.8	0.03533	3.7	0.04915
40	111001	5.3	0.005	45.5	0.03574	4.5	0.03809	3.2	0.03931
41	001010	11.2	0.011	81.7	0.26701	30.1	0.07766	12.9	0.15136
42	011010	10.7	0.011	81.7	0.26782	30.6	0.07639	10.6	0.09809
43	101010	7.6	0.008	50.5	0.07590	10.9	0.03261	6.4	0.08456
44	111010	7.4	0.007	52.1	0.07490	11.3	0.03079	5.7	0.06180
45	001011	8.1	0.008	67.6	0.11029	20.1	0.04729	10.5	0.13028
46	011011	7.7	0.008	67.7	0.10927	20.6	0.04529	8.9	0.08889
47	101011	4.4	0.004	46.2	0.03065	5.8	0.01664	4.0	0.05285
48	111011	4.5	0.005	48.4	0.02360	5.1	0.03118	2.8	0.03495
49	001100	8.7	0.009	93.6	0.06871	2.8	0.08202	9.7	0.12075
50	011100	9.5	0.009	93.5	0.06576	27.2	0.08882	7.6	0.08855
51	101100	7.0	0.007	53.8	0.03411	9.5	0.04596	5.2	0.06836
52	111100	7.5	0.007	53.7	0.03487	9.0	0.04942	4.2	0.05165
53	001101	6.8	0.007	79.8	0.05766	19.2	0.07122	7.7	0.09913
54	011101	7.5	0.007	79.7	0.05810	18.5	0.07719	6.1	0.07257
55	101101	4.3	0.004	48.5	0.02283	5.4	0.12339	3.4	0.04458
56	111101	4.5	0.005	48.4	0.02360	5.1	0.03118	2.8	0.03495
57	001110	7.0	0.007	94.15	0.07269	33.1	0.04433	10.4	0.12429
58	011110	6.7	0.007	94.20	0.07523	33.7	0.04189	8.7	0.08288
59	101110	6.2	0.006	54.5	0.02959	12.0	0.02602	5.6	0.07567
60	111110	6.1	0.006	54.5	0.02977	12.5	0.02422	5.0	0.05426
61	001111	5.5	0.005	80.6	0.05373	23.7	0.03969	8.4	0.10624
62	011111	5.2	0.005	80.7	0.05392	0.7	0.03690	7.2	0.07198
63	101111	3.7	0.00374	49.2	0.01944	7.1	0.01890	3.7	0.05258
64	111111	3.6	0.00364	49.3	0.01896	7.5	0.01736	3.4	0.03995
Average		12.2	0.0122	63.9	0.10040	14.8	0.06313	5.6	0.15704
SD		5.9	0.0	18.7	0.1	9.4	0.0	2.8	0.1
COV (%)		48.5	48.5	29.2	105.0	63.4	69.9	49.4	68.9
Tension (+), Compression (-)		+	+	-	+	-	+	-	-
Minimum		3.6	0.004	22.9	0.00035	0.7	0.00380	1.8	0.03495
Maximum		27.6	0.028	94.2	0.51000	33.7	0.19791	12.9	0.53100

base layer thicknesses, and modulus values for asphalt, base, subbase, and subgrade layers are shown in Table 46. Similar datasets were used to develop asphalt surface deflection plot at low and high level of modulus values for all four layers (Figure 67).

Table 46. Surface deflection values for various different treatment combinations

Low and high ASPHALT modulus and constant modulus values for base, subbase, subgrade layers									
Sequence no. (database)	Treatment combination	Uncracked pavement Low Level Factorial Design (0)							
		Asphalt (T1)	Subbase (T2)	Subgrade (E4)	Base (E2)	Subbase (E3)	Asphalt (E1)	mils	inches
1	000000	3	6	10,000	40,000	20,000	200,000	27.6	0.0280
5	000001	3	6	10,000	40,000	20,000	1,000,000	22.8	0.0228
3	100000	9	6	10,000	40,000	20,000	200,000	18.8	0.0190
7	100001	9	6	10,000	40,000	20,000	1,000,000	13.5	0.0135
Sequence no. (database)	Treatment combination	Uncracked pavement High Level Factorial Design (1)							
		Asphalt (T1)	Subbase (T2)	Subgrade (E4)	Base (E2)	Subbase (E3)	Asphalt (E1)	mils	inches
57	001110	3	6	50,000	200,000	100,000	200,000	7.0	0.007
61	001111	3	6	50,000	200,000	100,000	1,000,000	5.5	0.005
59	101110	9	6	50,000	200,000	100,000	200,000	6.2	0.006
63	101111	9	6	50,000	200,000	100,000	1,000,000	3.7	0.004

Low and high SUBBASE modulus and constant modulus values for asphalt, base, subgrade layers									
Sequence no. (database)	Treatment combination	Uncracked pavement Low Level Factorial Design (0)							
		Asphalt (T1)	Subbase (T2)	Subgrade (E4)	Base (E2)	Subbase (E3)	Asphalt (E1)	mils	inches
1	000000	3	6	10,000	40,000	20,000	200,000	27.6	0.0280
9	000010	3	6	10,000	40,000	100,000	200,000	23.2	0.0230
2	010000	3	12	10,000	40,000	20,000	200,000	26.1	0.0260
10	010010	3	12	10,000	40,000	100,000	200,000	20.2	0.0200
Sequence no. (database)	Treatment combination	Uncracked pavement High Level Factorial Design (1)							
		Asphalt (T1)	Subbase (T2)	Subgrade (E4)	Base (E2)	Subbase (E3)	Asphalt (E1)	mils	inches
53	001101	3	6	50,000	200,000	20,000	1,000,000	6.8	0.007
61	001111	3	6	50,000	200,000	100,000	1,000,000	5.5	0.005
54	011101	3	12	50,000	200,000	20,000	1,000,000	7.5	0.007
62	011111	3	12	50,000	200,000	100,000	1,000,000	5.2	0.005

Low and high BASE modulus and constant modulus values for asphalt, subbase, subgrade layers									
Sequence no. (database)	Treatment combination	Uncracked pavement with low modulus values for asphalt, subbase, subgrade layers							
		Asphalt (T1)	Subbase (T2)	Subgrade (E4)	Base (E2)	Subbase (E3)	Asphalt (E1)	mils	inches
1	000000	3	6	10,000	40,000	20,000	200,000	27.6	0.0280
17	000100	3	6	10,000	200,000	20,000	200,000	21.0	0.0210
45	001011	3	6	50,000	40,000	100,000	1,000,000	8.1	0.0080
61	001111	3	6	50,000	200,000	100,000	1,000,000	5.5	0.0050

Low and high SUBGRADE modulus and constant modulus values for asphalt, base, subbase layers									
Sequence no. (database)	Treatment combination	Uncracked pavement with low modulus values for asphalt, subbase, subgrade layers							
		Asphalt (T1)	Subbase (T2)	Subgrade (E4)	Base (E2)	Subbase (E3)	Asphalt (E1)	mils	inches
1	000000	3	6	10,000	40,000	20,000	200,000	27.6	0.0280
33	000100	3	6	50,000	40,000	20,000	200,000	13.6	0.0140
29	000111	3	6	10,000	200,000	100,000	1,000,000	15.3	0.0150
64	001111	3	6	50,000	200,000	100,000	1,000,000	3.6	0.0036

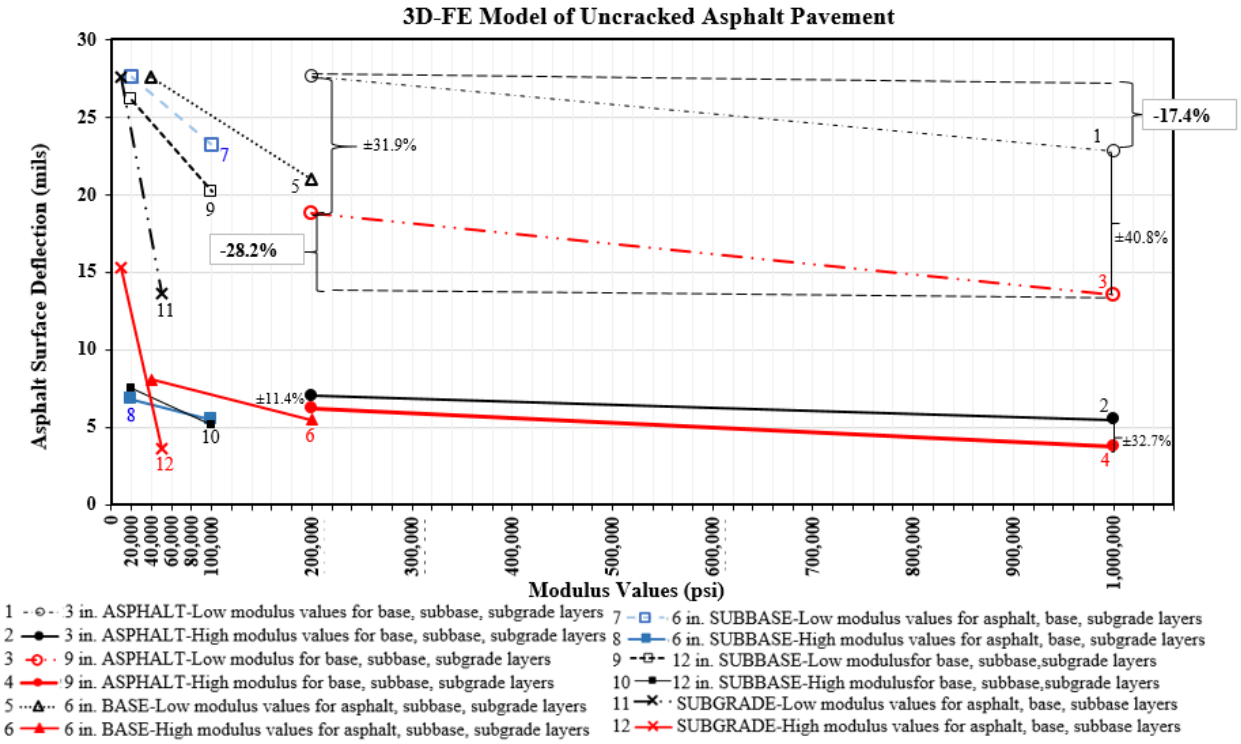

Figure 67. Asphalt surface deflections based on low and high modulus and thickness levels

Key findings from the analysis follow:

- The effect of layer thickness on surface deflection is greater as compared to the effect of asphalt modulus value, for asphalt layer with weak base, subbase, and subgrade layers. The surface deflection values differ by 36.4% (average) due to asphalt layer thickness changes, as compared to 21.1% (average) change of surface deflection value due to low and high levels of asphalt modulus values.
- However, the effect of modulus value is greater as compared to the effect of asphalt layer thickness for asphalt layer with strong base, subbase, and subgrade layers. The surface deflection values differ by 30.9% (average) due to low and high levels of asphalt modulus values, as compared to only 22.1% (average) change in surface deflection value due to different asphalt layer thicknesses.

V. 3D-FE MODELING OF ASPHALT PAVEMENTS WITH LONGITUDINAL CRACK

5.1 Literature Review of 3D-FE Modeling for Cracked Pavements and Motivation

The presence of asphalt surface discontinuity, such as surface crack, reduces the structural capacity of pavement systems. Continuous traffic load applications over the years caused surface crack distress on top of pavement surfaces. In the LTPP program, the selected test sections were evaluated for various different crack types including alligator and block cracking that are measured as an area in a square meter. In contrast, transverse and longitudinal cracks are measured as a unit length in meter. In general, the LTPP data indicates more severe cracking distresses on asphalt surface due to repeated load cycles, for the test sections without any major M&R treatments over the years [11].

Figure 68 shows the spatial map of average Pavement Condition Rating (PCR) in the state of Mississippi for 2016. The average PCR data for 82 counties indicated 70.7 percent are showing a fair condition of paved roads. Only two counties' road network is rated as in good condition, which are Greene (PCR = 81.6) and Harrison (PCR = 81.9) counties. The remaining counties (26.8%) recorded PCR of 71 or below, which indicated poor road conditions. The Lafayette County recorded a PCR of 80.2 over 100, which is under fair condition group (PCR 72 to 81) [120]. On the other hand, a statewide data summarized that out of 23,377 miles of MDOT state-maintained road network, 32.67% are in poor condition, 38.81% are in acceptable condition, while the remaining 28.52% of the inspected road network is in good condition [120].

These statistics show that it is needed to consider asphalt pavement surface discontinuity in the mechanistic empirical pavement analysis. Most of the layered elastic software used to study pavement responses do not consider any discontinuity. The following statements highlight the limitations in static linear layer elastic assumptions [121]:

- Inaccurate for pavement with cracking, discontinuities, and highly nonlinear material is used.
- The actual load is dynamic loading applications.

The only possible approach to study cracked pavement responses under the FWD and dynamic truck wheel loads are through the 3D-FE analysis. One of the advantages of the 3D-FE analysis is the capability to model discontinuity in asphalt pavement. The previous finite element studies reported that the INTERFACE element was used to simulate discontinuity in other structure materials [122, 123, 124, 125, 126]. Unfortunately, this element type was not suitable for simulating pavement cracks, which always have some aggregate interlock. However, more reasonable approaches to simulate discontinuity in asphalt surface layer were proposed and studied by Uddin and Pan [121] in 1995. The 3D-FE analysis of surface layer with discontinuity for concrete pavements was published by researchers in 1994, 1995, and 1997, respectively [127, 128, 129]. Previous researches related to both concrete and asphalt pavement modelings were studied, however, only asphalt pavement is considered in the 3D-FE analysis of this research.

Uddin et al. [127] studied the effects of pavement discontinuities on Portland cement concrete pavement. Prior to the 3D-FE analysis, the researchers optimized the pavement - subgrade structure of the model. Five important findings were reported, and two of them were used in this research. Those two findings follow;

(1) A 12.2 meter (40 feet) of subgrade depth simulates a semi-infinite subgrade, and

(2) The nodes at the bottom of the model were fixed, while rollers in the lateral sides of the model gave the best responses.

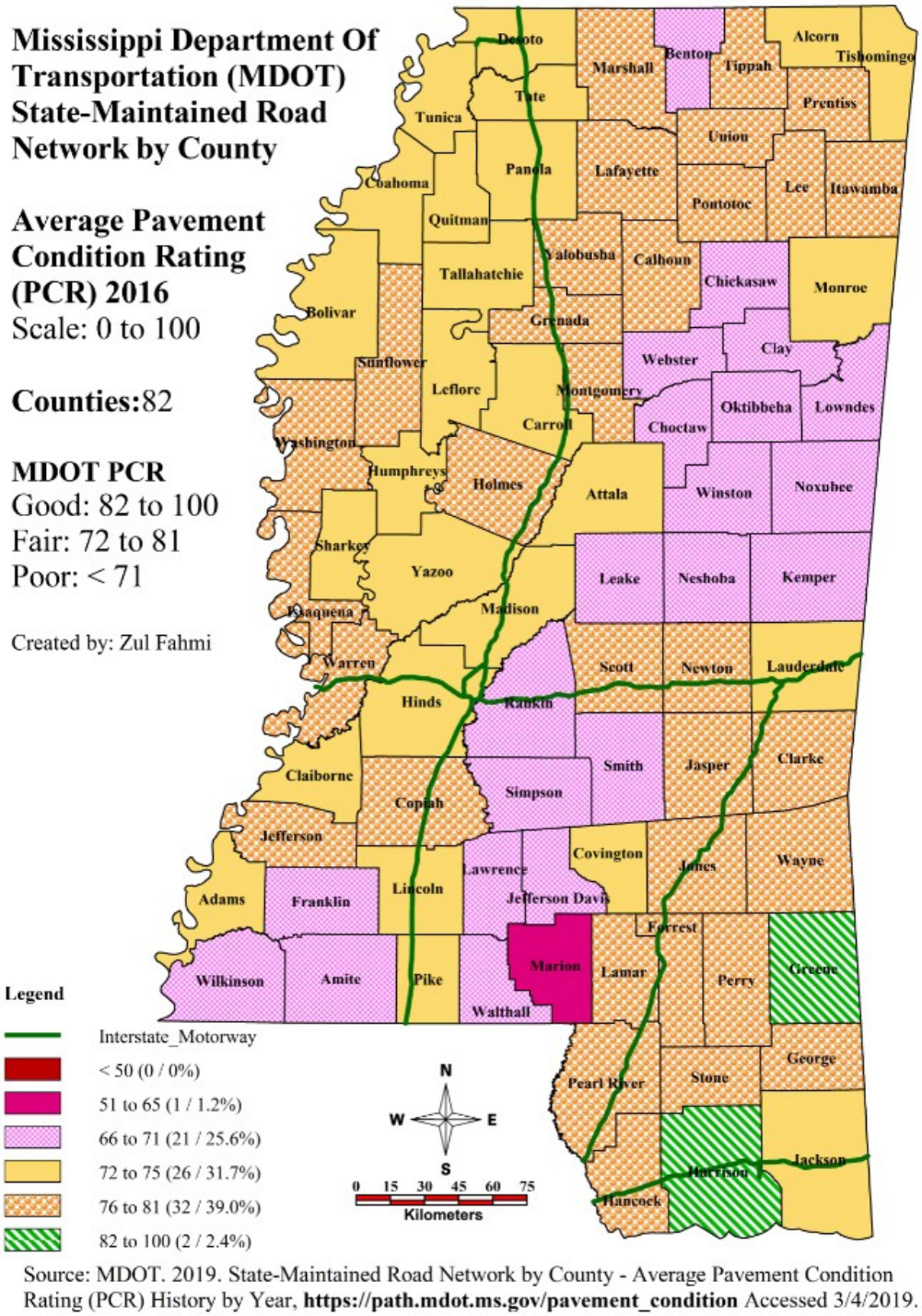

Figure 68. Spatial Map of 2016 Average Pavement Condition Rating (PCR) by Counties in Mississippi

The modulus values for the concrete, base, and subgrade layers were backcalculated from the deflection data using the FPEDD1 program. Later on, the BISAR computer program was used to predict the surface deflection under layer elastic static analysis. Then the deflection value was compared with the results from static analysis using ABAQUS software. Only one percent difference in the deflection values, which suggest that the geometry, mesh, and boundary condition of the 3D-FE model are adequate for further analysis.

For dynamic analysis, Uddin et al. [127] analyzed both implicit and explicit analysis approaches in the ABAQUS. It turns out that the deflection value based on the implicit approach shows 18 percent lesser difference compared to static analysis. The explicit approach shows more error, therefore, only the implicit approach is considered for pavement discontinuity analysis.

The researchers [127] also introduced an approach to simulate full-depth crack in concrete layer using special-purpose unidirectional gap element known as GAPUNI available in ABAQUS software. Gap elements allow a pair of continuous faces to be in contact (gap closure) or in separation (gap opening) with respect to particular directions and separation conditions. The gap elements control the interaction between the contact surfaces in such a way that these surfaces do not penetrate each other under contact pressure [121]. The mechanism of GAPUNI element that requires a friction coefficient was described in detail by the researchers. Before simulating the crack condition, parametric studies were conducted to determine the crack gap width. It was discovered that the crack widths of 0.2, 0.1, 0.05, 0.02 inches were insignificant because the crack remains open throughout the analysis. Further studies conclude that the gap width of 0.01 inch is most reasonable. This implies that the effect of the friction coefficient of 0.5 on surface deflection is significant. The gap width of 0.01 inch (0.25 mm) and a friction

coefficient of 0.5 were used between the two contact surface of gap elements. The friction coefficient of 0.5 was introduced to allow the contact surface to slide with a very minimal shear force developing during the simulation. These criteria were developed from a previous study conducted in 1994 by Uddin et al. [128] for cracked asphalt pavement.

Further analysis was conducted to compare the deflection values between the uncracked and cracked pavement under dynamic loads. Transverse and longitudinal cracks were simulated using the GAPUNI element and the deflection under the FWD load was observed. It was discovered that the dynamic loading causes 17 to 22 percent higher deflection responses at the center of the loading area for cracked pavement, as compared to the uncracked pavement. However, the difference becomes smaller as noticed from nodes farther away from the center of the loading area.

Uddin et al. [128] conducted a few case studies to evaluate the effectiveness of the 3D-FE analysis to predict the modulus values for Portland concrete pavement with CTB layers. The deflection values from the FWD tests for jointed concrete pavement with discontinuity were compared with the 3D-FE outputs. The 3D-FE model simulates the concrete pavement layer, CTB layer, and subgrade layer for U.S. Highway 78 in Marshall County, Mississippi. Both uncracked and cracked pavements were simulated incorporating layer modulus values backcalculated from PEDD1 backcalculation software.

As compared to the previous research [127], Uddin et al. not only simulated crack using GAPUNI element but also simulated a transverse joint with dowel bar within the concrete slab. The dowel bars were modeled using beam elements. The Gap element in the ABAQUS was also used to simulate body-to-body contact to specify the interactions between the dowel bar and the surrounding concrete medium. Similar to the previous study [127], the gap width of 0.01 inch

and a friction coefficient of 0.5 were used in the analysis. The modulus values for the following conditions were analyzed;

1) Uncracked concrete pavement and uncracked CTB layers,

2) Cracked concrete pavement and uncracked CTB layers,

3) Cracked concrete pavement and cracked CTB layers.

There are no changes applied to the subgrade layer with 24,400 psi modulus value. The iterative procedures using the 3D-FE models using the ABAQUS software were considered. The ABAQUS dynamic deflections were compared, and the modulus values were adjusted until the smallest differences were observed between the predicted and measured deflection values. In general, it was noted that the 3D-FE predictions match reasonably well with the measured deflections. For both concrete and base layers, the modulus values for the cracked condition are less as compared to the uncracked layers.

In 1997, Uddin et al. [25] enhanced the research on the concrete pavement with discontinuities using the ABAQUS software. This study not only simulates transverse joint with dowel bars but also simulates a void under the concrete slab. Similar to the previous study [127, 128] the gap width of 0.01 inch and a friction coefficient of 0.5 were adopted for simulating discontinuities using the Gap elements. The voids under the concrete pavement at certain pavement sections of US Highway 78 in Marshall County were detected using the thermographic equipment.

The following conditions were evaluated in the study using the 3D-FE model simulations for the 80kN (18-kip) dual wheel single axle truck at the midslab position, with a 100 psi tire pressure:

1) Uncracked pavement model

2) Crack only in concrete pavement layer

3) Cracked concrete pavement and cracked CTB layers

4) Cracked concrete and CTB with voids

In general, the researchers summarized that the surface deflection is the lowest for the uncracked model compared to models with the cracked condition. The comparison for the cracked condition follows;

- The deflection values are slightly higher for pavement with concrete cracked only, compared to uncracked pavement.
- The deflection values for cracked concrete and cracked CTB layer are higher compared to concrete cracked only.
- The highest deflection values were observed for cracked concrete and cracked CTB with voids, as compared to all other simulations.

This research highlights the capability of the 3D-FE program to simulate the sophisticated conditions of discontinuities, which cannot be done using the multilayer linear elastic analysis and other finite element programs that do not consider crack modeling and dynamic analysis [25].

A comprehensive study on finite element analysis of flexible pavements with discontinuities was conducted by Uddin and Pan [121] in 1995. The researchers used ABAQUS software to simulate longitudinal cracks, transverse cracks, and alligator cracks in the asphalt surface layer. The details of pavement-subgrade model parameters were described in the paper. Two major requirements of the 3D-FE models follow;

1) In order to capture the accurate responses results, the mesh size under the load must be smaller compared to other regions far from the loading area.

2) The size of the elements is gradually increased as it farther away from the simulated loading areas.

The seed modulus values for pavement layers were backcalculated using the PEDD1 computer program. The researchers stated that the backcalculated modulus values are reasonable and good estimates of the effective in situ modulus values for the selected test section. The modulus values were used in the 3D-FE analysis of cracked pavement. The deflections values from the 3D-FE models with continuities were compared with measured deflections.

Transverse and longitudinal cracks simulation procedures in ABAQUS were implemented by Uddin et al. [127] for full-depth cracked asphalt layer. High severity alligator cracks were modeled by using the gap elements in both longitudinal and transverse directions. The following observations were noted in this study based on the maximum deflection:

- The deflection values for asphalt pavement with transverse cracks is about 7% higher compared to the uncracked pavements.
- The deflection values for asphalt pavement with longitudinal cracks is about 17% higher compared to the uncracked pavements.
- The highest difference of 36% was observed for the asphalt layer with high severity of alligator cracks as compared to the uncracked pavements.

The studies showed that the ABAQUS software was capable of simulating the pavement discontinuities including surface cracks. However, the literature review did not show any study that described the modeling of the cracked area in asphalt pavements using the LS-DYNA

software. The previous studies reported that the INTERFACE element was used to simulate discontinuity on other structure materials [122, 123, 124, 125, 126]. This element was not suitable for simulating pavement cracks, which always have some aggregate interlock. For that reason, this research explores the potential of using LS-DYNA software to simulate the cracked asphalt layer and evaluate the responses under truck wheel loads.

5.2 LS-DYNA 3D-FE Modeling and Simulations of Longitudinal Crack in Asphalt Layer

This sub-chapter describes the development of the 3D-FE model with cracked pavement layer. The syntheses of literature reviews on the TDC indicated that the propagation of the longitudinal cracks started not only from the top and moved downwards. There is a probability of the crack to initiate from the middle of thick asphalt pavement, based on the research in Japan [27, 28]. Therefore, this research proposed the simulations of cracked asphalt pavement with longitudinal cracks in traffic direction. Four different crack locations are simulated in the 3D-FE models. The cracked locations are simulated at (1) top one-third, (2) middle one-third, (3) bottom one-third, and (4) full depth cracked of asphalt pavement layer.

5.2.1 TDC Modeling and Simulation

In this research, the following key steps were used to develop the 3D-FE model and simulate longitudinal crack in the surface layer.

1) The 3D-FE for cracked asphalt model was created similar to the dimensions of the uncracked 3D-FE pavement-subgrade model using the LS-DYNA software. However, the cracked pavement was set up with finer meshes to simulate a 0.1-inch width of the cracked area.

This crack area was set up in traffic direction all the way to the other ends of the 3D-FE model, for outside wheel path close to the shoulder. The middle of the crack area is 30.25 inches (about 2.52 feet) from the road shoulder. Figure 69 compares the surface views on top of the asphalt pavement layer for uncracked pavement (a) and cracked pavement (b).

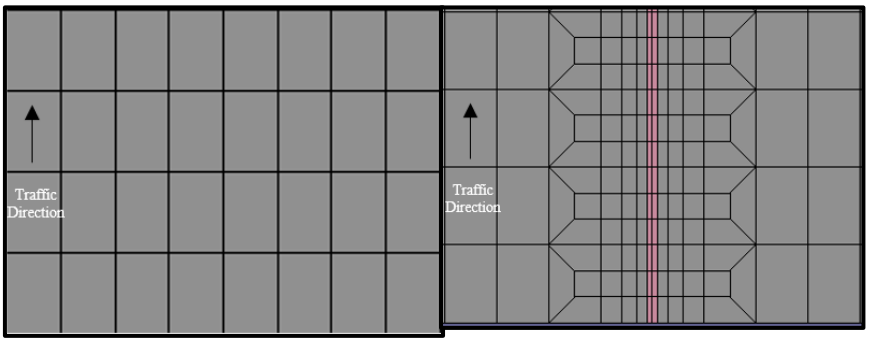

(a) (b)

Figure 69**.** Plan views on top of the asphalt pavement layer for uncracked pavement (a) and cracked pavement (b)

2) This research proposed the simulation of the longitudinal crack in asphalt pavement using the CONTACT SURFACE TO SURFACE definition in the LS-DYNA software [130]. Figure 70 shows the parameters required to set the CONTACT definition.

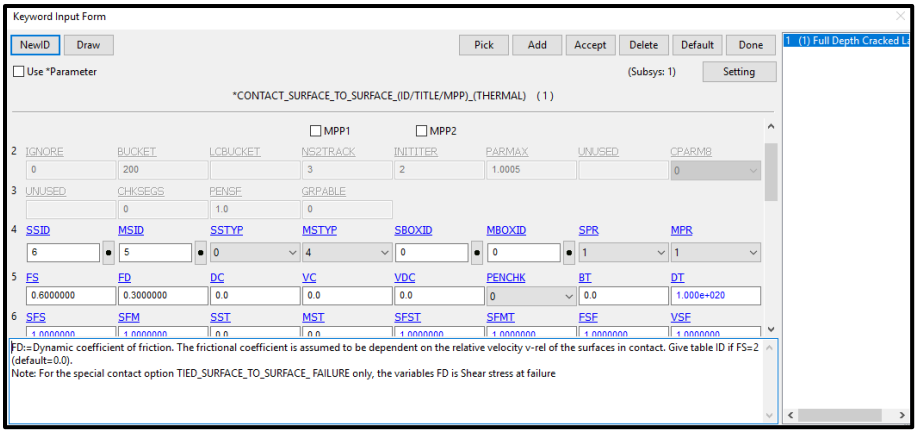

Figure 70. Keyword input form for CONTACT SURFACE TO SURFACE definition in the LS-DYNA software

There are two most important parameters, which are the definitions of the master segment (MSID) and slave segment (SSID), and static friction (FS) and dynamic friction (FD) of coefficient values. In this research, the FS of 0.6 and FD of 0.3 were used in the analysis. These friction coefficients are used to simulate the pavement cracks which always have some aggregate interlock. Details on part of the parameters are described in Appendix C (Figure C1).

Parametric studies were conducted earlier in this research to determine the effects of coefficient of friction values on the deflections. In the LS-DYNA software, the deflection value was determined from the nodes' output. The analysis evaluates the deflection values for the nodes on the asphalt surface layer, at the middle of the asphalt layer, and at the bottom of the asphalt layer. The following parametric studies were conducted to evaluate the effects of friction coefficients on the surface deflections.

- Parametric Study 1: Fix the FS at 0.7, and change the FD values from 0.1, 0.2, 0.3, 0.4, 0.5, 0.6, and 0.7, respectively.
- Parametric Study 2: Change FS values from 0.1, 0.2, 0.3, 0.4, 0.5, and 0.6, and fix the FD at 0.3 for each runs.

These two case studies were conducted for the nodes at the asphalt surface layer, at the middle of the asphalt layer, and at the bottom of the asphalt layer, respectively. The results are summarized in Appendix C (Table C1). It was discovered that the friction coefficient values did not affect the deflections, regardless of the node locations. Therefore based on certain engineering justification and experience, the final FS and FD used in this research are 0.6 and 0.3, respectively.

3) The FS and FD are used in between the master and slave segments of the 3D-FE cracked model. The master and slave segments are required as part of the surface CONTACT definition in the 3D-FE analysis The master segment is the asphalt vertical surfaces, and base layer horizontal surfaces surrounding the cracked areas. Figure 71 shows the master segment defined on the vertical surfaces of a wider asphalt layer on the left side of the cracked area (a), and the master segment defined on the vertical surfaces of asphalt layer on the right side (b), which is closer to the shoulder. Both pictures also show the master segments set on the surfaces of the base layer.

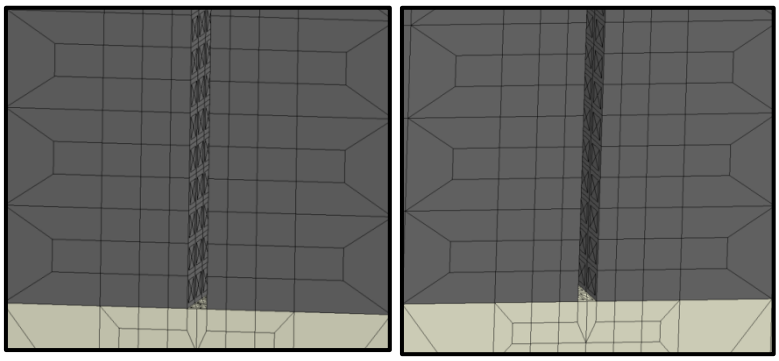

(a) (b)

Figure 71. Master segments defined on the vertical surfaces of the asphalt layer for both left (a) and right (b) sides of the cracked area

4) In contrast, the slave segment was set the horizontal and vertical surfaces of the cracked layer as shown in Figure 72. The SEGMENT SET command was used to define both master and slave segments.

Further analysis will be conducted to study the structural responses of uncracked and cracked asphalt pavements under the FWD and wheel loads by simulating cracks at the surface and several different depth levels.

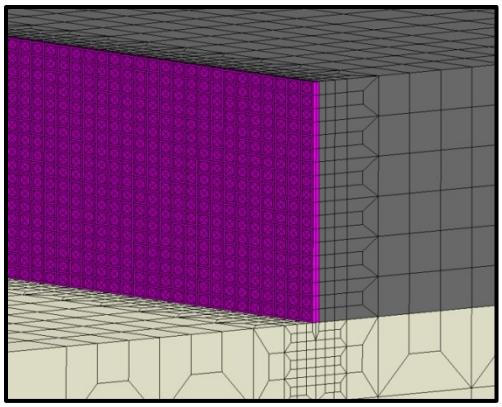

Figure 72. Slave segments defined on both the left and right sides of vertical surfaces, and horizontal surfaces at the bottom of the cracked element

5) Next, set the boundary conditions for the cracked 3D-FE models. Use roller-type boundary condition on all sides to unconstraint lateral motion. In the LS-DYNA, the translational and rotational constraint in the local x-axis, y-axis, or z-axis are controlled by using binary logic zero and one values. Choosing zero will restrain translation or rotation at the local axis. In contrast, the translation and rotation at the local axis are permitted if the binary logic of one is selected in the keyword input form. Appendix C (Figure C2 to C5) shows the screenshots of the keyword input form for boundary conditions set up for the cracked 3D-FE model.

6) Subsequently, the SEGMENT SET command was used to define the loading areas on top of the asphalt layer. Figure 73 shows the segments set to simulate the contact area between the truck tire and road surface on top of the cracked areas. This research modeled a standard 18-kips single axle truck with four tires, and the truck load of 4,500 lbs on each tire at 100 psi tire pressure [85]. However, the longitudinal cracked in the asphalt layer was simulated only for outside wheel path at about 2.5 feet from the road shoulder. Figure 74 shows the original sketch of the 18-kips single axle truck [85], and also the dimension of the tire contact area developed in

this research. The LS-DYNA peak deflections for this analysis were calculated using a pressure value of 100 psi over an area of 22.5 in^2, therefore the applied peak load was 4,500 lbf. The LS-DYNA calculated peak deflections were normalized to 4,500 lbf, multiplying the calculated peak deflections by the factor 1.00 (4,500 lbs / 4,500 lbf).

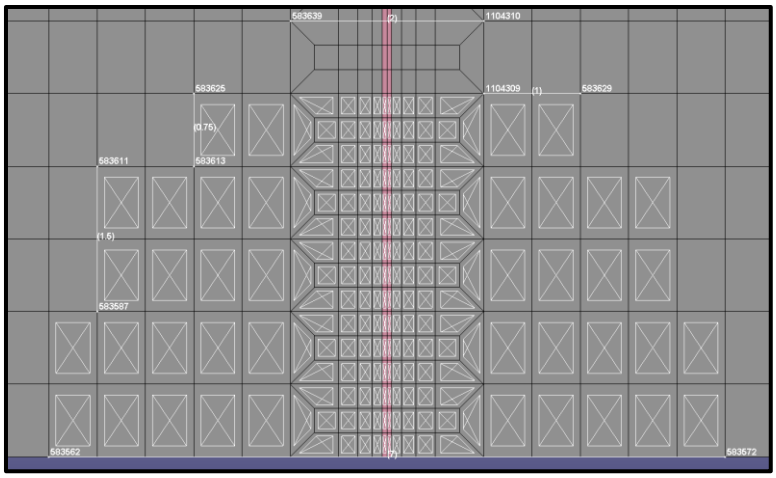

Figure 73. Truck tire contact area simulated in the 3D-FE analysis for cracked asphalt pavement

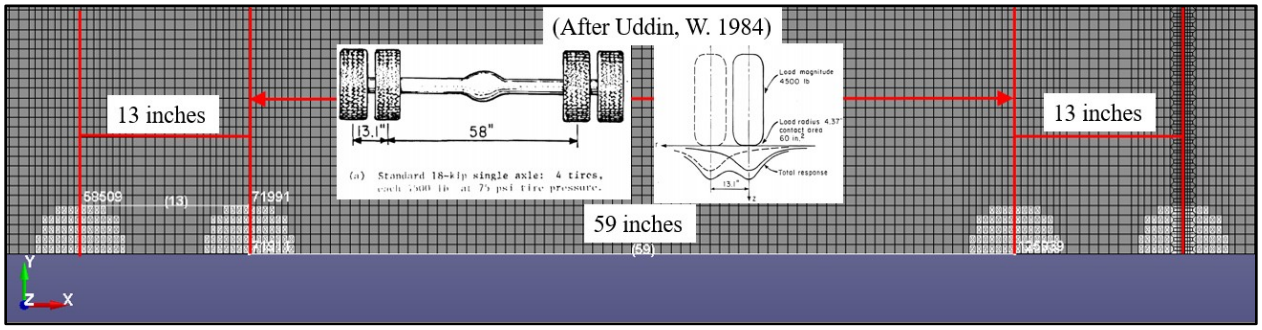

Figure 74. Original sketch of an 18-kips single axle truck with four tires and tire contact areas developed in this research

7) Once all the requirements in step one to step six are fulfilled, the 3D-FE model is ready for simulations based on the factorial design. Finally, the deflection values for specific nodes are available through NODOUT option under ASCII output command. Additionally, the stress and

strains results are available in ELOUT option under ASCII output command. The deflection, stress, and strain values are plotted, and the findings are compared between both uncracked and cracked asphalt pavement conditions.

5.2.1 Modeling of Cracked Element Using LS-DYNA Software

The modeling of the cracked element in the asphalt layer is another important contribution of this research. The following approaches are evaluated in this research to simulate the cracked area:

1) Initial or trial approach to developing cracked conditions using the existing spring element in the LS-DYNA software.

2) Final or selected approach to simulate cracked area in the LS-DYNA software.

5.2.1.1 Initial or Trial Approach using Spring Element

In this trial run, the 3D-FE model with uncracked asphalt surface layer was used to test the capability of the spring element to simulate discontinuity in the asphalt layer. Two spring elements were introduced at the symmetry area of the left and right sides asphalt layer. Those two spring elements were placed at the top of the first asphalt layer and at the bottom of the sixth asphalt layer to simulate full depth, as shown in Figure 75. The parameters used in the model and the deflection value from the trial runs are shown in Tables 47 and 48. The thickness and modulus values for the in situ, low level model, and high level model are shown in Table 49. The major findings from the trial runs follow:

- Table 47 shows that low level model (Model 000000) has the highest deflection value of 27.6 mils compared to high level model (Model 111111) and in situ condition.

- High level model (Model 111111) shows approximately 87% less deflection compared to low level model (Model 000000)
- This trial run was conducted to evaluate if the use of spring element is an appropriate approach to simulate discontinuity of asphalt layer.
- Additional run was conducted for uncracked asphalt layer using elastic spring constant, k calculated using the deflection value of model 000000 (Table 48).
- The analysis shows that the observed deflection values for models with the spring element are the same with the deflection value obtained from uncracked pavement without the spring element.

Therefore the proposal of using the spring element in the LS-DYNA to simulate cracked asphalt layer was not accepted, and replaced with another cracked simulation approach.

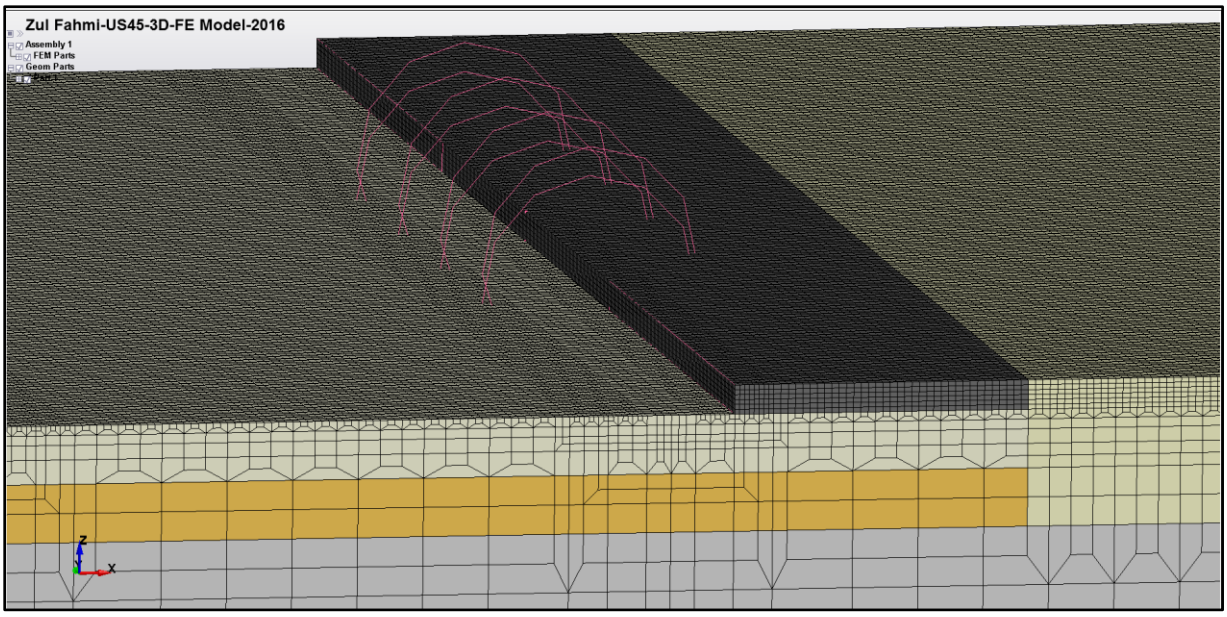

Figure 75. Trial run with two spring element on top and bottom of asphalt layer to simulate full depth cracked condition

Table 47. Summary of uncracked asphalt layer subjected to dynamic wheel load for models 000000 and 11111 without the spring element on top and bottom of sphalt layer

No.	Model Parameters for **Uncracked** Asphalt Layer	Model 000000	Model 111111
1	Type of element	Eight-node solid element (C3D8R)	
2	Number of elements	1,039,413	2,488,835
3	Number of nodes	1,113,195	2,571,316
4	Degree of freedom	3,313,429	7,677,534
5	CPU Time, (Xi®MTower™-S/N: 039617; 16 GB RAM, 64-bit Operating System	1 hour 49 minutes	4 hours 5 minutes
6	Initial model preparation time, days	14	
7	Load set up time, minutes	8	
8	Asphalt pavement surface deflection (load center), mils	27.6	3.60

Table 48. Summary of uncracked asphalt layer subjected to dynamic wheel load for In Situ Condition and Model 000000 with spring element on top and bottom of asphalt layer

No.	Model Parameters for **Uncracked** Asphalt Layer	In situ	Model 000000
1	Type of element	Eight-node solid element (C3D8R)	
2	Number of elements	1,039,413	
3	Number of nodes	1,113,195	
4	Degree of freedom	3,313,429	
5	CPU Time, (Xi®MTower™-S/N: 039617; 16 GB RAM, 64-bit Operating System	2 hours 46 minutes	1 hour 49 minutes
6	Elastic spring constant, k (psi/in)	7,299.3	4,739.3
7	Elastic spring constant, k used in LS-DYNA (force/deformation), lb-f/in	164,233.6	106,635.1
8	Asphalt pavement surface deflection (load center), mils	13.7	27.6

Table 49. Pavement structures for in situ, low level Model 000000, and high level Model 111111

	In situ value	Model 000000	Model 111111
Asphalt Layer	T_1 = 3 in	T_1 = 3 in	T_1 = 9 in
	E_1 = 332.2 ksi	E_1 = 200 ksi	E_1 = 1,000 ksi
Base Layer	6 in (fixed)	6 in (fixed)	
	E_2 = 132.5 ksi	E_2 = 40 ksi	E_2 = 200 ksi
Subbase Layer	T_2 = 6 in	T_2 = 6 in	T_2 = 12 in
	E_3 = 40.8 ksi	E_3 = 20 ksi	E_3 = 100 ksi
Subgrade Layer	480 in (fixed)	480 in (fixed)	
	E_4 = 17.74 ksi	E_4 = 10 ksi	E_4 = 50 ksi

5.2.1.2 Development of Cracked Layer using Solid Element

The cracked layer in the 3D-FE cracked asphalt model was developed using the eight-node solid element. The crack layer simulates longitudinal crack with a gap of 0.5-inch in width. It was assumed that the opening of the crack has a constant gap from top to bottom. This research proposes the modeling of longitudinal cracks at different depth level, which is top one-third, middle one-third, bottom-one-third, and full depth cracks in the asphalt pavement layer. Figures 76 to 79 show the cracked element for different depth levels. Both pre and post processing conditions are shown in the following figures.

It is important to know that the deflections are extracted from the NODOUT file under z-displacement, which means the deflection in vertical directions. On the other hands, the stress, and strain values are extracted from ELOUT file. For example, if the compressive stress values at certain element are required, the stress values are then extracted from “sig-zz” column. The “sig-zz” explains the sigma, which is the symbol of stress, and “zz” describe the measurement at the z direction. Additionally, the strain values are extracted from the “eps-zz” column. The “eps” explains the epsilon, which is the symbol for strain.

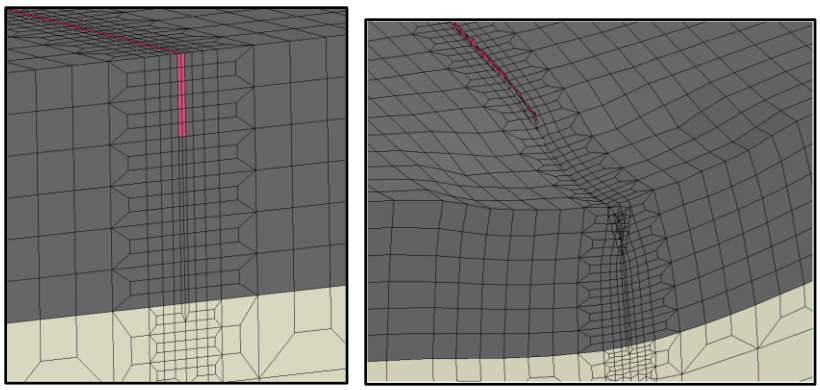

(a) (b)

Figure 76. Undeformed (a) and deformed (b) models for the top one-third cracked from overall asphalt thickness

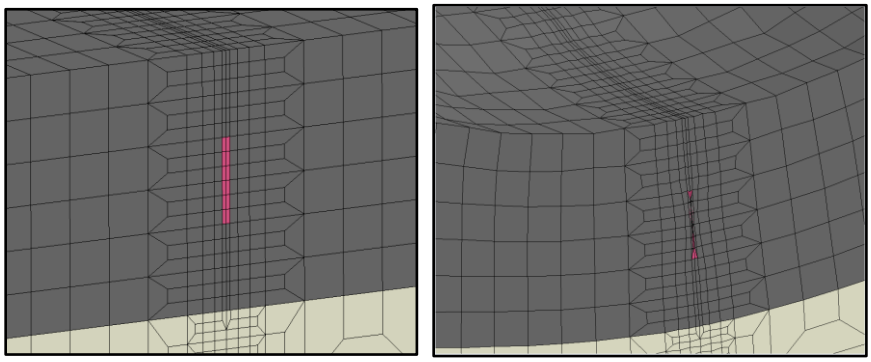

(a) (b)

Figure 77. Undeformed (a) and deformed (b) models for the middle one-third cracked from overall asphalt thickness

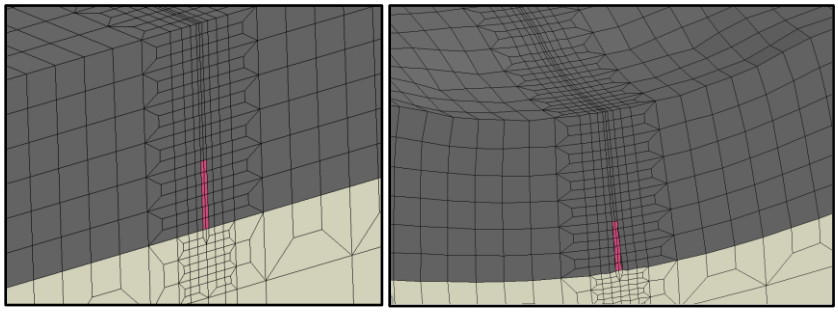

(a) (b)

Figure 78. Undeformed (a) and deformed (b) models for the bottom one-third cracked from overall asphalt thickness

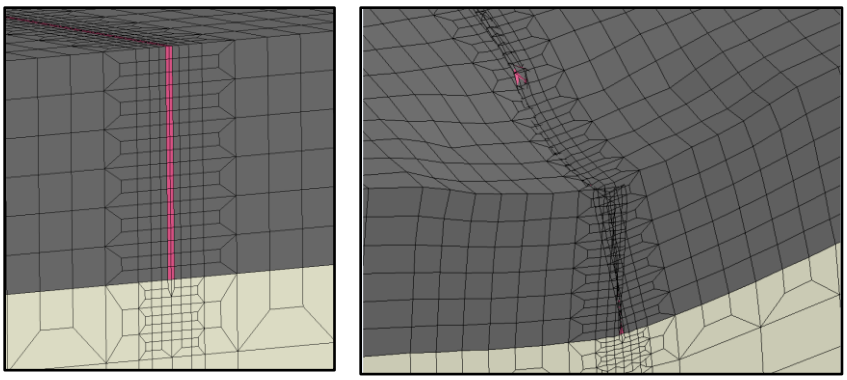

(a) (b)

Figure 79. Undeformed (a) and deformed (b) models for the full cracked asphalt layer

In the LS-DYNA software, the stress and strain values are measured at the centroid of the solid element [129]. Therefore, the stress and strain values reported in this research are the average of two elements on the left and right sides of the center line (dash-dash line in Figure 80).

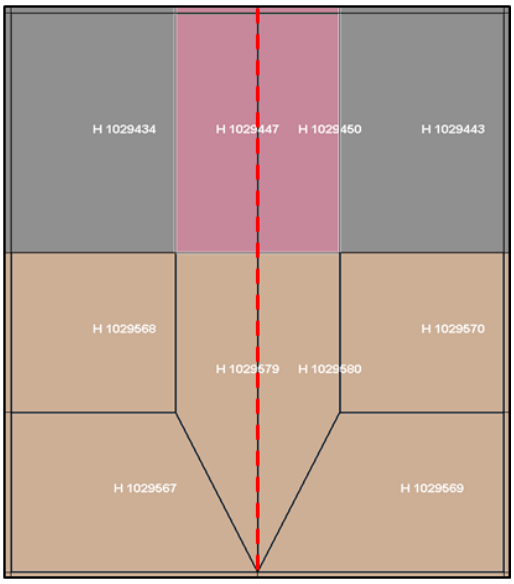

Figure 80. Close up view of the elements close to the center line of loading area

The required stress and strain values, for example at the asphalt surface layer, are actually measured slightly below the surface of asphalt layer. This implies that the stress and strain

depend on the configurations of the elements, which include the ratio between height and width of a solid element. Thus, it is important to ensure that the element has a reasonable height and width ratio of one over two (1:2) for a more accurate response value. The responses under the wheel load at the cracked areas are also influenced by the responses intrigued by the nearby wheel load as seen in Figure 81. The model developed in this research simulates the actual loading configuration of a single axle truck with two tires on each side.

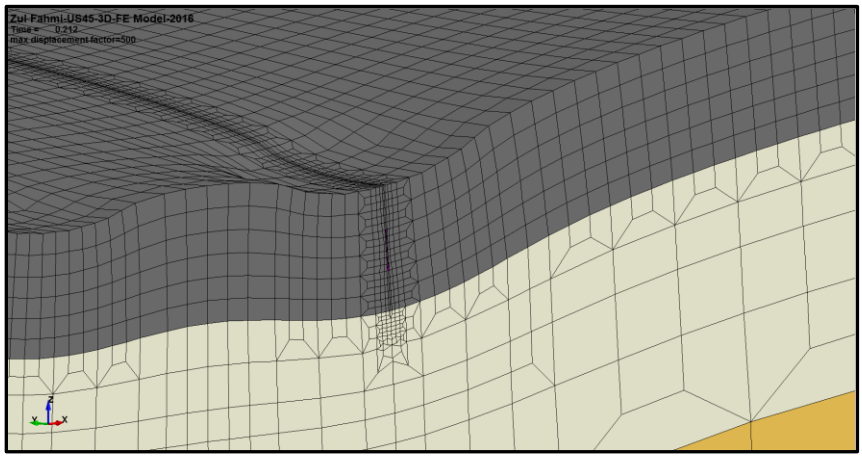

Figure 81. Example of the deformed cracked model with dual tires on each side

5.2.2 Parametric Study Conducted to Determine Modulus Value for the Cracked Layer

Earlier in this research, parametric studies were conducted to determine the modulus value for cracked element in the 3D-FE cracked model. The modulus value for the cracked layer must be lower than the surrounding asphalt modulus. Key steps to determine the modulus value for cracked layer follows:

1) This research proposed to provide the modulus value for cracked layer in the 3D-FE, based on the deflection ratios of uncracked and cracked asphalt layers. Therefore, the FWD data

was extracted from the LTPP database and the deflection values for test section 28-3085 were evaluated. Table 50 shows FWD data from 1995 and Figure 82 shows an example of distress map from the LTPP database only for the first 15 meter lengths of the surveyed test section. Multiple block cracks, longitudinal cracks, and transverse cracks were observed on the road surfaces. Based on the best visual assessments, the uncracked and cracked surface conditions were noted and recorded for further analysis. Similar approach was implemented for uncracked and cracked conditions in 2003 as shown in Table 51 and Figure 83.

Table 50. Summary of FWD data for the LTPP test section 28-3085 and asphalt surface conditions in 1995

State: Mississippi (28-3085), Test date: 11/9/1995, Deflection Unit ID: 8002-132, CN:1, Drop Number: 2										
No	Point Location	Pavement Surface Temperature (°C)	Drop Load				Pead Deflection (Sensor 1)			Asphalt Surface Condition
			kPa	psi	lbs	Factor (9,000 lbs / measured loads)	Micron	Mils	Normalized to 9,000 lbs (mils)	
1	0	9	570.5	82.7	9081	0.99	470	18.5	18.3	Cracked
2	8.2	9	555	80.5	8834	1.02	669	26.3	26.8	Cracked
3	15.2	10	561	81.4	8930	1.01	578	22.8	22.9	Cracked
4	22.9	11	567.8	82.3	9037	0.99	673	26.5	26.4	Cracked
5	31.1	11	565.8	82.1	9005	0.99	587	23.1	23.1	Cracked
6	38.7	12	561.3	81.4	8934	1.01	589	23.2	23.3	**Uncracked**
7	45.7	13	555.5	80.6	8842	1.02	921	36.2	36.9	Cracked
8	53.9	12	545.5	79.1	8683	1.04	825	32.5	33.7	Cracked
9	61.6	13	552.8	80.2	8798	1.02	492	19.4	19.8	Cracked
10	69.2	13	549	79.6	8739	1.03	572	22.5	23.2	Cracked
11	76.8	14	550	79.8	8754	1.03	496	19.5	20.1	Cracked
12	83.8	15	552.8	80.2	8798	1.03	513	20.2	20.7	Cracked
13	92	15	558.5	81	8890	1.02	588	23.1	23.4	Cracked
14	99.1	15	564.5	81.9	8985	1.01	436	17.2	17.2	Cracked
15	106.7	15	562.3	81.5	8949	1.01	408	16.1	16.1	Cracked
16	114.3	11	564.3	81.8	8981	1	370	14.5	14.6	Cracked
17	122.5	13	568.5	82.5	9049	0.99	262	10.3	10.3	**Uncracked**
18	129.5	13	576	83.5	9168	0.98	200	7.9	7.7	Cracked
19	137.2	8	563.3	81.7	8965	1	323	12.7	12.8	Cracked
20	145.4	10	535.8	77.7	8528	1.06	746	29.4	31	Cracked
21	152.4	11	546	79.2	8691	1.04	613	24.1	25	Cracked

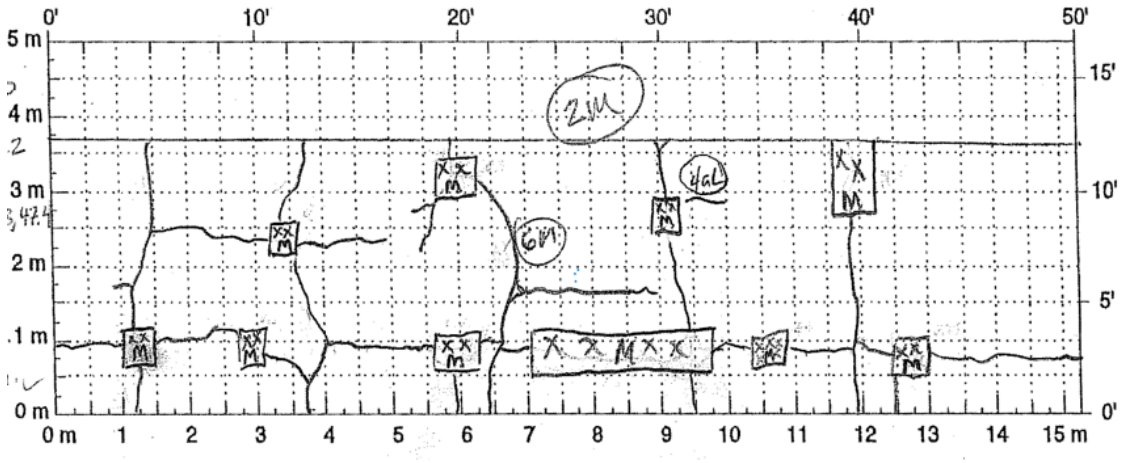

Figure 82. Example of the LTPP manual distress survey manual sketch (Test date: 11/9/1995)

Table 51. Summary of FWD data for the LTPP test section 28-3085 and asphalt surface conditions in 2003

State: Mississippi (28-3085), Test date: 3/7/2003, Deflection Unit ID: 8002-132, CN:3, Drop Number: 2										
No	Point Location	Pavement Surface Temperature (°C)	Drop Load				Pead Deflection (Sensor 1)			
			kPa	psi	lbs	Factor (9,000 lbs / measured loads)	Micron	Mils	Normalized to 9,000 lbs (mils)	Asphalt Surface Condition
1	0	7.3	571	82.8	9085	0.99	395	15.5	15.4	**Uncracked**
2	7.6	8	550	79.7	8746	1.03	538	21.2	21.8	**Uncracked**
3	15.2	7.8	559	81.1	8898	1.01	465	18.3	18.5	**Uncracked**
4	22.9	7.8	546	79.2	8691	1.04	578	22.7	23.6	**Uncracked**
5	30.5	9.6	537	77.9	8568	1.05	746	29.4	30.9	**Uncracked**
6	38.1	9.6	548	79.5	8723	1.03	692	27.2	28.1	**Uncracked**
7	45.7	9.8	540	78.4	8599	1.05	863	34	35.6	Cracked
8	53.3	11.3	545	79	8675	1.04	732	28.8	29.9	Cracked
9	61	10.5	540	78.3	8591	1.05	605	23.8	25	Cracked
10	68.6	11.4	538	78.1	8567	1.05	747	29.4	30.9	Cracked
11	76.2	11.5	540	78.3	8591	1.05	564	22.2	23.3	Cracked
12	83.8	10.9	534	77.5	8500	1.06	608	23.9	25.3	Cracked
13	91.4	11.7	552	80	8782	1.02	598	23.5	24.1	Cracked
14	99.1	13.3	543	78.7	8635	1.04	557	21.9	22.8	Cracked
15	106.7	13.2	543	78.8	8647	1.04	473	18.6	19.4	Cracked
16	114.3	5.7	541	78.4	8603	1.04	421	16.6	17.3	**Uncracked**
17	121.9	13.7	552	80.1	8786	1.02	293	11.5	11.8	**Uncracked**
18	129.5	9.2	560	81.2	8914	1.01	394	15.5	15.7	**Uncracked**
19	137.2	7.2	559	81.1	8902	1.01	231	9.1	9.2	Cracked
20	144.8	9.4	556	80.6	8842	1.02	444	17.5	17.8	**Uncracked**
21	152.4	12.2	539	78.2	8583	1.05	698	28.8	28.8	**Uncracked**

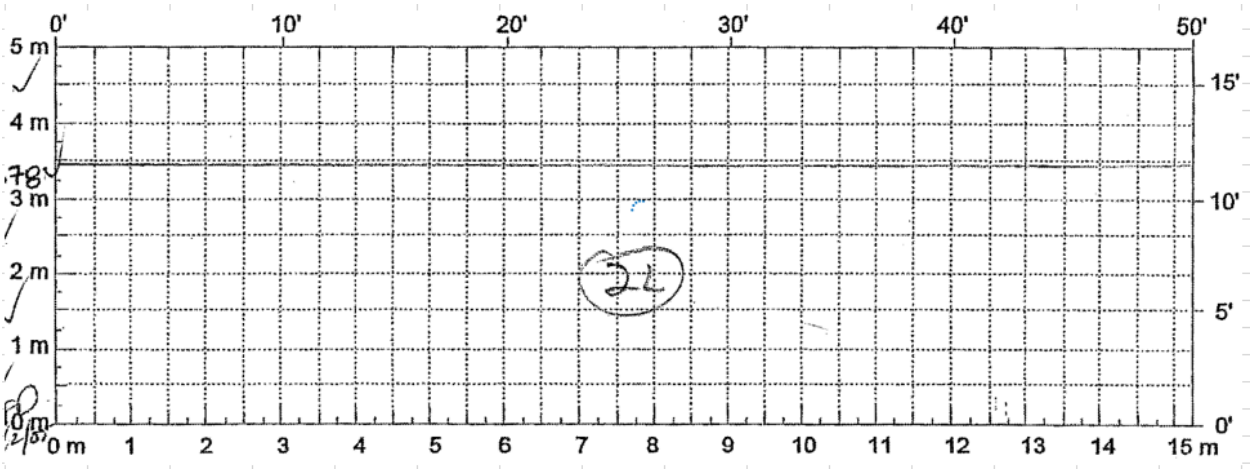

Figure 83. Example of manual distress survey manual sketch (Test date: 03/07/2003)

2) Table 52 shows sensor one peak deflection ratios between uncracked and cracked conditions.

Table 52. Peak deflection ratios between uncracked and cracked pavement for the LTPP test section 28-3085 (deflections normalized to 9,000 lbs)

No.	SHRP ID	Test Date: 11/9/1995		Test Date: 3/7/2003		Peak deflection ratio between cracked and uncracked pavements
		Deflections normalized to 9,000 lbs (mils)	Asphalt Surface Condition	Deflections normalized to 9,000 lbs (mils)	Asphalt Surface Condition	
1	28-3085	18.3	Cracked	15.4	Uncracked	1.19
2	28-3085	26.8	Cracked	21.8	Uncracked	1.23
3	28-3085	22.9	Cracked	18.5	Uncracked	1.24
4	28-3085	26.4	Cracked	23.6	Uncracked	1.12
5	28-3085	23.1	Cracked	30.9	Uncracked	0.75
16	28-3085	14.6	Cracked	17.3	Uncracked	0.84
18	28-3085	7.7	Cracked	15.7	Uncracked	0.49
20	28-3085	31	Cracked	17.8	Uncracked	1.74
21	28-3085	25	Cracked	28.8	Uncracked	0.87
Test Section 28-3085 in Mississippi					Mean	1.1
					SD	0.4
					COV (%)	34.4

The first 15 meter lengths of the surveyed test section in 2003 (Figure 83) shows no crack due to maintenance intervention. Figure 84 plot shows peak deflection ratios between uncracked and cracked asphalt pavements for nine selected data points in the LTPP test section. The calculated peak deflection ratio mean is 1.1 with a standard deviation of 0.4 and a COV of 34.4%.

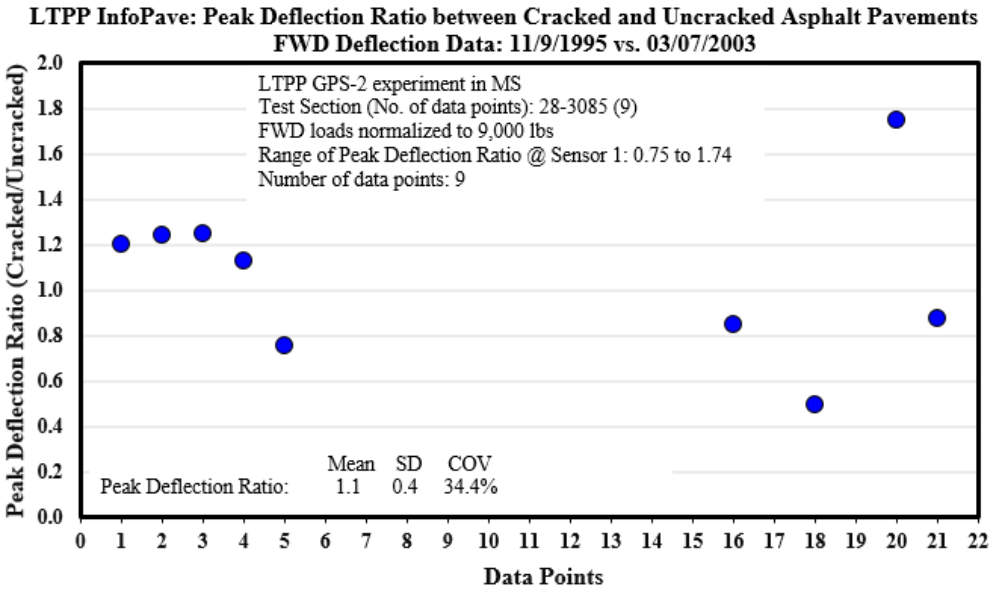

Figure 84. Peak deflection ratios plot of uncracked and cracked pavement for the LTPP test section 28-3085 (deflections normalized to 9,000 lbs)

3) Several values of low modulus of cracked asphalt layer (1,000 to 5,000 psi) and high modulus values of cracked asphalt layer (100,000 to 500,000 psi) were used to calculate the surface deflections. Figure 85 plots the calculated surface deflections for selected cracked layer modulus values.

4) The peak deflection values for cracked models were divided by the peak deflection of uncracked model of 13.7 mils for in situ condition with 332,200 psi modulus value. The resulted peak deflection ratios of cracked and uncracked pavements were summarized in Table 53 and

plotted in Figure 86. The mean for the peak deflection ratio is 1.1 and the standard deviation is 0.08.

5) As shown in Figure 86, the plot was used to interpolate the modulus value at 1.1 peak deflection ratio, and it was determined that the corresponding cracked layer modulus value is 20,000 psi. Therefore, the modulus value of 20,000 psi was assigned to the cracked layer at multiple depths.

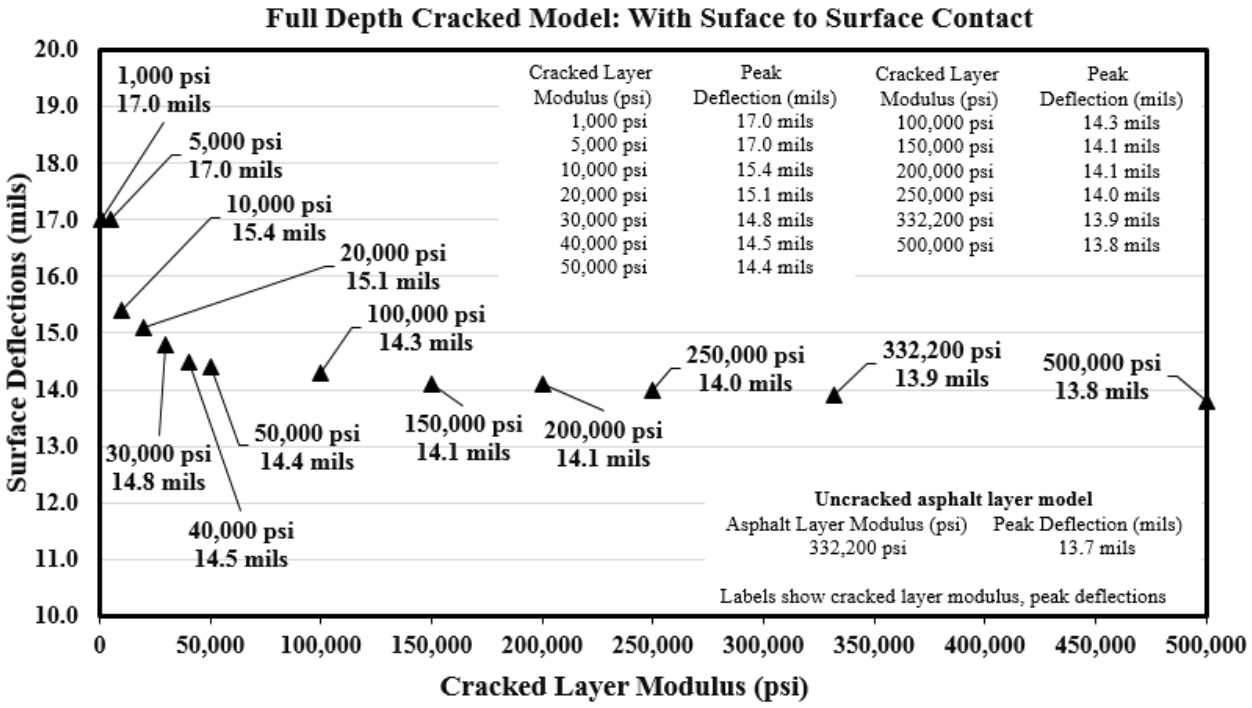

Figure 85. Surface deflections correspond to various different cracked layer modulus

Table 53. 3D-FE Cracked model: Surface deflections at the center of loading area with plus and minus 1 SD corresponding to various different cracked asphalt layer modulus values

Full Depth Cracked Model: With Surface to Surface Contact					
Cracked Layer Modulus (psi)	Peak Deflection (mils)	Peak Deflection Ratio (Cracked/Uncracked Model)	Peak Deflection Ratio - SD	Peak Deflection Ratio plus 1SD	Peak Deflection Ratio minus 1SD
1,000	17.0	1.24	0.09	1.33	1.15
5,000	17.0	1.24	0.09	1.33	1.15
10,000	15.4	1.12	0.09	1.21	1.03
20,000	15.1	1.10	0.09	1.19	1.01
30,000	14.8	1.08	0.09	1.17	0.99
40,000	14.5	1.06	0.09	1.15	0.97
50,000	14.4	1.05	0.09	1.14	0.96
100,000	14.3	1.04	0.09	1.13	0.95
150,000	14.1	1.03	0.09	1.12	0.94
200,000	14.1	1.03	0.09	1.12	0.94
250,000	14.0	1.02	0.09	1.11	0.93
332,200	13.9	1.01	0.09	1.10	0.92
500,000	13.8	1.01	0.09	1.10	0.92
Mean (mils)	14.8	1.1	Uncracked model peak deflection in situ condition: 13.7 mils (Asphalt layer modulus = 332,200 psi)		
SD (mils)	1.08	0.08			
COV (%)	7.31	7.31			

5.3 3D-FE Modeling and Simulations using Factorial Design for Cracked Asphalt pavement Subjected to Truck Axle Loading

The full factorial design for the 3D-FE cracked asphalt pavement model was similar to those implemented for the uncracked asphalt pavement model. Six factors are considered in this factorial experiment design for 3D-FE simulations. Each factor has two levels: low and high, which contributes to the complete factorial experiment design with a total of 64 possible

treatment combinations (2^6). However, the full factorial design is repeated four times depending on the crack locations (top one-third, middle one-third, bottom one-third, and full depth cracked).

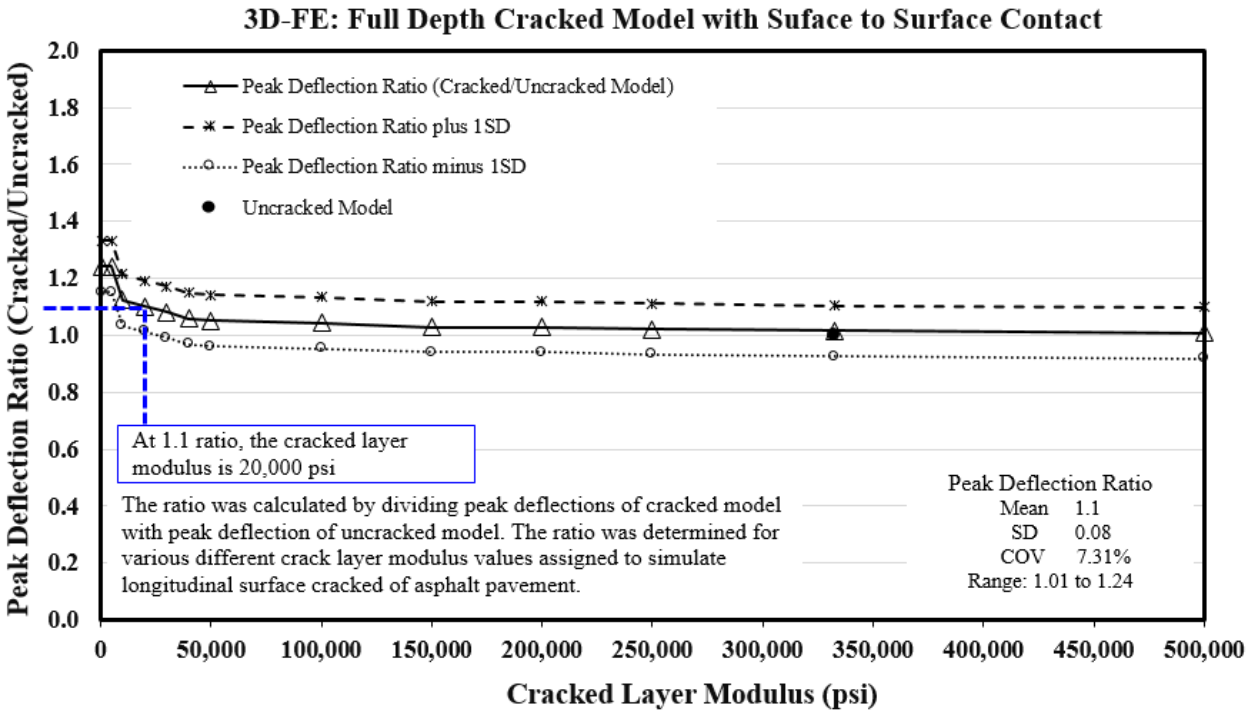

Figure 86. Peak deflection ratio for uncracked and cracked pavements: Surface deflections at the center of loading area corresponding to various different cracked layer modulus values

Once the simulations are completed, further research is recommended to analyze structural response of the asphalt highway pavement subjected to truck loads on the simulated longitudinal crack. This will help to investigate the effects of the crack depths on surface deflections and other structural responses of stresses and strains at various layer depths and on top of the subgrade. However, only selected combinations of the factorial were analyzed in this research due to the LS-DYNA software license expiry. It is recommended to complete the unfinished simulations of the cracked model in order to develop a more comprehensive structural response databases at multi-depth crack levels.

Table 54 shows 64 combinations the full factorial design proposed for the cracked 3D-FE asphalt pavement models. The thickness and modulus values for asphalt, base, subbase, and subgrade layers at low level (zero) and high level (one) are included in as well.

Table 54. Full factorial design for the 3D-FE cracked asphalt pavement model

Levels of the factors				**Layer Thickness - mm (in)**			
				0 Asphalt - 76.2 (3)		**1** Asphalt - 228.6 (9)	
Young's Modulus, E - MPa (ksi)				**0**	**1**	**0**	**1**
Subgrade (SG)	Base (B)	Subbase (SB)	Asphalt (A)	Subbase -152.4 (6)	Subbase - 304.8 (12)	Subbase -152.4 (6)	Subbase - 304.8 (12)
0 E_{SG1} - 68.9 (10)	**0** E_{B1} - 275.8 (40)	**0** E_{SB1} - 137.9 (20)	**0** E_{A1} - 1,379 (200)	**1** 000000	**2** 010000	**3** 100000	**4** 110000
			1 E_{A2} - 6,894.8 (1,000)	**5** 000001	**6** 010001	**7** 100001	**8** 110001
		1 E_{SB2} - 689.5 (100)	**0** E_{A1} - 1,379 (200)	**9** 000010	**10** 010010	**11** 100010	**12** 110010
			1 E_{A2} - 6,894.8 (1,000)	**13** 000011	**14** 010011	**15** 100011	**16** 110011
	1 E_{B2} - 1,379 (200)	**0** E_{SB1} - 137.9 (20)	**0** E_{A1} - 1,379 (200)	**17** 000100	**18** 010100	**19** 100100	**20** 110100
			1 E_{A2} - 6,894.8 (1,000)	**21** 000101	**22** 010101	**23** 100101	**24** 110101
		1 E_{SB2} - 689.5 (100)	**0** E_{A1} - 1,379 (200)	**25** 000110	**26** 010110	**27** 100110	**28** 110110
			1 E_{A2} - 6,894.8 (1,000)	**29** 000111	**30** 010111	**31** 100111	**32** 110111
1 E_{SG2} - 344.7 (50)	**0** E_{B1} - 275.8 (40)	**0** E_{SB1} - 137.9 (20)	**0** E_{A1} - 1,379 (200)	**33** 001000	**34** 011000	**35** 101000	**36** 111000
			1 E_{A2} - 6,894.8 (1,000)	**37** 001001	**38** 011001	**39** 101001	**40** 111001
		1 E_{SB2} - 689.5 (100)	**0** E_{A1} - 1,379 (200)	**41** 001010	**42** 011010	**43** 101010	**44** 111010
			1 E_{A2} - 6,894.8 (1,000)	**45** 001011	**46** 011011	**47** 101011	**48** 111011
	1 E_{B2} - 1,379 (200)	**0** E_{SB1} - 137.9 (20)	**0** E_{A1} - 1,379 (200)	**49** 001100	**50** 011100	**51** 101100	**52** 111100
			1 E_{A2} - 6,894.8 (1,000)	**53** 001101	**54** 011101	**55** 101101	**56** 111101
		1 E_{SB2} - 689.5 (100)	**0** E_{A1} - 1,379 (200)	**57** 001110	**58** 011110	**59** 101110	**60** 111110
			1 E_{A2} - 6,894.8 (1,000)	**61** 001111	**62** 011111	**63** 101111	**64** 111111

5.4 Evaluation and Comparison of Structural Response Analysis Results for Uncracked and Cracked Pavements

The structural response analysis of low level modulus of weak pavements (model 000000) for all depth levels was analyzed. Similar layer thickness and modulus values were used

for multi-depths crack layer analysis as shown in Table 55. Table 56 shows the deflection, stress, and strain values for cracked asphalt layer at various different crack depth levels.

Table 55. Layer thicknesses and modulus values for the 3D-FE analysis to study responses at different crack depth levels: Low Level Modulus (Model 000000)

Cracked Asphalt Pavement			Thickness (in)		Young's Modulus (psi)			
No.	Combination Treatments	Crack Location	Asphalt Layer	Subbase Layer	Subgrade (E4)	Base (E2)	Subbase (E3)	Asphalt (E1)
1	000000	**Uncracked**	3	6	10,000	40,000	20,000	200,000
2	000000	Top 1/3	3	6	10,000	40,000	20,000	200,000
3	000000	Middle 1/3	3	6	10,000	40,000	20,000	200,000
4	000000	Bottom 1/3	3	6	10,000	40,000	20,000	200,000
5	000000	Full Depth	3	6	10,000	40,000	20,000	200,000

Table 56. Deflection, stress, and strain responses for cracked asphalt layer at various different crack depth levels: Low Level Modulus (Model 000000)

Cracked Asphalt Pavement			Deflection at the center of loading area (mils)	Compressive vertical stress in the middle of asphalt layer (psi)	Tensile horizontal strain at the bottom of ashalt layer (÷1000)	Compressive vertical stress in the middle of base layer (psi)	Tensile horizontal strain at the bottom of base layer (÷1000)	Compressive vertical stress in the middle of subbase layer (psi)	Compressive vertical strain on top of subgrade layer (÷1000)
No.	Combination Treatments	Crack Location							
1	000000	**Uncracked**	27.6	-80.5	**0.268**	**-23.7**	0.198	**-8.40**	-0.531
2	000000	Top 1/3	28.5	-126.6	0.359	-27.1	0.205	-8.56	-0.538
3	000000	Middle 1/3	**27.5**	**-14.1**	0.293	-25.7	**0.197**	-8.41	-0.531
4	000000	Bottom 1/3	27.6	-67.9	0.679	-25.7	0.200	-8.39	**-0.530**
5	000000	Full Depth	28.6	-33.2	0.641	-29.8	0.206	-8.70	-0.543

The key findings for asphalt pavement with low level thickness and modulus values follow:

- The highest surface deflection was observed for asphalt layer with full-depth crack layer (28.6 mils).
- The highest compressive vertical stress in the middle of asphalt layer was observed for pavement with top one-third crack layer (126.6 psi).

- Tensile horizontal stains at the bottom of asphalt layer were higher for bottom one-third and full-depth crack layers as compared to other crack locations (more than 0.00064 in./in.)
- The compressive vertical stress in the middle of base layer was the highest for asphalt pavement with full-depth crack layer (29.8 psi).
- The tensile horizontal strain at the bottom of base layer was the highest for asphalt pavement with full-depth crack layer (0.000206 in./in.).
- The compressive vertical stress in the middle of subbase layer was the highest for asphalt pavement with full-depth crack layer (8.7 psi).
- The compressive vertical strain on top of subgrade layer (0.000543 in./in.)

Further analysis was conducted to compare structural responses between low level modulus and thin pavements (model 000000) high level modulus and thick pavements (model 111111). Various different combinations of factorial design were also evaluated in this research. Data sets in Table 57 were assigned to these models for the analysis. Table 58 summarizes the surface deflection, stress, and strain values measured at critical locations for both uncracked and full depth cracked asphalt layers.

Table 57. Layer thicknesses and modulus values for uncracked and full depth cracked asphalt layer at various different treatment combinations

Cracked Asphalt Pavement			Thickness (in)		Young's Modulus (psi)			
No.	Combination Treatments	Crack Location	Asphalt Layer	Subbase Layer	Subgrade (E4)	Base (E2)	Subbase (E3)	Asphalt (E1)
1	000000	**Uncracked**	3	6	10,000	40,000	20,000	200,000
2	111111	**Uncracked**	9	12	50,000	200,000	100,000	1,000,000
3	000000	Full Depth	3	6	10,000	40,000	20,000	200,000
4	000011	Full Depth	3	6	10,000	40,000	100,000	1,000,000
5	000111	Full Depth	3	6	10,000	200,000	100,000	1,000,000
6	001000	Full Depth	3	6	50,000	40,000	20,000	200,000
7	001011	Full Depth	3	6	50,000	40,000	100,000	1,000,000
8	001111	Full Depth	3	6	50,000	200,000	100,000	1,000,000
9	111111	Full Depth	9	12	50,000	200,000	100,000	1,000,000

Table 58. Deflection, stress, and strain responses for uncracked and full depth cracked asphalt layer at various different treatment combinations

Cracked Asphalt Pavement			Deflection at the center of loading area (mils)	Compressive vertical stress in the middle of asphalt layer (psi)	Tensile horizontal strain at the bottom of ashalt layer (÷1000)	Compressive vertical stress in the middle of base layer (psi)	Tensile horizontal strain at the bottom of base layer (÷1000)	Compressive vertical stress in the middle of subbase layer (psi)	Compressive vertical strain on top of subgrade layer (÷1000)
No.	Combination Treatments	Crack Location							
1	000000	**Uncracked**	27.6	-80.5	0.268	-23.7	0.198	-8.4	0.531
2	111111	**Uncracked**	**3.6**	-49.3	**0.019**	**-7.5**	**0.017**	**-3.4**	**-0.040**
3	000000	Full Depth	28.6	-33.2	0.641	-29.8	0.206	-8.7	-0.543
4	000011	Full Depth	20.5	-18.8	0.507	-22.9	0.064	-7.1	-0.336
5	000111	Full Depth	16.2	-22.3	-0.231	-31.9	0.054	-5.5	-0.251
6	001000	Full Depth	14.6	-27.8	0.676	-29.8	0.175	-13.0	-0.166
7	001011	Full Depth	9.4	**-13.2**	1.021	-24.3	0.062	-11.4	-0.138
8	001111	Full Depth	6.5	-16.2	0.048	-32.0	0.042	-9.3	-0.114
9	111111	Full Depth	7.0	-13.4	0.078	-9.6	0.022	-3.8	-0.043

The key finding for uncracked asphalt pavements follows:

- Low level modulus and thin pavement shows higher surface deflection, stress, and strain values at those critical locations as compared to high level modulus and thick pavement layer.

The key finding for full-depth cracked asphalt pavements follows:

- Low level modulus and thin pavement shows higher surface deflection, stress, and strain values at those critical locations as compared to high level modulus and thick pavement layer.

Comparison between the uncracked and full-depth cracked asphalt layer indicates that asphalt pavements with full-depth crack show higher surface deflection, stresses, and strains except for compressive vertical stress in the middle of asphalt layer, as compared to uncracked asphalt pavements. This finding applies to both model 000000 and model 111111, respectively.

5.5 Impacts of Longitudinal Crack on Backcalculation of Effective Asphalt Layer Modulus

This research also analyzed the impacts of the longitudinal cracks on the backcalculation of the asphalt layer modulus values. In general, the modulus values for the uncracked pavement are higher as compared to the cracked pavements. The effective modulus values will decrease due to the effect of full depth cracks. Table 59 describes the layer thicknesses and the modulus values for different combination treatments of the 3D-FE models that simulated full depth longitudinal cracks.

Table 59. Layer thicknesses and modulus values for various different treatments for the 3D-FE models that simulate full depth longitudinal cracks

Combination Treatments	Crack Location	Thickness, Inches			Modulus Values, psi			
		Asphalt Layer	Base Layer	Subbase Layer	Asphalt Layer	Base Layer	Subbase Layer	Subgrade Layer
000000	Full Depth	3	6	6	200,000	40,000	20,000	10,000
000011	Full Depth	3	6	6	1,000,000	40,000	100,000	10,000
000111	Full Depth	3	6	6	1,000,000	200,000	100,000	10,000
001000	Full Depth	3	6	6	200,000	40,000	20,000	50,000
001011	Full Depth	3	6	6	1,000,000	40,000	100,000	50,000
001111	Full Depth	3	6	6	1,000,000	200,000	100,000	50,000
111111	Full Depth	9	6	12	1,000,000	200,000	100,000	50,000

Further iterations were conducted to study the effective asphalt modulus values of full depth longitudinal cracks as compared to the modulus values of the uncracked asphalt pavements. The key steps to execute the iterations follow:

1) The deflection values at the center of the loading area (W_1) were extracted for the uncracked and cracked asphalt pavement models. Higher level models show smaller deflection values as compared to the low level models.

2) The GAMES linear elastic software was used to iterate the effective asphalt modulus values of full depth cracked models with different combination treatments. This software allows simulation of point loads at four different locations similar to the loading configurations in the 3D-FE models.

3) Initially, the deflection values for the uncracked models were compared with the deflection values obtained from the GAMES analysis, which assumes no discontinuity on the asphalt pavement surfaces. Less than 6.5% difference in the deflection values were noted, which suggest that the defection values from the 3D-FE analysis were reliable and acceptable.

4) Similar modulus values used in the 3D-FE analysis were used in the GAMES analysis for different combination treatments. Multiple iterations were conducted by changing only asphalt modulus values until the deflection values matched with the deflection values of full depth cracked models.

5) The iterated modulus values were not the final effective modulus values for cracked models. The iterated modulus values show the required reductions in the asphalt modulus to match the deflection values of the cracked asphalt pavements within ± 1% tolerance criteria. Therefore the final effective modulus values were obtained by substracting the iterated modulus values from the default modulus of uncracked pavements.

6) The effective asphalt modulus values for cracked models with full depth longitudinal cracks were calculated and compared with the uncracked asphalt modulus values.

Table 60 shows the effective modulus values for seven different combination treatments. The combination treatments represent the low and high levels of asphalt and subbase layer thicknesses, and low and high levels of modulus values for all layers.

Table 60. Comparisons of the effective asphalt pavement modulus values with uncracked pavements for seven different combination treatments

No.	Combination Treatments	Uncracked Asphalt Modulus (psi)	Effective Asphalt Modulus (Full Depth Cracked), psi	% Reduction in Asphalt Modulus
1	000000	200,000	38,000	81.0
2	000011	1,000,000	250,000	75.0
3	000111	1,000,000	100,000	90.0
4	001000	200,000	91,000	54.5
5	001011	1,000,000	541,000	45.9
6	001111	1,000,000	690,000	31.0
7	111111	1,000,000	865,000	13.5

Based on full-depth cracked 3D-FE model results low level modulus of weak pavements showed a higher reduction of 81.0% in the asphalt modulus compared to the uncracked 3D-FE model, while the high level modulus and thick pavement showed a reduction of 13.5% in the asphalt modulus of the uncracked pavement model.

VI. IMPLEMENTATION OF ENHANCED CONDITION MODELS FOR ASPHALT PAVEMENT DESIGN AND ASSET MANAGEMENT

6.1 Implementation for Mechanistic Empirical Design of Asphalt Pavement Design

The limitations of the MEPDG software pavement performance models include the following items:

- No consideration of cumulative equivalent single axle loads.
- No consideration of maintenance and rehabilitation history and climatic regions.
- No block cracking model, which is an important distress of low-temperature cracking.
- Longitudinal cracking model is used on the prediction of the top-down cracking distress.

Therefore, it is recommended to implement the enhanced pavement condition deterioration models in a mechanistic-empirical design method such as PADAP software.

6.1.1 Application of IRI Performance Condition Deterioration Model Equations

Both enhanced IRI multiple regression equation and ANN IRI model were proposed for asphalt pavement design purposes. The final multiple regression equation for IRI condition deterioration prediction is shown in Equation 6.1. It is important to point out that Equation 6.1 is applicable only high quality road networks with the IRI equal or less than 3 m/km. This includes the national highway system that is maintained periodically.

$$Y_I = 0.642 + 0.726\ (Y_{I0}) + 0.006\ (Age) - 0.045\ (SN) - 1.542x10^{-8}\ (CESAL) + 0.002\ (TEMP_{AIR}) - 0.000349\ (PRECIP) + 0.08\ (Reg\_D) - 0.105\ (CND) - 0.061\ (IRI\_D) \quad (6.1)$$

The necessary keys steps required in the implementation of the enhanced IRI multiple regression equation for pavement design follow:

- Set the initial IRI to 0.5 m/km for newly paved road network. For older road network, the most recent IRI data must be known in order to use the proposed multiple regression equation. The initial IRI value must be between 0.53 m/km to 3.55 m/km.
- Pavement age (year) is calculated from the last year since the major maintenance and rehabilitation has taken place. If there is no major maintenance and rehabilitation history recorded, the pavement age is calculated from the initial year when the road was opened to the traffic. If the pavement age in 2019 in 10 years, and the predicted IRI in 2029 is required, then the pavement age of 20 years will used in the equation. The pavement age must be between 0 to 48 years.
- Estimate the CESAL for the projected years based on a known traffic growth factor. If the recent CESAL is 500,000 in 2019, and the annual traffic growth factor is 0.01, the estimated CESAL in 2029 is 552,311 and will be used in the equation. The maximum CESAL is 36,669,857 and the minimum CESAL is 3,000.
- Calculate the SN based on the layer coefficients, layer thicknesses, and drainage coefficients for asphalt, base, and subbase layers, respectively. The minimum and maximum SN values are 1.4 to 10.8, respectively.

- Assume an average monthly air temperature (°C) based on the most recent year data that are available in the national database. The minimum and maximum air temperatures ranged from -8.3°C to 46°C, respectively.
- Assume an average monthly precipitation (mm) based on the most recent year data that are available in the national database. The average monthly precipitation ranged from 0 to 645 mm.
- For the LTPP climatic region factor (Reg_D), assign zero for the Southern region. In contrast, assign one for other regions.
- For major maintenance and rehabilitation intervention (CND) variable, assign zero if there is no major maintenance and rehabilitation has taken place. Assign one if old pavement layer has been removed and resurfaced.
- For IRI measurement location factor (IRI_D), assign zero for the outside wheel path, and one for the inside wheel path.

The $ANN_{7\text{-}5\text{-}1}$ provides the most optimum network for future IRI prediction. The $ANN_{7\text{-}5\text{-}1}$ refers to a total of seven inputs (Y_{I0}, Age, SN, CESAL, $TEMP_{AIR}$, PRECIP, and CND), five hidden nodes, and one output. Figure 87 shows the set up for the optimum network used in the analysis using the TRSEQ1 ANN computer program [68].

Figure 88 shows an example of the implementation of ANN model for future IRI prediction. This extended analysis intends to predict the remaining duration (years) before the surface roughness of in-service asphalt pavement located at LTPP test section 40-4165 in Southern region reaches the terminal IRI of 2.71m/km as outlined by the MEPDG. The prediction was carried out by changing only pavement age and traffic data at 3% annual CESAL growth in the ANN model. The initial IRI, SN, air temperature, and CND data are assumed

similar to the final measured data in 2005. Based on Figure 88 plot, asphalt surface roughness for test section 40-4165 will reach terminal IRI of 2.71 m/km in 2020.

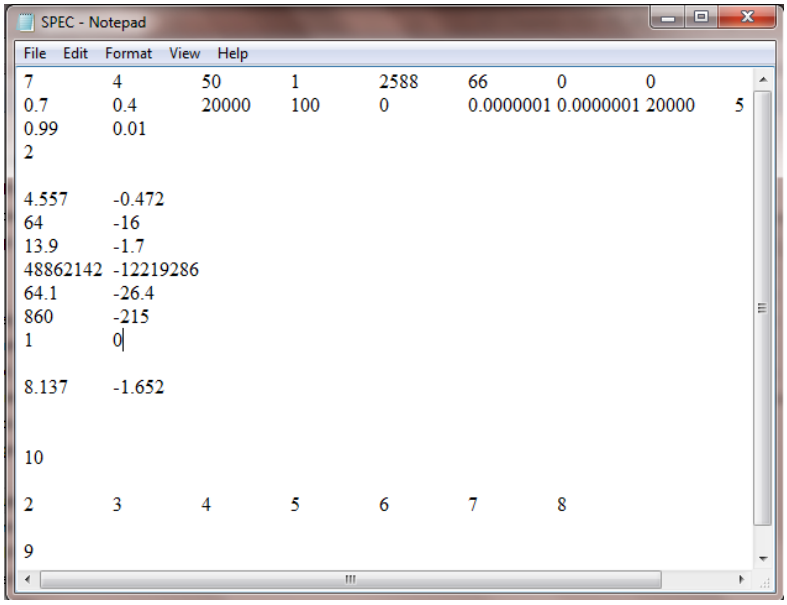

Figure 87. Example of SPEC file set up for IRI model using ANN method

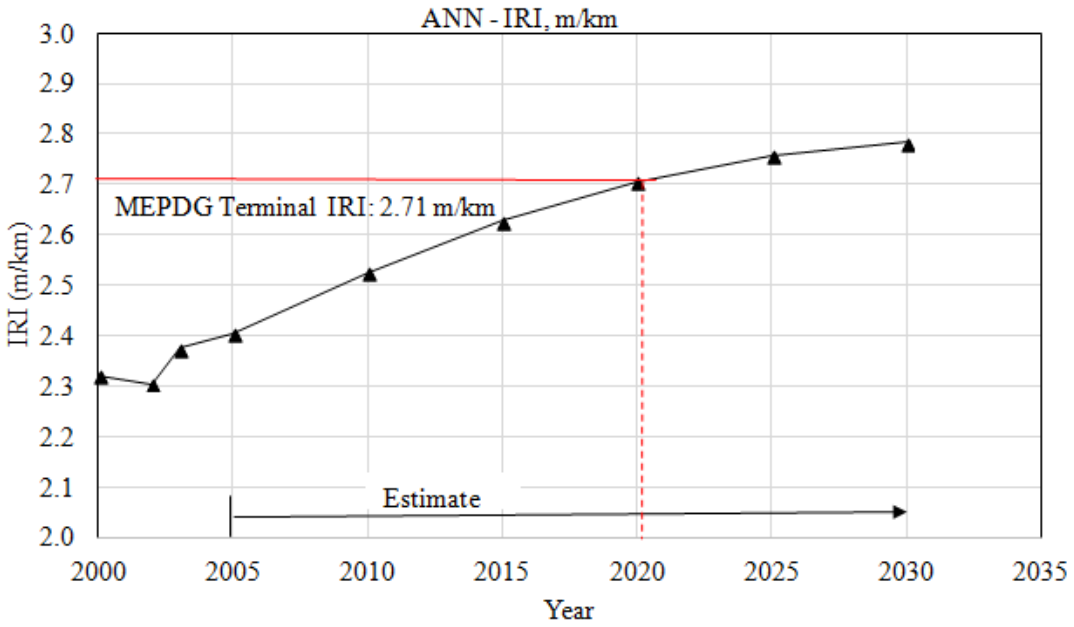

Figure 88. Implementation of the ANN model equation to predict future IRI value for LTPP test section 40-4165 in Southern region

Both enhanced rutting multiple regression equation and ANN rutting model were proposed for asphalt pavement design purposes. The final enhanced multiple regression equation for rutting condition deterioration prediction is shown in Equation 6.2.

$$\text{Log}_{10}(Y_R+0.5) = 0.058 + 0.952\ (\text{Log}_{10}\ (Y_{RO}+0.5)) - 0.000481\ (\text{Age}) + 2.962\text{x}10^{-9}\ (\text{CESAL}) + 0.021\ (\text{SN}) + 2.562\text{x}10^{-8}\ (E_1) - 1.356\text{x}10^{-7}\ (E_2) - 1.171\text{x}10^{-7}\ (E_3) + 2.348\text{x}10^{-7}\ (E_4) - 0.000141\ (\text{TEMP}_{AIR}) + 0.010\ (\text{Reg\_D}) + 0.006\ (\text{CND}) - 0.041(\text{Base\_D}) + 0.000259\ (T_T) - 0.011\ (T_1) \quad (6.2)$$

The necessary keys steps required in the implementation of the enhanced rutting multiple regression equation for pavement design follow:

- Set the initial IRI to zero mm for newly paved road network. For older road network, the rut depth data must be known in order to use the proposed multiple regression equation. The initial IRI value must be between 0 to 15 mm. Transform the rut depth value to Log_{10} $(Y_{RO}+0.5)$ for implementation in the enhanced rutting prediction equation.
- Pavement age (year) is calculated from the last year since the major maintenance and rehabilitation has taken place. If there is no major maintenance and rehabilitation history recorded, the pavement age is calculated from the initial year when the road was opened to the traffic. The pavement age must be between zero to 28 years.
- Estimate the CESAL for the projected years based on a known traffic growth factor. The maximum CESAL is 7,612,665 and the minimum CESAL is 3,000.
- Calculate the SN based on the layer coefficients, layer thicknesses, and drainage coefficients for asphalt, base, and subbase layers, respectively. The minimum and maximum SN values are 1.0 to 9.0, respectively.

- Asphalt layer modulus (E_1) value must be known and must be between 100,000 psi to 1,183,987 psi.
- Base layer modulus value (E_2) must be known and must be between zero (no base layer) to 1,346,116 psi.
- Subbase layer modulus value (E_3) must be known and must be between zero (no subbase layer) to 129,359 psi.
- Subgrade layer modulus value (E_4) must be known and must be between 9,034 psi to 53,270 psi.
- Assume an average monthly air temperature (°C) based on the most recent year data that are available in the national database. The minimum and maximum air temperatures ranged from -3.0°C to 31.1°C, respectively.
- Total pavement layers thicknesses (T_T) must be known and ranged from 7.2 to 34.7 inches.
- Asphalt layer thickness (T_1) must be known and ranged from 0.9 to 14.6 inches.
- For the LTPP climatic region factor (Reg_D), assign zero for the Southern region. In contrast, assign one for other regions.
- For major maintenance and rehabilitation intervention (CND) variable, assign zero if there is no major maintenance and rehabilitation has taken place. Assign one if old pavement layer has been removed and resurfaced.
- For base layer type factor (Base_D), assign zero for stabilized base, one for granular base.

The $ANN_{15\text{-}3\text{-}1}$ provides the most optimum network for future rutting prediction. The $ANN_{15\text{-}3\text{-}1}$ refers to a total of 15 inputs ($Log_{10}(Y_{R0}+0.5)$, Age, CESAL, SN, E_1, E_2, E_3, E_4, $TEMP_{AIR}$, Reg_D, CND, Base_D, T_T, T_1, DEF_{W1}), three hidden nodes, and one output

($Log_{10}(Y_R+0.5)$). Figure 89 shows the set up for the optimum network used in the analysis using the TRSEQ1 ANN computer program [78].

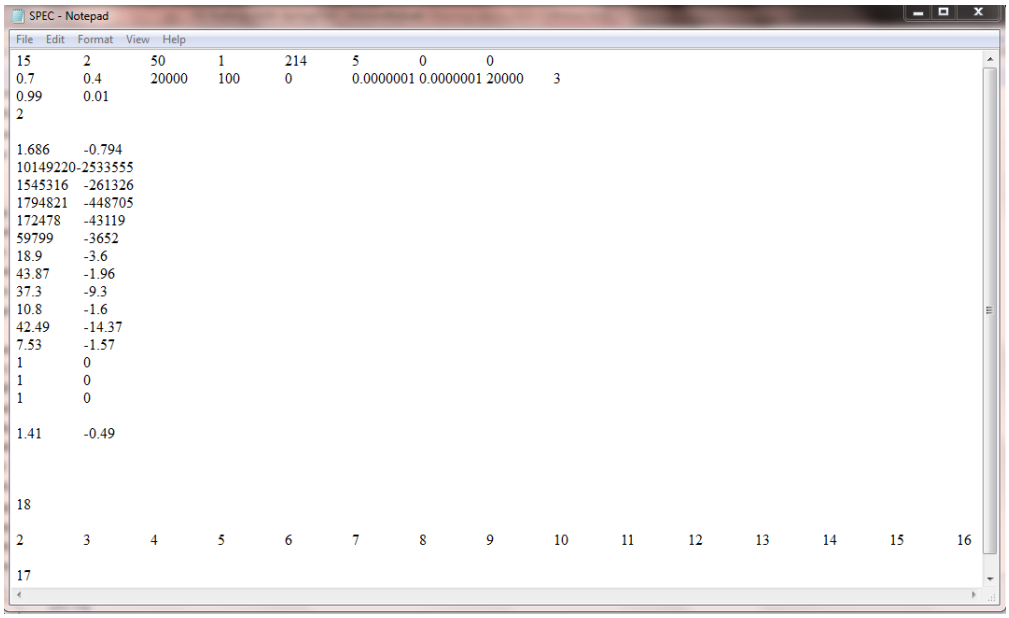

Figure 89. Example of SPEC file set up for rutting model using ANN method

6.1.3 Application of Cracking Performance Condition Prediction Model Equations

The ANN models for combined all cracking distress types and individual cracking type are better predictor for asphalt layer cracking distresses. Figure 90 shows the set up for the optimum network used in the analysis using the TRSEQ1 ANN computer program [78]. The optimum ANN cracking models follow:

- Combined UCI: $ANN_{21\text{-}9\text{-}1}$
- UCI for alligator crack: $ANN_{21\text{-}9\text{-}1}$
- UCI for block crack: $ANN_{21\text{-}9\text{-}1}$
- UCI for longitudinal crack: $ANN_{21\text{-}9\text{-}1}$
- UCI for transverse crack: $ANN_{21\text{-}8\text{-}1}$

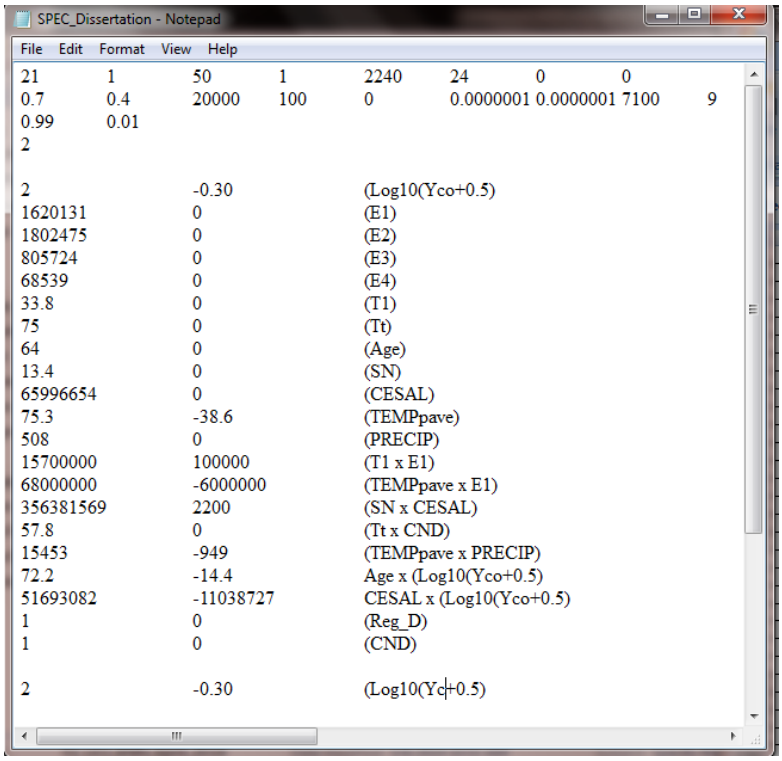

Figure 90. Example of SPEC set up for combined all cracking distresses (UCI)

6.2 Application of Condition Deterioration Predictive Equations for Asphalt Pavement Asset Management

Figure 91 shows and enhanced Pavement Asset Management (PAM) framework [63], which was developed based on the U.S. Governmental Accounting Standards Board (GASB) Statement 34 framework [131]. The influence of life-cycle M&R is significant for longer performing highway condition, as shown in Figure 92. It is recommended implementing the enhanced pavement deterioration model equations developed in this research for life-cycle asset management and M&R programs. A simplified M&R intervention criteria for PAM is shown in Table 61.

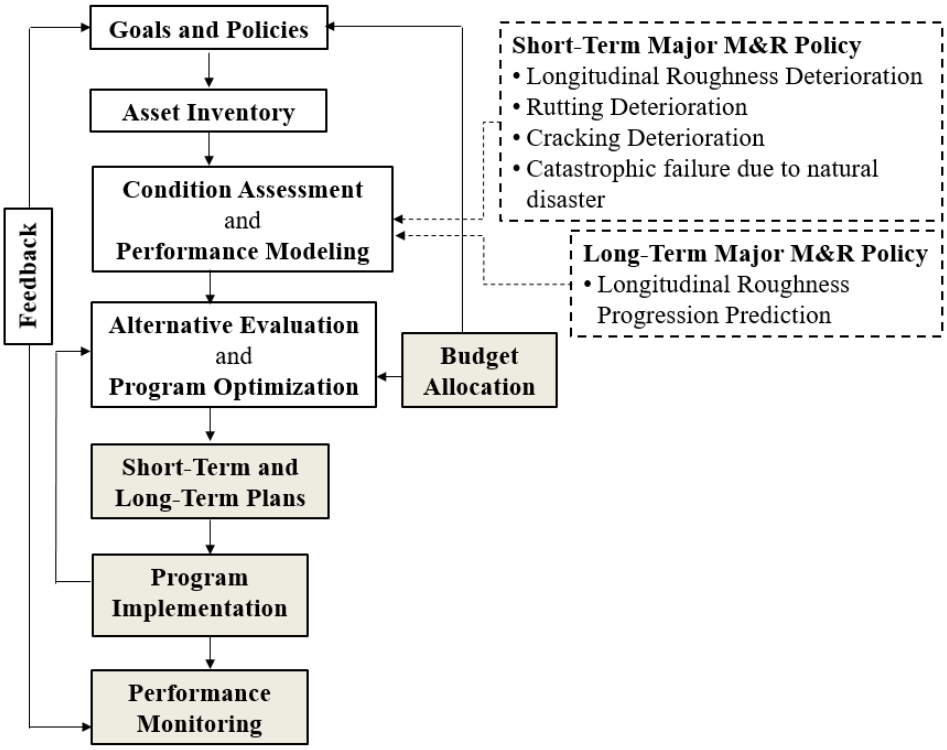

Figure 91. An Enhanced Pavement Asset Management (PAM) Framework [63]

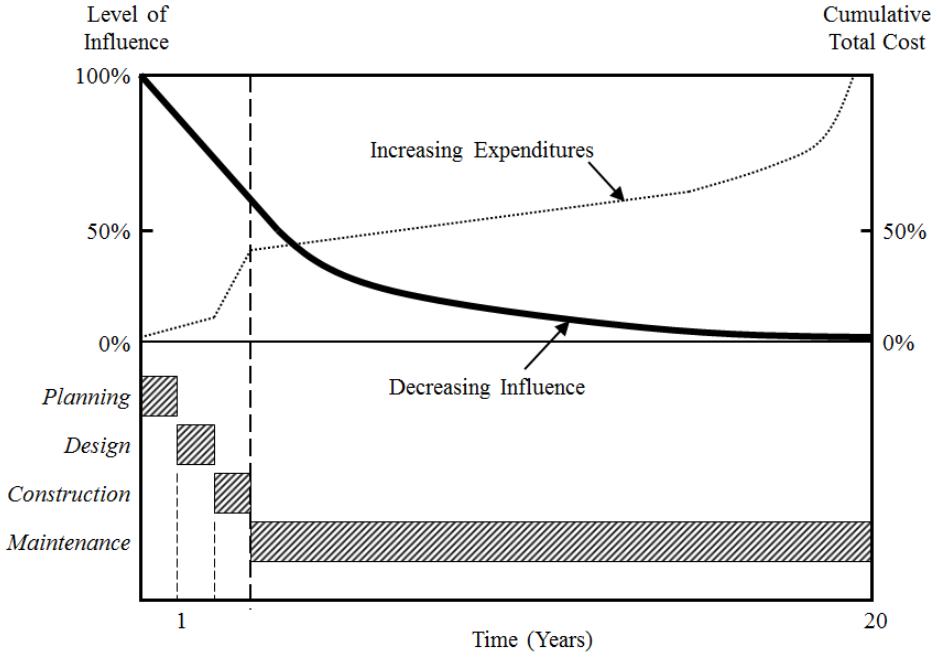

Figure 92. Basic Concept of Life Cycle Cost (LCC) [63]

Table 61. Simplified M&R intervention criteria for pavement asset management

1. Short Term or Single Year M,R&R Intervention Policy			
	Asphalt Pavement M,R&R	Intervention Criteria	M,R&R Treatment
(a)	Total Distress Area Low (L), Medium (M), High (H)	(L, M, H Severity) > 60%	**Asphalt Pavement:** M1 for freeway and highway; M2 for other roads **Concrete Pavement:** M1P for freeway and highway; M2P (extensive) for other roads
(b)	Cracking Area	< 60% H - Severity ≥ 20%	**Asphalt Pavement:** M3 (Minor, seal coat) **Concrete Pavement:** M2P (extensive)
(c)	Rutting Area	< 60% H - Severity ≥ 20%	**Asphalt Pavement:** M2 (Milling and inlay)
(d)	Total Distress Area	< 60% H - Severity < 20%	**Asphalt Pavement:** M4 **(**Local minor maintenance) **Concrete Pavement:** M4P (Local)
(e)	Longitudinal Roughness	IRI exceeds 5.2 m/km (Rough & Unsafe)	**Asphalt Pavement:** M3 **(**Minor, seal coat) **Concrete Pavement:** M2P (Extensive)
	(Only if distress repairs are not being applied)		
(f)	Catastrophic Failure Policy (Flood due to rain, hurricane, river overflow), Others: Earthquake	Rapid Condition Assessment to Identify: (1) Local Failure (> 60% area) (2) Mitigation by Major Maintenance & Rehabilitation	**Asphalt Pavement:** M3 **Concrete Pavement:** M2P Reconstruction as needed

Asphalt Pavement Treatment Codes		**Unit Cost, US $**
M1	Major maintenance, rehabilitation	1.5 inch milling, 4 inches asphalt overlay on freeways and highways, $6.0/sq. yard on 100% area
M2	Major, Milling and inlay	1.5 inch milling and asphalt inlay, $3.0/sq. yard on 100% area
M3	Minor, seal coat	Asphalt slurry seal or microsurfacing, $1.5/sq. yard on 100% area
M4	Local, minor for H - severity	Asphalt patching $2.5/sq. yard for rutted area; Crack sealing $1.5/sq. yard for cracked area
(If both M2 and M3 are selected then use **only** M2 for freeways and highways and use **only** M3 for other types of roads)		
Concrete Pavement M,R&R Treatment Codes		**Unit Cost, US $**
M1P	Major maintenance, rehabilitation	4 inches asphalt overlay on freeway and highway; $8.0/sq. yard on 100% area
M2P	Concrete pavement restoration	Extensive; $7.0/sq. yard on distressed area
M4P	Concrete pavement restoration	Local; $6.0/sq. yard on distressed area
2. Long Term or Multi Year M,R&R Intervention Policy		
Asphalt Pavement Intervention Criteria Based on Longitudinal Roughness		M2 if IRI equals or exceeds 5.2 m/km
Concrete Pavement Intervention Criteria		M1P if PSR equals or < 2.0
If PCR model is available (not in this dissertation), PCI ≤30 (Maintenance intervention level)		

6.5 Concluding Remarks

The developed enhanced condition deterioration model equations for asphalt highway pavement present a significant improvement on the models currently used in mechanistic-empirical pavement design method. It is recommended to calibrate the regression prediction model using condition and traffic data for selected pavement sections, if desired to implement in other geographic and different climatic regions.

VII. SUMMARY, CONCLUSIONS, AND RECOMMENDATIONS

7.1 Summary

A nation's economy and prosperity depends on an efficient and safe transportation networks for public mobility and freight transportation. A country's road network is recognized as one of the largest public infrastructure assets. Adverse pavement longitudinal roughness, rutting, cracking, potholes, and surface deterioration of road surface conditions require major maintenance and rehabilitation at significantly high costs. If timely maintenance and rehabilitation are not performed, the pavement damages inflicted by heavy truck traffic repetitions and environmental impacts may lead to life-threatening condition for road users.

The importance of considering maintenance and rehabilitation intervention factor in the condition deterioration prediction equations was never considered. This research considered the LTPP climatic regions and maintenance and rehabilitation intervention in the development and implementation of enhanced pavement condition deterioration prediction equations. The IRI prediction equation considered the IRI measurement location factor (outside and inside wheelpaths). The rutting prediction equation included additional factors of in situ modulus of pavement layers and base layer type. Additionally, variance stabilizing transformations were also considered in the development of the rutting and cracking prediction model equations. These considerations are vital for improved mechanistic-empirical structural design of the asphalt pavement and asset management practices. The regression equations are more objective, incorporate reasonable important independent variables, are easy to implement, and is easy to calibrate for future implementation in other geographical and climatic regions.

The enhanced asphalt highway pavement IRI, rutting, and cracking deterioration prediction equations were developed and evaluated in this research for LTPP data sets of 2,588 for IRI, 214 for rutting, and 2,240 for cracking. Comparatively, the AASHTO MEPDG performance equations were developed using less number of test sections.

The development of new cracking model using Unified Cracking Index combines all crack types (alligator, block, longitudinal, and transverse). Block cracking and the combined cracking models are not available in the MEPDG. The concept of Unified Cracking Index is practical and applicable for decision support system for the maintenance and rehabilitation programs. This approach together with intervention criteria of maintenance and rehabilitation is a significant enhancement for life-cycle asset management of asphalt highway pavements.

The 3D-FE models of uncracked and cracked pavement layer were also introduced in this research. A new approach to assess asphalt pavement structural responses under a single axle dual tires loads was developed and simulated using the 3D-FE dynamic analysis of the cracked and uncracked models. Reasonably good results of the model's verification as compared to linear elastic program and the previous 3D-FE simulations proved the reliability of the models used in the numerical analysis. These 3D-FE models of asphalt pavements are beneficial for structural response analysis as well as the pavement structural design. The analysis considers real-world pavement subgrade model size, truck load-time history, and a rational approach to simulate longitudinal crack in asphalt pavements at partial depths and full depth of the asphalt layers.

7.2 Conclusions

The main conclusions for each research topics are listed in the following sections:

7.2.1 Evaluation and Enhancement of Condition Deterioration Progression Models

- For model database, the IRI multiple regression of longitudinal roughness data shows R of 0.633, while the ANN IRI model shows R 0.717. The verifications using 18 data sets that was not in the model database show a better R of 0.664 for the IRI multiple regression equation as compared to the ANN's R of 0.483. Both IRI multiple regression equation and ANN model show a small RMSE less than 1.1, while the MARE values are 37.7% and 41.3% for the IRI multiple regression and ANN model, respectively.
- The prediction equations from multiple regression modeling and ANN modeling of rutting distress show high R values above 0.93 and 0.94, respectively, for the model database. For rutting verification data sets, both multiple regression equation and ANN model show similar R values of 0.99. Both rutting multiple regression equation and ANN model show the RMSE less than 1.0, while the MARE are 16.6% and 2.3% for the rutting multiple regression equation and ANN model, respectively.
- The combined UCI cracking equation for the model database shows correlation, R, of 0.551 for log model with the RMSE of 19.5% of crack densities in predictions compared to the measured LTPP data. The sigmoid transformed regression equation shows R of 0.511 with 4.1% error. In comparison, the ANN model for UCI showed significant improvement in R value (0.707) with 14.6% error. It is also showed high R value (0.861) and low error for the verification data sets.
- Individual ANN models of cracking (alligator, block, longitudinal, transverse) also showed reasonably accurate results.
- The developed asphalt pavement condition deterioration progression models are applicable to high quality pavements only.

7.2.2 Material Characterization of Asphalt Pavement Using Nondestructive Deflection Data

- Several modulus backcalculation software, based on the layered linear elastic static analysis were evaluated in this research. The comparison of the backcalculated modulus for the FWD deflection data used indicated that the backcalculated modulus values in the LTPP database were generally unreasonable using the EVERCALC 5.0 software. Overall, BAKFAA 2.0 and PEDD/UMPEDD backcalculated modulus values that were generally reasonable for all pavement layers.
- The results of a climate impact study revealed that the thickness design of longer lasting pavement performance depends on seasonal layer modulus values considering extreme weather and climate attributes.

7.2.3 3D-FE Modeling of Uncracked Asphalt Pavements

- The 3D-FE model of uncracked asphalt pavement layer was developed using the LS-DYNA finite element software and verified based on the measured peak surface deflection at the center of loading area under FWD load (9,000 lbf). The verification showed that the 3D-FE models predicted only -1.7% less surface deflection (13.8 mils) as compared to the measured surface deflection of 14.04 mils. Additional 3D-FE simulations subjected to 4,500 lbf of truck wheel load on each tire was conducted. The calculated surface deflection was compared with the surface deflection value calculated using the GAMES linear elastic static analysis program. The calculated % difference was -4.4% which suggested a reliable 3D-FE model developed in this research. A full factorial experiment for six independent variables at two levels was designed, and the simulations for all 64 treatment combinations were executed for the uncracked model.

7.2.4 3D-FE Modeling of Asphalt Pavements with Longitudinal Crack

- The 3D-FE models of the longitudinal crack in asphalt layer at multiple depths and full depths were also developed in this research. The cracked layer was simulated and subjected to truck wheel loads. The full depth crack, top one-third crack, middle one-third crack, and bottom one-third crack were simulated. However, only selected combinations of the factorial were analyzed due to the LS-DYNA software license expiry. The full depth cracked model shows higher surface deflections as compared to the uncracked model. The top one-third cracked models indicate the highest compressive vertical stress in the middle in the middle of the asphalt layer. Tensile horizontal strain at the bottom of the asphalt layer is the most critical for the bottom one-third cracked model ($\varepsilon = 0.000679$), which indicated 139% higher as compared to the uncracked pavements.
- Further analysis was conducted using the cracked model to study the effect of full depth crack on effective asphalt modulus values. Based on full-depth cracked 3D-FE model results at low level modulus values of weak pavements showed a significant reduction of 81.0 % in the asphalt modulus compared to the modulus of the uncracked 3D-FE model, while the high-level combination of modulus and thick layer values showed a small reduction of 13.5 % in the asphalt modulus of the uncracked pavement model. This analysis of reduction in the effective asphalt modulus due to cracked asphalt layer is not possible by using the traditional layered elastic static analysis that assumes no discontinuity in the pavement layer.

7.3 Recommendation for Future Research

a) Implementation of condition deterioration progression models

- Implement the reasonable condition deterioration progression models asphalt highway pavement, and calibrate if necessary, for other geographical and climate regions, such as the tropical country of Malaysia.
- Develop models for top-down cracking in asphalt pavements when the pavements relevant condition data is collected and made available.
- Use the LTPP database to develop enhanced condition equations for concrete pavements.

b) Extended database of the 3D-FE modeling of uncracked asphalt pavements

- Create a full factorial design of uncracked pavements by including medium level of thickness and modulus values for asphalt, base, subbase, and subgrade layers. Conduct additional 3D-FE simulations for extending 3D-FE structural response database.
- Develop structural response prediction equations using the 3D-FE response database.

c) Improvement of the 3D-FE modeling of cracked asphalt pavements

- Conduct 3D-FE simulations for the unfinished combinations of the full factorial design as conducted for the uncracked pavement models. However, the full factorial design is repeated four times depending on the crack locations (top one-third, middle one-third, bottom one-third, and full depth cracked). Once the simulations are completed, further research is recommended to analyze structural response of the asphalt highway pavement subjected to truck loads on the simulated longitudinal crack. This will help to investigate the effects of the crack depths on surface deflections and other structural responses of stresses and strains at various layer depths and on top of the subgrade.

LIST OF REFERENCES

[1] NAPA. 2019. Engineering Overview. National Asphalt Pavement Association (NAPA), http://www.asphaltpavement.org/index.php?option=com_content&view=article&id=14& Itemid=33 Accessed on April 17, 2019.

[2] USDOT. 2015. US Department of Transportation (USDOT), Bureau of Transportation Statistics. Table 1-36: Roadway Vehicle-Miles Traveled (VMT) and VMT per Lane-Mile by Functional Class (a), http://www.rita.dot.gov/bts/sites/rita.dot.gov.bts/files/publications/ national _transportation_statistics/html/table_01_36.html Accessed September 8, 2015.

[3] CBO. 2011. Economic and Budget Issue Brief. Spending and Funding for Highways. Congressional Budget Office (CBO), https://www.cbo.gov/sites/default/files/112th-congress-2011-2012/reports/01-19-highwayspendingbrief.pdf Accessed January 15, 2011.

[4] Pines Salomon Injury Laws, Top 25 Causes of Car Accidents. https://seriousaccidents. com/legal-advice/top-causes-of-car-accidents/ Accessed February 25, 2019.

[5] IIHS & HLDI. Motorcycles and ATCs. Insurance Institute for Highway Safety (IIHS) & Highway Loss Data Institute (HLDI), https://www.iihs.org/iihs/topics/t/motorcycles/fatalityfacts /motorcycles Accessed November 11, 2015.

[6] U.S Census Bureau. 2019. Population. https://www.census.gov/topics/population.html?

cssp=SERP Accessed on April 17, 2019.

[7] NHTSA. 2015. Occupant Protection. National Highway Traffic Safety Administration (NHTSA), https://one.nhtsa.gov/Driving-Safety/Occupant-Protection Accessed on November 11, 2015.

[8] Statistisches Bundesamt, Wiesbaden 2015. https://www.destatis.de/EN/Homepage.html Accessed on November 11, 2015.

[9] USDOT. 2017. Bureau of Transportation Statistics. Table 1-69: Annual Person-Hours of Highway Traffic Delay Per Auto Commuter. US Department of Transportation (USDOT) https://www.bts.gov/archive/publications/national_transportation_statistics/table_01_69 Accessed on April 17, 2019.

[10] USDOT. 2015. Bureau of Transportation Statistics. Annual Highway Congestion Cost. US Department of Transportation (USDOT). https://www.bts.gov/content/annual-highway-congestion-cost Accessed on November 11, 2015.

[11] FHWA. 2012. Long-Term Pavement Performance (LTPP). Federal Highway Administration (FHWA). LTPP Standard Data Release 26.0. DVD. January 2012.

[12] Mohamed Jaafar, Z. F., Uddin. W., and Ahlan, M. 2015. Modeling of Pavement Roughness Performance Using the LTPP Database for Southern Region in the U.S. Proceedings

of the 6th International Conference Bituminous Mixtures and Pavements, Thessaloniki, Greece, 2015, pp. 714-722.

[13] AASHTO. 2008. Mechanistic-Empirical Pavement Design Guide, Interim Edition: A Manual of Practice. American Association of State and Highway Transportation Officials (AASHTO), Washington, D.C, 2008.

[14] TRB. 2015. NCHRP 01-37A. Development of 2002 Guide for the Design of New and Rehabilitated Pavement Structures: Phase II. Transportation Research Board (TRB). http://apps.trb.org/cmsfeed/TRBNetProjectDisplay.asp?ProjectID=218 Accessed September 9, 2015.

[15] Uddin, W., Hudson, W.R., Haas, R. 2013. Pavement Design or Pavement Management? Good Design is Not Enough". Proceedings of the First International Journal of Pavement (IJP) Conference, Sao Paulo, Brazil, December 9-10, 2013.

[16] AASHTO. 2015. American Association of State Highway and Transportation Officials (AASHTO). Committee Correspondence. http://onlinepubs.trb.org/onlinepubs/archive/mepdg /AASHTO_memorandum.pdf Accessed September 9, 2015.

[17] Ahammed, M.A., Kass, S., and Hilderman, S. Implementing the AASHTOWare ME Design Guide: Manitoba Issues and Proposed Approaches. Paper Presented at the Pavement

Design Innovations to Implementation Session, Conference of the Transport Association of Canada, Winnipeg, Manitoba, 2013.

[18] Uddin, W. 2015. CE585-Highway Pavements. Course Lecture Notebook, University of Mississippi, September 2015.

[19] Uddin, W. 2013. A Synthesis Study of Noncontact Nondestructive Evaluation of Top-down Cracking in Asphalt Pavements. Final Report FHWA/MS-DOT-RD-13-255, Sponsored Research Study SS 255, Center for Advanced Infrastructure Technology Report UM-CAIT/2013-01, The University of Mississippi, for the Mississippi Department of Transportation, December 2013.

[20] Uddin, W. An Overview of GPR Applications for Evaluation of Pavement Thickness and Cracking. The 15th International Conference on Ground Penetration Radar (GPR), June 30, 2014 until July 4, 2014, pp. 925-930.

[21] Uddin, W., Noppakunwijai, P., and Chung, T. Performance Evaluation of Jointed Concrete Pavement Using Three-Dimensional Finite-Element Dynamic Analysis. Presented at 76th TRB Annual Meeting, January 12-16, 1997, Washington, D.C.

[22] Paterson, W. D. 1994. Proposal of Universal Cracking Indicator for Pavements. In Transportation Research Record No. 1455, TRB, National Research Council, Washington, D.C, 1994, pp. 69-76.

[23] Matsuno, S. and T. Nishizawa. Mechanism of Longitudinal Surface Cracking in Asphalt Pavement. Proceedings of the 7th International Conference on Asphalt Pavements. The University of Nottingham. Vol. 2, 1992, pp. 277–291.

[24] Taniguchi, S., I. Nishizaki, and A. Moriyoshi. Three Dimension Diagnosis of Pavement Damage using CT Scanner. Proceedings of the MAIREPAVE6 Conference, Torino, Italy, 2009, pp. 1-10.

[25] ARA Inc. 2004. NCHRP 1-37A: Guide for Mechanistic Empirical Design of New and Rehabilitated Pavement Structure. Final Report: Part 1 (Introduction) and Part 2 (Design Inputs), Prepared for NCHRP, TRB, National Research Council, 2004.

[26] Wambura, J.H.G., Maina, J., and H.R. Smith. 1999. Kenya Bituminous Materials Study. In Transportation Research Record 1681, TRB, National Research Council, Washington, D.C, 1999, pp 129-137.

[27] Rolt, J. 2000. Top-Down Cracking: Myth or Reality. Report GR45 6AU, Department for International Development (DFID), TRL Limited, Crowthore, Berkshire, United Kingdom, 2000, pp. 1-17.

[28] Dauzats, M. and R. Linder. 1982. A Method for the Evaluation of The Structural Condition of Pavements with Thick Bituminous Road Bases. Proceedings of the Fifth

International Conference on The Structural Design of Asphalt Pavements, The Delft University of Technology, The Netherlands, August 23 –August 26, 1982, Volume 1, pp. 387-409.

[29] Gerritsen, A.H., C.A.P.M. van Gurp, J.P.J. van der Heide, A.A.A. Molenaar, and A.C.Pronk. 1987. Prediction and Prevention of Surface Cracking in Asphaltic Pavements. Proceedings of the Sixth International Conference Structural Design of Asphalt Pavements, July 13-14, 1987, The University of Michigan Ann Arbor, Michigan, USA, Volume 1, pp. 378-391.

[30] Hugo, F. P.J. Strauss, G.P. Marais, and T.W. Kennedy. 1982. Four Asphalt Pavement Case Studies Using a Mechanistic Approach. Proceedings of the Fifth International Conference on The Structural Design of Asphalt Pavements, The Delft University of Technology, The Netherlands, August 23 - 26, 1982, Volume 1, pp. 275-284.

[31] Craus, J., A. Chen, J. Sousa, and C. Monismith. 1994. Development of Failure Curves and Investigation of Asphalt Concrete Pavement Cracking from Super-Overloaded Vehicles. Division of New Technology, Materials, and Research, California Department of Transportation, Sacramento, California, 1994.

[32] Myers, L. A., R. Roque, and B. Birgisson. 2001. Propagation Mechanisms for Surface-Initiated Longitudinal Wheelpath Cracks. In Transportation Research Record No. 1778, TRB, National Research Council, Washington, D.C., 2001, pp. 113–122.

[33] Freitas, E., P. Pereira, L. Picado-Santos, and A.T. Papagiannakis. 2005. Effect of Construction Quality, Temperature and Rutting on Initiation of Top-Down Cracking. In Transportation Research Record No. 1929, TRB, National Research Council, Washington, DC, 2005, pp. 174-182.

[34] Uhlmeyer, J. S., K. Willoughby, L. M. Pierce, and J. P. Mahoney. 2000. Top-Down Cracking in Washington State Asphalt Concrete Wearing Courses. Issues in Pavement Design and Rehabilitation. In Transportation Research Record No 1730, TRB, National Research Council, Washington, D.C., 2000, pp. 110–116.

[35] Svasdisant, T., M. G. Schorsch, Y. Baladi, and S. Pinyosunun. 2002. Mechanistic Analysis of Top-Down Cracking in Asphalt Pavements. In Transportation Research Record No. 1809, TRB, National Research Council, Washington, D.C., 2002, pp. 126–136.

[36] Pellinen, T.K., G. Rowe, and K. Boswas. 2004. Evaluation of Surface (Top-Down) Longitudinal Wheel Path Cracking. Final Report, Joint Transportation Research Program, Purdue University, Indiana, 2004.

[37] Harmelink, D., S. Shuler, and T. Aschenbrener. 2008. Top-Down Cracking in Asphalt Pavement: Causes, Effects, and Cures. Journal of Transportation Engineering, Vol. 134, No. 1, ASCE, January 2008, pp. 1-6.

[38] Dauzat, M. and Rampal, A. 1987. Mechanism of Surface Cracking in Wearing Courses. Proceedings of the Sixth International Conference Structural Design of Asphalt Pavements, July 13-14, 1987, The University of Michigan Ann Arbor, Michigan, USA, pp. 232-247.

[39] Hugo, F., and T.W. Kennedy. 1985. Surface Cracking of Asphalt Mixtures in Southern Africa. Proceedings, Association of Asphalt Paving Technologists, Vol. 54, 1985, pp 454-501.

[40] Myers, L.A., R. Roque, and B.E. Ruth. 1998. Mechanisms of Surface-Initiated Longitudinal Wheel Path Cracks in High-Type Bituminous Pavements. Journal of the Association of Asphalt Paving Technologists, Volume 67, 1998, pp. 401-432.

[41] Svasdisant, T., M. Schorsch, G.Y. Baladi, and S. Pinyosunun. 2000. Mechanistic Analysis of Top-Down Cracks in Asphalt Pavements. In Transportation Research Record No. 1809, TRB, National Research Council, Washington, D.C., 2000, pp. 126-136.

[42] Al-Qadi, Imad L. and Hao Wang. 2009. Evaluation of Pavement Damage Due to New Tire Design. Report FHWA-ICT-09-048, Illinois Center for Transportation, Department of Civil and Environmental Engineering, the University of Illinois at Urbana-Champaign, Urbana, Il., May 2009

[43] Park, H.J, Kim, Y.R. 2013. Investigation into the Top-Down Cracking of Asphalt Pavements in North Carolina. Transportation Research Record, No. 2368, TRB, National Research Council, Washington, D.C., 2013, pp 45–55.

[44] Robert L. L., Xue, L., Meng, L., Yu, C., Sheng, H., and Fan, G. A. 2018. Mechanical Empirical Model for Top Down Cracking of Asphalt Pavement Layers. NCHRP Web-Only Document 257, Contractor's Final Report for NCHRP Project 1-52, March 2018.

[45] Schorsch, M., Chnag, C-M., Baladi, G.Y. 2003. Effects of Segregation on the Initiation and Propagation of Top-Down Cracks. Paper presented in 82nd Transportation Research Board Annual Meeting, January 12-16, 2003.

[46] Freitas, E., P. Pereira, and L. Picado-Santos. 2003. Assessment of Top-Down Cracking Causes in Asphalt Pavements. Presented at the 3rd International Symposium on Maintenance and Rehabilitation of Pavements and Technological Control, Guimarães, Portugal, 2003, pp. 555–564.

[47] FHWA. 2014. About Long-Term Pavement Performance Program. LTPP Brochure. Federal Highway Administration (FHWA), Research and Technology, December 2014 https://www.fhwa.dot.gov/publications/research/infrastructure/pavements/ltpp/15018/index.cfm Accessed April 15, 2019.

[48] FHWA. 2015. About the Long-Term Pavement Performance Program. Part 1. Building and managing The LTPP Program. Federal Highway Administration (FHWA), https://www.fhwa.dot.gov/publications/research/infrastructure/pavements/ltpp/15049/003.cfm Accessed April 15, 2019.

[49] FHWA. 2015. (Federal Highway Administration), Evaluation of Long-Term Pavement Performance (LTPP) Climatic Data Use in Mechanistic-Empirical Pavement Design Guide (MEPDG) Calibration and Other Pavement Analysis, Chapter 7: Recommendations. https://www.fhwa.dot.gov/publications/research/infrastructure/pavements/ltpp/15019/008.cfm Accessed 17 February 2019.

[50] Heitzman, M., Timm, D., Takle, D., Herzmann, D., and Truax, D.D. 2011. Developing MEPDG Climate Data Input Files for Mississippi. Final Report FHWA/MS-DOT-RD-11-232, Research Study 232 for Mississippi Department of Transportation, June 2011.

[51] USDOE. 2019. Climate Zone Map. U.S. Department of Energy (USDOE). Office of Energy Efficiency and Renewable Energy. Washington, D.C. Climate Zones Map. https://www.hydrogen.energy.gov/images/h2a_climate_zone_map.jpg Accessed April 15, 2019.

[52] Uddin, W. 2019. Disaster Resilience Management of Infrastructure Systems: Computational Modeling and Geospatial Technologies. Taylor & Francis, CRC Press, 1st Edition. 2019.

[53] USDOE. 2019. About Climate Zones. U.S. Department of Energy (USDOE). Office of Energy Efficiency and Renewable Energy, Forrestal Building, Washington, D.C. https://www.energy.gov/eere/buildings/climate-zones Accessed April 15, 2019.

[54] AASHO. 1962. The AASHO Road Test: Report 5-Pavement Research. HRB Special Report 61-E, Highway Research Board, National Academy of Science, Washington, DC.

[55] Uddin, W. 2009. Highway Pavement Course Lecture Notebook (CE 585). University of Mississippi, Carrier Hall 203B, Oxford, Mississippi, USA. 2009-2014.

[56] ENR. 2006. About Industry's Largest R&D Effort Founded Interstate Construction, AASHO Road Test. Engineering News Record (ENR). March 13, 2006. http://www.eng.utoledo.edu/~nkissoff/pdf/CET-3120/AASHO%20Road%20Test.pdf Accessed May 2, 2019.

[57] Uddin, W. 2015. Appraisal of Mechanistic-Empirical Pavement Design Guide for Highways being Implemented in the United States and Complementary Needs for Pavement Asset Management. Proceedings of the 6th ICONFBMP, International Conference Bituminous Mixtures and Pavements, Thessaloniki, Greece, 10-12 June 2015, pp. 195-202.

[58] MDOT. 2017. Michigan DOT User Guide for Mechanistic-Empirical Pavement Design. https://www.michigan.gov/documents/mdot/MDOT_Mechanistic_Empirical_Pavement_Design_User_Guide_483676_7.pdf Accessed May 2, 2019.

[59] NCHRP. 2004. Mechanistic-Empirical Pavement Design Guide. NHCRP Project 1-37A, National Cooperative Highway Research Program (NCHRP), Transportation Research Board, Washington, DC. http://www.trb.org/mepdg/guide.htm Accessed May 2, 2019.

[60] AASHTO. 2019. About AASHTO Pavement ME Design Software. American Association of State Highway and Transportation Officials (AASHTO), Washington, DC. https://www.aashtoware.org/products/pavement/pavement-overview/ Accessed May 2, 2019.

[61] AASHTO. 1993. AASHTO Design Guide for Pavement Structures. American Association of the State Highway and Transportation Officials, Washington, D.C., 1993.

[62] Sayers, Michael W. Gillespie, Thomas D., Queiroz, Cesar A.V. 1986. The International Road Roughness Experiment (IRRE)-Establishing correlation and a calibration standard for measurements (English). World Bank Technical Paper No. WTP 45. Washington, DC. The World Bank. http://documents.worldbank.org/curated/en/326081468740204115/The-International-Road-Roughness-Experiment-IRRE-establishing-correlation-and-a-calibration-standard-for-measurements Accessed April 15, 2019.

[63] Uddin, W., Hudson, W.R., and Haas, R. 2013. Public Infrastructure Asset Management, Second Edition, McGraw-Hill, ISBN 0071820116 ISBN-13: 978-0071820110, 2013, 487 pages.

[64] Plati, C. 2011. Development of a Method to Establish Criteria for Pavement Roughness Evaluation. IJP – International Journal of Pavements, Vol. 10, No. 1-2-3, January-May-September 2011, pp. 95-105.

[65] FHWA. 2017. About National Highway System Daily Travel by Measured Pavement Roughness. Federal Highway Administration (FHWA), September 18, 2017.

https://www.fhwa.dot.gov/policyinformation/statistics/2016/hm47a.cfm Accessed April 15, 2019.

[66] AASHTO. Mechanistic-Empirical Pavement Design Guide, Interim Edition: A Manual of Practice. American Association of State and Highway Transportation Officials (AASHTO), Washington, D.C., 2008.

[67] Paterson, W. D. O. 1987. Road deterioration and maintenance effects: Models for planning and management. John Hopkins University Press for World Bank. Baltimore, MD.

[68] Paterson, W.D.O. 1989. A transferable causal model for predicting roughness progression in flexible pavements: 70-84. In Transportation Research Record 1215, TRB National Research Council, Washington, DC.

[69] Cardoso, S.H. & Macron, A.F. 1998. Pavement performance models for the State of Santa Carina, Brazil. In 4th International Conference on Managing Pavement: 568-582. Durban, South Africa.

[70] Queiroz, C.A.V. 1981. Performance prediction models for pavement management in Brazil. Ph.D. Dissertation. The University of Texas at Austin.

[71] Soncim, S. P. and Fernandes, J. L. Roughness Performance Model for Surface Treated Asphalt Highways. IJP – International Journal of Pavements, Vol. 11, No. 1-2-3, January-May-September 2012, pp. 93-102.

[72] Meegoda, J., and Gao, S. Roughness Progression Model for Asphalt Pavements using Long-Term Pavement Performance Data. Journal of Transportation Engineering, Vol. 140, No. 8, August 2014.

[73] Madanat, S., Nakat, Z., Farshidi, F., Sathaye, N., and Harvey, J. Development of Empirical Mechanistic Pavement Performance Models using Data from the Washington State PMS Database. Research Report. 2005, UCPRC-RR-2005-05.

[74] Rahim, A. M., Fiegel, G., Ghuzlan, K., and Khumann, D. Evaluation of International Roughness Index for Asphalt Overlays Placed Over Cracked and Seated Concrete Pavements. International Journal of Pavement Engineering, Vol. 10, No. 3, 2009, pp. 201-207.

[75] Choi, Jae-ho., Teresa, M. Adam., Hussain, U. Bahia. Pavement Roughness Modeling Using Back-Propagation Neural Networks. Journal of Computer-Aided Civil and Infrastructure Engineering, Vol. 19, No. 4, 2004, pp. 295-303.

[76] Attoh-Okine, N. O. Predicting Roughness Progression in Flexible Pavements using Artificial Neural Networks. Proceedings of the 3rd International Conference on Managing Pavements, San Antonio, Texas, Vol. 1, 1994, pp. 55-62.

[77] Kargah-Ostadi, N., Stoffels, S., and Tabatabaee, N. Network-Level Pavement Roughness Prediction Model for Rehabilitation Recommendations. In Transportation Research Record No. 2155, TRB, 2010, pp. 124-133.

[78] Najjar Y. 1999. Quick Manual for the Use of ANN program TRSEQ1. Department of Civil Engineering, Kansas State University, Manhattan, Kansas, USA.

[79] Mohamed Jaafar, Z. F., and Uddin. W. Modeling of Asphalt Pavement Rutting for LTPP Southern Region using Multiple Linear Regression Method. Proceedings of the 8th International Conference on Maintenance and Rehabilitation of Pavements. Thessaloniki, Greece, 2015, DOI:10.3850/978-981-11-0449-7-178-CD.

[80] FHWA. 2006. About Long-Term Pavement Performance (LTPP) Data Analysis Support: National Pooled Fund Study TPF-5 (013). Federal Highway administration (FHWA) https://www.fhwa.dot.gov/publications/research/infrastructure/pavements/ltpp/06121/index.cfm Accessed April 17, 2019.

[81] NCHRP 2004. Mechanistic-Empirical Pavement Design Guide. NCHRP Report Project 1-37A, National Cooperative Highway Research Program (NCHRP), Transportation Research Board, Washington, DC, https://apps.trb.org/cmsfeed/TRBNetProjectDisplay.asp?ProjectID=218 Accessed March 24, 2019.

[82] IBM. 2019. About IBM SPSS software. https://www.ibm.com/analytics/spss-statistics-software Accessed April 17, 2019.

[83] NCHRP. 2004. Guide for Mechanistic-Empirical Design of New and Rehabilitated Pavement Structures, Final Document - AppendixII-1: Calibration of Fatigue Cracking Models for Flexible Pavements, National Cooperative Highway Research Program (NCHRP), Transportation Research Board, National Research Council, Washington, D.C. http://onlinepubs.trb.org/onlinepubs/archive/mepdg/2appendices_II.pdf Accesses May 10, 2019.

[84] NCHRP. 2004. Guide for Mechanistic-Empirical Design of New and Rehabilitated Pavement Structures, Final Report – Part 3: Design Analysis, Chapter 3 – Design of New and Reconstructed Flexible Pavements, National Cooperative Highway Research Program (NCHRP), Transportation Research Board, National Research Council, Washington, D.C. http://onlinepubs.trb.org/onlinepubs/archive/mepdg/Part3_Chapter3_FlexibleDesign.pdf Accessed May 10, 2019.

[85] Uddin, W. 1984. A Structural Evaluation Methodology for Pavements Based on Dynamic Deflections, 1984, Ph.D. Dissertation.

[86] Paterson, W. D. 1994. Proposal of Universal Cracking Indicator for Pavements. In Transportation Research Record Issue Number 1455, Transportation Research Board, ISSN: 0361-1981, pp 69-75, National Academy of Science, Washington, D.C.

[87] Haas, R., Hudson, W.R., and Zaniewski, J. 1994. Modern Pavement Management. Krieger Publishing Company, Florida. 1994. 583p, ISBN 0-89464-588-9

[88] Huang, Y.H. 2004. Pavement Analysis and Design (Second Edition). 2004. Pearson Prentice Hall, New Jersey.775p, ISBN 0-13-142473-4

[89] Ullidtz, P. 1987. Pavement Analysis. Development in Civil Engineering, Vol. 19. ISBN 0-444-42817-8, 318p, 1987.

[90] Uddin, W. and Ricalde, L. 2000. Implementation of a User material Routine in 3D-FE Codes for Viscoelastic Modeling and Simulation of Highway and Airport Pavements. LS-DYNA User Conference, 2000, Session 6, pp 12-24

[91] FHWA. 2009. Using Falling Weight Deflectometer Data with Mechanistic-Empirical Design and Analysis, Vol. 1, Final Report, March 2017, FHWA-HRT-16-009, https://www.fhwa.dot.gov/publications/research/infrastructure/pavements/16009/002.cfm Accessed February 2019.

[92] FHWA. 1993. National Research Council. Strategic Highway Research Program (SHRP-P-651). Layer Moduli Backcalculation Procedure: Software Selection, October 1993, http://onlinepubs.trb.org/onlinepubs/shrp/SHRP-P-651.pdf Accessed on October 5, 2015.

[93] Uddin, W. and Garza, S.G. 2003. 3D-FE Simulation and Dynamic Response Analysis of FWD Impact Test on Asphalt Pavements. Proceedings of International Conference on Highway Pavement Data, Analysis and Mechanistic Design Applications, Columbus, OH, USA, September 8-10, 2003, Vol. 1, pp. 163-174.

[94] FHWA. 2006. The Long-Term Pavement Performance (LTPP) Program - Manual for Falling Weight Deflectometer Measurement Version 4, December 2006, http://www.fhwa.dot.gov/publications/research/infrastructure/pavements/ltpp/06132/ Assessed on September 15, 2015.

[95] Stubstad, R.N., Y.J. Jiang, and E.O. Lukanen. 2006. Guidelines for Review and Evaluation of Backcalculation Results. Project Report - FHWA-HRT-05-152. McLean, VA, 2006.

[96] M. Ameri, N. Yavari and T. Scullion. 2009. Comparison of Static and Dynamic Backcalculation of Flexible Pavement Layers Modulus Using Four Software Programs. Asian Journal of Applied Sciences, 2009, Vol. 2, pp. 197-210.

[97] U.S. Army Corps of Engineers. 2010. Pavement-Transportation Computer Assisted Structural Engineering (PCASE) Version 2.09. User Manual, September 2010.

[98] Priddy, Lucy P. 2015. Evaluation of Precast Portland Cement Concrete for Airfield Pavement Repairs." Engineer Research and Development Center (ERDC), U.S. Army Corps of Engineers, May 2015.

[99] Priddy, Lucy P., Bianchini, A., Gonzalez, Carlos R; Dossett, Cayce S. 2015. Evaluation of Procedures for Backcalculation of Airfield Pavement Moduli. Engineer Research and Development Center (ERDC), U.S. Army Corps of Engineers, August 2015.

[100] Washington State Department of Transportation (WSDOT). 2015. EVERSERIES© USER'S GUIDE Pavement Analysis Computer Software and Case Studies, August 2005, 2015.

[101] Uddin, W. 1998. Application of 3D-Finite Element Dynamic Analysis for Pavement Evaluation. Proceedings of the First National Symposium on 3D Finite Element Modeling for Pavement Analysis and Design, Charleston, West Virginia, Nov. 1998, (ISBN 0-937058-49-1), pp. 95-109.

[102] Uddin, W., S. Garza, and K. Boriboonsomsin. 2003. A 3D-FE Simulation Study of the Effects of Nonlinear Material Properties on Pavement Structural Response Analysis and Design. Proceedings of MAIREPAV03 - Third International Symposium on Maintenance and Rehabilitation of Pavements and Technological Control, (ISBN 972-8692, Universidade do Minho Publishers, Editors P. Pereira, and F. Branco), Guimarães, Portugal, July 7-10, 2003, pp. 99-108.

[103] Uddin, W. 1998. Application of Finite Element Dynamic Analysis for In Situ Material Characterization of Pavement Systems. Proceedings of the Fifth International Conference on the Bearing Capacity of Roads and Airfields, Trondheim, Norway, July 1998, Vol. 1, pp. 429-438.

[104] Boriboonsonsin, K. and H.G. Momm. 2002. Evaluation of Asphalt Pavement Damage Models Using LTPP Data in Northern Mississippi. International Contest on LTPP Data Analysis 3rd Year, 2001 - 2002.

[105] Ali, Galal A., Krizek, Raymond J., and Osterberg, Jorj. O. 1970. Influence of Poisson's Ratio on the Surface Deflection of Layered Systems. Highway Research Record No. 337, 1970, pp. 1-10.

[106] Federal Aviation Administration (FAA). 2011. Use of Nondestructive Testing in The Evaluation of Airport Pavements. Advisory Circular No. 150/5370-11B, September 2011, pp. 1-80.

[107] Mahoney, J. P., Winters, B. C., Jackson, N. C., and Pierce, L. M. 1993. Some Observations about Backcalculation and Use of a Stiff Layer Condition. In Transportation Research Board No. 1384, TRB, Washington D.C., 1993.

[108] George, K.P. and W. Uddin. Subgrade Characterization Study for Highway Pavement Design. Final Report - Sponsored Research Study SS 131, The University of Mississippi, for the Mississippi Department of Transportation, Report No. FHWA/MS- DOT-RD-00-131, December 2000.

[109] Uddin, W., A.H. Meyer, and W.R. Hudson. 1986. Rigid Bottom Considerations for Nondestructive Evaluation of Pavements. Transportation Research Record No. 1070, TRB, Washington, D.C., 1986, pp. 21-29.

[110] Uddin, W. and S. Garza. 2010. 3D-FE Simulation Study of Structural Response Analysis for Pavement-Subgrade Systems Subjected to Dynamic Loads. Trends in Engineering Mechanics Special Publication (TEMSP) 1, Pavements and Materials: Testing and Modeling in Multiple Length Scales, Editors: R.A. Tarefder, Yong-Park Kim, Zhanping, and Linbing Wang, ISBN 978-0-7844-1192-2, August 8-11, 2010, pp. 170-181. Also included in ASCE Conference Proceedings 385, 15 (2010).

[111] Garza, S. G. 2003. Integration of Pavement Nondestructive Evaluation, Finite Element Simulation, and Air Quality Modeling for Enhanced Transportation Corridor Assessment and Design. Ph.D. Thesis, Volume 1, May 2003.

[112] MDOT. 2013. Implementation of MEPDG in Mississippi-Draft Final Mississippi DOT Pavement ME Design User Input Guide. Report FHWA/MS-DOT-RD-013-170 Mississippi Department of Transportation, Jackson, Mississippi.

[113] Uddin, W. 1999. Improved Asphalt Thickness Design Procedures for New and Reconstructed Highway Pavements. Report FHWA/MS-DOT-RD-99-122, Final Report, State Study SS 122, Mississippi Department of Transportation.

[114] Uddin, W., Barros, R., and Mohamed Jaafar, Z. F. 2019. Sensitivity Analysis of Mechanistic-Empirical Pavement Structural Design Methods Considering Climate Impacts on Layer Modulus Values. Proceedings of the 7th International Conference Bituminous Mixtures and Pavements, Thessaloniki, Greece, 12-14 June 2019.

[115] Wang, P., Huang, X.M., Li, Q.F., and Yang, Z.T. 2008. Finite Element Analysis of Top-Down Cracking in Semi-Rigid Pavement Structure. Proceedings in 6th RILEM International Conference on Cracking in Pavements, Chicago, USA, 16-18 June, 2008, pp 327-331.

[116] Hajj, E., Thushanthan, P., Sebaaly, E.P. and Siddharthan, R.V. 2012. Influence of Tire-Pavement Stress Distribution, Shape, and Braking on Performance Predictions for Asphalt Pavement. Transportation Research Record: Journal of the Transportation Research Board. 2306. 73-85. 10.3141/2306-09.

[117] Connor, W.S. and Zelen, M. 1959. Fractional Factorial Experiment Designs for Factors at Three Levels. U.S. Department of Commerce, National Bureau of Standards, Applied Mathematics Series 54.

[118] James W. Maina, Yoshiaki Ozawa & Kunihito Matsui. 2012. Linear Eastic Analysis of Pavement Structure Under Non-Circular Loading, Road Materials and Pavement Design, 13:3, 403-421, DOI: 10.1080/14680629.2012.705419

[119] Nanagiri, Y. V. 2001. Pavement-Subgrade Material Characterization and Advanced Computer Simulations. Master Thesis. May 2001. University of Mississippi, Oxford, Mississippi, USA.

[120] MDOT. 2019. Mississippi Department of Transportation. County Pavement Condition Rating (PCR) History by Year. Jackson, Mississippi. https://path.mdot.ms.gov/pavement_condition Accessed March 2, 2019.

[121] Uddin, W. and Pan. Z. 1995. Finite-Element Analysis of Flexible Pavements with Discontinuities. Proceedings, ASCE Transportation Congress, American Society of Civil Engineers, San Diego, September 1995, Vol. 1, pp. 410-423.

[122] Nguyen, V. P. 2014. An Open Source Program to Generate Zero-Thickness Cohesive Interface Elements. Advance in Engineering Software. Volume 74, August 2014, pp. 27-39.

[123] Carol, I., Idiart, A., and Lopez, C. M. 2015. Advances in Meso-mechanical Analysis of Concrete Specimen using Zero-thickness Interface Elements. http://framcos.org/FraMCoS-6/194.pdf Accessed on November 15, 2015.

[124] Dias-da-Costa, D., Alfaiate, J., Sluys, L. J., and Julio, E. 2010. A Comparative Study on the Modeling of Discontinuous Fracture by Means of Enriched Nodal and Element Techniques and Interface Element. International Journal of Fracture, Volume 161, 2010, pp. 97-119.

[125] Muflahi, S. A., Mohamed, G. and Hallet, S. R. 2014. Investigation of Delamination Capabilities for Thin Composite Structure in LS-DYNA. 13th International LS-DYNA Users Conference, June 2014, Detroit, USA.

[126] Brunnet, S., Gilbert, M., Molyneaux, T., Beattie, G., and Hobbs, B. 2007. The Performance of Unreinforced Masonry Walls Subjected to Low Velocity Impacts: Finite Element Analysis. International Journal of Impact Engineering. Volume 34, Issue 8, August 2007, pp. 1433-1450.

[127] Uddin, W., D. Zhang, and F. Fernandez. 1994. Finite Element Simulation of Pavement Discontinuities and Dynamic Load Response. Transportation Research Record 1448, Journal of Transportation Research Board, Washington D.C., 1994, pp. 100-106.

[128] Uddin, W., R.M. Hackett, A. Joseph, Z. Pan, and A.B. Crawley. 1995. Three-Dimensional Finite-Element Analysis of Jointed Concrete Pavement Having Discontinuities. Transportation Research Record 1482, Journal of Transportation Research Board, Washington, D.C., 1995, pp. 26-32.

[129] LS-DYNA Support. 2019. Strain Measures of Solid Elements. Livermore Software Technology Corporation. https://www.dynasupport.com/howtos/element/strain-measures-of-solid-elements Accessed March 4, 2019.

[130] Livermore Software Technology Corporation (LSTC), LS-DYNA Keyword User's Manual, Volume 1, LS-DYNA R8.0 (r:6319), April 23, 2015.

[131] GASB. 2000. About Guide to Implementation of GASB Statement 34 on Basic Financial Statements and Management's Discussion and Analysis for State and Local Governments: Questions and Answers. Governmental Accounting Standards Board (GASB) of the Financial Accounting Foundation, Norwalk, CT. Library of Congress Card Number: 00-132271, ISBN 0-910065-84-5.

LIST OF APPENDICES

Appendix A: Prediction Model Equation for Condition Deterioration Progression

Model Summary[b]

Model	R	R Square	Adjusted R Square	Std. Error of the Estimate
1	.633[a]	.401	.399	.48694

a. Predictors: (Constant), IRI_D, CND, Air_Temperature, Total_Monthly_Precipitation, Initial_IRI_Per_Measurement_Year, Cumulative_Traffic, SN, Reg_D, Age

b. Dependent Variable: IRI_Per_Measurement_Year_Yi

Figure A1. IRI Roughness: Model summary

Coefficients[a]

Model		Unstandardized Coefficients		Standardized Coefficients	t	Sig.
		B	Std. Error	Beta		
1	(Constant)	.642	.053		12.207	.000
	Initial_IRI_Per_Measurement_Year	.726	.020	.581	36.331	.000
	Age	.006	.001	.086	4.552	.000
	SN	-.045	.007	-.114	-6.937	.000
	Cumulative_Traffic	-1.542E-8	.000	-.102	-5.970	.000
	Air_Temperature	.002	.001	.025	1.559	.119
	Total_Monthly_Precipitation	.000	.000	-.042	-2.668	.008
	Reg_D	.080	.022	.063	3.733	.000
	CND	-.105	.023	-.083	-4.582	.000
	IRI_D	-.061	.019	-.049	-3.212	.001

a. Dependent Variable: IRI_Per_Measurement_Year_Yi

Figure A2. IRI Roughness: Model coefficients

Model Summary[b]

Model	R	R Square	Adjusted R Square	Std. Error of the Estimate
1	.920[a]	.847	.836	.11315

a. Predictors: (Constant), Asphalt_Thickness_T1, Age, Subbase_Modulus_E3, Log10_Initial_Rut_Depth_Plus_0.5, CND, Air_Temperature, Subgrade_Modulus_E4, Cumu_ESALs, Base_D, Reg_D, Total_Thickness_Tt, Asphalt_Modulus_E1, SN, Base_Modulus_E2

b. Dependent Variable: Log10_Avg_Rut_Depth_Plus_0.5

Figure A3. Rutting: Model summary

Coefficients[a]

Model		Unstandardized Coefficients		Standardized Coefficients	t	Sig.
		B	Std. Error	Beta		
1	(Constant)	.058	.075		.775	.439
	Age	.000	.001	-.011	-.362	.718
	Cumu_ESALs	2.962E-9	.000	.010	.304	.761
	SN	.021	.011	.116	1.966	.051
	Asphalt_Modulus_E1	2.562E-8	.000	.037	.666	.506
	Base_Modulus_E2	-1.356E-7	.000	-.106	-1.569	.118
	Subbase_Modulus_E3	-1.171E-7	.000	-.011	-.296	.767
	Subgrade_Modulus_E4	2.348E-7	.000	.008	.219	.827
	Air_Temperature	.000	.001	-.004	-.118	.906
	Reg_D	.010	.025	.013	.380	.705
	CND	.006	.020	.010	.318	.751
	Base_D	-.041	.036	-.071	-1.121	.264
	Total_Thickness_Tt	.000	.002	.006	.134	.893
	Log10_Initial_Rut_Depth_Plus_0.5	.954	.033	.897	28.876	.000
	Asphalt_Thickness_T1	-.011	.005	-.127	-2.036	.043

a. Dependent Variable: Log10_Avg_Rut_Depth_Plus_0.5

Figure A4. Rutting: Model coefficients

Model Summary[b]

Model	R	R Square	Adjusted R Square	Std. Error of the Estimate
1	.577[a]	.333	.327	.54826

a. Predictors: (Constant), CND, Log10_Initial_UCI_Combined_All_Plus_0.5, Air_Temperature, Subbase_Modulus_E3, Precipitation, T1_X_E1, Asphalt_Thicknesses, Reg_D, Cumulative_ESALs, Total_Thicknesses, Age_Survey_Date, Base_Modulus_E2, Subgrade_Modulus_E4, Traffic_X_Log10_Initial_Yc_Plus_0.5, SN, Temperature_X_E1, Temperature_X_Precipitation, Age_X_Log10_Initial_Yc_Plus_0.5, TT_X_CND, Asphalt_Modulus_E1, SN_X_Cumulative_ESAL

b. Dependent Variable: Log10_UCI_Combined_All_Plus_0.5

Figure A5. UCI: Model summary for combined all crack types

Coefficients[a]

Model		Unstandardized Coefficients		Standardized Coefficients	t	Sig.
		B	Std. Error	Beta		
1	(Constant)	-.107	.101		-1.054	.292
	Log10_Initial_UCI_Combined_All_Plus_0.5	.781	.048	.763	16.182	.000
	Asphalt_Modulus_E1	1.413E-7	.000	.079	1.447	.148
	Base_Modulus_E2	5.277E-8	.000	.019	.864	.388
	Subbase_Modulus_E3	-7.136E-7	.000	-.026	-1.280	.201
	Subgrade_Modulus_E4	-3.742E-6	.000	-.048	-2.177	.030
	Asphalt_Thicknesses	-.002	.006	-.009	-.277	.782
	Total_Thicknesses	-.002	.002	-.025	-.901	.368
	Age_Survey_Date	.024	.002	.287	12.631	.000
	SN	.014	.013	.034	1.102	.271
	Cumulative_ESALs	3.500E-8	.000	.241	2.827	.005
	Air_Temperature	.001	.002	.022	.628	.530
	Precipitation	.001	.000	.140	3.283	.001
	T1_X_E1	9.234E-9	.000	.029	.832	.406
	Temperature_X_E1	2.083E-9	.000	.038	.805	.421
	SN_X_Cumulative_ESAL	-3.277E-9	.000	-.135	-1.569	.117
	TT_X_CND	-.002	.003	-.041	-.776	.438
	Temperature_X_Precipitation	-2.038E-5	.000	-.059	-1.252	.211
	Age_X_Log10_Initial_Yc_Plus_0.5	-.016	.002	-.343	-6.707	.000
	Traffic_X_Log10_Initial_Yc_Plus_0.5	-2.371E-8	.000	-.119	-4.950	.000
	Reg_D	-.090	.027	-.067	-3.383	.001
	CND	-.323	.066	-.238	-4.864	.000

a. Dependent Variable: Log10_UCI_Combined_All_Plus_0.5

Figure A6. UCI: Model coefficients for combined all crack types

Model Summary[b]

Model	R	R Square	Adjusted R Square	Std. Error of the Estimate
1	.569[a]	.324	.318	.55066

a. Predictors: (Constant), CND, Subbase_Modulus_E3, Air_Temperature, Cumu_ESAL_X_Log10_Initial_Yac_Plus_0.5, Precipitation, T1_X_E1, Reg_D, Asphalt_Thicknesses, Age_Survey_Date, Log10_Initial_UCI_Alligator_Crack_Plus_0.5, Total_Thicknesses, Base_Modulus_E2, Cumulative_ESALs, Subgrade_Modulus_E4, SN, Temperature_X_E1, Temperature_X_Precipitation, TT_X_CND, Age_X_Log10_Initial_Yac_Plus_0.5, Asphalt_Modulus_E1, SN_X_Cumulative_ESAL

b. Dependent Variable: Log10_UCI_Alligator_Crack_Plus_0.5

Figure A7. UCI: Model summary for alligator crack

Coefficients[a]

Model		Unstandardized Coefficients		Standardized Coefficients	t	Sig.
		B	Std. Error	Beta		
1	(Constant)	-.099	.100		-.995	.320
	Log10_Initial_UCI_Alligator_Crack_Plus_0.5	1.041	.055	.945	19.034	.000
	Asphalt_Modulus_E1	1.613E-7	.000	.090	1.650	.099
	Base_Modulus_E2	1.174E-8	.000	.004	.193	.847
	Subbase_Modulus_E3	-1.436E-6	.000	-.052	-2.563	.010
	Subgrade_Modulus_E4	-5.603E-6	.000	-.072	-3.247	.001
	Asphalt_Thicknesses	-.001	.006	-.004	-.108	.914
	Total_Thicknesses	-.003	.002	-.032	-1.139	.255
	Age_Survey_Date	.018	.002	.218	10.797	.000
	SN	.021	.013	.051	1.641	.101
	Cumulative_ESALs	3.454E-8	.000	.239	2.797	.005
	Air_Temperature	.000	.002	-.006	-.180	.857
	Precipitation	.001	.000	.122	2.839	.005
	T1_X_E1	-1.260E-8	.000	-.040	-1.131	.258
	Temperature_X_E1	4.467E-9	.000	.081	1.719	.086
	SN_X_Cumulative_ESAL	-5.167E-9	.000	-.213	-2.456	.014
	TT_X_CND	-.001	.003	-.017	-.320	.749
	Temperature_X_Precipitation	-1.318E-5	.000	-.038	-.805	.421
	Age_X_Log10_Initial_Yac_Plus_0.5	-.028	.003	-.533	-10.207	.000
	Cumu_ESAL_X_Log10_Initial_Yac_Plus_0.5	-2.452E-8	.000	-.118	-5.292	.000
	Reg_D	-.123	.026	-.091	-4.653	.000
	CND	-.228	.066	-.169	-3.433	.001

a. Dependent Variable: Log10_UCI_Alligator_Crack_Plus_0.5

Figure A8. UCI: Model coefficients for alligator crack

Model Summary[b]

Model	R	R Square	Adjusted R Square	Std. Error of the Estimate
1	.493[a]	.243	.236	.38165

a. Predictors: (Constant), CND, Subbase_Modulus_E3, Log10_Initial_UCI_Block_Crack_Plus_0.5, Air_Temperature, Precipitation, T1_X_E1, Reg_D, Cumulative_ESALs, Asphalt_Thicknesses, Age_Survey_Date, Total_Thicknesses, Base_Modulus_E2, Subgrade_Modulus_E4, SN, Temperature_X_E1, Cumu_ESAL_X_Log10_Initial_Ybc_Plus_0.5, Temperature_X_Precipitation, TT_X_CND, Asphalt_Modulus_E1, Age_X_Log10_Initial_Ybc_Plus_0.5, SN_X_Cumulative_ESAL

b. Dependent Variable: Log10_UCI_Block_Crack_Plus_0.5

Figure A9. UCI: Model summary for block crack

Coefficients[a]

Model		Unstandardized Coefficients		Standardized Coefficients	t	Sig.
		B	Std. Error	Beta		
1	(Constant)	-.363	.070		-5.189	.000
	Log10_Initial_UCI_Block_Crack_Plus_0.5	.621	.051	.645	12.188	.000
	Asphalt_Modulus_E1	2.742E-8	.000	.023	.404	.686
	Base_Modulus_E2	5.835E-8	.000	.033	1.382	.167
	Subbase_Modulus_E3	3.063E-7	.000	.017	.791	.429
	Subgrade_Modulus_E4	2.952E-6	.000	.058	2.468	.014
	Asphalt_Thicknesses	-.001	.004	-.010	-.295	.768
	Total_Thicknesses	-.001	.002	-.013	-.419	.676
	Age_Survey_Date	.003	.001	.055	2.377	.018
	SN	.024	.009	.089	2.737	.006
	Cumulative_ESALs	-1.308E-8	.000	-.138	-1.525	.127
	Air_Temperature	.002	.001	.042	1.129	.259
	Precipitation	.001	.000	.082	1.807	.071
	T1_X_E1	9.487E-9	.000	.045	1.227	.220
	Temperature_X_E1	2.333E-9	.000	.064	1.297	.195
	SN_X_Cumulative_ESAL	4.190E-10	.000	.026	.279	.780
	TT_X_CND	-.003	.002	-.082	-1.466	.143
	Temperature_X_Precipitation	-2.994E-5	.000	-.132	-2.643	.008
	Age_X_Log10_Initial_Ybc_Plus_0.5	-.008	.003	-.188	-3.274	.001
	Cumu_ESAL_X_Log10_Initial_Ybc_Plus_0.5	-2.755E-8	.000	-.095	-2.094	.036
	Reg_D	.019	.018	.022	1.056	.291
	CND	-.062	.046	-.070	-1.342	.180

a. Dependent Variable: Log10_UCI_Block_Crack_Plus_0.5

Figure A10. UCI: Model coefficients for block crack

Model Summary[b]

Model	R	R Square	Adjusted R Square	Std. Error of the Estimate
1	.502[a]	.252	.245	.30117

a. Predictors: (Constant), CND, Log10_Initial_UCI_Longitudinal_Crack_Plus_0.5, Subbase_Modulus_E3, Air_Temperature, Age_X_Log10_Initial_Ybc_Plus_0.5, Precipitation, T1_X_E1, Asphalt_Thicknesses, Cumulative_ESALs, Reg_D, Total_Thicknesses, Age_Survey_Date, Base_Modulus_E2, Subgrade_Modulus_E4, SN, Temperature_X_E1, Cumu_ESAL_X_Log10_Initial_Ybc_Plus_0.5, Temperature_X_Precipitation, TT_X_CND, Asphalt_Modulus_E1, SN_X_Cumulative_ESAL

b. Dependent Variable: Log10_UCI_Longitudinal_Crack_Plus_0.5

Figure A11. UCI: Model summary for longitudinal crack

Coefficients[a]

Model		Unstandardized Coefficients		Standardized Coefficients	t	Sig.
		B	Std. Error	Beta		
1	(Constant)	-.006	.055		-.109	.913
	Log10_Initial_UCI_Longitudinal_Crack_Plus_0.5	.462	.022	.426	21.101	.000
	Asphalt_Modulus_E1	-4.206E-8	.000	-.045	-.785	.432
	Base_Modulus_E2	5.789E-8	.000	.041	1.733	.083
	Subbase_Modulus_E3	1.207E-7	.000	.008	.395	.693
	Subgrade_Modulus_E4	-8.331E-7	.000	-.021	-.880	.379
	Asphalt_Thicknesses	.004	.003	.037	1.044	.297
	Total_Thicknesses	-.003	.001	-.068	-2.297	.022
	Age_Survey_Date	.004	.001	.096	4.399	.000
	SN	-.002	.007	-.011	-.332	.740
	Cumulative_ESALs	2.068E-8	.000	.275	3.061	.002
	Air_Temperature	.001	.001	.021	.572	.568
	Precipitation	-2.772E-5	.000	-.005	-.111	.911
	T1_X_E1	1.430E-8	.000	.086	2.340	.019
	Temperature_X_E1	-1.389E-9	.000	-.048	-.979	.328
	SN_X_Cumulative_ESAL	-1.942E-9	.000	-.154	-1.638	.102
	TT_X_CND	.003	.002	.118	2.128	.033
	Temperature_X_Precipitation	1.514E-5	.000	.084	1.694	.090
	Age_X_Log10_Initial_Ybc_Plus_0.5	-.001	.001	-.039	-1.583	.113
	Cumu_ESAL_X_Log10_Initial_Ybc_Plus_0.5	-9.902E-9	.000	-.043	-.960	.337
	Reg_D	-.003	.015	-.004	-.175	.861
	CND	-.165	.036	-.234	-4.549	.000

a. Dependent Variable: Log10_UCI_Longitudinal_Crack_Plus_0.5

Figure A12. UCI: Model coefficients for longitudinal crack

Model Summary[b]

Model	R	R Square	Adjusted R Square	Std. Error of the Estimate
1	.682[a]	.465	.460	.15750

a. Predictors: (Constant), CND, Log10_Initial_UCI_Transverse_Crack_Plus_0.5, Subbase_Modulus_E3, Air_Temperature, Precipitation, T1_X_E1, Asphalt_Thicknesses, Cumulative_ESALs, Reg_D, Total_Thicknesses, Age_Survey_Date, Base_Modulus_E2, Subgrade_Modulus_E4, Cumu_ESAL_X_Log10_Initial_Ytc_Plus_0.5, SN, Temperature_X_E1, Temperature_X_Precipitation, Age_X_Log10_Initial_Ytc_Plus_0.5, TT_X_CND, Asphalt_Modulus_E1, SN_X_Cumulative_ESAL

b. Dependent Variable: Log10_UCI_Transverse_Crack_Plus_0.5

Figure A13. UCI: Model summary for transverse crack

Coefficients[a]

Model		Unstandardized Coefficients		Standardized Coefficients	t	Sig.
		B	Std. Error	Beta		
1	(Constant)	.123	.029		4.233	.000
	Log10_Initial_UCI_Transverse_Crack_Plus_0.5	1.014	.044	1.000	23.064	.000
	Asphalt_Modulus_E1	-5.435E-8	.000	-.095	-1.943	.052
	Base_Modulus_E2	3.391E-8	.000	.039	1.914	.056
	Subbase_Modulus_E3	-2.367E-7	.000	-.027	-1.475	.140
	Subgrade_Modulus_E4	-2.394E-6	.000	-.095	-4.819	.000
	Asphalt_Thicknesses	-.001	.002	-.018	-.612	.540
	Total_Thicknesses	-.002	.001	-.060	-2.383	.017
	Age_Survey_Date	9.592E-5	.001	.004	.178	.858
	SN	-.008	.004	-.059	-2.147	.032
	Cumulative_ESALs	-3.404E-9	.000	-.073	-.872	.383
	Air_Temperature	.000	.001	-.021	-.658	.511
	Precipitation	-1.705E-5	.000	-.005	-.131	.896
	T1_X_E1	1.057E-8	.000	.103	3.306	.001
	Temperature_X_E1	1.479E-10	.000	.008	.199	.842
	SN_X_Cumulative_ESAL	-3.883E-10	.000	-.050	-.617	.538
	TT_X_CND	-.001	.001	-.069	-1.470	.142
	Temperature_X_Precipitation	4.908E-6	.000	.044	1.048	.295
	Age_X_Log10_Initial_Ytc_Plus_0.5	-.019	.002	-.412	-9.554	.000
	Cumu_ESAL_X_Log10_Initial_Ytc_Plus_0.5	-2.632E-8	.000	-.145	-6.262	.000
	Reg_D	-.016	.008	-.036	-1.963	.050
	CND	-.048	.019	-.111	-2.542	.011

a. Dependent Variable: Log10_UCI_Transverse_Crack_Plus_0.5

Figure A14. UCI: Model coefficients for transverse crack

Appendix B: Full factorial design for uncracked asphalt pavements

No.	Treatment Combinations	Layer thickness, in (T_1: Asphalt and T_2: Subbase) and Young's modulus, ksi (E_1:Asphalt, E_2: Base, E_3: Subbase, and E_4: Subgrade)					
		T_1	T_2	E_4	E_2	E_3	E_1
1	000000	3 in	6 in	10 ksi	40 ksi	20 ksi	200 ksi
2	010000	3 in	12 in	10 ksi	40 ksi	20 ksi	200 ksi
3	100000	9 in	6 in	10 ksi	40 ksi	20 ksi	200 ksi
4	110000	9 in	12 in	10 ksi	40 ksi	20 ksi	200 ksi
5	000001	3 in	6 in	10 ksi	40 ksi	20 ksi	1,000 ksi
6	010001	3 in	12 in	10 ksi	40 ksi	20 ksi	1,000 ksi
7	100001	9 in	6 in	10 ksi	40 ksi	20 ksi	1,000 ksi
8	110001	9 in	12 in	10 ksi	40 ksi	20 ksi	1,000 ksi
9	000010	3 in	6 in	10 ksi	40 ksi	100 ksi	200 ksi
10	010010	3 in	12 in	10 ksi	40 ksi	100 ksi	200 ksi
11	100010	9 in	6 in	10 ksi	40 ksi	100 ksi	200 ksi
12	110010	9 in	12 in	10 ksi	40 ksi	100 ksi	200 ksi
13	000011	3 in	6 in	10 ksi	40 ksi	100 ksi	1,000 ksi
14	010011	3 in	12 in	10 ksi	40 ksi	100 ksi	1,000 ksi
15	100011	9 in	6 in	10 ksi	40 ksi	100 ksi	1,000 ksi
16	110011	9 in	12 in	10 ksi	40 ksi	100 ksi	1,000 ksi
17	000100	3 in	6 in	10 ksi	200 ksi	20 ksi	200 ksi
18	010100	3 in	12 in	10 ksi	200 ksi	20 ksi	200 ksi
19	100100	9 in	6 in	10 ksi	200 ksi	20 ksi	200 ksi
20	110100	9 in	12 in	10 ksi	200 ksi	20 ksi	200 ksi
21	000101	3 in	6 in	10 ksi	200 ksi	20 ksi	1,000 ksi
22	010101	3 in	12 in	10 ksi	200 ksi	20 ksi	1,000 ksi
23	100101	9 in	6 in	10 ksi	200 ksi	20 ksi	1,000 ksi
24	110101	9 in	12 in	10 ksi	200 ksi	20 ksi	1,000 ksi
25	000110	3 in	6 in	10 ksi	200 ksi	100 ksi	200 ksi
26	010110	3 in	12 in	10 ksi	200 ksi	100 ksi	200 ksi
27	100110	9 in	6 in	10 ksi	200 ksi	100 ksi	200 ksi
28	110110	9 in	12 in	10 ksi	200 ksi	100 ksi	200 ksi
29	000111	3 in	6 in	10 ksi	200 ksi	100 ksi	1,000 ksi
30	010111	3 in	12 in	10 ksi	200 ksi	100 ksi	1,000 ksi

Full factorial design considering six factors at two levels (Total 64 cell)							
No.	Treatment Combinations	Layer thickness, in (T_1: Asphalt and T_2: Subbase) and Young's modulus, ksi (E_1:Asphalt, E_2: Base, E_3: Subbase, and E_4: Subgrade)					
		T_1	T_2	E_4	E_2	E_3	E_1
31	100111	9 in	6 in	10 ksi	200 ksi	100 ksi	1,000 ksi
32	110111	9 in	12 in	10 ksi	200 ksi	100 ksi	1,000 ksi
33	001000	3 in	6 in	50 ksi	40 ksi	20 ksi	200 ksi
34	011000	3 in	12 in	50 ksi	40 ksi	20 ksi	200 ksi
35	101000	9 in	6 in	50 ksi	40 ksi	20 ksi	200 ksi
36	111000	9 in	12 in	50 ksi	40 ksi	20 ksi	200 ksi
37	001001	3 in	6 in	50 ksi	40 ksi	20 ksi	1,000 ksi
38	011001	3 in	12 in	50 ksi	40 ksi	20 ksi	1,000 ksi
39	101001	9 in	6 in	50 ksi	40 ksi	20 ksi	1,000 ksi
40	111001	9 in	12 in	50 ksi	40 ksi	20 ksi	1,000 ksi
41	001010	3 in	6 in	50 ksi	40 ksi	100 ksi	200 ksi
42	011010	3 in	12 in	50 ksi	40 ksi	100 ksi	200 ksi
43	101010	9 in	6 in	50 ksi	40 ksi	100 ksi	200 ksi
44	111010	9 in	12 in	50 ksi	40 ksi	100 ksi	200 ksi
45	001011	3 in	6 in	50 ksi	40 ksi	100 ksi	1,000 ksi
46	011011	3 in	12 in	50 ksi	40 ksi	100 ksi	1,000 ksi
47	101011	9 in	6 in	50 ksi	40 ksi	100 ksi	1,000 ksi
48	111011	9 in	12 in	50 ksi	40 ksi	100 ksi	1,000 ksi
49	001100	3 in	6 in	50 ksi	200 ksi	20 ksi	200 ksi
50	011100	3 in	12 in	50 ksi	200 ksi	20 ksi	200 ksi
51	101100	9 in	6 in	50 ksi	200 ksi	20 ksi	200 ksi
52	111100	9 in	12 in	50 ksi	200 ksi	20 ksi	200 ksi
53	001101	3 in	6 in	50 ksi	200 ksi	20 ksi	1,000 ksi
54	011101	3 in	12 in	50 ksi	200 ksi	20 ksi	1,000 ksi
55	101101	9 in	6 in	50 ksi	200 ksi	20 ksi	1,000 ksi
56	111101	9 in	12 in	50 ksi	200 ksi	20 ksi	1,000 ksi
57	001110	3 in	6 in	50 ksi	200 ksi	100 ksi	200 ksi
58	011110	3 in	12 in	50 ksi	200 ksi	100 ksi	200 ksi
59	101110	9 in	6 in	50 ksi	200 ksi	100 ksi	200 ksi
60	111110	9 in	12 in	50 ksi	200 ksi	100 ksi	200 ksi
61	001111	3 in	6 in	50 ksi	200 ksi	100 ksi	1,000 ksi
62	011111	3 in	12 in	50 ksi	200 ksi	100 ksi	1,000 ksi
63	101111	9 in	6 in	50 ksi	200 ksi	100 ksi	1,000 ksi
64	111111	9 in	12 in	50 ksi	200 ksi	100 ksi	1,000 ksi

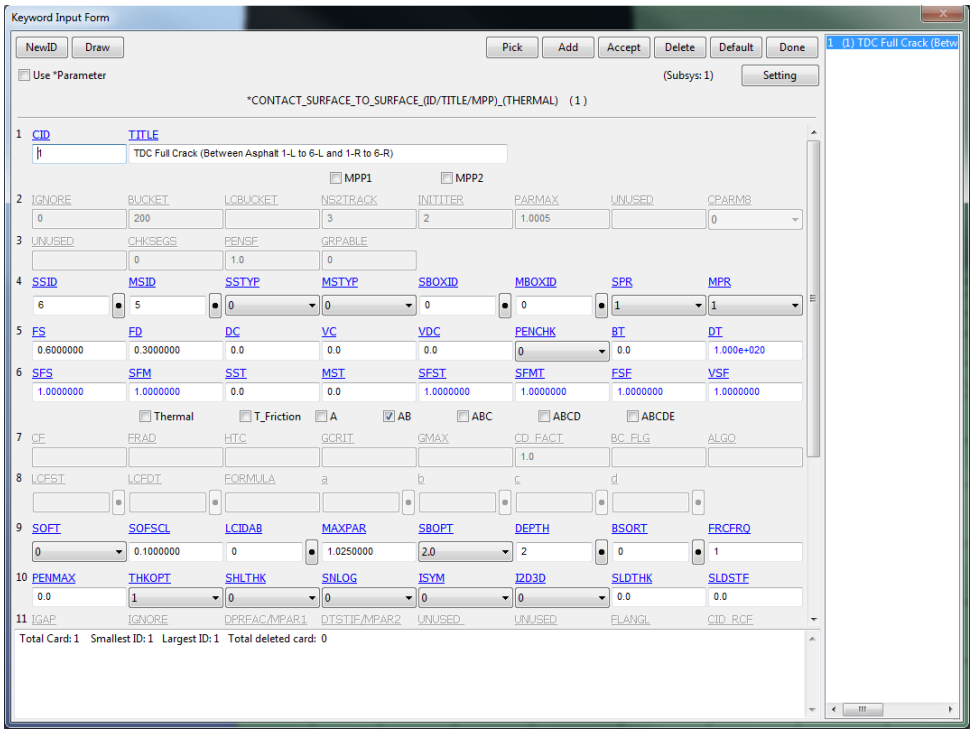

Figure C1. LS-DYNA CONTACT SURFACE TO SURFACE set up in the LS-DYNA software with Static Friction Coefficient (FS = 0.6) and Dynamic Friction of Coefficient (FD=0.3)

Parameters

SOFSCL: Scale factor for constraint forces of soft constraint option (default=.10). Values greater than 0.5 for single surface contact and 1.0 for a one way treatment are inadmissible.

MAXPAR: Maximum parametric coordinate in segment search (values 1.025 and 1.20 recommended). Larger values can increase cost. If zero, the default is set to 1.025. This factor allows an increase in the size of the segments. May be useful at sharp corners.

SBOPT: Segment-based contact options (SOFT=2).

EQ.0: Defaults to 2.

EQ.1: Pinball edge-edge contact (not recommended).

EQ.2: Assume planer segments (default).

EQ.3: Warped segment checking.

EQ.4: Sliding option

DEPTH: Search depth in automatic contact. Value of 1 is sufficiently accurate for most crash applications and is much less expensive. LS-DYNA for improved accuracy sets this value to 2. If zero, the default is set to 2.

LT.0: |DEPTH| is the load curve ID defining searching depth versus time.

FRCFRQ: Number of cycles between contact force updates for penalty contact formulations. This option can provide a significant speed-up of the contact treatment. If used, values exceeding 3 or 4 are dangerous. Considerable care must be exercised when using this option, as this option assumes that contact does not change FRCFRG cycles.

EQ.0: FRCFRG is set to 1 and force calculations are performed each cycle-strongly recommended.

PENMAX:=Maximum penetration distance for old type 3, 5, 8, 9, and 10 contact or the segment thickness multiplied by PENMAX defines the maximum penetration allowed (as a multiple of the segment thickness) for contact types a 3, a 5, a10, 13, 15, and 26.

EQ.0.0 for old type contacts 3, 5, and 10: Use small penetration search and value calculated from thickness and XPENE, see *CONTROL_ CONTACT.

EQ.0.0 for contact types a 3, a 5, a10, 13, and 15: Default is 0.4, or 40 percent of the segment thickness

EQ.0.0 for contact type26: Default is 200.0 times the segment thickness

THKOPT: Thickness option for contact types 3, 5, and 10:

EQ.0: default is taken from control card, *CONTROL_CONTACT,

EQ.1: thickness offsets are included,

EQ.2: thickness offsets are not included (old way).

SNLOG: Disable shooting node logic in thickness offset contact. With the shooting node logic enabled, the first cycle that a slave node penetrates a master segment, that node is moved back to the master surface without applying any contact force.

EQ.0: logic is enabled (default),

EQ.1: logic is skipped (sometimes recommended for metal forming calculations).

SLDTHK: Optional solid element thickness. A nonzero positive value will activate the contact thickness offsets in the contact algorithms where offsets apply. The contact treatment with then be equivalent to the case where null shell elements are used to cover the brick elements. The contact stiffness parameter below, SLDSTF, may also be used to override the default value.

SLDSTF: Optional solid element stiffness. A nonzero positive value overrides the bulk modulus taken from the material model referenced by the solid element.

FS: Static coefficient of friction if FS > 0 and not equal to 2.

EQ.-1.0: If the frictional coefficients defined in the *PART section are to be used, set FS to a negative number.

EQ. 2: For contact types SURFACE_TO_SURFACE and ONE_WAY_ SURFACE_TO_SURFACE, the dynamic coefficient of friction points to the table, see DEFINE_TABLE (The table ID is give by FD below.), giving the coefficient of friction as a function of the relative velocity and pressure. This option must be used in combination with the thickness offset option.

FD: Dynamic coefficient of friction. The frictional coefficient is assumed to be dependent on the relative velocity v-rel of the surfaces in contact. Give table ID if FS=2 (default=0.0).

SSID: Slave Segment Set Up

MSID: Master Segment Set Up.

Table C1. Parametric studies conducted to determine Static Friction Coefficient (FS) and Dynamic Friction of Coefficient (FD) values by comparing the deflection values for the nodes at the center of loading area

Layer Type	Measurement point depth mm (in) from surface layer	Nodes (center of wheel load contact area)	Crack Condition at vertical surface	Static Coefficient of Friction (FS)	Dynamic Coefficient of Friction (FD)	Time (Sec)	Deflection, mm (inch)
Asphalt	0 (0)	584853	TDC - From top to bottom of the first asphalt layer	0.7	0.1	0.212	0.3454 (0.0136)
				0.7	0.2	0.212	0.3454 (0.0136)
				0.7	0.3	0.212	0.3454 (0.0136)
				0.7	0.4	0.212	0.3454 (0.0136)
				0.7	0.5	0.212	0.3454 (0.0136)
				0.7	0.6	0.212	0.3454 (0.0136)
				0.7	0.7	0.212	0.3454 (0.0136)
				0.1	0.3	0.212	0.3454 (0.0136)
				0.2	0.3	0.212	0.3454 (0.0136)
				0.3	0.3	0.212	0.3454 (0.0136)
				0.4	0.3	0.212	0.3454 (0.0136)
				0.5	0.3	0.212	0.3454 (0.0136)
				0.6	0.3	0.212	0.3454 (0.0136)
	38.1 (1.5)	629949	TDC - From top to bottom of the first asphalt layer	0.7	0.1	0.212	0.3429 (0.0135)
				0.7	0.2	0.212	0.3429 (0.0135)
				0.7	0.3	0.212	0.3429 (0.0135)
				0.7	0.4	0.212	0.3429 (0.0135)
				0.7	0.5	0.212	0.3429 (0.0135)
				0.7	0.6	0.212	0.3429 (0.0135)
				0.7	0.7	0.212	0.3429 (0.0135)
				0.1	0.3	0.212	0.3429 (0.0135)
				0.2	0.3	0.212	0.3429 (0.0135)
				0.3	0.3	0.212	0.3429 (0.0135)
				0.4	0.3	0.212	0.3429 (0.0135)
				0.5	0.3	0.212	0.3429 (0.0135)
				0.6	0.3	0.212	0.3429 (0.0135)
	76.2 (3)	681147	TDC - From top to bottom of the first asphalt layer	0.7	0.1	0.212	0.3353 (0.0132)
				0.7	0.2	0.212	0.3353 (0.0132)
				0.7	0.3	0.212	0.3353 (0.0132)
				0.7	0.4	0.212	0.3353 (0.0132)
				0.7	0.5	0.212	0.3353 (0.0132)
				0.7	0.6	0.212	0.3353 (0.0132)
				0.7	0.7	0.212	0.3353 (0.0132)
				0.1	0.3	0.212	0.3353 (0.0132)
				0.2	0.3	0.212	0.3353 (0.0132)
				0.3	0.3	0.212	0.3353 (0.0132)
				0.4	0.3	0.212	0.3353 (0.0132)
				0.5	0.3	0.212	0.3353 (0.0132)
				0.6	0.3	0.212	0.3353 (0.0132)

BOUNDARY SPC SET used in the LS-DYNA to set boundary conditions for the 3D-FE model of cracked asphalt layer

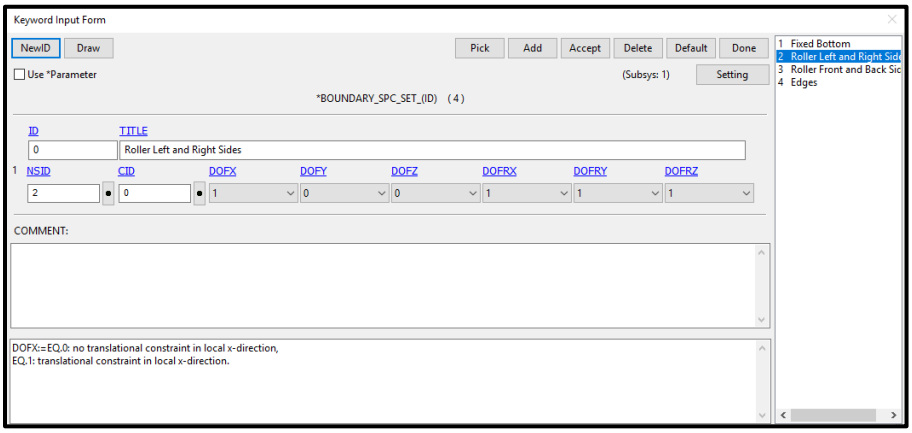

Figure C2. Boundary condition set up for the left and right sides of the 3D-FE model

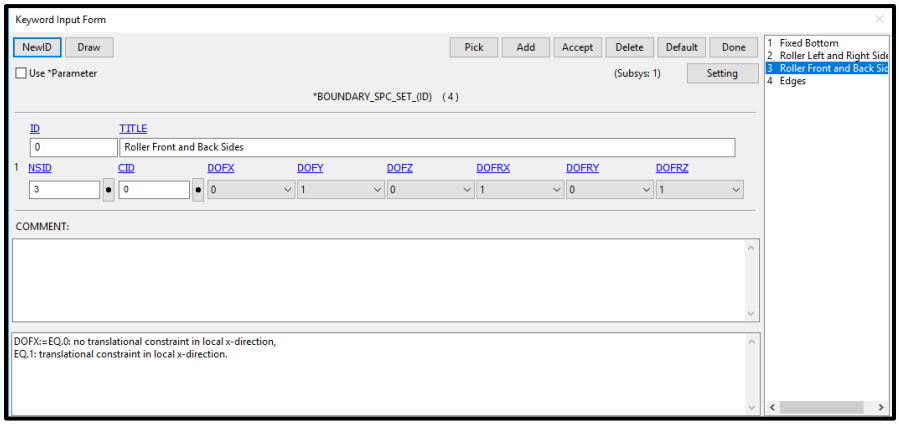

Figure C3. Boundary condition set up for the front and back sides of the 3D-FE model

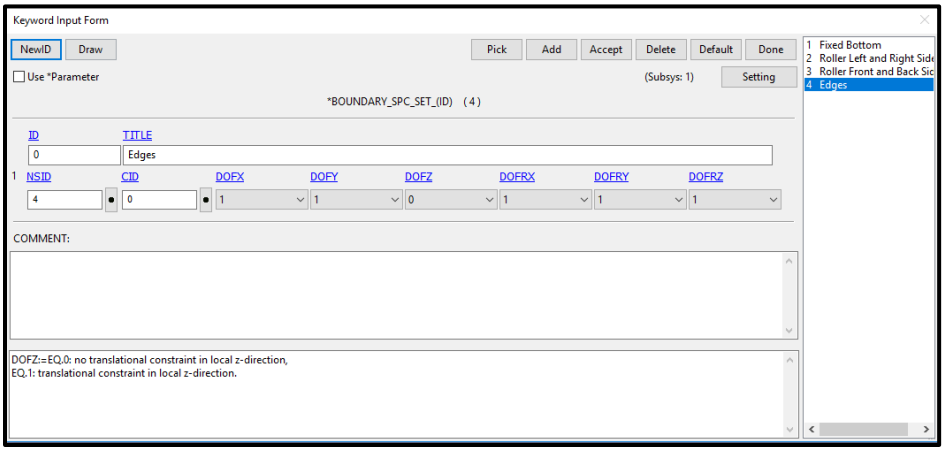

Figure C4. Boundary condition set up for the edges of the 3D-FE model

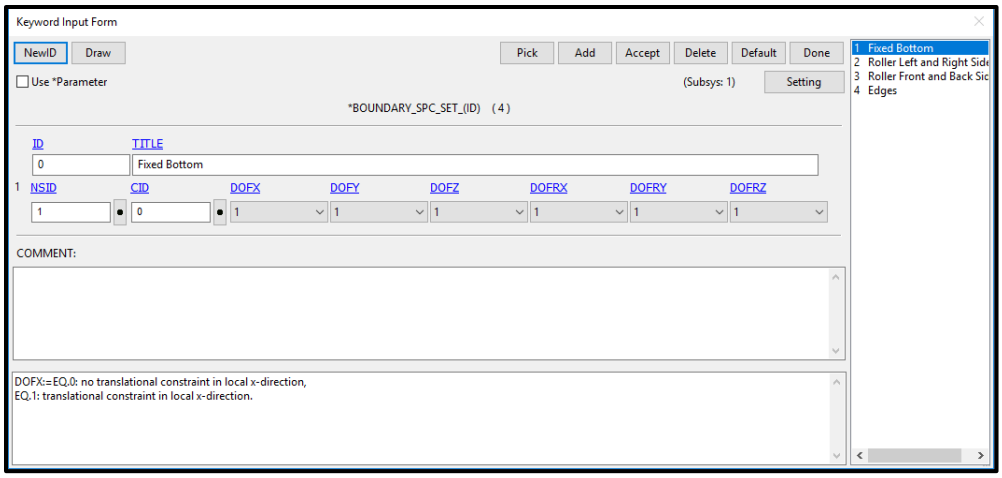

Figure C5. Boundary condition set up for the bottom of the 3D-FE model

Location	Boundary Condition	No. of Nodes	Axis with rotational constraint	Axis with translational constraint	DOF per node (based on translational constraint)	No. of nodes x DOF
Top	Free					
Bottom	Fixed	50	x, y, and z	x, y, and z	0	0
Left and Right	Roller	4,323	x, y, and z	x	2	8,646
Front and Back	Roller	8,807	x and z	y	2	17,614
Edges	Roller	88	x, y, and z	x and y	1	88
Degree of freedom = (# nodes x # DOF per node) - prescribed DOF					Prescribed DOF	26,348
The number of DOF per node for solid element is three (translation in x,y, and z)						
# of nodes = 1,113,195 (3D-FE model)						
# of elements = 1,039,413 (3D-FE model)						
Degree of freedom = (1,113,195 x 3) - 26,348 = 3,313,237						

Figure C6. Calculation of degree of freedom (DOF) for **uncracked** asphalt model

Location	Boundary Condition	No. of Nodes	Axis with rotational constraint	Axis with translational constraint	DOF per node (based on translational constraint)	No. of nodes x DOF
Top	Free					
Bottom	Fixed	50	x, y, and z	x, y, and z	0	0
Left and Right	Roller		x, y, and z	x	2	0
Front and Back	Roller	18,149	x and z	y	2	36,298
Edges	Roller	116	x, y, and z	x and y	1	116
Degree of freedom = (# nodes x # DOF per node) - prescribed DOF					Prescribed DOF	36,414
The number of DOF per node for solid element is three (translation in x,y, and z)						
# of nodes = 2,571,316 (3D-FE model)						
# of elements = 2,488,835 (3D-FE model)						
Degree of freedom = (2,571,316 x 3) - 36,414 = 7,677,534						

Figure C7. Calculation of degree of freedom (DOF) for **cracked** asphalt model

VITA

Zul Fahmi Bin Mohamed Jaafar was born in Kota Bharu, Kelantan, Malaysia, on February 4, 1985. He attended elementary, middle, and high schools in the hometown. He received his Bachelor of Science degree (2008) and Master of Science degree (2012) from Universiti Sains Malaysia (USM) in Pulau Pinang, Malaysia, both in Civil Engineering. He came to the United States in January 2013 to pursue his doctorate degree in the Department of Civil Engineering at the University of Mississippi, Oxford, Mississippi, United States. He received merit scholarships from Ministry of Education (MOE) Malaysia and Universiti Sains Malaysia. During his doctoral research at the University of Mississippi, he worked under the guidance of Dr. Waheed Uddin, professor and founder director of the Center for Advance Infrastructure Technology. His main field of interest is pavement and transportation engineering. He received the degree of Doctor of Philosophy in Engineering Science in May 2019.